ABSTRACT

MAXWELL, BRYAN MARET. Opening the “Black Box” : Improved Spatiotemporal Data Resolution in Agricultural BMPs using Continuous Multi-point Monitoring (Under the direction of Dr. François Birgand).

Our understanding of agricultural best management practices (BMP) has been constrained to partial information collected using infrequent monitoring methods. Advancements in monitoring technologies (e.g. field spectrophotometers) provide improved temporal resolution of water quality data. A multiplexed pumping system (MPS) was developed to extend the temporal resolution benefits to the spatial scale. The MPS technology and field spectrophotometers were deployed in lab and field studies to observe nutrient dynamics of two BMPs at the site scale.

A small volume MPS was designed to minimize sample volume while still providing high frequency data. The system was tested for cross contamination between multiple sources and two applications of the technology are reported. Cross contamination from multiple sources was negligible when using recommended procedures. Short-circuiting of flow in a bioreactor was directly observed through high frequency porewater sampling, and the MPS showed high seasonal and spatial variability of nitrate removal in stream sediments using *in situ* mesocosms. The results show it is possible to obtain high frequency data in volume-limited applications for observing pore water solute dynamics.

In eleven 24-hour experimental trials at the Claridge Nursery stream restoration the small volume MPS measured sediment-driven [NO_3] reduction in *in situ* open to air mesocosms. There was high seasonal variability in NO_3 removal rates that followed temperature changes. Mean NO_3 removal in organic muck sediments was greater by 114 mg N m^{-2} d^{-1}, relative to low-organic sand sediments. Greater NO_3 flux in organic muck sediments was supported by diffusive film porewater samplers. Spatial variability in some trials was high, with NO_3 removal rates varying by 2 – 4x in mesocosms < 1 m apart. Zero and first order models were both well-suited to modeling the observed data. Sampling frequency of < 1 hour was recommended for best estimates of removal rates.

A 287-day experiment investigated the effects of DRW cycles on NO_3 removal in woodchip columns. Columns were exposed to continuous saturation (SAT) or to weekly, 8-h drying-

rewetting (8 h of aerobiosis followed by saturation) cycles (DRW). Nitrate concentrations were measured at the column outlets using the small volume MPS. Drying-rewetting columns showed greater export of total and dissolved organic carbon and increased NO_3 removal rates. Nitrate removal rates in DRW columns increased by up to 80%, relative to SAT columns, although DRW removal rates decreased quickly after rewetting. Increased NO_3 removal in DRW columns continued even after 39 DRW cycles, with ~33% higher total NO_3 mass removed over each weekly DRW cycle.

A second 105-day experiment investigated the effect of DRW duration on NO_3 removal in woodchips. An 8 h DRW cycle increased NO_3 removal by similar percentage as the previous experiment, and a 24 h DRW cycle increased NO_3 removal by 114±29%, relative to SAT columns. A 2 h DRW cycle did not substantially increase NO_3 removal. Rate of DOC leaching significantly impacted NO_3 removal in both studies. Temperature and hydraulic residence time had a positive and negative effect, respectively, on NO_3 removal. Results provide strong support that NO_3 removal in woodchip bioreactors can be increased using DRW cycles, and that aerobically-produced DOC is the major cause of increased rates.

The MPS was deployed in three 2 – 4 week monitoring periods at Iowa and New Zealand field bioreactors. High frequency monitoring was able to accurately measure NO_3 removal rates (0.7 – 2.5 g N m^{-3} d^{-1}) and showed current calculations using instantaneous values can be misleading due to lagged nutrient pulses. Cumulative NO_3 loads were calculated with uncertainty of 1 – 4%. Internal porewater sampling showed vertical [NO_3] gradients related to spatially-variable porosity and residence time, and NO_3 pulse tracking revealed apparent “dead-zones” and preferential flow.

Opening the “Black Box” : Improved Spatiotemporal Data Resolution in Agricultural BMPs using Continuous Multi-point Monitoring

by
Bryan Maret Maxwell

A dissertation submitted to the Graduate Faculty of
North Carolina State University
in partial fulfillment of the
requirements for the degree of
Doctor of Philosophy

Biological and Agricultural Engineering

Raleigh, North Carolina
2019

APPROVED BY:

_____	_____
Dr. François Birgand Committee Chair	Dr. Michael Burchell
_____	_____
Dr. Garry Grabow	Dr. Louis Schipper External Member
_____	
Dr. Dean Hesterberg	

DEDICATION

I would like to dedicate this dissertation to my immediate and extended family who, without your help, none of this would have been possible, and to those friends and family close to me who I wish could have still been around as I finished this journey of mine before the end of theirs.

BIOGRAPHY

Bryan Maret Maxwell arrived to Raleigh at the end of a southern arc that began in California and ended on the Atlantic coast. He was born the first son of Ruth Allyn Banks and Paul Bryan Maxwell, the first of two sons, both of which would eventually pass through the bricked pathways of North Carolina State University. Bryan, for the middle name of his father; Maret, for the middle name of his father's brother; Maxwell, for his father's family name which extends much further than any family member he ever met having traveled across the Atlantic from the ancestral home of the Maxwell clan, seated in a castle now turned to rubble in Dumfries, Scotland.

Bryan's arrival to Raleigh came at the end of a trail shaped by his father's career and his mother's best intentions. Just after the birth of his broth Craig Ian Maxwell, the family moved from Los Angeles to a suburb on the periphery of Dallas where his father continued his metallurgical career. The layover in Texas was brief, however, after his father's company transferred him to manage a plant in South Carolina. This would lead the Maxwell family to once again pick up their shallow roots and move to the third home in five years, inexorably drawn towards the East Coast. Their home in the small town outside of Orangeburg would become his first lessons in agriculture and the customs of the South. Their house was host to a small pepper garden, five shabby goats, and one lucky chicken that had survived the dogs. Their town was host to, among other things, a collection of tobacco and cotton farms, one doctor who worked out of a double-wide, and several cemeteries split between two groups whose defining requisite were where your ancestors arrived from. If it was his father that dictated the move to the Palmetto State, it was his mother that demanded their departure. After his brother's near-fatal acquaintance with anaphylaxis, his mother forced their move from the town she considered too rural to be trusted with her children's welfare.

It was after this last move that Bryan would arrive in North Carolina. It wasn't until North Carolina that the Maxwell family finally set down roots. Bryan's childhood was shaped by the contours around Charlotte, the marshes and beaches to the east and the long spine of Appalachia to the west. His father's penchant for travel would take him around the country and beyond its borders, giving Bryan, at a young age, the fortune of short glimpses into a world that existed outside of the States.

The bulk of Bryan's early education unfolded in North Carolina as he moved from childhood into adolescence. Much of this education would take place outside of school hours and fluorescent recitations. His parents picked up where the school's curriculum left off, his formal lessons in grammar and algebra countered by the informal study of music and art. School would attempt to teach him a physical education, that formalized arena of play, but it was his father that taught him to love sports and outdoor adventure. School would make him literate, but it was his mother that taught him to love books and writing. Bryan's grandparents picked up where his parents left off. His grandfather helped teach him the lifelong lessons of tackle and lures and bait and crab pots outside of Beaufort, South Carolina. His grandmother taught him manners and walks in the woods and enough humility and humor to appreciate the absurdity of writing a third-person autobiography at thirty years old.

When it came time to move from high school into college, Bryan's university ambitions ended at North Carolina State University where he has spent the last ten years. The grandson of a engineer for skyscrapers and bridges, the son of an engineer for metals and alloys, it was a natural choice to go to the only major college for engineering in the state which was the closest he had to a thing called home. After three years of studying civil engineering Bryan realized he didn't share his grandfather's passion for structural design. He stayed within the discipline, moving into a field more closely connected to the land, and has studied agricultural engineering ever since. Bryan has spent the last five years of his doctorate improving understanding of water quality treatment practices and the removal of excess nitrogen from the landscape. After he finishes his degree Bryan intends to remain on the same trajectory, a perpetual student of life and the world.

ACKNOWLEDGMENTS

I would first like to begin with the sort of acknowledgements intended for this section. There have been a significant number of institutions, organizations, and individuals who, without their financial support, much of the work in this dissertation would not have been possible. I would like to thank the North Carolina Department of Transportation for funding the development of the in situ mesocosm method for measuring sediment-driven nitrogen removal at the Claridge Nursery stream restoration. I would like to thank the US Department of Agriculture's NIFA grant program for entirely funding the lab and field research of woodchip bioreactors. I would like to thank the Water Resources and Research Institute for funding research into floating islands, work not included in the scope of this dissertation. And I certainly have to thank North Carolina State University and the Department of Biological and Agricultural Engineering for financially supporting me through the doctorate program. I most certainly would like to thank my advisor, Dr. Francois Birgand, for helping support me financially, helping direct this research, and providing oversight for experiments and the technical writing of this dissertation. I would also like to thank the members of my committee, Drs. Dean Hesterberg, Louis Schipper, Michael Burchell, and Garry Grabow for their vital input. Among the other supporting staff and faculty in the BAE department, I am grateful for the help of: Heather Austin (for always being helping me keep myself on track), Neil Bain (for shop help and patience with my absent-mindedness), Shiying Tian (for being incredibly helpful as a consult), Sam Garvey (for helping design an MPS that didn't have to be baby-sat), Phil Harris, Cong Tu, Mike Boyette (for convincing me to come to graduate school), John Classen, Garey Fox, Lacey Parrish, Tim Seaboch, Ken Pecinovsky (an Iowa farmer not in our department, but who definitely deserves mentioning), and Caleb Ray.

On a more personal note, I would like to acknowledge an incredible cast of characters in the department who were consistently there to help along the way. The work in Plymouth, North Carolina would have been much harder and much lonelier without the help of Wenlong Liu, who has also been a source of feedback and advice. Getting started on my early research would have been much harder without the help of Kyle Aveni-Deforge who not only made himself available as a great lab technician, but also as a mentor and friend. Despite an undergraduate workload that could have been a graduate thesis, Danielle Winter was a huge help for much of the work within

and without this dissertation, and I hope I was as helpful to her as she was to me. I appreciated the huge help in the field and lab that was given to me by members of our lab group, including Chiao-Wen Lin, Elizabeth Allen, Sheida Moin, and Qianyu Hang. Further, without the fellowship of other students in the BAE department my time here would have much less enjoyable. The BAE roots run deep, and I don't doubt I've made some lifelong friends in the process. I can only hope that fellowship extends into the future. It is one of the best resources the department has for graduate students. The same should be said for everyone who provided me support and comradery outside the department, whose names I hopefully don't need to list and are aware who they are. The world can be a lonely place, and an ear to speak into and a face to laugh with are something of immeasurable value.

On an even more personal note, I would like to acknowledge the support of my family. My gratitude towards my family runs well beyond the pages of this manuscript and my time in school. I would never have been able to pursue graduate school without my parents' generosity of paying for my undergraduate schooling. And these are only my financial debts. I have been blessed with two parents who supported my ambitions, and lack thereof, who encouraged me with my gifts, who provided me guidance, in life and finance and love, and who offered to and did jump on a plane to come to Raleigh when things got hairy. None of this would have been possible without my parents. There is a book of gratitude somewhere whose handwriting is mine and whose pages have no end and whose title is the names of my parents. I would like to thank my brother, too, who was also there during challenging times, and my aunt Sue and uncle Doug who were a much needed mountain refuge of family when the rest of mine was so far away. Finally, I would like to thank my grandmother, who I think would have joined me in wishing that she could be here for the end of this journey of mine before seeing the end of hers. I'm not sure I've ever had more admiration for someone in their faith. I will always be grateful for a grandmother who always told me she enjoyed my writing, and was proud of me for simply showing up and getting taller.

I would finally like to acknowledge that big beautiful blue-green house on the hill, without which I doubt I would be as motivated or inspired to work in this particular field.

TABLE OF CONTENTS

LIST OF TABLES

LIST OF FIGURES

CHAPTER 1: **A Small-volume Multiplexed Pumping System for Automated, High-frequency Water Chemistry Measurements in Volume-limited Applications**. Maxwell, B. M., Birgand, F., Smith, B., & Aveni-Deforge, K. (2018). *Hydrology and Earth System Sciences, 22*(11), 5615-5628.

1.1. Introduction

Recent UV-vis field spectrometers provide an opportunity for high frequency *in situ* monitoring to increase temporal resolution of water quality data. Water quality has been measured with these instruments by correlating absorbance with chemical concentration (Crumpton et al. 1992; Suzuki and Kuroda 1987; Finch et al. 1998; Johnson & Coletti 2002; Rochelle-Newall & Fisher 2002; Saraceno et al. 2009). Rieger et al. (2006) and Torres & Bertrand-Krajewski (2008) measured total suspended solids (TSS) in wastewaters using partial least squares regression (PLSR) to correlate absorbance fingerprints to concentrations. Etheridge et al. (2014) expanded the technique to measure light- and non-absorbing constituents including PO_4^{3-}, total phosphorus (TP), nitrate (NO_3^-), total Kjeldahl nitrogen (TKN), TSS, dissolved organic carbon (DOC), and salinity in a brackish North Carolina marsh. Birgand et al. (2016) have shown that the technique might also be used to measure iron and silica in lakes and reservoirs.

Among the spatial heterogeneity of biological and chemical processes in the environment (Merill & Tonjes, 2014; Kahlert et al., 2002; Dent & Grimm, 1999; Parkin, 1987), patches referred to as 'hot spots' are particularly interesting (e.g. riparian buffers, hyporheic zones). These 'hot spots' have been observed to have a disproportionate impact on biogeochemical cycles, and can be particularly active over short periods of time referred to as 'hot moments' (McClain et al., 2003; Vidon et al., 2010). While temporal resolution has and will provide invaluable information at a particular monitoring station (e.g. Etheridge et al., 2014), expanding resolution to spatial data could illuminate tightly coupled processes and would greatly magnify the value of these instruments. Documenting the short-term fate of reactive nutrients within identified 'hot spots' might provide new insight into nutrient cycles and their controlling factors.

An automated large volume multiplexed pumping system (MPS) capable of pumping water from up to 12 sources to a UV-vis spectrophotometer was previously reported (Birgand et al., 2016). The MPS is a 'multiplexed' system in that it delivers sample volumes from separate sources to a single probe used to consecutively observe water chemistry at all sources. The 3.18 mm inside

diameter (ID) tubing yields an average volume of 100 mL of water per sample, which is very well adapted when the source can easily accommodate such withdrawal without consequences on the source or the processes studied. Certain applications, however, may require minimizing sample withdrawal to avoid disturbing the observed process while still obtaining high frequency data. Observing solute dynamics in soils or sediments, particularly those with low drainable porosity, is one such example of a volume-limited application.

In this article, we are reporting the capabilities offered by a small volume MPS coupled with a field spectrophotometer to obtain high resolution water quality data in both time and space. This system can accommodate small volumes (< 15 mL) from up to 12 different sources located within a 10 m distance of the instrument and provide absorbance measurements at better than hourly intervals at each location. This system was designed to minimize inline volumes for volume-limited applications. This article describes the instrument and the challenges involved, evaluates its performance, and reports two applications of this system in such volume-limited conditions.

1.2. Small volume multiplexed pumping system

The principle followed for this instrument is to use a portable spectrophotometer as a central portable laboratory, coupled with the MPS able to sequentially pump water from several points within a reasonable distance of the probe. The small volume MPS is designed for high frequency sampling in volume-limited applications. The solution to minimizing sample volume is small diameter tubing and a low volume flow-through measurement cell. The challenges of this design include clogging of tubing and high head losses due to surface tension forces in the tubing. The latter implies higher pump suction and tends to generate sample residuals left after purging along the length of the tubing, increasing the potential for cross contamination between samples. This drawback demands specific evaluation of the small volume MPS before use.

The major components of the system include: 1) a UV-vis spectrophotometer fitted with a flow-through cuvette, 2) a bidirectional peristaltic pump, 3) small diameter Polytetrafluoroethylene (PTFE or Teflon) tubing, 4) an Arduino control board (Arduino, www.arduino.cc), 5) a 12 port valve, 6) a 3 way valve manifold, and 7) an optional fractional volume collector.

The general automated ‘sampling sequence’ for the system starts with pumping from source *n* to a flow-through spectrophotometer cuvette via 0.9 mm I.D. PFTE tubing and a peristaltic pump.

After the water has entered the cuvette the spectrophotometer takes a measurement and water is then purged back either to the source, to a fractional volume collector, or to waste using a 3 way valve manifold. The multi-port valve then selects source *n+1* and a similar 'sampling sequence' takes place. Up to 12 'sampling sequences' corresponding to the 12 ports of the multi-port valve can occur during a 'sampling cycle'. A fractional volume collector can be used to collect selected sample volumes so that readings by the spectrophotometer can be compared to lab measured concentrations.

Control of the MPS pumping, purging, valve actuation, and activity logging is performed by an Arduino Mega 53 pin control chip (Arduino, www.arduino.cc). This inexpensive control board utilizes open-source software for easy-to-use programming and hardware interfacing, although other similar board/microprocessors can be used. The high frequency water quality probe used is a UV-vis field spectrophotometer Spectro::Lyser™ by s::can™ fitted with a 4 mm path length, 1.1 mL flow-through quartz cuvette (Starna Cells, Inc. model 46-Q-4) placed vertically to facilitate cuvette drainage by gravity during purging. The water quality probe is used as a 'master' instrument to dictate the MPS 'slave' system when to begin a 'sampling sequence'. We use an existing capability of the spectrophotometer to send a 12 V signal at an adjustable time prior to a measurement as a trigger for the MPS, although any other triggering method (e.g. time-based using the Arduino control board) could be used.

A peristaltic pump provides pumping and purging at 20 mL min^{-1} flow rate acceptable for the 0.9 mm I.D. tubing used. A MOSFET h bridge controlled by the Arduino reverses DC polarity at the pump to alternate between pumping and purging. The 12 port valve used is a low pressure Cheminert® 12 position valve from Valco Instruments. The multi-port valve advances to the next desired port using a pneumatic actuator powered by compressed air (bottle or 12 V compressor). Although the valve advances through ports sequentially, the user can select the ports to use with the Arduino controller. Three Arduino-controlled 3 way solenoid valves (Takasago MTV series) are used for different sampling and purging configurations. The Arduino board is fitted with an SD card reader/writer for activity logging, an RTC clock for time-keeping, an LCD panel for system output display, and operable switches for manual control.

The system has been designed for unattended operation for long periods of time (e.g. days or weeks), although it is limited by the spectrometer data storage, fouling of the cuvette, and battery power (and sample storage of the fractional volume collector if used). The time for a 'sampling sequence' is limited by the longest pumping time from furthest source. Ultimately this determines the frequency of spectrometer measurements since the probe has a set time interval between measurements. The sampling frequency for each source depends on the 'sampling sequence' time intervals and on the number of sources (1 to 12).

1.3. System configurations

Several configurations have been programmed to increase versatility of the instrument and minimize cross contamination between samples (Figure 1-1) by actuating one or more of the 3 way valves using the Arduino control board.

1.3.1. Pumping from source to probe and purging back to source.

When it is necessary to purge all sample volume back to the source, the system is configured as Figure 1-1(a) during pumping (downward arrow on the peristaltic pump) and as Figure 1-1(b) during purging (upward arrow on the peristaltic pump). To measure absorbance in the 1.1 mL cuvette used, a minimum sample volume of ~7 mL is required which includes cuvette volume ($V_{cuvette}$) plus inline tubing volume. The system is purged by air by running the pump in reverse. To minimize cross contamination without using a DI rinse, the cuvette can be rinsed by pumping sample volume >7 mL temporarily stored in the post-cuvette storage volume.

1.3.2. Purge to waste

In this configuration, it is not desired that the sample be purged to the source, so it is purged to waste (Figure 1-1(c)).

1.3.3. Pump to waste

This configuration is used for purging residuals of the sample drawn from the previous source *n - 1* that remain in the tubing and rinsing with sample volume from the current source *n* (Figure 1-1(d)). After the estimated time for new water from the current source to reach the waste valve has elapsed, the system switches to configuration in Figure 1-1(a) for sample measurement by probe.

1.3.4. Fractional volume collection (FVC)

This configuration is used for collecting measured sample volumes to compare values given by the probe to later lab analysis (Figure 1-1(e)). The actual sequence consists in purging the FVC tubing with air using Figure 1-1(e) configuration but in the pumping mode (downward arrow on the peristaltic pump, not shown) until water has passed the 3 way valve closest to the FVC, then use Figure 1-1(c) to purge any cross contaminated water to waste before samples are sent to the FVC using configuration in Figure 1-1(e). Any water left in tubing after the FVC sample vial is full is purged to waste.

1.3.5. DI water rinse

Between each sample, the user may choose to rinse the tubing and cuvette with DI water to create consistent cross contamination between samples and residual DI water droplets (Figure 1-1(f)). This configuration draws water in from a DI water source and pumps it through the lines and into the cuvette. Consistent cleaning of the quartz cuvette decreases optical fouling over time. The cuvette and post-cuvette storage volume are rinsed and the water is then purged to waste.

1.4. System testing

In laboratory continuous flow systems, the risk for cross contamination between consecutive samples is mechanically minimized by having unidirectional flow and by rinsing the lines with a carrier liquid between samples. Our system has been designed to allow for bidirectional flow, purging the lines instead with air. Because of surface tension forces purging with air can leave micro-droplet residuals in the lines, opening the possibility for cross contamination between consecutive samples. This is particularly problematic since sample volumes needed for analysis each time are by design small. Although this is admittedly undesirable, this can still be acceptable as long as the potential for contamination is evalutated and solutions to minimize the risks are known. Potential solutions for minimizing cross-contamination include a pre-measurement rinse with the current source water or extended purging of the lines with air after each measurement.

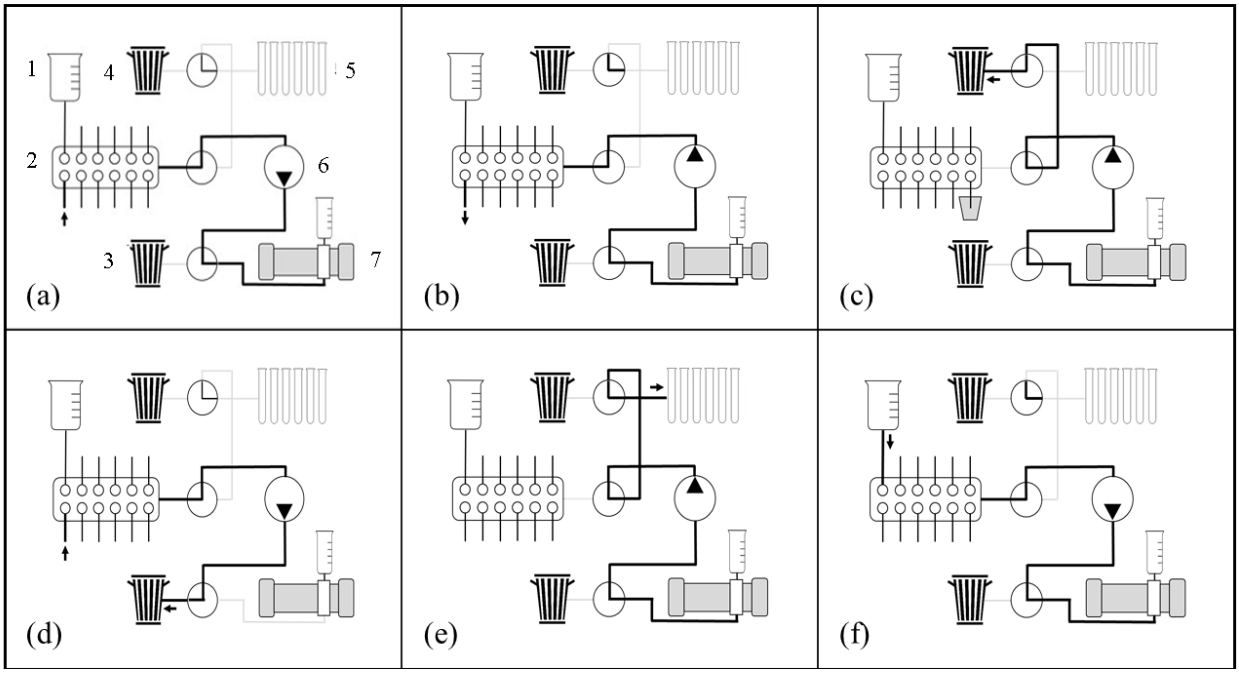

Figure 1-1. Graphical depiction of small volume multiplexed pumping system (MPS) configurations which include 1) DI water source, 2) 12 port intake valve, 3 & 4) waste or air purge, 5) fractional volume collector (FVC), 6) bidirectional peristaltic pump, and 7) spectrophotometer with cuvette housing. An Arduino microcontroller actuates a series of 3 way valves to move between separate configurations (a) – (f).

Cross contamination could arise from two processes. First, cuvette contamination could occur when a water sample inside the cuvette during instrument reading is contaminated by droplets from the previous sample, either in the cuvette or in the MPS tubing. Second, cross contamination of the source, or source contamination, could occur when the 'purging back to source' configuration is used (Figure 1-1(b)) and the source itself is contaminated by residuals from other sources. Both contamination possibilities were evaluated in two separate experiments. A third test of performance quantified the relationship between sampling frequency and the distance from the source to the system, since increased pumping time for a 'sampling sequence' leads to lower data frequency.

Methods for evaluating cuvette contamination and source contamination were identical to those used in Birgand et al. (2016). Alternating measurements between sources of high and low NO_3^- concentration ($[NO_3]_{high}$ and $[NO_3]_{low}$, respectively) was used to determine contamination. The spectrophotometer's estimates of NO_3^- based on the absorbance fingerprint (method detailed

further in Supplemental Material) were used to quantify contamination. The primary difference in testing the small volume MPS for contamination between sources was the size of the flow-through cell. In this system a 1.1 mL flow-through quartz cuvette was used. In addition to testing cross contamination when rinsing with sample volume from the current source, a DI rinse was tested to see if it resulted in decreased contamination by residuals.

For testing pump timings, external tubes of various lengths were cut and fitted to the inlet port of the system. The length of time required to pump from the source to fill the cuvette and the time required to purge the line were recorded. Pump times for each tube length were measured twice with use of a stopwatch and average pump time was recorded.

1.4.1. Cross contamination results

The cross contamination trial results are summarized in Table 1-1. The first two columns report p-values testing for significant difference (α=0.05) between spectrophotometric estimates of NO_3^- concentration in the source (10 repeated measurements) and subsequent 10 measurements after pumping sample volume from the alternate NO_3^- source between each measurement (i.e. if $p>0.05$, there was no statistical difference between initial and subsequent measurements for NO_3^-, implying negligible cross contamination). The results show that without a DI rinse and when measuring high concentration samples after low concentration samples the cuvette must be rinsed with the current sample by at least ten times $V_{cuvette}$ to make cuvette contamination by previous sample negligible. With rinsing only two times $V_{cuvette}$, concentrations were underestimated at about 13.25 mg NO_3-N L^{-1}, lower than the $[NO_3]_{high}$ = 14.72 mg NO_3-N L^{-1} reference. Cross contamination was divided by 10 by rinsing with four times $V_{cuvette}$, but was still measurable and significant.

For the low concentration samples measured after high concentrations, rinsing 10 times the $V_{cuvette}$ could not fully eliminate cross contamination as it still appeared to be significant, yielding readings around 0.14 mg NO_3-N L^{-1}instead of the initial 0.06 mg NO_3-N L^{-1}. Adding a DI rinse appeared to eliminate cross contamination for $[NO_3]_{low}$ by rinsing with ten times $V_{cuvette}$ (<0.01 mg L^{-1} difference), but the same treatment significantly diluted $[NO_3]_{high}$.

Table 1-1. Results of testing cross contamination of cuvette. Treatment indicates the volume of sample pumped from the current source for cuvette rinsing relative to cuvette volume ($V_{cuvette}$), and whether or not a prior DI rinse was used. *** indicates that the protocol used resulted in no significant difference between initial [NO_3^-] and subsequent measurements (α=0.05).

Trial #	Treatment	Initial concentrations (mg NO_3-N L^{-1})		p-value for difference in means of $[NO_3]_{High}$	p-value for difference in means of $[NO_3]_{Low}$	95% C.I. for difference in means, $[NO_3]_{High}$ (mg NO_3-N L^{-1})	95% C.I. for difference in means, low NO_3^- source (mg NO_3-N L^{-1})
		$[NO_3]_{High}$	$[NO_3]_{Low}$				
1	2x $V_{cuvette}$	14.71 ± 0.02	0.12 ±0.01	<0.0001	<0.0002	(-1.59, -1.37)	(1.29, 2.10)
2	4x $V_{cuvette}$	14.71 ± 0.01	0.09 ±0.01	<0.0001	<0.0001	(-0.19,-0.14)	(0.15,0.18)
3	10x $V_{cuvette}$	14.75 ± 0.01	0.06 ±0.01	0.236***	<0.0001	(-0.03,0.01)	(0.06,0.09)
4	DI rinse, 2x $V_{cuvette}$,	14.74 ± 0.01	0.08 ±0.01	<0.0001	<0.0001	(-1.74,-1.41)	(0.28,0.35)
5	DI rinse, 4x $V_{cuvette}$	14.74 ± 0.01	0.11 ±0.02	<0.0001	<0.0001	(-0.11,-0.07)	(0.04,0.08)
6	DI rinse, 10x $_{cuvette}$	15.14 ± 0.01	0.09 ±0.02	0.003	0.615***	(-0.06,-0.02)	(-0.02,0.04)

These results suggest that there is no one solution to fully eliminate cross contamination when consecutive samples differ drastically in solute concentration. These results were obtained for extreme changes of conditions where consecutive concentrations were roughly 150-fold different. For applications where this ratio may be common between consecutive samples, rinsing with >10 times $V_{cuvette}$ is recommended and values for lower concentration should be taken with caution. For most applications, however, such ratios between consecutive concentrations are unlikely. For ratios of 50, 10 and 5 (i.e 0.50 to 25.0, 0.5 to 5.0 and 0.5 to 2.5 mg NO_3-N L^{-1}), the differences in mean concentrations reported in Table 1-1 would be divided by a factor of 3, 10 and 30, respectively. Rinsing with four times $V_{cuvette}$ would reduce the absolute concentration difference from 0.19 mg NO_3-N L^{-1} in the worst-case scenario to 0.06, 0.02 and less than 0.01 mg NO_3-N L^{-1}, respectively, although the concentrations may still be significantly over- or underestimated.

These values are within the 5% measurement uncertainties often found to be acceptable from analytical instruments.

1.4.2. Source contamination

Source contamination (or cross contamination of the source) testing results are shown in Figure 1-2. As expected, $[NO_3]_{high}$ and $[NO_3]_{low}$ became diluted and concentrated, respectively, as residual volumes from the previous samples contaminated the sources. This source contamination increased with increasing difference in initial concentrations (Figure 1-2 and Table 1-2). Over 40 purges back to the source, the concentration and dilution effects were approximately linear and regression lines were fitted to the data to calculate effective residual volumes (V_{res}). The 95% confidence interval for the slope and intercept of the regression lines were used to calculate the uncertainty on the calculated residual volumes. Standard errors of the regression residuals were twice those of the reference measurements. This indicates additional source(s) of random error, which could include some variability in the residual volumes and/or non-uniform mixing of the sources between consecutive samples. Estimates of V_{res} were calculated to vary between 0.28 and 0.46 mL (Table 1-2). In trial (a) and (c), V_{res} were statistically different when calculated using $[NO_3]_{high}$ and $[NO_3]_{low}$, and also differed between trials (a) and (b) for $[NO_3]_{low}$. Practically, our results show that when using the 'purge back to source' configuration (Figure 1-1(b)) less than 0.5 mL of water (5% of sample volume pumped) from the previous sample may contaminate the source measured. This is comparable to previous analysis of the large volume MPS showing V_{res} of 4% sample volume pumped (Birgand et al., 2016). This volume may correspond to droplets left in the 0.9 mm ID tubing.

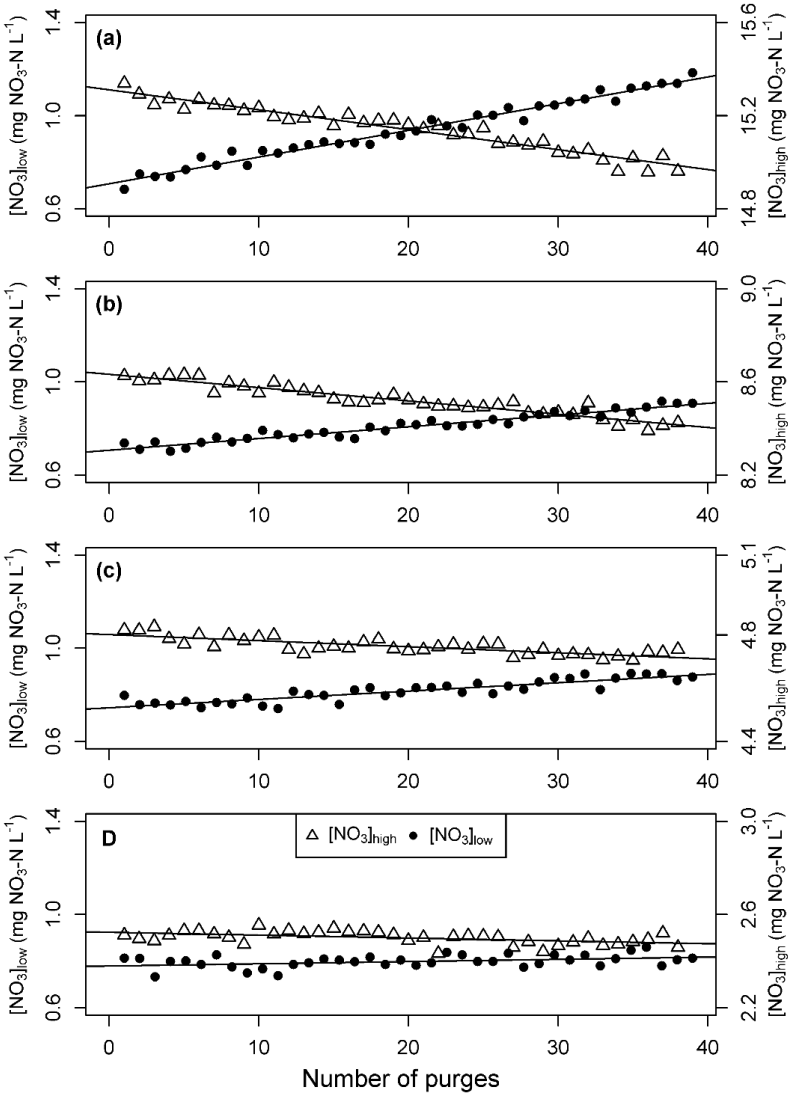

Figure 1-2. Changes in $[NO_3^-]$ in low ($[NO_3]_{low}$) and high ($[NO_3]_{high}$) concentration sources (0.5 L) resulting from residual volumes purged to the alternate source. Greater concentration or dilution effects were seen with increasing differences in initial NO_3^- concentrations of the sources during Trials (a) – (d).

Table 1-2. Initial NO_3^- concentrations, calculated effective residual volumes (V_{res}) and 95% confidence interval (C.I.) from source contamination Trials (a) – (d).

	$[NO_3]_{Low}$			$[NO_3]_{High}$		
Trial	Initial concentration (mg NO_3-N L^{-1})	V_{res} (mL)	95 % C.I. (mL)	Initial concentration (mg NO_3-N L^{-1})	V_{res} (mL)	95 % C.I. (mL)
(a)	0.71	0.41	(0.39, 0.43)	15.3	0.32	(0.29, 0.35)
(b)	0.71	0.35	(0.32, 0.38)	8.63	0.39	(0.34, 0.43)
(c)	0.74	0.46	(0.38, 0.55)	4.80	0.28	(0.21, 0.36)
(d)	0.78	0.30	(0.06, 0.52)	2.52	0.39	(0.15, 0.60)

Although this residual volume is significant, its effect depends on the application. When alternating between 3 and 5 mg NO_3-N L^{-1} of NO_3^- sources 50 L in volume, it would take 500 purges to source before a 0.01 mg NO_3-N L^{-1} change in the concentration would be detectable as a result of residuals purged to the alternate source. In the same situation with a 0.5 L source, only 5 purges would induce the same level of change. These results suggest that the 'purge to source configuration' should be used in short lived experiments and only in applications with a high source volume (>10 L), which would keep this artifact undetectable. For small-volume applications (e.g. porewater sampling) source contamination may be significant and the 'purge to waste' routine is recommended, rather than 'purge back to source'.

1.4.3. Pump time requirement results

Times required for a single sampling sequence (pumping and purging from source) for variable tube lengths was not linear with tubing length (data not shown), and best described using the following equation: $Time = 0.0001 \times length^2 + 0.0662 \times length + 79.4$, where *time* corresponds to the cumulative time in seconds required to pump and purge from the source to the cuvette, and *length* is the tube length from the source to the MPS in cm. From this equation, the time for a sampling sequence between consecutive sources was calculated with 60 s added to

account for cuvette rinsing for the spectrophotometer measurement time. For applications with sources up to 1, 4, and 9 m away from the MPS, time for one sample sequence would be 147, 182, and 280 s, respectively. The results suggest that roughly 30 min resolution water quality data can be obtained for up to 10 sources with sources up to 4 m away. The resolution would fall to 47 min for the same number of sources up to 9 m away.

1.5. Frequent porewater sampling in a woodchip bioreactor

Woodchip bioreactors, also called denitrification beds, are a popular agricultural conservation practice for the treatment of NO_3^- in subsurface drainage. These anaerobic systems provide woodchips as a carbon source and promote denitrification to remove NO_3^- from the aquatic environment. Soil pits typically ~1 m deep, ~5 m wide and ~25 m long are filled with woodchips through which drainage water percolates. Over twenty years of research on woodchip bioreactors has shown their potential to reduce NO_3^- concentrations, but has also shown troubling variability in reported treatment efficacy (e.g. 81% to 3%; David et. al 2016), or bioreactor volumetric removal rates (e.g., 2 to 22 g N m^{-3} d^{-1}, reviewed by Schipper et. al, 2010; 0.42 to 7.76 g N m^{-3} d^{-1}, Chistianson et. al, 2012). Variation in treatment performance has been attributed to various factors, including hydraulic residence time (HRT), temperature, influent concentration, and age (Addy et al., 2016; Hoover et al., 2016). An important part of the reported uncertainty and variability seems to be associated with measurement methods ill-suited to quantify NO_3^- fluxes into, within, and leaving bioreactors. Woodchip bioreactors are mostly treated as 'black box' systems.

There is evidence that internal hydraulic flowpaths and short-circuiting may result in overall treatment inefficiencies, although this has been inferred indirectly in field and lab experiments using tracers (Chistianson et al., 2013; Cameron & Schipper, 2011; Hoover et al., 2016). We report results from a preliminary experiment showing that the small volume MPS can help improve understanding of bioreactors as 'black box' systems.

1.5.1. Materials and methods

Nitrate dynamics were studied in a (1.20 x 1.20 x 0.45 m deep) lab bioreactor at North Carolina State University using the small volume MPS (Figure A-2 and A-3). This bioreactor is a lab-scale model of field bioreactors where inlet and outlet manifolds installed at opposite corners create

diagonal flow from the inlet at the top to the outlet at the bottom (Figure A-2). Eight sampling wells within the bioreactor woodchip media were monitored for NO_3^- concentrations using the small volume MPS. Sample wells were placed at shallow (S) or deep (D) zones (20.9 and 41.9 cm depth, respectively) and at 55.9 and 100.2 cm from the inlet along two longitudinal transects. Transects were located along the centerline and 21.6 cm from left sidewall (Figure A-2). Wells were made of stainless steel tubing (0.32 cm O.D.) with vertical slits cut at the tip to draw water into the well. Wells tips were covered with fine plankton netting (60 μm mesh) to prevent clogging of MPS tubing. Well names were assigned based on their location in the bioreactor. Wells S1 and S2 were shallow wells located near the inlet on the centerline and 21.6 cm from the sidewall, respectively. Wells S3 and S4 were shallow wells located near the outlet on the centerline and 21.6 cm from the sidewall, respectively. The same convention was used for deep wells D1 – D4.

For these experiments a dual sampling/analyzing system was used. The small volume MPS did not directly sample water from each well. Instead, to obtain synchronized NO_3^- concentrations in the bioreactor, all wells were sampled simultaneously using an 8 channel ISMATEC peristaltic pump triggered by the MPS Arduino board. The 8 channel pump simultaneously delivered sample volumes from each well to an intermediate manifold of eight 40 mL syringes. The small volume MPS was then used to sequentially pump water to the cuvette for analysis by the spectrophotometer. The probe was calibrated for NO_3^- using PLSR techniques described previously (Etheridge et al., 2014).

1.5.2. Small volume MPS reveals short-circuiting inside a woodchip bioreactor

In the first MPS application, we conducted a 76 h constant NO_3^- injection experiment from April 30 – May 4 2015 in a saturated bioreactor receiving 60 L h^{-1} tap water flow for a theoretical HRT of ~5.7 h. Nitrate from a concentrated KNO_3 stock solution was injected using a precision piston pump (Fluid Metering Inc. Model QBG, 1.2 g L^{-1}) for a target inflow NO_3^- concentration of 20 mg NO_3-N L^{-1}. The eight wells were sampled and analyzed every 40 min with the system described in Sec. 3.1. Ports 9 and 10 of the 12 port valve directly sampled the inlet and outlet weirs after consecutively analyzing sample volumes from each of the eight wells. In the first experiment, KNO_3 injection began at 8:10 AM on May 1 (14.2 h after MPS monitoring began, Figure 1-3). From 14.2 to 22.4 h NO_3^- concentrations were stable around 18.3 mg NO_3-N L^{-1}. After this period inlet concentrations rose until 37 h and was variable over the 76 h injection. Inlet NO_3^-

concentration ranged from 18.2 - 20.6 mg NO_3-N $L^{-1}$and varied by 12% of the target inlet concentration. Variability in inlet NO_3^- concentration was higher than anticipated due to degassing in the KNO_3 solution tank, with accumulation of air bubbles partially restricted flow through the piston pump.

Nitrate concentrations at the inlet rose quickly to 18.4 mg NO_3-N L^{-1} within 47 min of starting the KNO_3 injection (Figure 1-3). Inlet NO_3^- concentration likely passed 18 mg NO_3-N L^{-1} sooner, but the sampling time resolution of 47 min was insufficient to capture the exact time of the arrival. Three of the four wells nearest the inlet (S1, D1, and D2) showed nearly identical increases in NO_3^-, with concentrations at these wells passing 18 mg NO_3-N L^{-1} within 4.5 – 8.2 h of the injection. The shallow inlet well located along the side wall (S2) showed a noticeable lag, with NO_3^- staying below 18 mg NO_3-N L^{-1}until 19.7 h after the injection began. Nitrate concentrations at this well were significantly lower over the entire injection, relative to other wells near the inlet. All four inlet wells showed increases and decreases in NO_3^- concentrations that corresponded to changes in concentration at the inlet, although variability at S2 was much higher than the other three inlet wells. Nitrate concentrations in deep wells near the inlet closely followed one another during each sample interval, with an average difference of only 0.13 mg NO_3-N L^{-1}. Shallow wells near the inlet varied greatly with an average difference of 2.04 mg NO_3-N L^{-1}.

Four hours after injection NO_3^- was detected at the deep middle well near the outlet (D3), but outlet NO_3^-concentrations did not become stable until about 25 hours, or 5 times the theoretical HT of 5.7 hours. The very long lag for stabilization of NO_3^- concentrations at the outlet weir was likely due to the variability of injected NO_3^- to move through the bioreactor, as apparent from the 16.9, 17.5, and 21.2 h taken for S3, S4, and D3 to reach 18 mg NO_3-N L^{-1}.

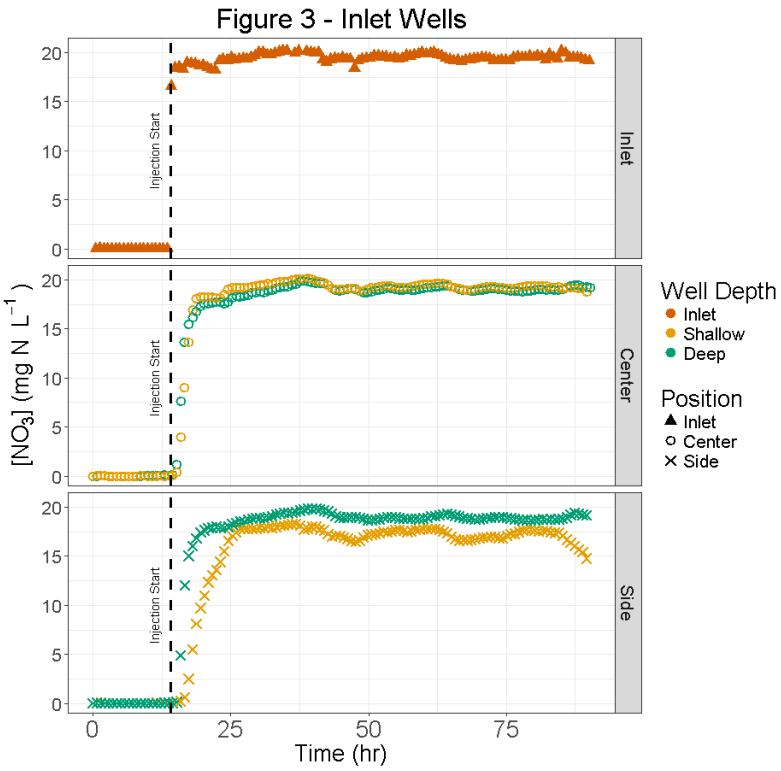

Figure 1-3. Nitrate concentration at inlet and wells near the inlet before and during the KNO_3 injection. Color indicates bioreactor inlet and depth of sampling wells, shape indicates the position of the well transect (centerline or near side wall).

Nitrate concentrations were significantly greater in deep wells relative to shallow wells at side wells near the inlet and at middle wells near the outlet. Shallow wells had higher NO_3^- concentration at side outlet wells and middle inlet wells. Variance in NO_3^- concentration was higher in shallow wells than deep wells at all four well pairs, illustrating that water moved quickly diagonally through the bioreactor and short-circuited most of the bioreactor volume. Lag and lower NO_3^- concentrations observed in the shallow wells (e.g., S2 and S4, Figure 1-4) suggest that areas further away from the direct diagonal flowpath may have slower hydraulic exchange and higher HRT (e.g., S2) and act as 'dead zones'.

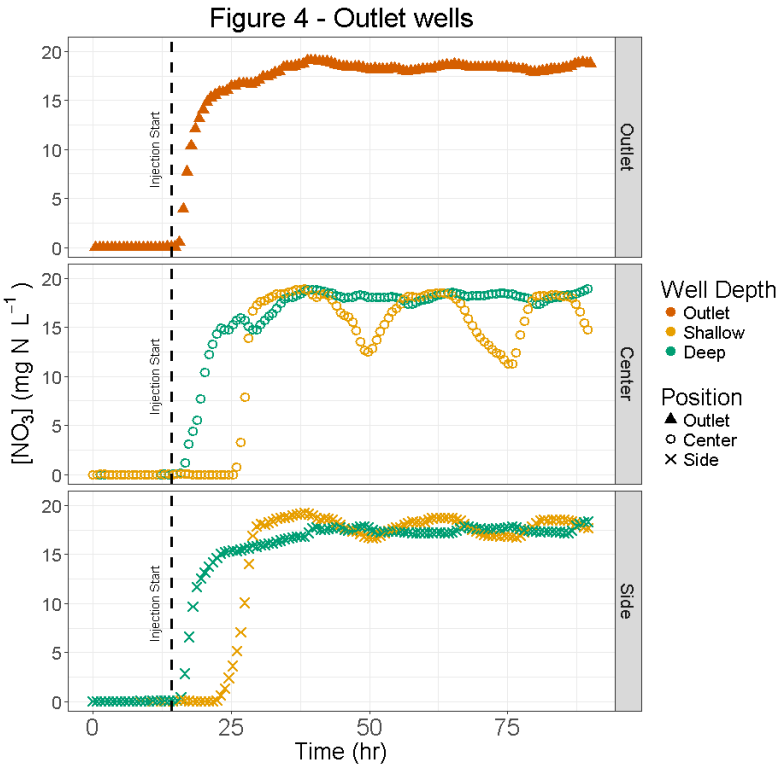

Figure 1-4. Nitrate concentration at outlet and wells near the outlet before and during the KNO_3 injection. Color indicates bioreactor outlet and depth of sampling wells, shape indicates the position of the well transect (centerline or near side wall).

To our knowledge, short-circuiting and 'dead zones' had never been observed directly but only inferred through high dispersion indices (MDI) shown in field reactors (Chistianson et al.; 2013) and in lab reactors (Hoover et al., 2016). Delayed time of arrival for NO_3^- at wells farther from the shortest flowpath indicate hydraulic inefficiencies, however several shallow wells also showed cyclic patterns in NO_3^- concentrations. Microbial and gas clogging has been documented and can be caused by creation of biofilm pore walls by microbial cells or fungi (Oberdorfer & Peterson, 1985; Okubo & Matsumoto, 1979; Vandivivere et al., 1995) or by extracellular polymers (Shaw et al., 1985; Vandevivere & Baveye, 1992). Gas clogging due to the accumulation of microbial-produced gas bubbles and influencing hydraulic conductivity in peat (Kellner et al., 2004; Beckwith & Baird, 2001) seems to explain some observed transient low conductivity (Kellner et al., 2004). These changes in hydraulic conductivity could explain the NO_3^- concentration fluctuations of the S2, S3, and S4wells, which exhibited regular decreases and increases of NO_3^- concentrations

1.5.3. Internal nitrate removal kinetics

In a second set of bioreactor experiments, NO_3^- reduction kinetics were measured at each well. The lab bioreactor was fully drained for a period of 24 hours. Following this drain event, the woodchips were re-saturated with the same KNO_3 spiked tap water made by the same method described in Sec. 3.2. Inflow NO_3^- concentration was 14 mg NO_3-N L^{-1} at 108 L h^{-1}. After pumping 4.5 pore volumes through the reactor, flow was stopped and the outlet weir raised to prevent any outflow. Each well was sampled every 3 h over 24 h during five trials from March 26 – April 12 using the MPS and 8 channel pump. Times series of NO_3^- concentrations at each well were fitted to zero order kinetics models (Eq. 1.1). Time series were fitted using the nls() function in R which calculates least-squares estimates for model parameters. In fitting the zero order model, only the concentrations after flow was stopped and above 2 mg NO_3-N L^{-1} were used. Other than both shallow outlet wells, NO_3^- concentrations at each well peaked at 12.5-13.5 mg NO_3-N L^{-1}after flow was stopped. Both shallow outlet wells had much lower peaks of 9.5-10.5 mg NO_3-N L^{-1}, consistent with observations in the first experiment that wells in this zone were slower to receive new water.

Over the five trials zero order NO_3^- removal rates ranged from 0.13 to 0.54 mg NO_3-N L^{-1} h^{-1} (Table 1-3). For this experimental bioreactor with a measured porosity of 0.59, this equates to a range of 1.84 – 7.65 g N m^{-3} d^{-1} (m^3 of reactor volume). Having access to eight points provided a range of removal rates and illustrated variability within the bioreactor. Spatial variability in the volumetric NO_3^- removal rates approached those reported across many field bioreactors (reviewed by Schipper et al., 2010). While there was high variability in NO_3^- removal rates within trials, there was no significant difference in mean values between wells when considering all five trials. The five lowest removal rates measured (Table 1-3) were in shallow outlet wells S3 and S4 (observed dead zones), and indicate that there may be a causality between NO_3^- removal rates and hydraulic inefficiencies or clogging.

Table 1-3. Zero order NO_3^- removal rates, *k*, at eight well locations during five experimental trials. Zero order kinetics model was fitted to time series of NO_3^- concentrations after flow was stopped to the lab bioreactor.

Well Location	Zero order, *k* (mg L^{-1} h^{-1})	R^2	RMSEP (mg L^{-1} h^{-1})
D1	0.25 – 0.43	0.96 – 0.99	0.002 – 0.003
D2	0.27 – 0.43	0.94 – 0.99	0.002 – 0.005
D3	0.29 – 0.38	0.84 – 0.99	0.002 – 0.010
D4	0.30 – 0.38	0.93 – 0.99	0.001 – 0.008
S1	0.30 – 0.44	0.93 – 0.99	0.002 – 0.008
S2	0.30 – 0.54	0.97 – 0.99	0.002 – 0.006
S3	0.15 – 0.34	0.88 – 0.98	0.003 – 0.006
S4	0.13 – 0.36	0.91 – 0.99	0.001 - 0.010

1.6. High frequency measurements in *in situ* stream mesocosms

Among the many methods used to measure NO_3^- removal kinetics in streams, the *in situ* mesocosm method is attractive as it involves minimal disturbance of the sediment, is effective for investigating spatial variability under field conditions, and can be performed at different times of the year (reviewed by Birgand et al., 2007). *In situ* mesocosms consist of open bottom containers inserted into the sediment which isolate water inside the mesocosm from the surrounding stream, making it possible to estimate process kinetics from changes in nutrient concentrations over time. Water recirculation is often applied to mimic ambient stream velocity.

The standard method consists in manual sample withdrawal several times (most often 4-7 times; reviewed by Birgand et al., 2007) over the duration of the experiment (typically <48 h). In laboratory mesocosms the volume of the water withdrawn is a minor issue as one can account for the mass of nutrients removed (e.g., Birgand et al., 2016; Messer et al., 2017). For *in situ* mesocosms water withdrawal is more significant as this water will, over time, be replaced by water upwelling from the sediment porewater. This discourages taking more samples during the experiment to reduce uncertainty in kinetics estimates. The inherent conflict between kinetics

uncertainties and porewater interference in *in situ* stream mesocosms can be solved with the small volume MPS used in the 'back to source' configuration (Fig 1(b)).

1.6.1. Materials and methods

To characterize NO_3^- removal kinetics of a stream prior to its restoration (Claridge Nursery, Goldsboro, NC; 35.4° N, 78.0° W), the small volume MPS was used with *in situ* mesocosms in two distinct sections of the reach to be restored. The upper reach of the ditch (1.6 km) has submerged vegetation and a thick muck sediment (20-30 cm depth) with high organic content (2-26% organic matter). The lower reach (0.6 km) has no instream vegetation and sandy sediment with low organic content (0.1-9.0 % organic matter). The upper and lower reaches are referred to as Muck and Sand, respectively.

In eleven 24 h experimental trials from August 2014 – March 2015, four mesocosms made of open bottomed barrels were gently inserted into the sediment down to approximately 10 cm within a 1 m radius of each other (Figure A-4). Each 57 cm diameter barrel inserted into the sediment are referred to as Sediment mesocosms and covered 0.26 m^2 of stream bottom. A fifth, closed bottom barrel (referred to as Control mesocosm) placed in the stream for temperature adjustment and containing only stream water served as a control, representing NO_3^- removal processes occurring in the water column. Water depth in Sediment mesocosms was measured manually. Recirculating DC pumps (3 L min^{-1}) were placed on the sidewall of the barrel (Figure A-5) and their flow was adjusted to mimic ambient stream velocity (0.02 – 0.10 m s^{-1}). Sample lines were placed near the recirculating pumps to obtain a well-mixed sample volume. Mesocosms were removed at the end of each experiment to allow hydrologic connection with the stream between trials. Four 24 h trials were completed at each Muck site and three trials performed at the downstream Sand site across four seasons.

At the beginning of each trial a 2 L solution of KNO_3 was added to each mesocosm to reach an initial NO_3^- concentration of 5-6 mg NO_3-N L^{-1}. The overlying water was gently stirred and left to equilibrate. The addition of the KNO_3 solution generating extra head inside the mesocosm helped prevent upwelling from groundwater (Solder et al., 2015) which might have otherwise occurred. Each sample volume pumped by the MPS temporarily withdrew ~25 mL of sample over <4 min,

corresponding to <0.1 mm drop in head, which we assumed was not high or long enough to generate significant upwelling.

Mesocosms were sampled every 36 min for 24 h using the small volume MPS. The measurement cuvette (1.1 mL, 4 mm path length) was rinsed with >10 times V_{res} to prevent cross contamination. Zero order, first order, and efficiency loss (EL) kinetics models accounting for water depth (D) (Equation 1.1-1.3) were fitted to the [NO_3^-] time series (~40-50 data points per mesocosm per trial) to 1) compare NO_3^- removal rates between sites and across seasons and 2) determine which model best predicted the observed data.

$$C_t = C_0 - \frac{\rho_{ZO}}{D} * t \qquad \text{(Equation 1.1)}$$

$$C_t = C_0 * e^{-\left(\frac{\rho_{FO}}{D} * t\right)} \qquad \text{(Equation 1.2)}$$

$$C_t = \left(\frac{\rho_{EL}{}^{(\alpha-1)}}{D} * t + C_0{}^{(1-\alpha)}\right)^{\left(\frac{1}{1-\alpha}\right)} \qquad \text{(Equation 1.3)}$$

Methods of model fitting and evaluation were the same as those presented in Section 1.5 (Messer et al.,2017; Birgand et al.,2016). The *nls* package in R Studio was used to fit observed data to a model predicting [NO_3^-] at time t, C_t, from estimates of initial concentration, C_0, depth-compensated removal constants (ρ_{ZO}, ρ_{FO}, ρ_{EL}), and the efficiency loss constant α. Commonly reported rate constant, k, was calculated by dividing ρ coefficients by depth, D.

1.6.2. Nitrate uptake kinetics

There was little preference between zero and first order models in the time series of decreasing [NO_3^-] (Table 1-4), with R^2 values for both models typically >0.95. Residuals of both models were nearly identical in most cases and differences in model R^2 were generally <0.01. All time series of decreasing [NO_3^-] from Sand trials showed better fit for zero order kinetics. Higher R^2 and improved residuals for a first order model, relative to a zero order model, were seen in trials with greater decreases in [NO_3^-] over the experiment. This was the case in Mar-18 and Aug-28 trials where net NO_3^- reduction in several mesocosms approached 2-3 mg NO_3-N L^{-1} over 24 h. The poorest model fitting occurred when fitting models to time series with little to no reduction in [NO_3^-], when total variability of [NO_3^-] was close to the precision of the spectrophotometer or

transient, short-term changes in [NO_3^-] were large relative to net reduction. The EL model was not useful in these short-term experiments.

Table 1-4. Time series of [NO_3^-] in Sediment mesocosms were fitted to zero and first order kinetics models. Results indicate that for the short duration experiment (<24 hr) and the observed range of [NO_3^-] (2-6 mg NO_3-N L^{-1}), removal was described equally well by either model, although first order kinetics better fitted NO_3^- time series during trials with large changes in [NO_3^-].

Trial Date (Sediment)	Zero-order, *k* mg NO_3-N m^{-2} d^{-1}	R^2	RMSEP mg NO_3-N m^{-2} d^{-1}	First-order, *k* m d^{-1}	R^2	RMSEP m d^{-1}
Aug. 28 (Muck)	500 - 580	0.99	30 - 60	0.15 - 0.17	0.99	0.02 - 0.05
Oct. 1 (Muck)	200 - 250	0.95 – 0.98	30 - 60	0.06 – 0.07	0.95 – 0.98	0.03 – 0.05
Nov. 6 (Muck)	140 - 260	0.93 – 0.98	40 - 70	0.04 – 0.07	0.93 – 0.98	0.03 – 0.06
Nov. 13 (Muck)	160 - 200	0.89 – 0.98	20 - 60	0.05 – 0.06	0.89 – 0.98	0.02 – 0.06
Jan. 29 (Muck)	-40 - 180	0.00 – 0.93	10 - 40	0.00 – 0.05	0.00 – 0.93	0.00 – 0.04
Feb. 3 (Muck)	40 - 120	0.76 – 0.99	20 - 30	0.01 – 0.04	0.76 – 0.99	0.02 – 0.03
Mar. 11 (Muck)	180 - 320	0.93 – 0.99	20 - 40	0.04 – 0.09	0.92 – 0.99	0.02 – 0.04
Mar 18 (Muck)	90 - 300	0.97 – 0.99	20 - 60	0.03 – 0.13	0.97 – 0.99	0.02 – 0.05
Sep 18 (Sand)	10 - 110	0.10 – 0.86	20 - 50	0.00 – 0.03	0.10 – 0.85	0.02 – 0.05
Dec 17 (Sand)	140 - 240	0.97 – 0.98	20 - 30	0.03 – 0.06	0.96 – 0.98	0.02 – 0.03
Mar 16 (Sand)	20 - 50	0.63 – 0.84	20 - 30	0.01 – 0.02	0.63 – 0.86	0.02 – 0.03

These results are somewhat contradictory to results obtained in lab wetland mesocosms of similar size where data were not well-fitted by a zero order model and where the EL model was performed best (Birgand et al., 2016). It is possible that the experiments were not long enough for [NO_3^-] to decrease enough for differences to appear among models, or for first order and EL kinetics to be apparent. In these *in situ* experiments, the results suggest that NO_3^- removal kinetics at the diurnal scale in nutrient-rich streams were adequately predicted by zero order models. In Muck trials, ρ values ranged from 10 – 580 mg NO_3-N m^{-2} d^{-1} (Table 1-4). Removal rates in Sand mesocosms were much lower, ranging from 10 – 240 mg NO_3-N m^{-2} d^{-1}. The results show that for NO_3^- removal rates less than 300 mg N m^{-2} L^{-1}, the zero order rate model was sufficient to fit the data, but the first order model appeared better for higher NO_3^- removal rates generally found in agricultural streams (350 and 1,250 mg N m^{-2} d^{-1}; Birgand et al., 2007).

1.6.3. Seasonal and spatial variability

In Muck trials NO_3^- removal rates followed a predictable seasonal pattern with removal rates highest in the month of August, decreasing in October and November trials, lowest during the winter months, and increasing again during March. This is consistent with observations that the rates of microbial processes increase with temperature. Nitrate removal rates during the Aug-18 trial (25 °C) were 4-14 times greater than those during Feb-3 (8 °C) at the same site. The opposite trend was seen among Sand trials. The Dec-17 trial with the coldest temperatures among Sand trials (10 °C) showed the highest NO_3^- removal rates. A seasonal influx of available carbon was likely the cause of this trend. Accumulated leaf packs at the Sand site, included in the Dec-17 mesocosms, provided available carbon and substrate for denitrification to occur. Nitrate removal rates during this trial were even higher than rates in Muck trials with similar temperature (Jan-29 and Feb-3).

The *in situ* mesocosm method revealed high variability in NO_3^- removal rates within trials, even when mesocosms were within a 1 m radius. High variability in Muck trials in the month of March was caused by the presence of emergent vegetation along the stream bank (Figure A-6). In Mar-11 and Mar-18 trials, mesocosms placed in this near-bank vegetated zone showed removal rates 48-81% and 74-240% higher than those in mesocosms placed in the unvegetated stream center, respectively. In the Jan-29 trial, a single mesocosm showed removal rates 300-2500% higher than

the other Sediment mesocosms. Muck trials had a higher degree of within-trial variability relative to Sand, indicating that sediment NO_3^- removal potential at the Sand site was more homogenous.

1.7. Conclusions

The first report of the MPS illustrated the ability of this technology to increase temporal and spatial resolution of water quality data (Birgand et al., 2016). The small volume MPS increases the number of potential applications for this method by significantly decreasing sample volume. The small volume MPS minimized the volume of the flow-through measurement cell (1.1 mL quartz cuvette), contrasting with the 40 mL flow-through cell used previously. In order to prevent cross contamination of samples caused by pumping from different sources, an adequate pre-measurement rinse with the current sample volume must be used. For the larger volume MPS this would require pumping roughly 36 times more volume past the flow-through cell for adequate rinsing. In the stream mesocosms, removing 25 mL of sample for <4 min to measure absorbance resulted in temporary head drop <0.1 mm and minimized sample withdrawal to allow 40-50 NO_3^- measurements to be made over 24 h without significantly affecting mesocosm hydraulics.

The small volume MPS allows continuous multi-point sampling to be extended to applications where sample volume is limited or must be minimized. The most obvious application is for porewater sampling, where sample withdrawal rate should not exceed the rate at which water moves through the medium. Total volume extracted must also be small to avoid significantly affecting the observed environment. Drainable porosity in soils is much less than the total volume of soil, leading to a zone of influence which size depends on the total sample volume extracted and the drainable porosity. For example, sampling every 1 or 6 h over 24 h from a soil with a 0.1 drainable porosity, this zone of influence (assuming 15 mL required sample volume for the small volume MPS) would be 3600 and 600 cm^3, respectively. Assuming this zone is spherical, it would have a diameter of 19 and 10 cm, which is not insignificant. Sampling interval should be short enough to adequately capture temporal variation while avoiding excessive water withdrawal to avoid interdependence between sampling points that are hydraulically connected. When removal kinetics were measured in the lab bioreactor during stopped flow, a sample interval of 3 h was used over 24 h. With an observed drainable porosity of 0.58, the zone of influence at each of the eight points was 7.3 cm and accounted for 0.4% of water in the bioreactor. Sampling wells were no closer than 21 cm, so an assumption of independence between sampling points was reasonable.

The small volume MPS was able to observe for the first time short-circuiting in a woodchip bioreactor which had been surmised in the literature although never fully shown. We were also able to measure NO_3^- removal rates at multiple locations within the bioreactor. The application of the MPS in stream mesocosms opened the possibility to measure NO_3^- removal kinetics *in situ* in replicated experiments by eliminating potential contamination by groundwater. The small-volume MPS has high potential for providing quality data sets for improving new and existing solute transport models for saturated or partially saturated soils and opens the possibility to be used in replicated experiments.

Due to the small diameter of the fittings and tubing in this system, several pumping concerns are magnified compared to the large volume MPS. Water micro-droplets or residuals in the tubing lines are more susceptible to freezing and caution should be used when deploying this system under freezing conditions. Valves and tubing are also more susceptible to clogging. In both applications a plankton net fabric (60 μm mesh) was used and no clogging occurred, even in the case of the woodchip bioreactor application with high dissolved organic matter. The small sample volume potentially limits the number of sondes and sensors to which the MPS can be coupled. The design of the s::can spectrophotometer allows for such a small volume flow-through measurement cell to be used, while other available water quality sensors typically require much larger sample volumes for which this system might not be well-suited. The volume-limited applications presented include sampling an overlying water column and porewater in coarse woodchips. Porewater sampling in fine soils or sediments may be more restrictive and will result in a larger sphere of influence around the sampling point. While the minimum volume required for measurement using the MPS is small (~7 mL) and comparable to other small volume sediment samplers (e.g. Rhizon *in situ* samplers, Seeberg-Elverfeldt et al., 2005), bi-directional pumping from multiple sources by the MPS requires closer to 10-15 mL to reduce cross contamination for accurate solute measurement. Sampling of fine soils with low hydraulic conductivity using the MPS can be aided by the use of small diameter sampling wells.

1.8. References

Beckwith, C. W., & Baird, A. J. (2001). Effect of biogenic gas bubbles on water flow through poorly decomposed blanket peat. *Water Resources Research, 37*(3), 551-558.

Birgand, F., Aveni-Deforge, K., Smith, B., Maxwell, B., Horstman, M., Gerling, A. B., et al. (2016). First report of a novel multiplexer pumping system coupled to a water quality probe to collect high temporal frequency in situ water chemistry measurements at multiple sites. *Limnology and Oceanography: Methods, 14*(12), 767-783.

Birgand, F., Skaggs, R. W., Chescheir, G. M., & Gilliam, J. W. (2007). Nitrogen removal in streams of agricultural catchments—a literature review. *Critical Reviews in Environmental Science and Technology, 37*(5), 381-487.

Cameron, S. G., & Schipper, L. A. (2011). Evaluation of passive solar heating and alternative flow regimes on nitrate removal in denitrification beds. *Ecological Engineering, 37*(8), 1195-1204.

Christianson, L. E., Bhandari, A., Helmers, M. J., Kult, K. J., Sutphin, T., & Wolf, R. (2012). Performance evaluation of four field-scale agricultural drainage denitrification bioreactors in iowa. *Transactions of the ASABE, 55*(6), 2163.

Christianson, L., Helmers, M., Bhandari, A., & Moorman, T. (2013). Internal hydraulics of an agricultural drainage denitrification bioreactor. *Ecological Engineering, 52*, 298-307.

Crumpton, W. G., Isenhart, T. M., & Mitchell, P. D. (1992). Nitrate and organic N analyses with second-derivative spectroscopy. *Limnology and Oceanography, 37*(4), 907-913.

David, M. B., Gentry, L. E., Cooke, R. A., & Herbstritt, S. M. (2016). Temperature and substrate control woodchip bioreactor performance in reducing tile nitrate loads in east-central illinois. *Journal of Environmental Quality, 45*(3), 822-829.

Dent, C. L., & Grimm, N. B. (1999). Spatial heterogeneity of stream water nutrient concentrations over successional time. *Ecology, 80*(7), 2283-2298.

Etheridge, J. R., Birgand, F., Osborne, J. A., Osburn, C. L., Burchell, M. R., & Irving, J. (2014). Using in situ ultraviolet-visual spectroscopy to measure nitrogen, carbon, phosphorus, and suspended solids concentrations at a high frequency in a brackish tidal marsh. *Limnology and Oceanography: Methods, 12*(1), 10-22.

Finch, M. S., Hydes, D. J., Clayson, C. H., Weigl, B., Dakin, J., & Gwilliam, P. (1998). A low power ultra violet spectrophotometer for measurement of nitrate in seawater: Introduction, calibration and initial sea trials. *Analytica Chimica Acta, 377*(2), 167-177.

Johnson, K. S., & Coletti, L. J. (2002). In situ ultraviolet spectrophotometry for high resolution and long-term monitoring of nitrate, bromide and bisulfide in the ocean. *Deep Sea Research Part I: Oceanographic Research Papers, 49*(7), 1291-1305.

Kahlert, M., Hasselrot, A. T., Hillebrand, H., & Pettersson, K. (2002). Spatial and temporal variation in the biomass and nutrient status of epilithic algae in lake erken, sweden. *Freshwater Biology, 47*(7), 1191-1215.

Kellner, E., Price, J. S., & Waddington, J. (2004). Pressure variations in peat as a result of gas bubble dynamics. *Hydrological Processes, 18*(13), 2599-2605.

McClain, M. E., Boyer, E. W., Dent, C. L., Gergel, S. E., Grimm, N. B., Groffman, P. M., et al. (2003). Biogeochemical hot spots and hot moments at the interface of terrestrial and aquatic ecosystems. *Ecosystems, 6*(4), 301-312.

Merill, L., & Tonjes, D. J. (2014). A review of the hyporheic zone, stream restoration, and means to enhance denitrification. *Critical Reviews in Environmental Science and Technology, 44*(21), 2337-2379.

Messer, T. L., Burchell II, M. R., Birgand, F., Broome, S. W., & Chescheir, G. (2017). Nitrate removal potential of restored wetlands loaded with agricultural drainage water: A mesocosm scale experimental approach. *Ecological Engineering, 106*, 541-554.

Oberdorfer, J. A., & Peterson, F. L. (1985). Waste-water injection: Geochemical and biogeochemical clogging processes. *Groundwater, 23*(6), 753-761.

Okubo, T., & Matsumoto, J. (1979). Effect of infiltration rate on biological clogging and water quality changes during artificial recharge. *Water Resources Research, 15*(6), 1536-1542.

Parkin, T. B. (1987). Soil microsites as a source of denitrification variability. *Soil Science Society of America Journal, 51*(5), 1194-1199.

Rieger, L., Langergraber, G., & Siegrist, H. (2006). Uncertainties of spectral in situ measurements in wastewater using different calibration approaches. *Water Science and Technology, 53*(12), 187-197.

Rochelle-Newall, E., & Fisher, T. (2002). Chromophoric dissolved organic matter and dissolved organic carbon in chesapeake bay. *Marine Chemistry, 77*(1), 23-41.

Saraceno, J. F., Pellerin, B. A., Downing, B. D., Boss, E., Bachand, P. A., & Bergamaschi, B. A. (2009). High-frequency in situ optical measurements during a storm event: Assessing relationships between dissolved organic matter, sediment concentrations, and hydrologic processes. *Journal of Geophysical Research: Biogeosciences, 114*(G4)

Schipper, L. A., Robertson, W. D., Gold, A. J., Jaynes, D. B., & Cameron, S. C. (2010). Denitrifying bioreactors—an approach for reducing nitrate loads to receiving waters. *Ecological Engineering, 36*(11), 1532-1543.

Seeberg-Elverfeldt, J., Schlüter, M., Feseker, T., & Kölling, M. (2005). Rhizon sampling of porewaters near the sediment-water interface of aquatic systems. *Limnology and Oceanography: Methods, 3*(8), 361-371.

Shaw, J. C., Bramhill, B., Wardlaw, N. C., & Costerton, J. W. (1985). Bacterial fouling in a model core system. *Applied and Environmental Microbiology, 49*(3), 693-701.

Solder, J. E., Gilmore, T. E., Genereux, D. P., & Solomon, D. K. (2016). A tube seepage meter for in situ measurement of seepage rate and groundwater sampling. *Groundwater, 54*(4), 588-595.

Suzuki, N., & Kuroda, R. (1987). Direct simultaneous determination of nitrate and nitrite by ultraviolet second-derivative spectrophotometry. *Analyst, 112*(7), 1077-1079.

Torres, A., & Bertrand-Krajewski, J. (2008). Partial least squares local calibration of a UV–visible spectrometer used for in situ measurements of COD and TSS concentrations in urban drainage systems. *Water Science and Technology, 57*(4), 581-588.

Vandevivere, P., Baveye, P., Lozada, D. S., & DeLeo, P. (1995). Microbial clogging of saturated soils and aquifer materials: Evaluation of mathematical models. *Water Resources Research, 31*(9), 2173-2180.

Vandevivere, P., & Baveye, P. (1992). Effect of bacterial extracellular polymers on the saturated hydraulic conductivity of sand columns. *Applied and Environmental Microbiology, 58*(5), 1690-1698.

Vidon, P., Allan, C., Burns, D., Duval, T. P., Gurwick, N., Inamdar, S., et al. (2010). Hot spots and hot moments in riparian zones: Potential for improved water quality management. *JAWRA Journal of the American Water Resources Association, 46*(2), 278-298.

A Small-volume Multiplexed Pumping System for Automated, High-frequency Water Chemistry Measurements in Volume-limited Applications. Maxwell, B. M., Birgand, F., Smith, B., & Aveni-Deforge, K. (2018). *Hydrology and Earth System Sciences, 22*(11), 5615-5628.

Role in Authorship of Paper : Primary author and contributor of research described herein.

Hydrol. Earth Syst. Sci., 22, 5615–5628, 2018
https://doi.org/10.5194/hess-22-5615-2018

Hydrology and Earth System Sciences
Open Access
EGU

A small-volume multiplexed pumping system for automated, high-frequency water chemistry measurements in volume-limited applications

Bryan M. Maxwell[1], **François Birgand**[1], **Brad Smith**[2], **and Kyle Aveni-Deforge**[1]

[1]Biological and Agricultural Engineering, North Carolina State University, 3110 Faucette Drive, Raleigh, 27695, USA
[2]Sungate Design Group, 905 Jones Franklin Road, Raleigh, 27606, USA

Correspondence: Bryan M. Maxwell (bmmaxwel@ncsu.edu)

Received: 23 April 2018 – Discussion started: 31 May 2018
Revised: 26 September 2018 – Accepted: 9 October 2018 – Published: 30 October 2018

Abstract. An automated multiplexed pumping system (MPS) for high-frequency water chemistry measurements at multiple locations previously showed the ability to increase spatial and temporal data resolution and improve understanding of biogeochemical processes in aquatic environments and at the land–water interface. The design of the previous system precludes its use in volume-limited applications in which highly frequent measurements requiring a large sample volume would significantly affect observed processes. A small-volume MPS was designed to minimize the sample volume while still providing high-frequency data. The system was tested for cross-contamination between multiple sources, and two applications of the technology are reported. Cross-contamination from multiple sources was shown to be negligible when using recommended procedures. Short-circuiting of flow in a bioreactor was directly observed using high-frequency porewater sampling in a well network, and the small-volume MPS showed high seasonal and spatial variability of nitrate removal in stream sediments, enhancing data collected from in situ mesocosms. The results show it is possible to obtain high-frequency data in volume-limited applications. The technology is most promising at the reach or transect scale for observing porewater solute dynamics over daily timescales, with data intervals < 1 h for up to 12 locations.

1 Advancements in high-frequency water quality monitoring

Recent UV–VIS field spectrometers provide an opportunity for high-frequency in situ monitoring to increase the temporal resolution of water quality data. Water quality has been measured with these instruments by correlating absorbance with chemical concentration (Crumpton et al., 1992; Suzuki and Kuroda, 1987; Finch et al., 1998; Johnson and Coletti, 2002; Rochelle-Newall and Fisher, 2002; Saraceno et al., 2009). Rieger et al. (2006) and Torres and Bertrand-Krajewski (2008) measured total suspended solids (TSS) in wastewaters using partial least-squares regression (PLSR) to correlate absorbance fingerprints to concentrations. Etheridge et al. (2014) expanded the technique to measure light- and non-absorbing constituents including PO_4^{3-}, total phosphorus, nitrate (NO_3^-), total Kjeldahl nitrogen, TSS, dissolved organic carbon, and salinity in a brackish North Carolina marsh. Birgand et al. (2016) have shown that the technique might also be used to measure iron and silica in lakes and reservoirs.

Among the spatial heterogeneity of biological and chemical processes in the environment (Merill and Tonjes, 2014; Kahlert et al., 2002; Dent and Grimm, 1999; Parkin, 1987), patches referred to as "hotspots" are particularly interesting (e.g., riparian buffers, hyporheic zones). These hotspots have been observed to have a disproportionate impact on biogeochemical cycles, and can be particularly active over short periods of time referred to as "hot moments" (McClain et al., 2003; Vidon et al., 2010). While temporal resolution has and will provide invaluable information at a particular moni-

Published by Copernicus Publications on behalf of the European Geosciences Union.

toring station (e.g., Etheridge et al., 2014), expanding resolution to spatial data could illuminate tightly coupled processes and would greatly magnify the value of these instruments. Documenting the short-term fate of reactive nutrients within identified hotspots might provide new insight into nutrient cycles and their controlling factors.

An automated large volume multiplexed pumping system (MPS) capable of pumping water from up to 12 sources to a UV–VIS spectrophotometer was previously reported (Birgand et al., 2016). The MPS is a "multiplexed" system in that it delivers sample volumes from separate sources to a single probe used to consecutively observe water chemistry at all sources. The 3.18 mm inside diameter (i.d.) tubing yields an average volume of 100 mL of water per sample, which is very well adapted when the source can easily accommodate such withdrawal without consequences for the source or the processes studied. Certain applications, however, may require minimizing sample withdrawal to avoid disturbing the observed process while still obtaining high-frequency data. Observing solute dynamics in soils or sediments, particularly those with low drainable porosity, is one such example of a volume-limited application.

In this article, we are reporting the capabilities offered by a small-volume MPS coupled with a field spectrophotometer to obtain high-resolution water quality data in both time and space. This system can accommodate small volumes (< 15 mL) from up to 12 different sources located within a 10 m distance of the instrument and provide absorbance measurements at better than hourly intervals at each location. This system was designed to minimize inline volumes for volume-limited applications. This article describes the instrument and the challenges involved, evaluates its performance, and reports two applications of this system in such volume-limited conditions.

2 Small-volume multiplexed pumping system

The principle followed for this instrument is to use a portable spectrophotometer as a central portable laboratory, coupled with the MPS able to sequentially pump water from several points within a reasonable distance of the probe. The small-volume MPS is designed for high-frequency sampling in volume-limited applications. The solution to minimizing sample volume is small-diameter tubing and a low-volume flow-through measurement cell. The challenges of this design include clogging of tubing and high head losses due to surface tension forces in the tubing. The latter implies higher pump suction and tends to generate sample residuals left after purging along the length of the tubing, increasing the potential for cross-contamination between samples. This drawback demands specific evaluation of the small-volume MPS before use.

2.1 System design and hardware

The major components of the system include (1) a UV–VIS spectrophotometer fitted with a flow-through cuvette, (2) a bidirectional peristaltic pump, (3) small-diameter polytetrafluoroethylene (PTFE or Teflon) tubing, (4) an Arduino control board (Arduino), (5) a 12-port valve, (6) a three-way valve manifold, and (7) an optional fractional volume collector.

The general automated "sampling sequence" for the system starts with pumping from source n to a flow-through spectrophotometer cuvette via 0.9 mm i.d. PFTE tubing and a peristaltic pump. After the water has entered the cuvette the spectrophotometer takes a measurement and water is then purged back either to the source, to a fractional volume collector, or to waste using a three-way valve manifold. The multi-port valve then selects source $n+1$, and a similar sampling sequence takes place. Up to 12 sampling sequences corresponding to the 12 ports of the multi-port valve can occur during a "sampling cycle". A fractional volume collector can be used to collect selected sample volumes so that readings by the spectrophotometer can be compared to lab-measured concentrations.

Control of the MPS pumping, purging, valve actuation, and activity logging is performed by an Arduino Mega 53 pin control chip (Arduino, www.arduino.cc). This inexpensive control board utilizes open-source software for easy-to-use programming and hardware interfacing, although other similar board/microprocessors can be used. The high-frequency water quality probe used is a UV–VIS field spectrophotometer Spectro::Lyser™ by s::can™ fitted with a 4 mm path length, 1.1 mL flow-through quartz cuvette (Starna Cells, Inc. model 46-Q-4) placed vertically to facilitate cuvette drainage by gravity during purging. The water quality probe is used as a "master" instrument to dictate to the MPS "slave" system when to begin a sampling sequence. We use an existing capability of the spectrophotometer to send a 12 V signal at an adjustable time prior to a measurement as a trigger for the MPS, although any other triggering method (e.g., time-based using the Arduino control board) could be used.

A peristaltic pump provides pumping and purging at 20 mL min^{-1} flow rate acceptable for the 0.9 mm I.D. tubing used. A MOSFET H bridge controlled by the Arduino reverses DC polarity at the pump to alternate between pumping and purging. The 12-port valve used is a low-pressure Cheminert™ 12-position valve from Valco Instruments. The multi-port valve advances to the next desired port using a pneumatic actuator powered by compressed air (bottle or 12 V compressor). Although the valve advances through ports sequentially, the user can select the ports to use with the Arduino controller. Three Arduino-controlled three-way solenoid valves (Takasago MTV series) are used for different sampling and purging configurations (Sect. 2.2). The Arduino board is fitted with an SD card reader/writer for activity logging, an RTC clock for timekeeping, an LCD panel

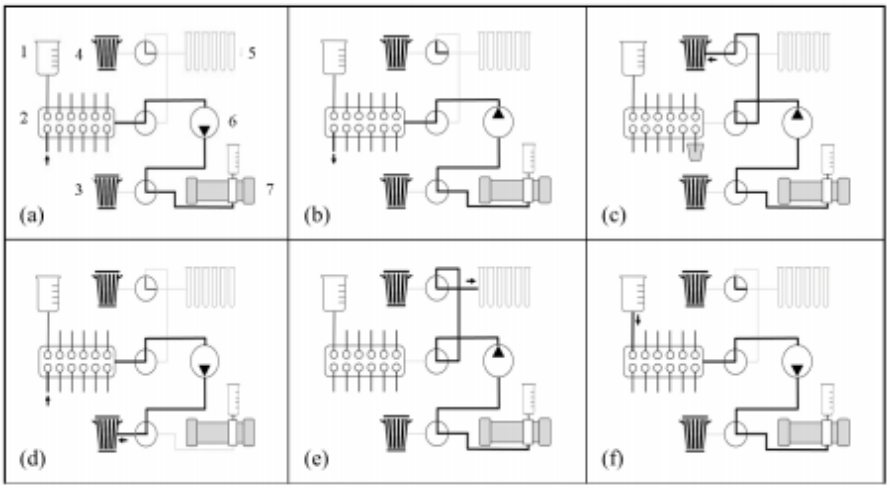

Figure 1. Graphical depiction of small-volume multiplexed pumping system (MPS) configurations which include (1) DI water source, (2) 12-port intake valve, (3, 4) waste or air purge, (5) fractional volume collector (FVC), (6) bidirectional peristaltic pump, and (7) spectrophotometer with cuvette housing. An Arduino microcontroller actuates a series of three-way valves to move between separate configurations **(a–f)** described in Sects. 2.2.1–2.2.5.

for system output display, and operable switches for manual control.

The system has been designed for unattended operation for long periods of time (e.g., days or weeks), although it is limited by the spectrometer data storage, fouling of the cuvette, and battery power (and sample storage of the fractional volume collector if used). The time for a sampling sequence is limited by the longest pumping time from furthest source. Ultimately this determines the frequency of spectrometer measurements since the probe has a set time interval between measurements. The sampling frequency for each source depends on the sampling sequence time intervals and on the number of sources (1 to 12).

2.2 System configurations

Several configurations have been programmed to increase versatility of the instrument and minimize cross-contamination between samples (Fig. 1) by actuating one or more of the three-way valves using the Arduino control board.

2.2.1 Pumping from source to probe and purging back to source

When it is necessary to purge all sample volume back to the source, the system is configured as Fig. 1a during pumping (downward arrow on the peristaltic pump) and as Fig. 1b during purging (upward arrow on the peristaltic pump). To measure absorbance in the 1.1 mL cuvette used, a minimum sample volume of ~ 7 mL is required, which includes cuvette volume (V_{cuvette}) plus inline tubing volume. The system is purged by air by running the pump in reverse. To minimize cross-contamination without using a deionized (DI) rinse, the cuvette can be rinsed by pumping sample volume > 7 mL temporarily stored in the post-cuvette storage volume.

2.2.2 Purge to waste

In this configuration, it is not desired that the sample be purged to the source, so it is purged to waste (Fig. 1c).

2.2.3 Pump to waste

This configuration is used for purging residuals of the sample drawn from the previous source $n-1$ that remain in the tubing and rinsing with sample volume from the current source n (Fig. 1d). After the estimated time for new water from the current source to reach the waste valve has elapsed, the system switches to the configuration in Fig. 1a for sample measurement by probe.

2.2.4 Fractional volume collection

This configuration is used for collecting measured sample volumes to compare values given by the probe to later lab analysis (Fig. 1e). The actual sequence consists in purging the fractional volume collector (FVC) tubing with air using Fig. 1e configuration but in the pumping mode (downward

arrow on the peristaltic pump, not shown) until water has passed the three-way valve closest to the FVC, then use the Fig. 1c configuration to purge any cross-contaminated water to waste before samples are sent to the FVC using the configuration in Fig. 1e. Any water left in tubing after the FVC sample vial is full is purged to waste.

2.2.5 DI water rinse

Between each sample, the user may choose to rinse the tubing and cuvette with DI water to create consistent cross-contamination between samples and residual DI water droplets (Fig. 1f). This configuration draws water in from a DI water source and pumps it through the lines and into the cuvette. Consistent cleaning of the quartz cuvette decreases optical fouling over time. The cuvette and post-cuvette storage volume are rinsed and the water is then purged to waste.

2.3 System testing

In laboratory continuous flow systems, the risk for cross-contamination between consecutive samples is mechanically minimized by having unidirectional flow and by rinsing the lines with a carrier liquid between samples. Our system has been designed to allow for bidirectional flow, purging the lines instead with air. Because of surface tension forces purging with air can leave micro-droplet residuals in the lines, opening the possibility for cross-contamination between consecutive samples. This is particularly problematic since sample volumes needed for analysis each time are small by design. Although this is admittedly undesirable, this can still be acceptable as long as the potential for contamination is evaluated and solutions to minimize the risks are known. Potential solutions for minimizing cross-contamination include a pre-measurement rinse with the current source water or extended purging of the lines with air after each measurement.

Cross-contamination could arise from two processes. First, cuvette contamination could occur when a water sample inside the cuvette during instrument reading is contaminated by droplets from the previous sample, either in the cuvette or in the MPS tubing. Second, cross-contamination of the source, or source contamination, could occur when the "purging back to source" configuration is used (Fig. 1b) and the source itself is contaminated by residuals from other sources. Both contamination possibilities were evaluated in two separate experiments. A third test of performance quantified the relationship between sampling frequency and the distance from the source to the system, since increased pumping time for a sampling sequence leads to lower data frequency.

Methods for evaluating cuvette contamination and source contamination were identical to those used in Birgand et al. (2016). Alternating measurements between sources of high and low NO_3^- concentration ($[NO_3]_{high}$ and $[NO_3]_{low}$, respectively) were used to determine contamination. The spectrophotometer's estimates of NO_3^- based on the absorbance fingerprint (method detailed further in the Supplement) were used to quantify contamination. The primary difference in testing the small-volume MPS for contamination between sources was the size of the flow-through cell. In this system a 1.1 mL flow-through quartz cuvette was used. In addition to testing cross-contamination when rinsing with sample volume from the current source, a DI rinse was tested to see if it resulted in decreased contamination by residuals.

For testing pump timings, external tubes of various lengths were cut and fitted to the inlet port of the system. The length of time required to pump from the source to fill the cuvette and the time required to purge the line were recorded. Pump times for each tube length were measured twice with use of a stopwatch, and average pump time was recorded.

2.3.1 Cross-contamination results

The cross-contamination trial results are summarized in Table 1. The first two columns report p values testing for a significant difference ($\alpha = 0.05$) between spectrophotometric estimates of NO_3^- concentration in the source (10 repeated measurements) and subsequent 10 measurements after pumping sample volume from the alternate NO_3^- source between each measurement (i.e., if $p > 0.05$, there was no statistical difference between initial and subsequent measurements for NO_3^-, implying negligible cross-contamination). The results show that without a DI rinse and when measuring high-concentration samples after low-concentration samples, the cuvette must be rinsed with the current sample by at least $10 \times V_{cuvette}$ to make cuvette contamination by the previous sample negligible. With only rinsing $2 \times V_{cuvette}$, concentrations were underestimated at about 13.25 mg NO_3–N L^{-1}, lower than the $[NO_3]_{high} = 14.72$ mg NO_3–N L^{-1} reference. Cross-contamination was divided by 10 by rinsing with $4 \times V_{cuvette}$, but was still measurable and significant.

For the low-concentration samples measured after high concentrations, rinsing $10 \times V_{cuvette}$ could not fully eliminate cross-contamination as it still appeared to be significant, yielding readings around 0.14 mg NO_3–N L^{-1} instead of the initial 0.06 mg NO_3–N L^{-1}. Adding a DI rinse appeared to eliminate cross-contamination for $[NO_3]_{low}$ by rinsing with $10 \times V_{cuvette}$ (< 0.01 mg L^{-1} difference), but the same treatment significantly diluted $[NO_3]_{high}$.

These results suggest that there is not one solution to fully eliminate cross-contamination when consecutive samples differ drastically in solute concentration. These results were obtained for extreme changes of conditions for which consecutive concentrations were roughly 150-fold different. For applications in which this ratio may be common between consecutive samples, rinsing with $> 10 \times V_{cuvette}$ is recommended and values for lower concentration should be taken with caution. For most applications, however, such ratios between consecutive concentrations are unlikely. For ratios of 50, 10, and 5 (i.e 0.50 to 25.0, 0.5 to 5.0, and 0.5 to 2.5 mg NO_3–N L^{-1}), the differences in mean con-

Table 1. Results of testing cross-contamination of cuvette. Treatment indicates the volume of sample pumped from the current source for cuvette rinsing relative to cuvette volume ($V_{cuvette}$), and whether or not a prior DI rinse was used. C.I. denotes the confidence interval.

Trial no.	Treatment	Initial concentrations ($mg\,NO_3{-}N\,L^{-1}$)		p value for difference in means of		95 % C.I. for difference in means ($mg\,NO_3{-}N\,L^{-1}$)	
		$[NO_3]_{High}$	$[NO_3]_{Low}$	$[NO_3]_{High}$	$[NO_3]_{Low}$	$[NO_3]_{High}$	low NO_3^- source
1	$2 \times V_{cuvette}$	14.71 ± 0.02	0.12 ± 0.01	< 0.0001	< 0.0002	$(-1.59, -1.37)$	$(1.29, 2.10)$
2	$4 \times V_{cuvette}$	14.71 ± 0.01	0.09 ± 0.01	< 0.0001	< 0.0001	$(-0.19, -0.14)$	$(0.15, 0.18)$
3	$10 \times V_{cuvette}$	14.75 ± 0.01	0.06 ± 0.01	0.236^*	< 0.0001	$(-0.03, 0.01)$	$(0.06, 0.09)$
4	DI rinse, $2 \times V_{cuvette}$,	14.74 ± 0.01	0.08 ± 0.01	< 0.0001	< 0.0001	$(-1.74, -1.41)$	$(0.28, 0.35)$
5	DI rinse, $4 \times V_{cuvette}$	14.74 ± 0.01	0.11 ± 0.02	< 0.0001	< 0.0001	$(-0.11, -0.07)$	$(0.04, 0.08)$
6	DI rinse, $10 \times V_{cuvette}$	15.14 ± 0.01	0.09 ± 0.02	0.003	0.615^*	$(-0.06, -0.02)$	$(-0.02, 0.04)$

* indicates that the protocol used resulted in no significant difference between the initial NO_3^- concentration and subsequent measurements ($\alpha = 0.05$).

Table 2. Initial NO_3^- concentrations, calculated effective residual volumes (Vres), and 95 % confidence interval (C.I.) from source contamination trials (a)–(d).

Trial	$[NO_3]_{low}$			$[NO_3]_{high}$		
	Initial concentration ($mg\,NO_3{-}N\,L^{-1}$)	V_{res} (mL)	95 % C.I. (mL)	Initial concentration ($mg\,NO_3{-}N\,L^{-1}$)	V_{res} (mL)	95 % C.I. (mL)
(a)	0.71	0.41	(0.39, 0.43)	15.3	0.32	(0.29, 0.35)
(b)	0.71	0.35	(0.32, 0.38)	8.63	0.39	(0.34, 0.43)
(c)	0.74	0.46	(0.38, 0.55)	4.80	0.28	(0.21, 0.36)
(d)	0.78	0.30	(0.06, 0.52)	2.52	0.39	(0.15, 0.60)

centrations reported in Table 1 would be divided by a factor of 3, 10, and 30, respectively. Rinsing with $4 \times V_{cuvette}$ would reduce the absolute concentration difference from $0.19\,mg\,NO_3{-}N\,L^{-1}$ in the worst-case scenario to 0.06, 0.02, and less than $0.01\,mg\,NO_3{-}N\,L^{-1}$, respectively, although the concentrations may still be significantly over- or underestimated. These values are within the 5 % measurement uncertainties often found to be acceptable from analytical instruments.

2.3.2 Source contamination

Source contamination (or cross-contamination of the source) testing results are shown in Fig. 2. As expected, $[NO_3]_{high}$ and $[NO_3]_{low}$ became diluted and concentrated, respectively, as residual volumes from the previous samples contaminated the sources. This source contamination increased with increasing difference in initial concentrations (Fig. 2 and Table 3). Over 40 purges back to the source, the concentration and dilution effects were approximately linear, and regression lines were fitted to the data to calculate effective residual volumes (V_{res}). The 95 % confidence interval for the slope and intercept of the regression lines was used to calculate the uncertainty on the calculated residual volumes. Standard errors of the regression residuals were twice those of the reference measurements. This indicates additional source(s) of random error, which could include some variability in the residual volumes and/or nonuniform mixing of the sources between consecutive samples. Estimates of V_{res} were calculated to vary between 0.28 and 0.46 mL (Table 2). In trials (a) and (c), V_{res} were statistically different when calculated using $[NO_3]_{high}$ and $[NO_3]_{low}$, and also differed between trials (a) and (b) for $[NO_3]_{low}$. Practically, our results show that when using the purging back to source configuration (Fig. 1b) less than 0.5 mL of water (5 % of sample volume pumped) from the previous sample may contaminate the source measured. This is comparable to previous analysis of the large volume MPS showing V_{res} of 4 % sample volume pumped (Birgand et al., 2016). This volume may correspond to droplets left in the 0.9 mm i.d. tubing.

Although this residual volume is significant, its effect depends on the application. When alternating between 3 and $5\,mg\,NO_3{-}N\,L^{-1}$ of NO_3^- sources 50 L in volume, it would take 500 purges to source before a $0.01\,mg\,NO_3{-}N\,L^{-1}$ change in the concentration would be detectable as a result of residuals purged to the alternate source. In the same situation with a 0.5 L source, only five purges would induce the same level of change. These results suggest that the purge to source configuration should be used in short-lived experiments and only in applications with a high source volume (> 10 L), which would keep this artifact undetectable. For small-volume applications (e.g., porewater sampling) source

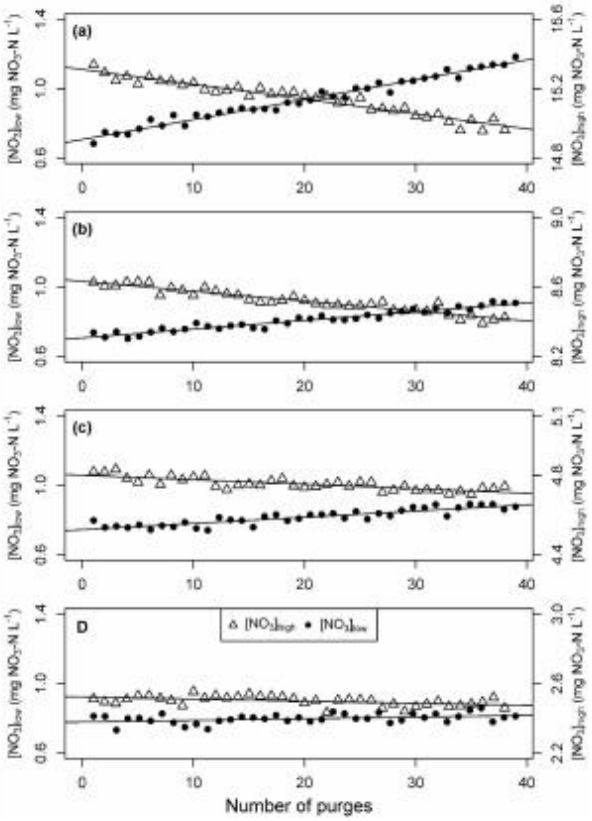

Figure 2. Changes in NO_3^- concentrations in low ($[NO_3]_{low}$) and high ($[NO_3]_{high}$) concentration sources (0.5 L) resulting from residual volumes purged to the alternate source. Greater concentration or dilution effects were seen with increasing differences in initial NO_3^- concentrations of the sources during trials **(a)**–**(d)**.

contamination may be significant and the "purge to waste" routine is recommended, rather than the purging back to source configuration.

2.3.3 Pump time requirement results

Times required for a single sampling sequence (pumping and purging from source) for variable tube lengths were not linear with tubing length (data not shown), and best described using the following equation: time $= 0.0001 \times \text{length}^2 + 0.0662 \times \text{length} + 79.4$, where time corresponds to the cumulative time in seconds required to pump and purge from the source to the cuvette, and length is the tube length from the source to the MPS in centimeters. From this equation, the time for a sampling sequence between consecutive sources was calculated with 60 s added to account for cuvette rinsing for the spectrophotometer measurement time. For applications with

Table 3. Zero-order NO_3^- removal rates, k, at eight well locations during five experimental trials. The zero-order kinetics model was fitted to time series of NO_3^- concentrations after flow to the lab bioreactor was stopped. RMSEP refers to the root mean square error of prediction.

Well location	Zero order, k ($mg\,L^{-1}\,h^{-1}$)	R^2	RMSEP ($mg\,L^{-1}\,h^{-1}$)
D1	0.25–0.43	0.96–0.99	0.002–0.003
D2	0.27–0.43	0.94–0.99	0.002–0.005
D3	0.29–0.38	0.84–0.99	0.002–0.010
D4	0.30–0.38	0.93–0.99	0.001–0.008
S1	0.30–0.44	0.93–0.99	0.002–0.008
S2	0.30–0.54	0.97–0.99	0.002–0.006
S3	0.15–0.34	0.88–0.98	0.003–0.006
S4	0.13–0.36	0.91–0.99	0.001–0.010

sources up to 1, 4, and 9 m away from the MPS, the time for one sample sequence would be 147, 182, and 280 s, respectively. The results suggest that roughly 30 min resolution water quality data can be obtained for up to 10 sources with sources up to 4 m away. The resolution would fall to 47 min for the same number of sources up to 9 m away.

3 Frequent porewater sampling in a woodchip bioreactor

Woodchip bioreactors, also called denitrification beds, are a popular agricultural conservation practice for the treatment of NO_3^- in subsurface drainage. These anaerobic systems provide woodchips as a carbon source and promote denitrification to remove NO_3^- from the aquatic environment. Soil pits typically ~ 1 m deep, ~ 5 m wide, and ~ 25 m long are filled with woodchips through which drainage water percolates. Over 20 years of research on woodchip bioreactors has shown their potential to reduce NO_3^- concentrations, but has also shown troubling variability in reported treatment efficacy (e.g., 81 % to 3 %; David et al., 2016) or bioreactor volumetric removal rates (e.g., 2 to 22 g N m^{-3} d^{-1}, reviewed by Schipper et al., 2010; 0.42 to 7.76 g N m^{-3} d^{-1}, Christianson et al., 2012). Variation in treatment performance has been attributed to various factors, including hydraulic residence time (HRT), temperature, influent concentration, and age (Addy et al., 2016; Hoover et al., 2016). An important part of the reported uncertainty and variability seems to be associated with measurement methods ill-suited to quantify NO_3^- fluxes into, within, and leaving bioreactors. Woodchip bioreactors are mostly treated as "black box" systems.

There is evidence that internal hydraulic flow paths and short-circuiting may result in overall treatment inefficiencies, although this has been inferred indirectly in field and lab experiments using tracers (Christianson et al., 2013; Cameron and Schipper, 2011; Hoover et al., 2016). We report results from a preliminary experiment showing that the small-volume MPS can help improve understanding of bioreactors as black box systems.

3.1 Materials and methods

Nitrate dynamics were studied in a (1.20 × 1.20 × 0.45 m deep) lab bioreactor at North Carolina State University using the small-volume MPS (Figs. S2 and S3 in the Supplement). This bioreactor is a lab-scale model of field bioreactors in which inlet and outlet manifolds installed at opposite corners create diagonal flow from the inlet at the top to the outlet at the bottom (Fig. S2). Eight sampling wells within the bioreactor woodchip media were monitored for NO_3^- concentrations using the small-volume MPS. Sample wells were placed at shallow (*S*) or deep (*D*) zones (20.9 and 41.9 cm depth, respectively) and at 55.9 and 100.2 cm from the inlet along two longitudinal transects. Transects were located along the centerline and 21.6 cm from the left sidewall (Fig. S2). Wells were made of stainless steel tubing (0.32 cm O.D.) with vertical slits cut at the tip to draw water into the well. Wells tips were covered with fine plankton netting (60 µm mesh) to prevent clogging of MPS tubing. Well names were assigned based on their location in the bioreactor. Wells S1 and S2 were shallow wells located near the inlet on the centerline and 21.6 cm from the sidewall, respectively. Wells S3 and S4 were shallow wells located near the outlet on the centerline and 21.6 cm from the sidewall, respectively. The same convention was used for deep wells D1–D4.

For these experiments a dual sampling–analyzing system was used. The small-volume MPS did not directly sample water from each well. Instead, to obtain synchronized NO_3^- concentrations in the bioreactor, all wells were sampled simultaneously using an eight-channel ISMATEC peristaltic pump triggered by the MPS Arduino board. The eight-channel pump simultaneously delivered sample volumes from each well to an intermediate manifold of eight 40 mL syringes. The small-volume MPS was then used to sequentially pump water to the cuvette for analysis by the spectrophotometer. The probe was calibrated for NO_3^- using PLSR techniques described previously (Etheridge et al., 2014).

3.2 Small-volume MPS reveals short-circuiting inside a woodchip bioreactor

In the first MPS application, we conducted a 76 h constant NO_3^- injection experiment from 30 April to 4 May 2015 in a saturated bioreactor receiving 60 L h^{-1} tap water flow for a theoretical HRT of ~ 5.7 h. Nitrate from a concentrated KNO_3 stock solution was injected using a precision piston pump (Fluid Metering Inc. Model QBG, 1.2 g L^{-1}) for a target inflow NO_3^- concentration of 20 mg NO_3–N L^{-1}. The eight wells were sampled and analyzed every 40 min with the system described in Sect. 3.1. Ports 9 and 10 of the 12-port valve directly sampled the inlet and outlet weirs after consecutively analyzing sample volumes from each of the eight wells. In the first experiment, KNO_3 injection began at 08:10 on 1 May (14.2 h after MPS monitoring began, Fig. 3). From 14.2 to 22.4 h NO_3^- concentrations were stable around 18.3 mg NO_3–N L^{-1}. After this period, inlet concentrations rose until 37 h and were variable over the 76 h injection. Inlet NO_3^- concentration ranged from 18.2 to 20.6 mg NO_3–N L^{-1} and varied by 12 % of the target inlet concentration. Variability in inlet NO_3^- concentration was higher than anticipated due to degassing in the KNO_3 solution tank, with accumulation of air bubbles partially restricting flow through the piston pump.

Nitrate concentrations at the inlet rose quickly to 18.4 mg NO_3–N L^{-1} within 47 min of starting the KNO_3 injection (Fig. 3). Inlet NO_3^- concentration likely passed 18 mg NO_3–N L^{-1} sooner, but the sampling time resolution of 47 min was insufficient to capture the exact time of the ar-

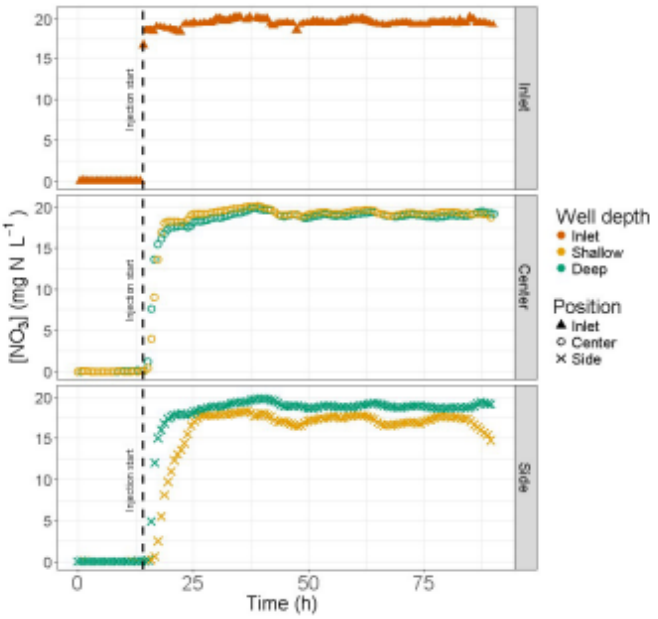

Figure 3. Nitrate concentration at inlet and wells near the inlet before and during the KNO_3 injection. Color indicates bioreactor inlet and depth of sampling wells, and shape indicates the position of the well transect (centerline or near the side wall).

rival. Three of the four wells nearest the inlet (S1, D1, and D2) showed nearly identical increases in NO_3^-, with concentrations at these wells passing 18 mg NO_3–N L^{-1} within 4.5–8.2 h of the injection. The shallow inlet well located along the side wall (S2) showed a noticeable lag, with NO_3^- staying below 18 mg NO_3–N L^{-1} until 19.7 h after the injection began. Nitrate concentrations at this well were significantly lower over the entire injection, relative to other wells near the inlet. All four inlet wells showed increases and decreases in NO_3^- concentrations that corresponded to changes in concentration at the inlet, although variability at S2 was much higher than the other three inlet wells. Nitrate concentrations in deep wells near the inlet closely followed one another during each sample interval, with an average difference of only 0.13 mg NO_3–N L^{-1}. Shallow wells near the inlet varied greatly, with an average difference of 2.04 mg NO_3–N L^{-1}.

A period of 4 h after injection, NO_3^- was detected at the deep middle well near the outlet (D3), but outlet NO_3^- concentrations did not become stable until about 25 h, or 5 times the theoretical HRT of 5.7 h. The very long lag for stabilization of NO_3^- concentrations at the outlet weir was likely due to the variability of injected NO_3^- to move through the bioreactor, as apparent from the 16.9, 17.5, and 21.2 h taken for S3, S4, and D3 to reach 18 mg NO_3–N L^{-1}.

Nitrate concentrations were significantly greater in deep wells relative to shallow wells at side wells near the inlet and at middle wells near the outlet. Shallow wells had higher NO_3^- concentration at side outlet wells and middle inlet wells. Variance in NO_3^- concentration was higher in shallow wells than deep wells at all four well pairs, illustrating that water moved quickly diagonally through the bioreactor and short-circuited most of the bioreactor volume. Lag and lower NO_3^- concentrations observed in the shallow wells (e.g., S2 and S4; Fig. 4) suggest that areas further away from the direct diagonal flow path may have slower hydraulic exchange and higher HRT (e.g., S2) and act as "dead zones".

To the best of our knowledge, short-circuiting and dead zones have never been observed directly but only inferred through dispersion indices (Morrill Dispersion Index) shown in field reactors (Christianson et al., 2013) and in lab reactors (Hoover et al., 2016). Delayed time of arrival for NO_3^- at wells farther from the shortest flow path indicates hydraulic inefficiencies; however several shallow wells also showed cyclic patterns in NO_3^- concentrations. Microbial and gas clogging has been documented and can be caused by the creation of biofilm pore walls by microbial cells or fungi (Oberdorfer and Peterson, 1985; Okubo and Matsumoto, 1979; Vandevivere et al., 1995) or by extracellular polymers (Shaw et al., 1985; Vandevivere and Baveye, 1992). Gas clogging

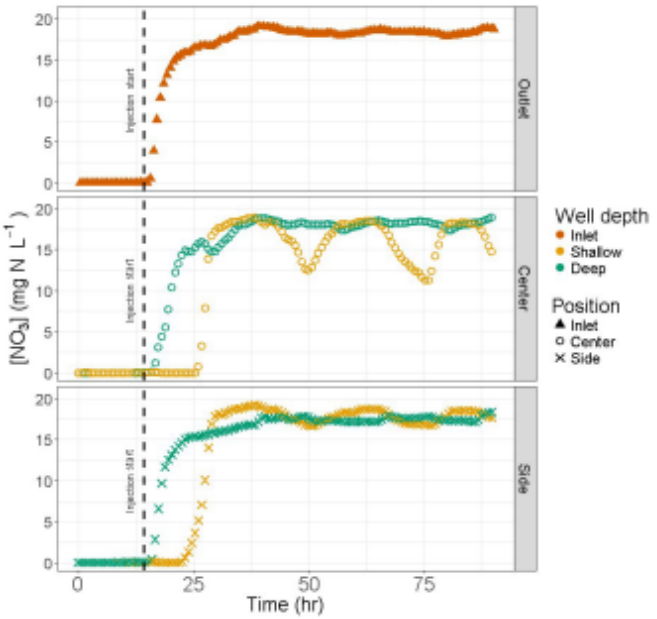

Figure 4. Nitrate concentration at outlet and wells near the outlet before and during the KNO_3 injection. Color indicates bioreactor outlet and depth of sampling wells, and shape indicates the position of the well transect (centerline or near the side wall).

due to the accumulation of microbial-produced gas bubbles and influencing hydraulic conductivity in peat (Kellner et al., 2004; Beckwith and Baird, 2001) seems to explain some observed transient low conductivity (Kellner et al., 2004). These changes in hydraulic conductivity could explain the NO_3^- concentration fluctuations of the S2, S3, and S4 wells, which exhibited regular decreases and increases of NO_3^- concentrations.

3.3 Internal nitrate removal kinetics

In a second set of bioreactor experiments, NO_3^- reduction kinetics were measured at each well. The lab bioreactor was fully drained for a period of 24 h. Following this drain event, the woodchips were re-saturated with the same KNO_3 spiked tap water made by the same method described in Sect. 3.2. Inflow NO_3^- concentration was 14 mg $NO_3-N\,L^{-1}$ at 108 $L\,h^{-1}$. After pumping 4.5 pore volumes through the reactor, flow was stopped and the outlet weir raised to prevent any outflow. Each well was sampled every 3 h over 24 h during five trials from 26 March to 12 April using the MPS and eight-channel pump. Times series of NO_3^- concentrations at each well were fitted to zero order kinetics models (Eq. 1). Time series were fitted using the nls() function in R which calculates least-squares estimates for model parameters. In fitting the zero-order model, only the concentrations after flow were stopped and above 2 mg $NO_3-N\,L^{-1}$ were used. Other than both shallow outlet wells, NO_3^- concentrations at each well peaked at 12.5–13.5 mg $NO_3-N\,L^{-1}$ after flow was stopped. Both shallow outlet wells had much lower peaks of 9.5–10.5 mg $NO_3-N\,L^{-1}$, consistent with observations in the first experiment that wells in this zone were slower to receive new water.

Over the five trials, zero-order NO_3^- removal rates ranged from 0.13 to 0.54 mg $NO_3-N\,L^{-1}\,h^{-1}$ (Table 3). For this experimental bioreactor with a measured porosity of 0.59, this equates to a range of 1.84–7.65 g $N\,m^{-3}\,d^{-1}$ (m^3 of reactor volume). Having access to eight points provided a range of removal rates and illustrated variability within the bioreactor. Spatial variability in the volumetric NO_3^- removal rates approached those reported across many field bioreactors (reviewed by Schipper et al., 2010). While there was high variability in NO_3^- removal rates within trials, there was no significant difference in mean values between wells when considering all five trials. The five lowest removal rates measured (Table 3) were in shallow outlet wells S3 and S4 (observed dead zones), and indicate that there may be a causality between NO_3^- removal rates and hydraulic inefficiencies or clogging.

4 High-frequency measurements in in situ stream mesocosms

Among the many methods used to measure NO_3^- removal kinetics in streams, the in situ mesocosm method is attractive as it involves minimal disturbance of the sediment, is effective for investigating spatial variability under field conditions, and can be performed at different times of the year (reviewed by Birgand et al., 2007). In situ mesocosms consist of open-bottom containers inserted into the sediment which isolate water inside the mesocosm from the surrounding stream, making it possible to estimate process kinetics from changes in nutrient concentrations over time. Water recirculation is often applied to mimic ambient stream velocity.

The standard method consists in manual sample withdrawal several times (most often 4–7 times; reviewed by Birgand et al., 2007) over the duration of the experiment (typically < 48 h). In laboratory mesocosms the volume of the water withdrawn is a minor issue as one can account for the mass of nutrients removed (e.g., Birgand et al., 2016; Messer et al., 2017). For in situ mesocosms water withdrawal is more significant as this water will, over time, be replaced by water upwelling from the sediment porewater. This discourages taking more samples during the experiment to reduce uncertainty in kinetics estimates. The inherent conflict between kinetics uncertainties and porewater interference in in situ stream mesocosms can be solved with the small-volume MPS used in the purging back to source configuration (Fig. 1b).

4.1 Materials and methods

To characterize NO_3^- removal kinetics of a stream prior to its restoration (Claridge Nursery, Goldsboro, NC; 35.4° N, 78.0° W), the small-volume MPS was used with in situ mesocosms in two distinct sections of the reach to be restored. The upper reach of the ditch (1.6 km) has submerged vegetation and a thick muck sediment (20–30 cm depth) with high organic content (2 %–26 % organic matter). The lower reach (0.6 km) has no instream vegetation and sandy sediment with low organic content (0.1 %–9.0 % organic matter). The upper and lower reaches are referred to as Muck and Sand, respectively.

In 11 24 h experimental trials from August 2014 to March 2015, four mesocosms made of open-bottom barrels were gently inserted into the sediment down to approximately 10 cm within a 1 m radius of each other (Fig. S4). Each 57 cm diameter barrel inserted into the sediment is referred to as a Sediment mesocosm and covered 0.26 m^2 of the stream bottom. A fifth, closed-bottom barrel (referred to as Control mesocosm) placed in the stream for temperature adjustment and containing only stream water served as a control, representing NO_3^- removal processes occurring in the water column. Water depth in Sediment mesocosms was measured manually. Recirculating DC pumps (3 L min^{-1}) were placed on the sidewall of the barrel (Fig. S5) and their flow was adjusted to mimic ambient stream velocity (0.02–0.10 m s^{-1}). Sample lines were placed near the recirculating pumps to obtain a well-mixed sample volume. Mesocosms were removed at the end of each experiment to allow hydrologic connection with the stream between trials. Four 24 h trials were completed at each Muck site and three trials performed at the downstream Sand site across four seasons.

At the beginning of each trial a 2 L solution of KNO_3 was added to each mesocosm to reach an initial NO_3^- concentration of 5–6 mg NO_3–N L^{-1}. The overlying water was gently stirred and left to equilibrate. The addition of the KNO_3 solution generating extra head inside the mesocosm helped prevent upwelling from groundwater (Solder et al., 2015) which might have otherwise occurred. Each sample volume pumped by the MPS temporarily withdrew ~ 25 mL of sample over < 4 min, corresponding to > 0.1 mm drop in head, which we assumed was not high or long enough to generate significant upwelling.

Mesocosms were sampled every 36 min for 24 h using the small-volume MPS. The measurement cuvette (1.1 mL, 4 mm path length) was rinsed with $> 10 \times V_{res}$ to prevent cross-contamination. Zero-order, first-order, and efficiency loss (EL) kinetics models accounting for water depth (D) (Eq. 1–3) were fitted to the NO_3^- concentration time series ($\sim$ 40–50 data points per mesocosm per trial) to (1) compare NO_3^- removal rates between sites and across seasons and (2) determine which model best predicted the observed data.

$$C_t = C_0 - \frac{\rho_{ZO}}{D} \cdot t \tag{1}$$

$$C_t = C_0 \cdot e^{-\left(\frac{\rho_{FO}}{D} \cdot t\right)} \tag{2}$$

$$C_t = \left(\frac{\rho_{EL}^{(\alpha-1)}}{D} \cdot t + C_0^{(1-\alpha)}\right)^{\left(\frac{1}{1-\alpha}\right)} \tag{3}$$

Methods of model fitting and evaluation were the same as those presented in Sect. 3.3 (Messer et al., 2017; Birgand et al., 2016). The nls() package in R Studio was used to fit observed data to a model predicting NO_3^- concentration at time t, C_t, from estimates of initial concentration, C_0, depth-compensated removal constants (ρ_{ZO}, ρ_{FO}, ρ_{EL}), and the efficiency loss constant α. The commonly reported rate constant, k, was calculated by dividing ρ coefficients by depth, D.

4.2 Nitrate uptake kinetics

There was little preference between zero- and first-order models in the time series of decreasing NO_3^- concentrations (Table 4), with R^2 values for both models typically > 0.95. Residuals of both models were nearly identical in most cases and differences in model R2 were generally > 0.01. All time series of decreasing NO_3^- concentrations from Sand trials showed better fit for zero-order kinetics. Higher

Table 4. Time series of NO_3^- concentrations in Sediment mesocosms were fitted to zero- and first-order kinetics models. Results indicate that for this short-duration experiment (< 24 h) and at the observed range of NO_3^- concentrations (2–6 mg NO_3–N L^{-1}), removal was described equally well by either model, although first-order kinetics better fitted NO_3^- time series during trials with large changes in NO_3^- concentration. RMSEP refers to the root mean square error of prediction.

Trial date (sediment)	Zero order, k mg NO_3–N m^{-2} d^{-1}	R^2	RMSEP mg NO_3–N m^{-2} d^{-1}	First order, k m d^{-1}	R^2	RMSEP m d^{-1}
28 Aug (Muck)	500–580	0.99	30–60	0.15–0.17	0.99	0.02–0.05
1O Oct (Muck)	200–250	0.95–0.98	30–60	0.06–0.07	0.95–0.98	0.03–0.05
6 Nov (Muck)	140–260	0.93–0.98	40–70	0.04–0.07	0.93–0.98	0.03–0.06
13 Nov (Muck)	160–200	0.89–0.98	20–60	0.05–0.06	0.89–0.98	0.02–0.06
29 Jan (Muck)	−40–180	0.00–0.93	10–40	0.00–0.05	0.00–0.93	0.00–0.04
3 Feb (Muck)	40–120	0.76–0.99	20–30	0.01–0.04	0.76–0.99	0.02–0.03
11 Mar (Muck)	180–320	0.93–0.99	20–40	0.04–0.09	0.92–0.99	0.02–0.04
18 Mar (Muck)	90–300	0.97–0.99	20–60	0.03–0.13	0.97–0.99	0.02–0.05
18 Sep (Sand)	10–110	0.10–0.86	20–50	0.00–0.03	0.10–0.85	0.02–0.05
17 Dec (Sand)	140–240	0.97–0.98	20–30	0.03–0.06	0.96–0.98	0.02–0.03
16 Mar (Sand)	20–50	0.63–0.84	20–30	0.01–0.02	0.63–0.86	0.02–0.03

R^2 and improved residuals for a first-order model, relative to a zero-order model, were seen in trials with greater decreases in NO_3^- concentrations over the experiment. This was the case in 18 March and 28 August trials during which net NO_3^- reduction in several mesocosms approached 2–3 mg NO_3–N L^{-1} over 24 h. The poorest model fitting occurred when fitting models to time series with little to no reduction in NO_3^- concentrations, when total variability of NO_3^- was close to the precision of the spectrophotometer or transient, short-term changes in NO_3^- were large relative to net reduction. The EL model was not useful in these short-term experiments.

These results are somewhat contradictory to results obtained in lab wetland mesocosms of similar size, whereby data were not fitted well by a zero-order model and whereby the EL model performed best (Birgand et al., 2016). It is possible that the experiments were not of long enough duration for NO_3^- concentrations to decrease enough for differences to appear among models, or for first-order and EL kinetics to be apparent. In these in situ experiments, the results suggest that NO_3^- removal kinetics at the diurnal scale in nutrient-rich streams were adequately predicted by zero-order models. In Muck trials, ρ values ranged from 10 to 580 mg NO_3–N m^{-2} d^{-1} (Table 4). Removal rates in Sand mesocosms were much lower, ranging from 10 to 240 mg NO_3–N m^{-2} d^{-1}. The results show that for NO_3^- removal rates less than 300 mg N m^{-2} L^{-1}, the zero-order rate model was sufficient to fit the data, but the first-order model appeared better for higher NO_3^- removal rates generally found in agricultural streams (350 and 1250 mg N m^{-2} d^{-1}; Birgand et al., 2007).

4.3 Seasonal and spatial variability

In Muck trials NO_3^- removal rates followed a predictable seasonal pattern, with removal rates highest in the month of August, decreasing in October and November trials, lowest during the winter months, and increasing again during March. This is consistent with observations that the rates of microbial processes increase with temperature. Nitrate removal rates during the 18 August trial (25 °C) were 4–14 times greater than those during 3 February (8 °C) at the same site. The opposite trend was seen among Sand trials. The 17 December trial with the coldest temperatures among Sand trials (10 °C) showed the highest NO_3^- removal rates. A seasonal influx of available carbon was likely the cause of this trend. Accumulated leaf packs at the Sand site, included in the 17 December mesocosms, provided available carbon and substrate for denitrification to occur. Nitrate removal rates during this trial were even higher than rates in Muck trials with similar temperature (29 January and 3 Februry).

The in situ mesocosm method revealed high variability in NO_3^- removal rates within trials, even when mesocosms were within a 1 m radius. High variability in Muck trials in the month of March was caused by the presence of emergent vegetation along the stream bank (Fig. S6). In 11 and 18 March trials, mesocosms placed in this near-bank vegetated zone showed removal rates 48 %–81 % and 74 %–240 % higher than those in mesocosms placed in the unvegetated stream center, respectively. In the 29 January trial, a single mesocosm showed removal rates 300 %–2500% higher than the other Sediment mesocosms. Muck trials had a higher degree of within-trial variability relative to Sand, indicating that sediment NO_3^- removal potential at the Sand site was more homogenous.

5 Conclusions

The first report of the MPS illustrated the ability of this technology to increase temporal and spatial resolution of water quality data (Birgand et al., 2016). The small-volume MPS increases the number of potential applications for this method by significantly decreasing sample volume. The small-volume MPS minimized the volume of the flow-through measurement cell (1.1 mL quartz cuvette), contrasting with the 40 mL flow-through cell used previously. In order to prevent cross-contamination of samples caused by pumping from different sources, an adequate pre-measurement rinse with the current sample volume must be used. For the larger volume MPS this would require pumping roughly 36 times more volume past the flow-through cell for adequate rinsing. In the stream mesocosms, removing 25 mL of sample for < 4 min to measure absorbance resulted in a temporary head drop < 0.1 mm and minimized sample withdrawal to allow 40–50 NO_3^- measurements to be made over 24 h without significantly affecting mesocosm hydraulics.

The small-volume MPS allows continuous multi-point sampling to be extended to applications for which the sample volume is limited or must be minimized. The most obvious application is for porewater sampling, for which sample withdrawal rate should not exceed the rate at which water moves through the medium. Total volume extracted must also be small to avoid significantly affecting the observed environment. Drainable porosity in soils is much less than the total volume of soil, leading to a zone of influence in which the size depends on the total sample volume extracted and the drainable porosity. For example, if sampling every 1 or 6 h over 24 h from a soil with a 0.1 drainable porosity, this zone of influence (assuming 15 mL required sample volume for the small-volume MPS) would be 3600 and 600 cm^3, respectively. Assuming this zone is spherical, it would have a diameter of 19 and 10 cm, which is not insignificant. The sampling interval should be short enough to adequately capture temporal variation while avoiding excessive water withdrawal to avoid interdependence between sampling points that are hydraulically connected. When removal kinetics were measured in the lab bioreactor during stopped flow, a sample interval of 3 h was used over 24 h. With an observed drainable porosity of 0.58, the zone of influence at each of the eight points was 7.3 cm and accounted for 0.4 % of water in the bioreactor. Sampling wells were no closer than 21 cm, so an assumption of independence between sampling points was reasonable.

For the first time, the small-volume MPS was able to observe short-circuiting in a woodchip bioreactor, which had been surmised in the literature although never fully shown. We were also able to measure NO_3^- removal rates at multiple locations within the bioreactor. The application of the MPS in stream mesocosms has allowed the possibility to measure NO_3^- removal kinetics in situ in replicated experiments by eliminating potential contamination by groundwater. The small-volume MPS has high potential for providing quality data sets for improving new and existing solute transport models for saturated or partially saturated soils and presents the possibility of being used in replicated experiments.

Due to the small diameter of the fittings and tubing in this system, several pumping concerns are magnified compared to the large volume MPS. Water micro-droplets or residuals in the tubing lines are more susceptible to freezing and caution should be used when deploying this system under freezing conditions. Valves and tubing are also more susceptible to clogging. In both applications a plankton net fabric (60 µm mesh) was used and no clogging occurred, even in the case of the woodchip bioreactor application with high dissolved organic matter. The small sample volume potentially limits the number of sondes and sensors to which the MPS can be coupled. The design of the s::can spectrophotometer allows for such a small-volume flow-through measurement cell to be used, while other available water quality sensors typically require much larger sample volumes for which this system might not be well suited. The volume-limited applications presented include sampling an overlying water column and porewater in coarse woodchips. Porewater sampling in fine soils or sediments may be more restrictive and will result in a larger sphere of influence around the sampling point. While the minimum volume required for measurement using the MPS is small (~ 7 mL) and comparable to other small-volume sediment samplers (e.g., Rhizon in situ samplers; Seeberg-Elverfeldt et al., 2005), bidirectional pumping from multiple sources by the MPS requires a volume closer to 10–15 mL to reduce cross-contamination for accurate solute measurement. Sampling of fine soils with low hydraulic conductivity using the MPS can be aided by the use of small-diameter sampling wells, similar to those described in Sect. 3.1.

Data availability. All data presented in this paper in Sects. 2.3.1, 2.3.2, 3.1, 3.2, 4.2, and 4.3 are provided in .csv files in an online Zenodo repository at https://doi.org/10.5281/zenodo.1453353 (Maxwell, 2018). The online repository also includes the R code (R Studio Ver.1.1.442 or greater) used to generate plots and calculate coefficients for NO_3^- removal kinetic equations.

The Supplement related to this article is available online at: https://doi.org/10.5194/hess-22-5615-2018-supplement

Author contributions. Direction of research, funding, and initial development of the small-volume MPS was provided by FB. Early design and prototyping of the small-volume MPS was provided by BS and KAD, and development of protocols for testing cross-contamination was contributed to by KAD.

Competing interests. The authors declare that they have no conflict of interest.

Acknowledgements. The authors would like to acknowledge the NCSU BAE Environmental Analysis Lab for water chemistry analysis. Stream mesocosm research was funded by the NCDOT under grant agreement 2013-37, and bioreactor porewater sampling research was funded in part by NIFA USDA grant 2016-67019-25279 and USDA multistate project S1063.

Edited by: Matthew Hipsey
Reviewed by: two anonymous referees

References

Addy, K., Gold, A., Christianson, L., David, M., Schipper, L., and Ratigan, N.: Denitrifying bioreactors for nitrate removal: A meta-analysis, J. Environ. Qual., 45, 873–871, 2016.

Beckwith, C. W. and Baird, A. J.: Effect of biogenic gas bubbles on water flow through poorly decomposed blanket peat, Water Resour. Res., 37, 551–558, 2001.

Birgand, F., Skaggs, R. W., Chescheir, G. M., and Gilliam, J. W.: Nitrogen removal in streams of agricultural catchments – a literature review, Crit. Rev. Env. Sci. Tec., 37, 381–487, 2007.

Birgand, F., Aveni-Deforge, K., Smith, B., Maxwell, B., Horstman, M., Gerling, A. B., and Carey, C. C.: First report of a novel multiplexer pumping system coupled to a water quality probe to collect high temporal frequency in situ water chemistry measurements at multiple sites, Limnol. Oceanogr.-Meth., 14, 767–783, 2016.

Cameron, S. G. and Schipper, L. A.: Evaluation of passive solar heating and alternative flow regimes on nitrate removal in denitrification beds, Ecol. Eng., 37, 1195–1204, 2011.

Christianson, L., Helmers, M., Bhandari, A., and Moorman, T.: Internal hydraulics of an agricultural drainage denitrification bioreactor, Ecol. Eng., 52, 298–307, 2013.

Christianson, L. E., Bhandari, A., Helmers, M. J., Kult, K. J., Sutphin, T., and Wolf, R.: Performance evaluation of four field-scale agricultural drainage denitrification bioreactors in iowa, T. ASABE, 55, 2163–2174, 2012.

Crumpton, W. G., Isenhart, T. M., and Mitchell, P. D.: Nitrate and organic N analyses with second-derivative spectroscopy, Limnol. Oceanogr., 37, 907–913, 1992.

David, M. B., Gentry, L. E., Cooke, R. A., and Herbstritt, S. M.: Temperature and substrate control woodchip bioreactor performance in reducing tile nitrate loads in east-central illinois, J. Environ. Qual., 45, 822–829, 2016.

Dent, C. L. and Grimm, N. B.: Spatial heterogeneity of stream water nutrient concentrations over successional time, Ecology, 80, 2283–2298, 1999.

Etheridge, J. R., Birgand, F., Osborne, J. A., Osburn, C. L., Burchell, M. R., and Irving, J.: Using in situ ultraviolet-visual spectroscopy to measure nitrogen, carbon, phosphorus, and suspended solids concentrations at a high frequency in a brackish tidal marsh, Limnol. Oceanogr.-Meth., 12, 10–22, 2014.

Finch, M. S., Hydes, D. J., Clayson, C. H., Weigl, B., Dakin, J., and Gwilliam, P.: A low power ultra violet spectrophotometer for measurement of nitrate in seawater: Introduction, calibration and initial sea trials, Anal. Chim. Acta, 377, 167–177, 1998.

Johnson, K. S. and Coletti, L. J.: In situ ultraviolet spectrophotometry for high resolution and long-term monitoring of nitrate, bromide and bisulfide in the ocean, Deep-Sea Res. Pt I, 49, 1291–1305, 2002.

Kahlert, M., Hasselrot, A. T., Hillebrand, H., and Pettersson, K.: Spatial and temporal variation in the biomass and nutrient status of epilithic algae in lake erken, sweden, Freshwater Biol., 47, 1191–1215, 2002.

Kellner, E., Price, J. S., and Waddington, J.: Pressure variations in peat as a result of gas bubble dynamics, Hydrol. Process., 18, 2599–2605, 2004.

Maxwell, B.: Replication data for : A small volume multiplexed pumping system for automated, high frequency water chemistry measurements in volume-limited applications, Zenodo, https://doi.org/10.5281/zenodo.1453353, 2018.

McClain, M. E., Boyer, E. W., Dent, C. L., Gergel, S. E., Grimm, N. B., Groffman, P. M., Hart, S. C., Harvey, J. W., Johnston, C. A., and Mayorga, E.: Biogeochemical hot spots and hot moments at the interface of terrestrial and aquatic ecosystems, Ecosystems, 6, 301–312, 2003.

Merill, L. and Tonjes, D. J.: A review of the hyporheic zone, stream restoration, and means to enhance denitrification, Crit. Rev. Env. Sci. Tec., 44, 2337–2379, 2014.

Messer, T. L., Burchell II, M. R., Birgand, F., Broome, S. W., and Chescheir, G.: Nitrate removal potential of restored wetlands loaded with agricultural drainage water: A mesocosm scale experimental approach, Ecol. Eng., 106, 541–554, 2017.

Oberdorfer, J. A. and Peterson, F. L.: Waste-water injection: Geochemical and biogeochemical clogging processes, Groundwater, 23, 753–761, 1985.

Okubo, T. and Matsumoto, J.: Effect of infiltration rate on biological clogging and water quality changes during artificial recharge, Water Resour. Res., 15, 1536–1542, 1979.

Parkin, T. B.: Soil microsites as a source of denitrification variability, Soil Sci. Soc. Am. J., 51, 1194–1199, 1987.

Rieger, L., Langergraber, G., and Siegrist, H.: Uncertainties of spectral in situ measurements in wastewater using different calibration approaches, Water Sci. Technol., 53, 187–197, 2006.

Rochelle-Newall, E. and Fisher, T.: Chromophoric dissolved organic matter and dissolved organic carbon in chesapeake bay, Mar. Chem., 77, 23–41, 2002.

Saraceno, J. F., Pellerin, B. A., Downing, B. D., Boss, E., Bachand, P. A., and Bergamaschi, B. A.: High-frequency in situ optical measurements during a storm event: Assessing relationships between dissolved organic matter, sediment concentrations, and hydrologic processes, J. Geophys. Res., 114, G00F09, https://doi.org/10.1029/2009JG000989, 2009.

Seeberg-Elverfeldt, J., Schlüter, M., Feseker, T., and Kölling, M.: Rhizon sampling of porewaters near the sediment-water interface of aquatic systems, Limnol. Oceanogr.-Meth., 3, 361–371, 2005.

Schipper, L. A., Robertson, W. D., Gold, A. J., Jaynes, D. B., and Cameron, S. C.: Denitrifying bioreactors – an approach for reducing nitrate loads to receiving waters, Ecol. Eng., 36, 1532–1543, 2010.

Shaw, J. C., Bramhill, B., Wardlaw, N. C., and Costerton, J. W.: Bacterial fouling in a model core system, Appl. Environ. Microb., 49, 693–701, 1985.

Solder, J. E., Gilmore, T. E., Genereux, D. P., and Solomon, D. K.: A tube seepage meter for in situ measurement of seepage rate and groundwater sampling, Groundwater, 54, 588–595, 2016.

Suzuki, N. and Kuroda, R.: Direct simultaneous determination of nitrate and nitrite by ultraviolet second-derivative spectrophotometry, Analyst, 112, 1077–1079, 1987.

Torres, A. and Bertrand-Krajewski, J.-L.: Partial least squares local calibration of a UV-visible spectrometer used for in situ measurements of cod and tss concentrations in urban drainage systems, Water Sci. Technol., 57, 581–588, 2008.

Vandevivere, P. and Baveye, P.: Effect of bacterial extracellular polymers on the saturated hydraulic conductivity of sand columns, Appl. Environ. Microb., 58, 1690–1698, 1992.

Vandevivere, P., Baveye, P., Lozada, D. S., and DeLeo, P.: Microbial clogging of saturated soils and aquifer materials: Evaluation of mathematical models, Water Resour. Res., 31, 2173–2180, 1995.

Vidon, P., Allan, C., Burns, D., Duval, T. P., Gurwick, N., Inamdar, S., Lowrance, R., Okay, J., Scott, D., and Sebestyen, S.: Hot spots and hot moments in riparian zones: Potential for improved water quality management, J. Am. Water Resour. As., 46, 278–298, 2010.

CHAPTER 2: Measuring In-Stream Nitrate Removal Using Open-Ended *in situ* Mesocosms in a North Carolina Coastal Plain Stream Prior to Restoration

2.1. Introduction

Streams and rivers provide a range of ecosystem services and provisions. Among those services are hydrologic control (e.g., Kondolf, 1996), water supply (e.g., Postel et al., 1997), habitat (e.g., Arthington et al., 2010), carbon sequestration (e.g., Wohl et al., 2012), benefits to social and mental health (e.g., Kaplan, 1995; Frumkin, 2001), and pollution abatement (e.g., Mulholland et al., 2004; Birgand et al., 2007). Abatement of nitrogen (N) pollution from urban and agricultural land uses is a well-studied ecosystem service of streams and rivers which participate in the nitrogen cycle via processes inherent to their healthy functioning (Mulholland et al., 2004). As the nitrogen cycle becomes increasingly destabilized by the burning of fossil fuels and agricultural inputs (Fields, 2004) the environment's ability to respond to these impacts is of serious concern. Although nitrogen abatement efforts would ideally target prevention and treatment of nitrogen at its source, we rely heavily on these natural systems to remediate some of the N pollution.

Where aquatic ecosystems are disturbed by human development the post-development ecosystem can be reduced in size or functionally impaired, providing diminished hydrologic or biogeochemical services. Ecosystem services are lost that, even when mitigated for, often function below their capacity prior to disturbance (Bernhardt et al., 2005). Ecosystem rehabilitation (e.g. stream restoration) is used to refurbish lost services. In some cases, this has proven to be successful while in others, restoration failed to provide lost services (Bernhardt et al., 2005). Even when successful methods for restoration are implemented it is difficult to quantitatively show that services were restored or improved. Obstacles that prevent assessing success include lack of pre-monitoring efforts, lack of long-term post-restoration monitoring on the time scale at which ecosystem services usually return, or failure of sound methodologies to quantify the services provided (Pander, 2013). If services cannot be accurately valuated, the ability to accurately determine restoration success is highly uncertain. Accurate and repeatable methods for appraising ecosystem services are needed.

Nitrogen abatement in streams has been studied via pathways of immobilization (e.g., Ashenkas et al., 2004), mineralization (e.g., Seper, 1981), nitrification (e.g., Bernhardt et al., 2002), denitrification and DNRA (e.g., Burgin & Hamilton, 2007), or through nutrient balance methods (reviewed in Birgand et al, 2007). Methods for measuring denitrification, considered to be a major pathway in natural systems for removing N from the aqueous phase, are well-reported in the literature. Representative cores can be used to measure denitrification occurring in sediments (e.g., Groffman et al., 1993; Payne et al. 1991; Sorenson 1978; Aulakh et al. 1991). One major theoretical advantage of the sediment core method is that it allows the observation of a large number of samples at relative ease and low cost. The acetylene-blocking technique has been widely used (Parkin et al., 1985; Christensen et al., 1990) which promotes incomplete denitrification and measures N_2O production, an intermediate N species prior to the complete reduction of NO_3^- to N_2. The method, however, can fail to account for NO_3 produced by nitrification and subsequent denitrification since acetylene also prevents nitrification from occurring (Groffman et al., 2006). Other concerns include the incomplete diffusion of C_2H_2 in the sediment core, degradation of C_2H_2 over time, and even scavenging of NO by C_2H_2, underestimating denitrification rates (e.g., Groffman et al., 2006). A study on lake sediments by Seitzinger et al. (1993) compared the acetylene blocking technique to two other core methods and found that the acetylene blocking technique did not account for coupled nitrification/denitrification and failed to measure up to 50% of the N_2O production due to incomplete N_2 inhibition.

Nitrogen isotope tracers (e.g., ^{15}N) have also been used to determine the fate of nitrogen in streams and rivers. Groffman et al. (1989) reviewed several studies that utilized both the acetylene and ^{15}N approach and found that resulting denitrification measurements were comparable. A separate study compared the ^{15}N tracer method to the acetylene and N_2 flux method, however, and showed denitrification rate estimates using the tracer approach were <35% of those made by other methods (Seitzinger et al., 1993). The ^{15}N approach can be cost-prohibitive, requiring expensive analyzing equipment and ^{15}N tracer (Huack et al. 1976; Groffman, 2006). Mulholland et al. (2004) admitted this technique could be increasingly cost-prohibitive and difficult to measure N transformation in streams with high background N, limiting the applicability of this method to agricultural watersheds.

Additional measurement error comes from analyzing sediment cores removed from streams, precluding the ability to observe *in-situ* conditions. Risgaard-Peterson (1999) showed incubated sediment cores from a lake failed to account for wave forces that fluidized the sediment, resulting in an order of magnitude difference between core measurements and system mass balance. A study on nitrogen dynamics in tropical forest soil cores showed that laboratory cores underestimated mineralization and NH_4^+ consumption and higher NO_3^- assimilation relative to *in-situ* chambers (Arnold et al., 2008). The authors concluded that extracted cores alter the soil to an extent that findings are not indicative of true soil conditions. Hart et al. (1985) showed discrepancies between an *in-situ* method and laboratory cores when evaluating nitrification in forest soils. Birgand et al. (2007) showed in a review of all methods quantifying surficial removal rates that rates obtained from undisturbed sediment cores less than 10 cm in diameter were systematically lower than those obtained from in situ methods and from reach scale approaches. Birgand et al. (2007) attributed the methodological biases to the underrepresentation of advective exchanges associated with the small scale of cores. A method was needed to represent 'enough' of the spatial variability of the sediment heterogenous surface, and to represent 'enough' of the advective exchanges to eliminate much of the potential methodological bias observed with small cores, and that could be used as a benchmark method to determine *in-situ* behavior of nitrogen transformations in streams and river.

This chapter presents a method for measuring NO_3 removal driven by sediment and other processes under *in-situ* conditions. The method utilizes large *in-situ* mesocosms, a field spectrophotometer, and the small-volume multiplexed pumping system (MPS) designed for sample volume-limited applications. The objective of this study was to monitor sediment-driven NO_3 flux in an agricultural stream in eastern North Carolina prior to a stream restoration. The study presented in this chapter is the same study presented as an application of the small volume MPS in Chapter 1. The MPS was used to measure [NO_3] at 30 min intervals in replicate *in-situ* mesocosms to determine NO_3 removal rates from August 2014 to March 2015. It was hypothesized that the high-resolution data would capture seasonal and spatial variability of NO_3 removal rates by reducing uncertainty of rate estimates.

2.2. Methods

2.2.1. Site description

The stream selected for this study was historically used as a drainage ditch within the Claridge State Nursery in Goldsboro, NC (35.42^{O} N, 78.02^{O} W). The contributing watershed was zoned mostly agricultural with some low-density residential land use. The stream was highly channelized and disconnected from its floodplain. The total length of the reach to be restored is 2,200 m (Lin, 2016). This reach of the stream consists of two primary sediment zones: organic muck (L~1600 m) and sand (L~600 m), with an abrupt transition zone dividing the two. The stream reach consisting of muck had a thick organic layer (depth = 20 – 30 cm, 2 – 26% organic matter), submerged and emergent vegetation within the channel, and a narrow buffer with no overhead canopy. The transition to a sandy zone occurred along incoming tributaries to the stream. Several of these tributaries drain effluent leaving a nearby gravel washing operation and hog farm. The transition to a sand zone is well defined at a point ~1,600 m from the head of the reach where the sediment was primarily sand with little organic content (0.1 – 9.0% organic matter). These two sediment zones are referred to as Muck and Sand.

Sources of organic matter for the stream are both allochthonous and autochthonous. Typical surface water [NO_3] in this stream was 2 – 5 mg NO_3-N L^{-1}. The Muck zone was devoid of any tree canopy supporting dense bank vegetation and in-stream plants during Spring and Summer. This Muck reach was also characterized by little to no riparian buffer and bordered by agricultural fields and a dirt road on both sides. The Sand zone was located within a much wider riparian zone (>40 m) and shaded by dense canopy cover with no in-stream vegetation. Sediment carbon content for the Muck and Sand zone samples were 2.5±1.7 and 0.7±0.5% (Table B-1), respectively, analyzed using combustion at 1350 °C with infrared detection for carbon and thermal conductivity detection for nitrogen (BAE Environmental Analysis Lab).

2.2.2. *In situ* mesocosms

During each experimental trial four open-ended 59 cm diameter barrels of cross-sectional area (0.27 m^2) were placed in the sediment (Figure 2-1). At the beginning of each experimental trial mesocosms were inserted into the sediment and leveled to vertical. These open-bottom barrels

isolated the water in the mesocosm and the underlying sediment from the surrounding stream, creating a control volume in which changes in water chemistry could be measured over time. A closed-bottom barrel used as a control was also placed in the stream and filled to a similar depth with stream water to provide comparable temperature and water composition. The open and closed-bottom barrel mesocosms are referred to as Sediment and Control, respectively. Depth to which barrels were inserted depended on sediment resistance (depth = 10 – 15 cm in Sand; depth = 15 – 30 cm in Muck). Depth to sediment surface below the water level was taken as the average of 17 measurements within the mesocosm. These measurements were used to estimate volume of the water column overlying the sediment. A walking platform across the stream at both Muck sites prevented disturbance of the loose, organic sediment by foot traffic when inserting the barrels and when barrels were removed at the end of each 24 h trial (Figure 2-2).

Figure 2-1. Photo of *in situ* mesocosm method used at the downstream Sand site. Mesocosms were <1 m apart, with four Sediment mesocosms and one Control mesocosm used. Mesocosms were inserted in the sediment immediately prior to and removed at the end of each experiment.

Figure 2-2. Overhead view of mesocosms installed at the midstream Muck site. Low flow DC pumps were installed on the sidewall to mimic stream flow, incorporating advective processes. Use of an elevated bridge prevented disturbance of sediments by foot traffic.

In order to mimic stream flow within the hydraulically-isolated mesocosms low-flow, DC water pumps (3 L min^{-1}) were installed along the inside walls of the barrel (Figure 2-2). Flow was directed along the wall of the barrel resulting in radial flow within the mesocosm. Water velocity was measured using a Marsh McBirney FLO-MATE. Water velocity inside the mesocosm (0.02-0.10 m s^{-1}) was similar to ambient stream velocity and visually the flows were comparable.

Each Sediment mesocosm was assumed to be hydraulically isolated from the surrounding stream. This was made possible by inserting the barrels 10-30 cm in the sediment. Scouring along the upstream edge of the barrels was prevented using polyurethane skirts extending 30 cm around each barrel that were buried in the sediment. The addition of a 5 L KNO_3 spiking solution at the beginning of each trial generated extra head inside the mesocosm to prevent upwelling from groundwater (Solder et al., 2015), which might have otherwise occurred.

2.2.3. High-frequency NO_3 measurements in mesocosms

Water chemistry measurements in mesocosms were initiated two hours after inserting the mesocosms into the sediment to allow the system to stabilize. Mesocosms were spiked with 5 L of KNO_3 solution (~ 50 mg N L^{-1}) at the beginning of each trial to bring the NO_3-N

concentration to 4 – 5 mg N L^{-1}. In each separate trial the same mass and volume of KNO_3 was added to mesocosms regardless of ambient stream [NO_3]. Samples were drawn from each mesocosm using an automated, multiplexed pumping system (MPS) for small-volume applications (Maxwell et al., 2018). During measurements the MPS temporarily withdrew ~25 mL of sample over <4 min, corresponding to <0.1 mm drop in head, which was assumed to be not high or long enough to generate significant upwelling. The 25 mL pumped was >18x cuvette volume (1.1 mL), providing an adequate pre-measurement rinse to reduce cuvette contamination (Maxwell et al., 2018). In this experiment, samples were purged back to source once they were measured. Samples were drawn at a depth halfway between the water surface and the sediment and 5-10 cm from the inside wall of the mesocosm near the circulating pumps to obtain well-mixed sample volumes.

Samples were drawn from a mesocosm every 6 min resulting in 30-min data intervals for each of the five mesocosms over 24 h. During one sample sequence a sample volume (25 mL) was pumped from a mesocosm to the 4 mm path length quartz cuvette within the spectrophotometer. Following measurement by the probe, if the sample volume was not used for lab analysis the volume was purged back to the source mesocosm to conserve volume. If the sample was collected for lab analysis the volume was purged to a separate outlet line for collection in amber glass vials. Cross-contamination between samples was minimized by purging each line with air. Residual micro-volumes purged to an alternate source were assumed to have a negligible effect on water chemistry due to high source volume (>50 L; Maxwell et al., 2018).

Some adjustments in the multiplexer sampling cycle were made during the study. In the first three trials a sixth inlet line was added to the MPS. This additional line drew water from a container of deionized water (DI) after the fifth mesocosm was sampled, serving as a periodic rinse of the cuvette and internal lines. It was observed that since water chemistry differences between stream and DI water were much greater than differences between mesocosms, the DI rinse actually impaired measurements on the next sample by significantly diluting solute concentrations. After the first three trials the DI rinse was removed. During the final three trials in Spring 2014 adjustments were made to the volume of sample pumped to the probe. Rather than drawing less water (10 mL) when sample collection was not needed each sample sequence drew the same amount of water (25 mL) as those sequences when a lab sample was needed. This

change was made after observing that increasing the volume of the current sample pumped through the quartz cuvette during measurement led to decreased influence of residuals from the previous sample.

To estimate NO_3 removal rates of the stream reach the study incorporated both sediment zones, i.e. Muck and Sand. Three observation sites were chosen within the stream reach with two sites in the Muck zone and one site in the Sand zone. Experiments were run at upstream (Muck), midstream (Muck), and downstream (Sand) locations. Four 24 h trials were performed at each of the Muck sites, and three trials performed at the downstream Sand site.

2.2.4. Probe calibration

The spectro::lyser by s::can used in this study measures absorbance of a water sample in the UV-visible range at wavelengths from 200-750 nm at 2.5 nm intervals. The resulting spectral fingerprint for a given water sample gives 220 decadal absorbance coefficients (m^{-1}) measured at each wavelength emission. The probe is provided with an algorithm that, based off the manufacturer's global calibration, makes estimates of [NO_3] and [DOC]. To verify that the probe's results were calibrated to the water chemistry at this site, however, a site-specific calibration method was used.

Samples for lab analysis were collected during each of the eleven 24 h trials. Up to 25 samples were collected per trial (5 per mesocosm) for lab analysis of NO_3^- and NH_4^+. Sample loss occurred in some trials giving fewer lab-verified measurements. A partial least squares regression (PLSR) package in R (Mevik et al., 2011), developed for use in multi-variate linear regressions and chemometrics, was used to develop a predictive model for each trial. Etheridge et. al (2014) used this technique to develop prediction models for [NO_3] and [DOC]. The R *pls* package is well designed for this application and is described thoroughly in Mevik and Wehrens (2015). Predictive models for [NO_3] were developed. Samples were filtered using a Millipore Sterivex-GP 0.22 μm filter. Chemical analysis for NO_3^- and NH_4^+ was done using standard autoanalyzer techniques (LaChat QuickChem 8000).

The PLSR model was run with spectral fingerprints fitted using lab values (Etheridge et al., 2014). The results of the model's fit were given using 1-10 components with 10-fold cross-

validation. Selection of the ideal number of predictive components was based on the output of the selectNcomp function (method="onesigma") in the *pls* package which chooses the optimum number of components based on the first model where the optimal cross-validation is within one standard deviation of the previous model.

2.2.5. Sediment-driven NO_3 removal rates

NO_3 removal rates were calculated in terms of 1) areal removal rates and 2) uptake velocity. Areal removal rate (Equation 2.1) was calculated as the difference between the initial and final concentrations of the lab-analyzed sample volumes taken from each mesocosm at the beginning and end of each trial. This method used values reported from lab analysis only, and was not based on measurements made by the field spectrophotometer. The total areal mass removal rate (mg N m^{-2} d^{-1}) was calculated as:

$$\text{Areal Removal} = \frac{([NO_3^-]_{intial,lab} - [NO_3^-]_{final,lab}) \times V}{A \times \Delta t} \qquad \text{(Equation 2.1)}$$

where $[NO_3^-]_{initial,\ lab}$ and $[NO_3^-]_{final,\ lab}$ are lab-reported $[NO_3]$ in each mesocosm at the beginning and end of each trial, respectively; V is the volume of the mesocosm using manual depth measurements; A is the cross-sectional area of the open-bottomed barrels; and Δt is the difference in time between when initial and final samples were drawn.

Water chemistry measurements taken by the field spectrophotometer provided time series of $[NO_3]$ in each mesocosm at short data intervals of 30 min. Zero-order (ZO, 2.2), first-order (FO, 2.3), and efficiency loss (EL, 2.4) equations were fitted to $[NO_3]$ time series to determine reaction kinetics. In these models reaction rate, k, is replaced by the term ρ/d, where ρ is the uptake velocity and d is depth of the water column. Substituting ρ/d for k allows apparent removal rates to be normalized by depth. Uptake velocity (2), ρ (m d^-), is widely reported in analyses of stream removal processes (Birgand et al, 2007; Mulholland et al, 2008). Zero-order, first-order, and EL models were fitted to $[NO_3]$ time series for each mesocosm using the *nls* routine in R, a function of the *stats* package that determines the weighted least-squares estimates of parameters for a non-linear model using a relative-offset convergence criterion (Birgand et al., 2016; Messer et al., 2017).

$$C = C_0 - \frac{\rho_{ZO}}{d} * t \qquad \text{(Equation 2.2) Zero-order, } \alpha=0$$

$$C = C_0 * e^{\frac{\rho_{FO}}{d} * t} \qquad \text{(Equation 2.3) First-order, } \alpha=1$$

$$C = \frac{\rho}{d} * t * (\alpha - 1) + {C_0}^{1-\alpha^{1/(1-\alpha)}} \qquad \text{(Equation 2.4) Efficiency loss model, } 0<\alpha<1$$

$$\rho = \rho_{20} * \theta^{T-20} \qquad \text{(Equation 2.5) Arrhenius equation}$$

Mesocosm trials were performed at the three sites on the following dates in 2014 – 2015: Oct-1, Nov-13, Jan-29, Mar-11 (upstream, Muck); Aug-28, Nov-6, Feb-3, Mar-18 (midstream, Muck); Sep-18, Dec-17, Mar-16 (downstream, Sand). Statistical differences in removal metrics between the three sites were assessed using a paired t-test with Satterthwaite correction for non-homogenous variances (unequal population sizes). In order to account for temperature differences between trials, calculated ρ values were normalized using a form of the Arrhenius Equation (2.4) to obtain ρ_{20} values. Temperature coefficients, θ, were calculated by plotting the calculated ρ for each mesocosm at a particular site against temperature. The slope of the linear regression of this data is equal to log(θ). The θ value calculated for each site along with the average water temperature was used to calculate ρ_{20} values for each mesocosm.

2.2.6. Sediment pore water samplers

Sediment pore water samplers were used to measure vertical gradients of $[NO_3]$ and $[NH_4]$ in the sediment pore water (Figure 2-3). Samplers (37 x 10 cm) were made of 2.5 cm thick fiberglass with grooves cut through the sampler at 1 cm spacing creating a vertical array of hollow cells. Cells were filled with DI water then covered by a semi-permeable membrane held in place by two plates fastened across both faces of the sampler. Spectra/Por 1™ regenerated cellulose membrane (molecular weight cutoff = 6 – 8 kDa) was used to allow diffusion of ions into the cells. Samplers were inserted into the sediment and left to reach equilibrium with the soil pore water for up to a week. The result is a vertical profile of ion concentrations in the pore water at 1 cm spacing. Previous studies have observed biogeochemical processes occurring in the sediment based on a similar approach (Kuypers et al, 2003; Vanderborght and Billen, 1975). Porewater

profiles approximated conditions during each mesocosm trial as samplers were placed at the Muck and Sand sites and left for one week at the start of each trial. Sample volumes were extracted from each cell by inserting a 10 mL syringe needle into the cellulose membrane and slowly extracting the cell volume (~5 mL). The syringe was rinsed twice with DI water and air between consecutive cell extractions. These samples were analyzed for NO_3^- and NH_4^+ by standard autoanalyzer techniques (LaChat QuickChem 8000).

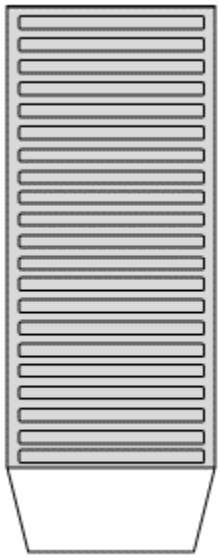

Figure 2-3. Pore water sampler constructed of fiberglass with hollow, fully-penetrating cells at 1 cm intervals. Cells were covered with semi-permeable membrane to allow diffusion of ions from the sediment pore water into the DI water filled cells to establish a vertical profile of [NO_3] and [NH_4] in the sediment pore water.

2.2.7. Temperature measurements

Temperature in the water column of each mesocosm was measured by HOBO Data Loggers with TMC-H1 Outdoor Sensors. Two temperature sensors were placed in each mesocosm. One sensor was located within the water column placed near the multiplexer sampling line. The second sensor was inserted into the sediment to a depth of 5 – 8 cm. Temperature was logged every 15 minutes over the 24 h trial.

2.3. Results

2.3.1. Probe calibration

Separate PLSR models were developed for each trial (Table 2-1). In 9 of 11 trials the correlation between PLSR-predicted and lab-analyzed NO_3^- values was greater than $R^2>0.97$ (0.976-0.999), consistent with findings from other studies showing PLSR models had high accuracy in fitting $[NO_3^-]$ to absorbance fingerprints. Values of the root mean square prediction error (RMSEP) were between 0.037-0.268 and are included in the error terms for uptake velocity ρ in first and zero-order models. A 2 – 4 component model provided the best fit for calibration, with separate components consisting of absorbance fingerprints used to predict estimates of $[NO_3]$. Models with greater than four components generally resulted in greater noise in the predicted time series data.

In only two trials was $R^2<0.97$ (Jan-29, $r^2=0.935$; Mar-18, $r^2=0.948$) and RMSEP noticeably higher than other trials. Poor fit in the Mar-18 PLSR calibration was due to poor calibration of the Lachat auto-analyzer which likely produced erroneous $[NO_3]$ values used in the calibration. Correction of the Mar-18 dataset using a PLSR model with better fit was tested. The Aug-28 PLSR model, which had a high R^2 (0.997) and low RMSEP (0.046), was applied to Mar-18 fingerprints to estimate $[NO_3]$ based on the spectral fingerprints of the Mar-18 trial. This resulted in significantly lower $[NO_3]$ estimates, consistent with lab errors for Mar-18. Additionally, the corrected estimates were similar to those given using the Feb-3 model ($r^2=0.994$; RMSEP=0.050). The model for the Aug-28 trial was applied to the Mar-18 fingerprints to estimate $[NO_3]$.

The cause of lower R^2 for the Jan-29 model is less clear, as the calibration standard for the Lachat was off by <0.1 mg L^{-1}. Applying the Aug-28 and Feb-3 models to Jan-29 fingerprints yielded similar results. The Jan-29 trial did not use a correction model and, along with all others except the Mar-18 trial, used the model developed from lab samples collected from the respective trial.

Table 2-1. Results of the PLSR manual calibration in each trial for both Sand and Muck. For each trial, 20-25 samples were collected following a probe measurement and later analyzed for [NO_3]. Most trials had high r^2 and low RMSEP model values, indicating the PLSR method was adequate for calibration during each trial, with lower model performance in Mar-18 and Jan-29 trials.

Trial	# of components	R^2	RMSEP
28-Aug	4	0.997	0.046
6-Nov	4	0.988	0.044
3-Feb	3	0.994	0.050
18-Mar	3	0.948	0.268
1-Oct	3	0.976	0.106
13-Nov	4	0.995	0.045
29-Jan	2	0.935	0.144
11-Mar	3	0.990	0.067
18-Sep	2	0.993	0.059
17-Dec	4	0.992	0.054
16-Mar	5	0.999	0.037

2.3.2. Time Series of [NO_3]

Calibrated [NO_3] estimates for the four Sediment and one Control mesocosms in each of the 11 trials are shown in Figure 2-4. The MPS was able to collect 40-50 data points per mesocosm in each 24 h trial. In two trials (Feb-3 and Mar-16) low overnight temperatures caused water in the small-diameter MPS tubing to freeze, resulting in gaps in the [NO_3] time series.

Uptake velocity for these trials were calculated using the available data. In the Oct-1, Nov-6, and Nov-13 trials a DI rinse was used at the end of every fourth sample cycle to try to provide cuvette cleaning. This DI rinse, however, produced errors at regular intervals on the mesocosm sampled immediately after the DI rinse. The data for this Sediment mesocosm in these three trials was corrected by removing these points where [NO_3] estimates were affected by the DI rinse before calculating uptake velocity. Additions of KNO_3 raised [NO_3] by 0.7 – 1.6 mg L^{-1},

with Figure 2-4 showing [NO_3] after dissolved KNO_3 was added to mesocosms only. In the Mar-11, Mar-16, and Mar-18 trials only two mesocosms were spiked with KNO_3 to confirm that apparent removal was not just an artifact of dilution from groundwater.

Decreases in mesocosm [NO_3] were seen in nearly all Muck trials, particularly in warmer months. Lower decreases in [NO_3] for Muck mesocosms were seen in the Jan-29 and Feb-3 trials, with Sediment [NO_3] time series closely resembling [NO_3] in the Control mesocosm. Mean net change in [NO_3] in all other Muck trials was 1.00±0.68 and 0.03±0.09 mg N L^{-1} (mean±standard deviation) for Sediment and Control mesocosms, respectively. In the Jan-29 and Feb-3 trials at colder temperatures average mean net change in [NO_3] was 0.21±0.22 and 0.07±0.05 mg N L^{-1} for Sediment and Control mesocosms. Decreases in [NO_3] in Sand Sediment mesocosms were much lower, generally, than in Muck Sediment mesocosms. Mean net change in [NO_3] in Sand trials was 0.37±0.19 and 0.12±0.04 mg N L^{-1} for Sediment and Control mesocosms, respectively, over 24 h.

Cross-contamination in the cuvette was assumed to be negligible in this study as sample volumes were >10x cuvette and differences in [NO_3] between mesocosms was <0.5 mg N L^{-1} (2 mg N L^{-1} in March trials). To preserve water volume in each mesocosm, samples were returned following measurement. Source-contamination was also negligible in this study as concentrations varied by less than 2 mg N L^{-1} and only 40 – 50 purges back to an alternate source occurred on source volumes >30 L (Maxwell et al., 2018).

2.3.3. Kinetics model fitting

There was no preference of either the zero or first-order model, with high R^2 for both models (Table 2-2). Rate constants for zero and first-order models were calculated fitting the observed [NO_3] time series to Equations 2.2 and 2.3, respectively. Range of zero and first-order rate constants, k, in columns 2 and 5 include calculated rates from all four mesocosms in each respective trial. Out of 44 time series for [NO_3] in Sediment mesocosms, 25 had higher R^2 when fitting the first-order model, 14 had higher R^2 using the zero-order model, and 4 were equally fitted by both. Average difference in R^2 between the zero and first-order models, however, was generally <0.02, indicating either kinetics model was well suited to modeling the [NO_3] time series. Both models fitted the data sets well with high R^2 (>0.95) in most cases. All [NO_3] time

series in Sand trials showed better fit for the zero-order model. Quantile-quantile plots of the residuals of zero and first-order models were nearly identical, with first-order residuals showing less heteroscedasticity for those trials with greater total changes in $[NO_3]$ (Mar-18, Aug-28).

Poor model fits were the result of several factors. Some poor model fits ($R^2<0.9$) were associated with $[NO_3]$ time series in which concentration rate changes were both positive and negative (Sep-18, Oct-1, Nov-6, Jan-29, Mar-16). Poor model fits were also associated with trials in which total changes in $[NO_3]$ were low. In these cases, overall change in $[NO_3]$ was low relative to measurement variability. Sources of measurement variability could include the probe's coefficient of variance, cross-contamination within the MPS, or incomplete mixing in the mesocosm. Estimates of ρ from the fitted models are shown in Figure 2-5 and 2-6, with error bars representing the standard error for ρ given from the *nls* function output. One $[NO_3]$ time series in the Jan-29 trial resulted in negative ρ estimates, or net $[NO_3]$ increase.

The efficiency loss (EL) model proved to be a poor model for this application with the exception of a few $[NO_3]$ series. The EL model was able to produce a better fit than either zero or first-order models in the Aug-28 and Mar-18 trials. These trials had high removal rates and visibly non-linear time series with decreasing slope at lower $[NO_3]$. When total decrease in $[NO_3]$ over the trial was high, these time series were able to observe the non-linear decrease in uptake velocity with decreasing $[NO_3]$ concentration. In nearly every other times series the EL model produced results with no practical meaning ($\rho>50$, or $1<\alpha<0$) or did not find ρ or α statistically significant in the model. In other cases, EL approached the same fit (R^2) of the zero-order model as α approached zero, essentially reducing the EL model to zero-order. Reasons for poor fit of the EL model may be the model is not easily fitted at the daily time interval, the data from this experiment doesn't provide a sufficient total decrease in $[NO_3]$ for the EL model to be observed, or that the EL model is not well-fitted when $[NO_3]$ is much greater than 2 mg N L^{-1}.

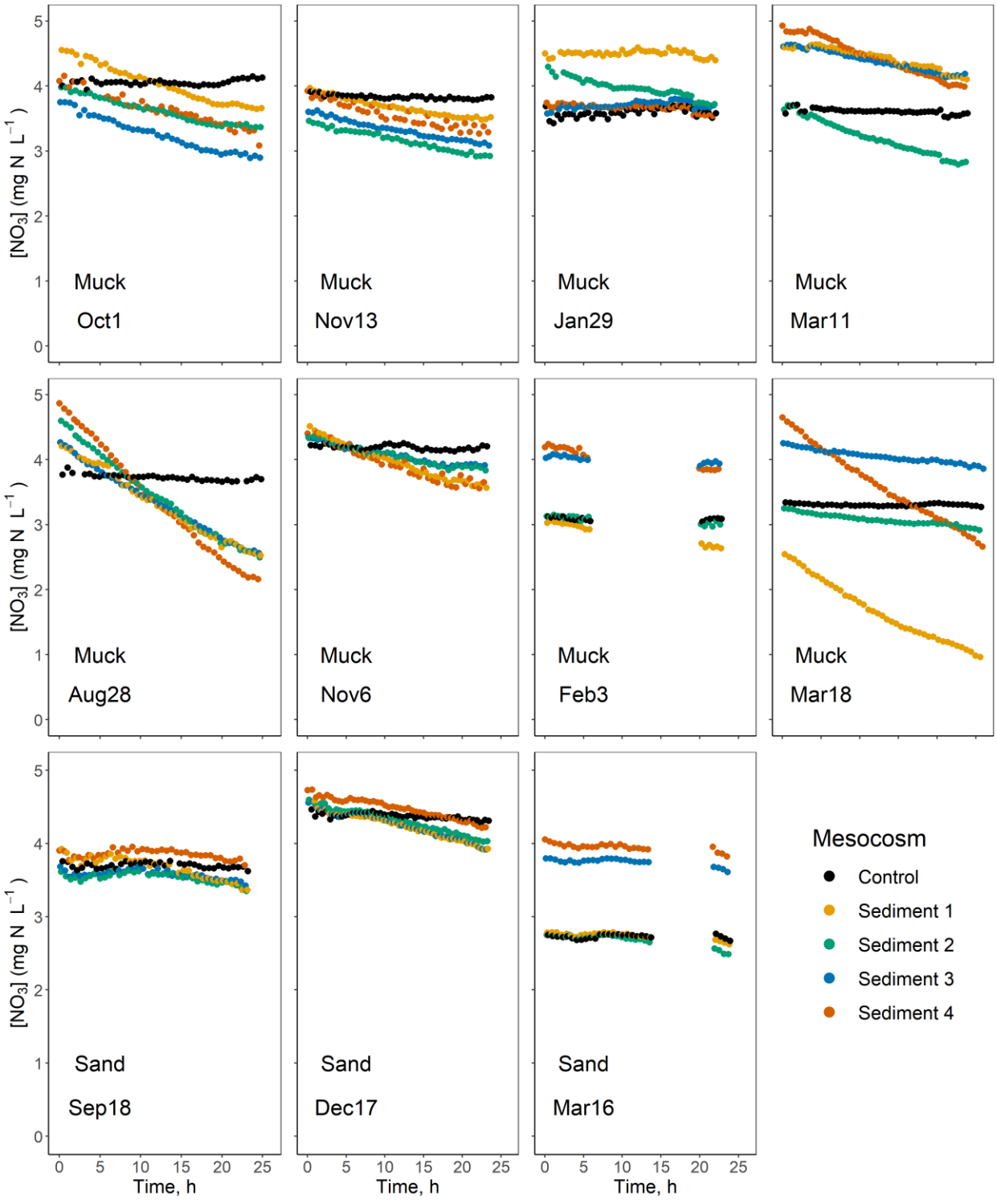

Figure 2-4. Time series of [NO_3] over each 24 h experimental trial. Legend at bottom right labels Sediment and Control mesocosms. Time series only show [NO_3] measurements taken after KNO_3 was added to each mesocosm.

Table 2-2. Time series of [NO_3] in Sediment mesocosms were fitted to zero and first-order kinetics models. Range of ρ values include estimates from fitted time series in all four Sediment mesocosms. Results indicate that for this short duration experiment (<24 h) and at the observed range of [NO_3] (2-6 mg NO_3-N L^{-1}), removal was described equally well by either model, although first order kinetics better fitted [NO_3] time series during trials with large changes in [NO_3].

Trial Date (Sediment)	Zero-order, ρ mg NO_3-N m^{-2} d^{-1}	R^2	Standard Error mg NO_3-N m^{-2} d^{-1}	First-order, ρ m d^{-1}	R^2	Standard Error m d^{-1}
Aug. 28 (Muck)	498 - 584	0.99	5 – 10	0.149 – 0.173	0.99	0.001 – 0.002
Oct. 1 (Muck)	204 – 251	0.95 – 0.98	6 – 8	0.057 – 0.071	0.95 – 0.98	0.001 – 0.002
Nov. 6 (Muck)	145 – 257	0.93 – 0.98	6 – 11	0.036 – 0.065	0.93 – 0.98	0.001 – 0.003
Nov. 13 (Muck)	162 – 201	0.89 – 0.98	4 – 10	0.045 – 0.63	0.89 – 0.98	0.001 – 0.003
Jan. 29 (Muck)	-38 – 182	0.00 – 0.93	7 – 9	0.000 – 0.046	0.00 – 0.93	0.001 – 0.003
Feb. 3 (Muck)	45 – 122	0.76 – 0.99	3 – 6	0.011 – 0.043	0.76 – 0.99	0.001 – 0.002
Mar. 11 (Muck)	177 – 321	0.93 – 0.99	4 – 7	0.040 – 0.093	0.92 – 0.99	0.001 – 0.002
Mar 18 (Muck)	87 – 296	0.97 – 0.99	2 – 3	0.028 – 0.127	0.97 – 0.99	0.001
Sep 18 (Sand)	14 – 113	0.10 – 0.86	6 – 10	0.004 – 0.030	0.10 – 0.85	0.002 – 0.003
Dec 17 (Sand)	144 – 244	0.97 – 0.98	4 – 6	0.032 – 0.058	0.96 – 0.98	0.001 – 0.002
Mar 16 (Sand)	22 – 54	0.63 – 0.84	3 – 5	0.007 – 0.020	0.63 – 0.86	0.001 – 0.002

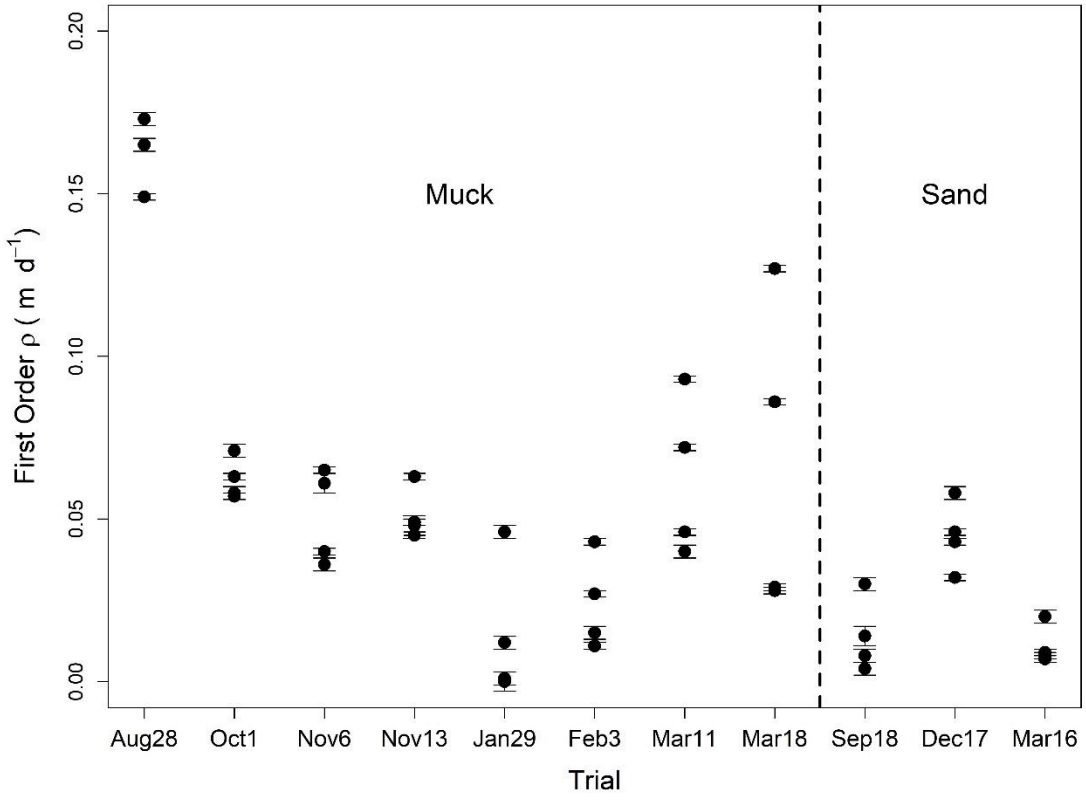

Figure 2-5. First-order removal constants, ρ (m d^{-1}), calculated from the [NO_3] time series during Muck and Sand trials. Trials are shown in chronological order and separated between Muck and Sand trials (dashed line).

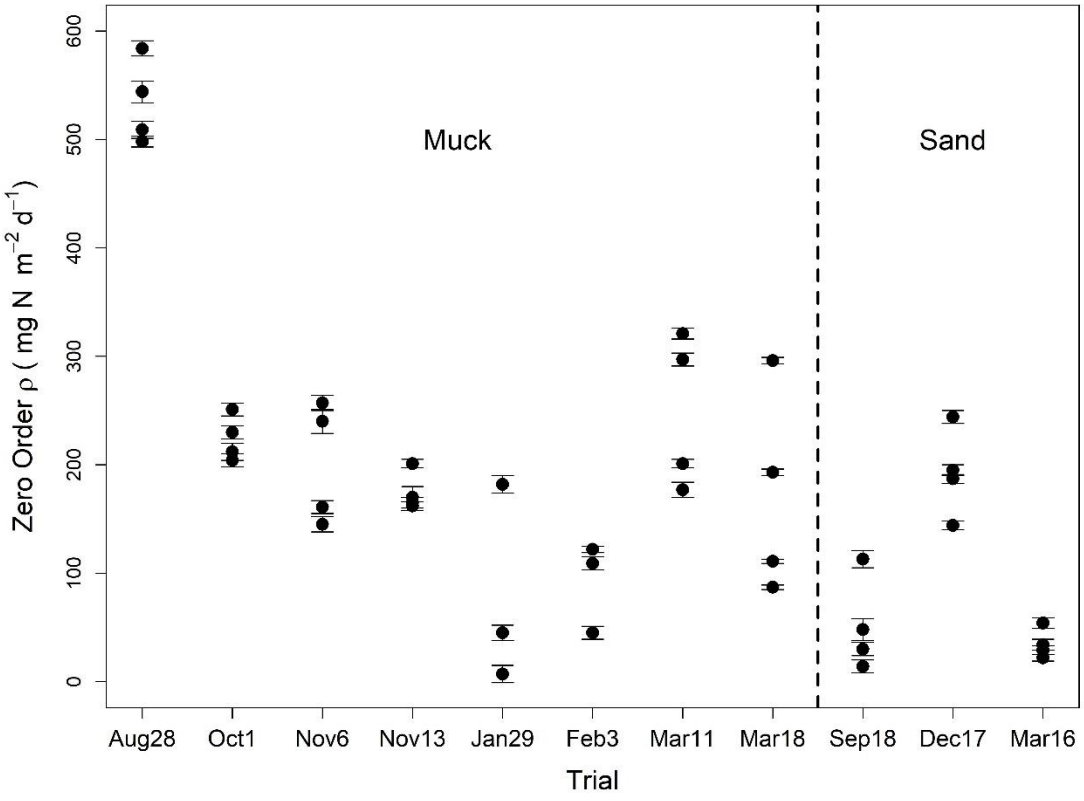

Figure 2-3. Zero-order removal constants, ρ (mg N m^{-2} d^{-1}), calculated from the [NO_3] time series during Muck and Sand trials. Trials are shown in chronological order and separated between Muck and Sand trials (dashed line).

2.3.4. Temperature-corrected removal rates

Temperature coefficients, θ, for Muck1, Muck2, and Sand sites were 1.008±0.006, 1.017±0.006, and 0.989±0.005, respectively. For ρ_{20} values obtained from first-order estimates, there was no significant difference in calculated ρ_{20} values between Muck1 and Muck2 (95% C.I. {-0.054, 0.006}, p=0.105). There were significant differences in ρ_{20} between Muck1 and Sand (95% C.I. {0.016, 0.047}, p<0.001) and Muck2 and Sand (95% C.I. {0.026, 0.085}, p<0.001). Both Muck1 and Muck2 had significantly greater mean ρ_{20} means than Sand. Results were the same when using zero-order estimates for ρ. Using ρ values from zero-order models θ = 1.030 (1.010,1.051), 1.061 (1.047, 1.075), and 0.952 (0.931, 0.973) for Muck1, Muck2, and Sand, respectively. As

with first-order estimates, there were only significant differences in ρ_{20} between Muck1 and Sand (95% C.I. {0.082, 0.200}, $p<0.001$) and Muck2 and Sand (95% C.I. {0.135, 0.280}, $p<0.001$).

The Dec-17 trial was an outlier for Sand trials and caused the temperature coefficient, θ, to be <1. Removing this trial, for the Sand site $\theta = 1.003 \pm 0.017$ from first-order ρ estimates. With this correction, there were still significant differences in ρ_{20} between Muck1 and Sand (95% C.I. {0.026, 0.054}, $p<0.001$) and Muck2 and Sand (95% C.I. {0.036, 0.093}, $p<0.001$).

2.3.5. Pore water profiles

Vertical profiles of pore water [NO_3] and [NH_4] are shown in Figure 2-7. Two pore water samplers were deployed on each date at the same site, and are referred to as Profile 1 and Profile 2. At both Muck sites the sediment surface was a loose and uncompacted layer composed of loose mud, organic matter, and filamentous biofilms. For Muck profiles the surface elevation (0 cm) was less well-defined with a ± 2 cm error. Sand profiles were more precisely defined, assuming neglible measurement error for the surface elevation .

Cross-contamination of cells did not appear to be a problem. On Mar-11 Profile 1 showed signs of cross-contamination, with variable [NO_3] in adjacent cells rather than smooth, directional trends seen on previous dates. [NO_3] also did not decrease quickly to <0.1 mg N L^{-1} near the sediment surface. Inspection of the sampler showed the screwholes holding the faceplate to the fiberglass sampler had become dethreaded, allowing movement of water between cells. This occurred for both samplers in Mar-16 and Mar-18 trials and profiles for these trials are not shown.

In Muck pore water profiles [NO_3] decreased to <0.1 mg N L^{-1} within 1-2 cm of the sediment surface. In several profiles [NO_3] decreased to <0.1 mg N L^{-1} above the sediment surface, although for each Muck profile a ±2 cm error in sediment surface elevation was assumed. Profiles for [NH_4] concentration in Muck sediments showed an opposite trend, with [NH_4] <0.1 above the sediment surface and increasing below the surface. Profiles of [NH_4] were more variable than [NO_3], both within and between sampling dates. Increases in [NH_4] below the

sediment surface ranged from 1.0 mg N L^{-1} in one Nov-6 sampler to 8.7 mg N L^{-1} in Nov-13 samplers. Trends in pore water [NH_4] or [NO_3] were not clearly or consistently related to season.

Pore water profiles in Sand sediments showed different trends than Muck. Although [NO_3] also decreased with depth, [NO_3] was >0.1 mg N L^{-1} up to 10-15 cm below the sediment surface in the Sep-18 trial. This contrasted sharply with Muck profiles in which [NO_3] was <0.1 mg N L^{-1} within 2 cm of the surface. The Dec-17 Sand profiles for [NO_3] showed trends similar to Muck profiles. Sand profiles of [NH_4] differed from Muck in that [NH_4] was <0.3 mg N L^{-1} in nearly all instances. Profiles on Sep-18 and Dec-17 did not show a large increase in [NH_4] moving from above to below the sediment surface.

Nitrate concentrations in the water column above the sediment were comparable to [NO_3] in mesocosms prior to spiking with KNO_3, suggesting that [NO_3] and [NH_4] results from pore water profiles were comparable to conditions seen in the mesocosm trials.

2.3.6. Temperature

Temperatures varied significantly over the 24 h trial with low variability between mesosms within the same trial (Figure 2-8). Temperatures from only one mesocosm in each trial is shown. Differences in water and sediment temperatures between mesocosms were <2º and 1º C, respectively. Control mesocosms were closed-bottom barrels with only water temperature recorded. Mean water temperatures varied by 0.2 – 1.0º C between Control and Sediment mesocosms of the same trial. HOBO dataloggers were not available for the Aug-28 or Sep-18 trials. Water temperature during these trials was measured manually, with temperatures of 25 and 17º C during Aug-28 and Sep-18, respectively (not shown in Figure 2-8).

Sediment temperatures were less variable than water temperatures over the experiment. During the calculation of θ and ρ_{20} in Equation 2.5, mean water temperature for the trial was used for the temperature parameter. Sediment temperatures were less variable than water temperatures over the expeirment. Unshaded Muck sediments (Muck1 and Muck2) appeared to have warmer temperatures relative to Sand in trials during the same time period (i.e. March trials at all sites). Because only water temperature was available for all trials, mean water temperature for the trial was used for the temperature parameter, T, during the calculation of θ and ρ_{20} in Equation 2.5.

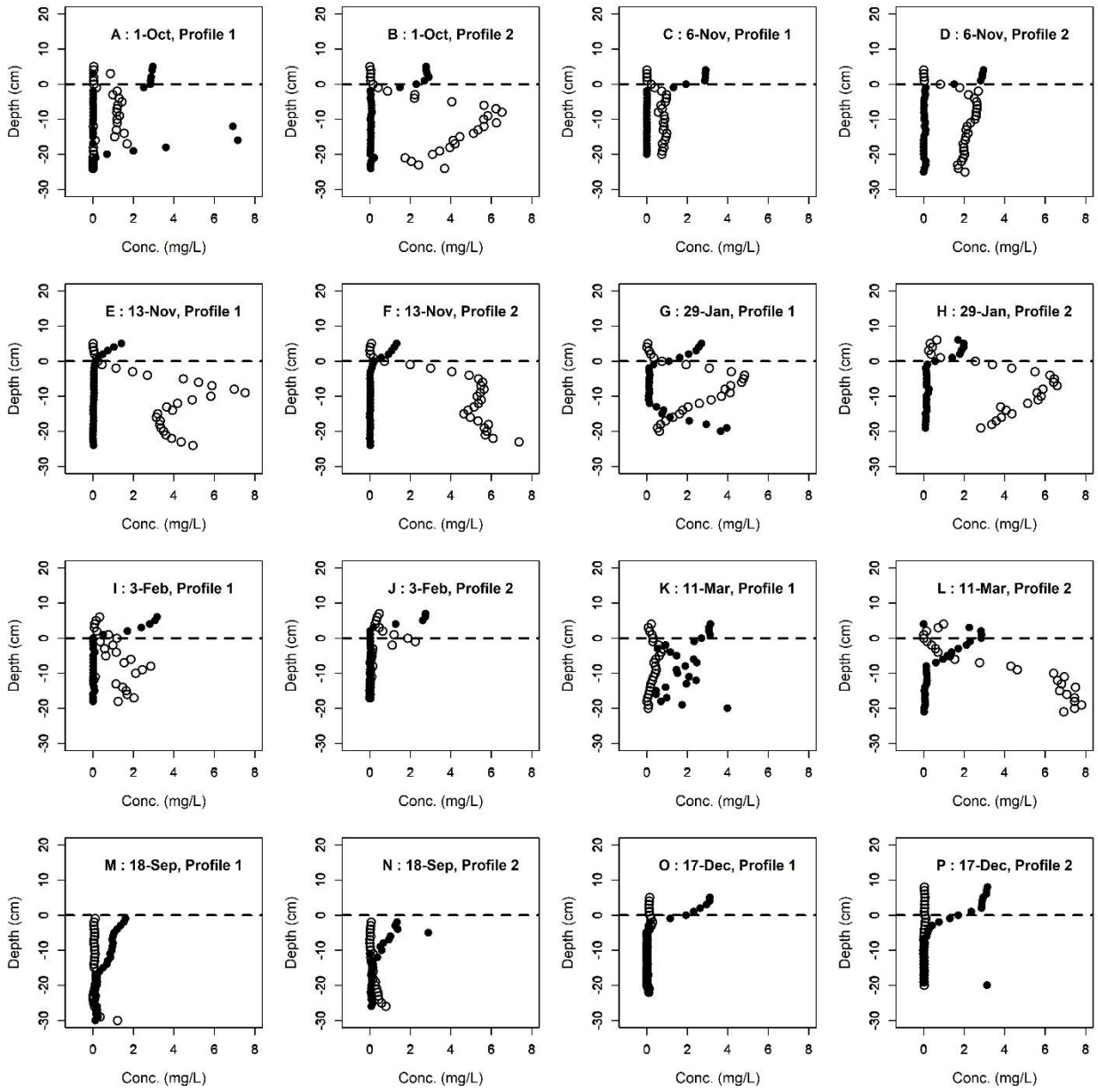

Figure 2-7. Sediment pore-water profiles using discrete volume samplers. Figures A-J indicate samplers placed in Muck sediments, figures K-P indicate samplers placed in Sand sediments. ● = [NO_3], ○ = [NH_4]. Dashed line indicates the sediment surface elevation.

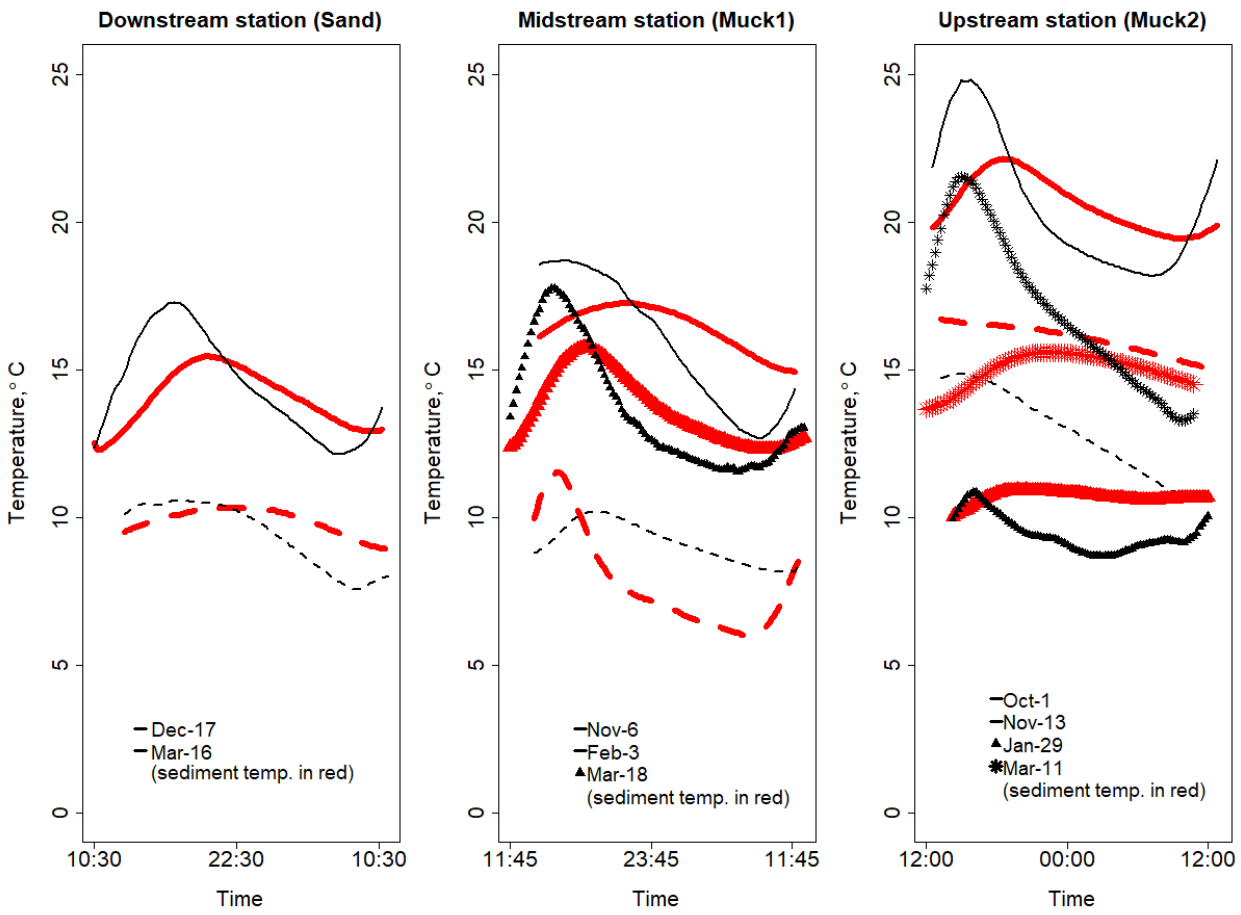

Figure 2-8. Water and sediment temperatures during each of the mesocosm trials. Due to low variability between mesocosms within the same trial, only temperatures from one mesocosm are shown. Temperature data-logging for the Aug-28 and Sep-18 is not shown, when temperatures were measured manually.

2.4. Discussion

2.4.1. In situ mesocosm method

The use of this mesocosm method requires the assumptions that water within each mesocosm was not significantly affected by surface or groundwater. This entails that mesocosms were 1) hydraulically isolated from adjacent surface water and 2) not significantly affected by upwelling low [NO_3] groundwater moving from the sediment into the mesocosm. If these assumptions are valid, then [NO_3] decreases and flux estimates, ρ or *k*, would reflect sediment-driven and possibly other NO_3 consumption.

While this experiment did not quantify or test the validity of these assumptions, the data collected provides some support for these assumptions. In the Mar-11, Mar-16, and Mar-18 trials only two mesocosms were spiked with KNO_3 to confirm that apparent NO_3 removal was not just an artifact of dilution from ground or surface water. Spiked and non-spiked mesocosms in Mar-11 and Mar-18 trials both behaved similarly, with similar slopes of the [NO_3] time series. If dilution from groundwater were driving [NO_3] concentration decreases, slope of the time series would be greater at higher initial [NO_3]. If groundwater upwelling had a substantial effect on mesocosm [NO_3] we would also expect greater apparent removal in Sand mesocosms, since coarse sand sediments tend to have greater hydraulic conductivity then organic sediments (Sebok et al., 2014). Rather, apparent removal was significantly lower in Sand trials, although Sand porewater samplers did show higher [NO_3] in shallow sediments. Additionally, hydraulic head differential measured at this site was < 1 cm. When mesocosms were spiked with 6 L of dissolved KNO_3 this head differential was effectively overcome by adding 2.2 cm of water to the mesocosm.

In one Mar-18 Sediment mesocosm which did not receive a KNO_3 addition, [NO_3] fell to 0.7 mg N L^{-1}, below the initial 2.5 – 3.3 mg N L^{-1} when the trial was started, supporting the assumption that water within mesocosms was not simply being diluted by infiltrating stream water adjacent to the barrel. In this instance slope of the non-spiked Sediment mesocosm was similar to the KNO_3 spiked mesocosm, even as [NO_3] fell below that of stream. If dilution from infiltrating stream water were driving [NO_3] decreases, higher slopes would be expected at higher initial [NO_3]. The strong effect of temperature in Muck sediments also supports that downward flux of NO_3^- was the primary driver of [NO_3] decreases, rather than upwelling of low [NO_3] groundwater or surface water infiltration.

2.4.2. Seasonal trends

In Muck sediments NO_3 removal rates followed seasonal trends that were correlated with temperature. Zero-order uptake velocities, k_{ZO}, followed similar trends and were highest during August (T_{mean} = 25 °C) at 500 - 580 mg NO_3-N m^{-2} d^{-1}. Moving into the fall k_{ZO} declined during the October (T_{mean} = 21 °C) and November trials (T_{mean} = 12 and 16 °C) to 200 - 250 mg NO_3-N m^{-2} and 140 – 260 mg NO_3-N m^{-2}, respectively. Uptake velocity was at a minimum during the winter trials of January (-40 – 180 mg NO_3-N m^{-2}, T_{mean} = 9 °C) and February (40 – 120 mg

NO_3-N m^{-2}, T_{mean} = 7 °C). With increasing temperatures in both Mar-11 (T_{mean} = 17 °C) and Mar-18 trials (T_{mean} = 12 °C) k_{ZO} increased to 90 – 320 mg NO_3-N m^{-2}. The highest uptake velocities seen in March trials were significantly greater than in October, even though temperatures on Oct-1 were 4 and 10°C warmer than Mar-11 and Mar-18. For this site, the data indicate that predicting NO_3 removal from temperature alone, even at the same site, would fail to capture seasonal variability. Nitrate removal appeared to resume quickly following long periods of low temperature through the winter, with March rates comparable to those seen at the end of summer even at lower temperatures.

Sand trials had an opposite seasonal trend. Zero-order uptake velocity was low during Sep-18 (T_{mean} = 17°C) and Mar-16 (T_{mean} = 14°C) at 10 – 110 mg NO_3-N m^{-2} d^{-1} and 20 – 50 mg NO_3-N m^{-2} d^{-1}, respectively. During the coldest Sand trial in December (T_{mean} = 9.4°C) rates were significantly higher (140 - 240 mg NO_3-N m^{-2} d^{-1}) than the other two warmer Sand trials. The highest NO_3 removal rates were seen during the coldest month at the Sand site, again indicating that sediment-driven NO_3 removal is not predicted well by temperature only.

Control mesocosms performed as expected, although in some cases gave surprising results. Control mesocosms contained stream water only and were expected to be mostly unreactive. In trials where free-floating, filamentous algae were present in the stream they were included in both the Sediment and Control mesocosms. Autotrophs in the water column immobilizing NO_3 could have produced some apparent reduction but N removal was expected to be sediment-driven. Feb-3, Mar-11, and Mar-18 Controls had negative areal removal rates, an apparent NO_3 source. This could have been the result of autotrophic exudates or mineralization/nitrification, although differences in initial and final [NO_3] in Feb-3 and Mar-11 Controls were less than the probe's uncertainty. In two of the trials, Jan-29 (Muck) and Sep-18 (Sand), uptake velocities in the Control were within the 95% C.I. of rates seen in Sediment mesocosms.

2.4.3. Effect of sediment

Muck trials had significantly greater uptake velocity than Sand, even when values were normalized for temperature. This is most likely due to the higher carbon content of the sediment fueling denitrification (Table B-1). Muck1 and Muck2 were not significantly different in their uptake velocities. Both sites can be considered part of the Muck zone of this stream reach, and

zero-order ρ values for this sediment type ranged from 7-584 mg N m^{-2} d^{-1} throughout the year showing high seasonal variability. Muck ρ_{20} ranged from 10-483 mg N m^{-2} d^{-1}, with Sand ρ_{20} ranging from 12-185 mg N m^{-2} d^{-1}. By normalizing to ρ_{20} it is clear that differences in uptake velocities are the result of differences in the sites. Other contributing factors could include the in-stream vegetation that as present in some Muck trials. At the Sand site there was no in-stream vegetation present throughout the year.

The sediment pore water profiles showed in Muck soils [NO_3] was reduced to <0.1 mg N L^{-1} within 2-3 cm of the surface. In most cases decreases in [NO_3] began 1-3 cm above the surface, showing a strong downward gradient and an apparent sink in the sediment. Some trials (Oct-1 and Jan-29) showed the presence of potential aerobic microzones at depths below which NO_3 appeared to be depleted. Sand profiles (Sep-18) did not exhibit as strong a downward gradient with [NO_3] remaining 10-13 cm below the surface, although on Dec-17 nitrate profiles at the Sand site were similar to Muck. While the [NO_3] time series provide ample data showing removal was higher in Muck trials, results of the pore water samplers provide further support that removal is sediment driven. The higher organic content of the Muck sediments would prevent denitrification from being carbon limited, reducing NO_3 more quickly over a shorter distance as it diffuses into the soil.

For this stream, the length consisting of Muck sediments (~1,600 m) would provide most of the NO_3 removal services. Considering all values Muck mean removal was greater than sand by 114 mg N m^{-2} d^{-1}. Excluding the Dec-17 trial, removal was greater by 165 mg N m^{-2} d^{-1} with Muck mean nitrate removal 5x greater than that in Sand.

A number of studies on nutrient cycling in streams illustrate the effect of sediment organic content on nitrogen transformations. Arango and Tank (2007) showed that the greatest predictor of annual denitrification rates in agricultural and forested streams was sediment C content. Both denitrification and nitrification were positively correlated with sediment C. The authors also found that denitrification was not significantly correlated with stream DOC concentration, similar to findings by Bernhardt and Likens (2002) during an acetate addition in a forested stream. Waters et al. (2014) found that, among four northeastern streams, that denitrification was largely C limited. Arango et al. (2008) also showed that benthic organic matter significantly

impacted denitrification rates in Midwest streams when [NO_3] was above published half-saturation constants (0.2 – 1.3 mg NO_3-N L^{-1}). In the present study, [NO_3] in the Claridge stream were always above N-limiting conditions for denitrification. It would be expected that, in this agricultural setting with high N inputs, denitrification is primarily C limited.

2.4.4. Effect of leaf litter

As previously discussed, Dec-17 was an outlier among the Sand trials. During late December leaf packs accumulated in the bottom of the stream, trapped by low velocity and in-stream obstacles. Leaf packs were likely from dense overhead canopy at the Sand site, rather than the upstream reach which had virtually no tree cover. Mesocosms during this trial were placed over the top of these 2-5 cm deep leaf packs and inserted into the sediment isolating packs within the barrel. Significant increases in NO_3 removal were seen, with Dec-17 mean uptake velocity equal to 193 mg N m^{-2} d^{-1} and greater than Mar-16 and Sep-18 by 158 and 141 mg N m^{-2} d^{-1}, respectively, despite temperatures on Dec-17 being 9.4 °C, i.e., 5.0 and 7.3 °C lower (Table 2-2). Dec-17 for the sand sediment had comparable mean uptake velocity to Nov-6 and Nov-13 Muck trials where temperatures were 3-4°C warmer, and 2-4 times the mean removal of Jan-29 and Feb-3 Muck trials at similar temperatures.

Pore water samplers placed within leaf packs indicated a stronger downward [NO_3] gradient relative to Sep-18 (Figure 2-7). The Sand site, lacking in available carbon for most of the year, showed significant increases in NO_3 removal once carbon was present. While this could be interpreted as Sand having a higher treatment potential than Muck when carbon is present, this should not be attributed to the sediment itself. Rather the overlying leaf pack provided carbon substrate for denitrifiers and likely led to lower DO levels within the leaf pack as carbon was consumed. This may indicate that available carbon in the water column, rather than the sediment, better facilitates denitrification since exchange is more rapid in the water column relative to diffusion into the sediment. This is supported by the fact that mean NO_3 removal on Dec-17 was higher than rates seen in Muck trials at similar temperatures.

2.4.5. Submerged vegetation

Submerged vegetation resulted in significant heterogeneity of nitrate removal rates. At the end of February submerged and emergent macrophytes believed to be pennywort (*Hydrocotyle ranunculoides*) appeared at the Muck sites. The Mar-18 trial was the only trial to capture the effect of vegetation. Two mesocosms (Sediment 1 & 4) on the side of the channel included this dense vegetation while the other two mesocosms (Sediment 2 & 3) were placed in the middle of the stream containing little to no vegetation (Figure 2-9). One of each mesocosm in both vegetated zones was spiked with KNO_3 while the other was not. Zero-order uptake velocities were 259 and 171 mg N m^{-2} d^{-1} in vegetated columns and 83 and 89 mg N m^{-2} d^{-1} in unvegetated, with first-order velocities of 0.086 and 0.064 m d^{-1} in vegetated columns and 0.026 and 0.021 m d^{-1} in unvegetated. This vegetated zone, present for roughly 8 months of the year, saw 2-4 times the removal potential of the less vegetated stream center. Some of the NO_3 removal would have been caused by plant uptake and the biofilm present on this substrate. Using the mean removal rate of unvegetated mesocosms in this trial (86 mg N m^{-2} d^{-1}), the sediment would have been only responsible for 33 – 50% of NO_3 removed. Reddy (1983) found areal removal rates of 200 mg N m^{-2} d^{-1} for pennywort, while Reddy et al. (1985) found a range of 321-645 mg N m^{-2} d^{-1} for the same species. It is probable that NO_3 uptake was vastly increased in this zone by plant uptake rather than microbial activity, although lab samples showed increases in $[NH_4]$ over the course of the Mar-18 trial in Vegetated mesocosms. Plants preferentially take up NH_4^+ as an inorganic N source; Reddy et al. (1983) showed 84% of N uptake by pennywort was NH_4 rather than NO_3 when applied at equal amounts. If ammonia concentrations did not decline and actually increased, it is less clear that plant uptake was predominantly responsible for N removal. Since only changes in $[NO_3]$ and $[NH_4]$ were measured, rather than direct measurements of denitrification products (e.g. N_2, N_2O), the method used in this study cannot separate plant uptake from denitrification or other NO_3 removal pathways.

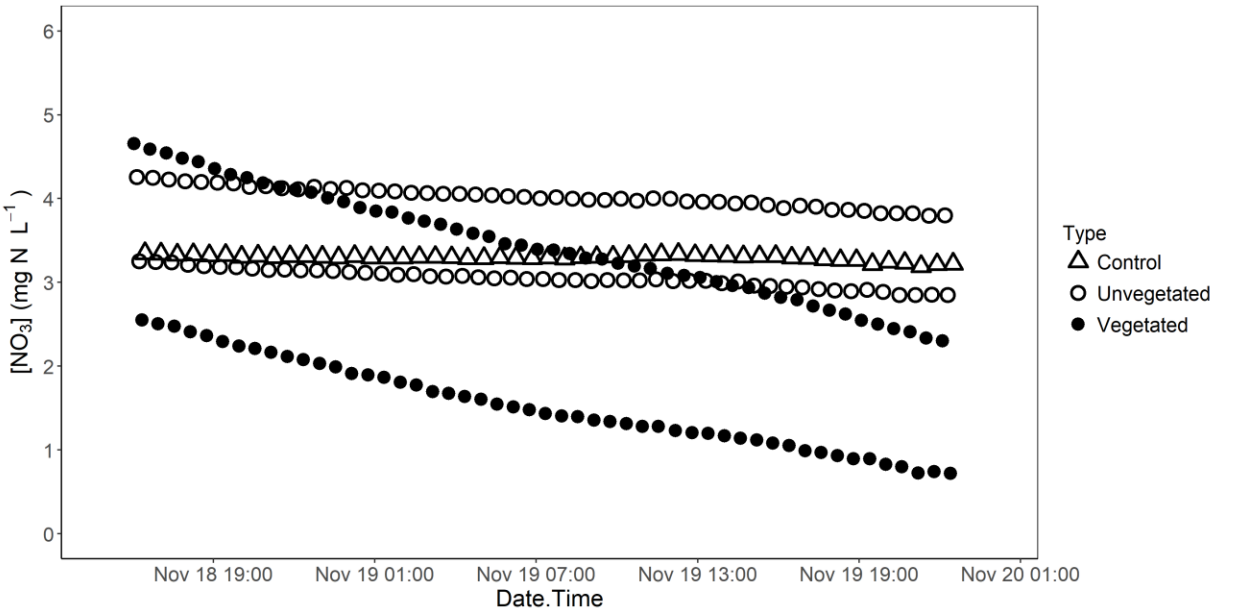

Figure 2-9. Time series of [NO_3] during the Mar-18 trial in which two mesocosms were placed over submerged vegetation (Vegetated) and two mesocosms were placed over sediment without vegetation (Unvegetated). Mesocosms containing submerged vegetation had 2 – 4x greater NO_3 removal, compared with mesocosms without.

Several studies have looked at the impact of carbonaceous substrate, in the water column or sediment, on denitrification rates. O'Brien et al. (2018) showed stimulated nitrate removal in a stream following additions of leaf litter relative to a reference stream. A number of studies have shown the ability of denitrification to occur within epiphyton biofilms found on submerged vegetation (Eriksson and Weisner, 1996; Law et al. 1993). Denitrification can occur on woody material (Healy et al., 2006; Saliling et al., 2007), periphyton (Sirivedhin and Gray, 2006), and suspended particles (Michotey and Bonin, 1997), even within well-mixed aerobic water columns. Anoxic conditions on submerged surfaces provide microsites for denitrification to occur.

An important question is whether these extrusive features (e.g. plants, leaf packs, attached biofilms) in a well-mixed water column contribute greater potential for nitrate removal, relative to sediment-driven processes. While denitrification can be limited by both carbon and nitrogen (i.e. supply-limited), it can also be constrained by rates of diffusion (i.e. rate-limited). Denitrification in a well-mixed water column is less limited by diffusion of NO_3 to the active site, as NO_3 depleted in the nearby boundary is quickly replaced. Emergent vegetation, such as in the Mar-11 and Mar-18 trials, provide surfaces for denitrifying biofilms to attach and be directly

adjacent to NO_3-rich water, although the higher rate of NO_3 delivery may be counteracted by the inhibition of DO on denitrification rates. Alternatively, dense leaf packs in the water column may provide zones where nutrient-rich water moves easily to the denitrifying sites, while also provide a thick enough zone for DO to be sufficiently depleted. In this sense, leaf packs function more similarly to three-dimensional denitrifying zones (e.g. woodchip bioreactors, denitrification walls) rather than diffusion of NO_3 across a large distance (i.e. depth of water column) to denitrifying sites across a two-dimensional surface (i.e. stream sediment). In dense leaf packs, the diffusive boundary layer is small, hydraulic residence time and likelihood of anoxic conditions high, and rate of substrate turnover (i.e. NO_3) high. Further research could examine the relative contributions of both sites, sediments and leaf packs, to overall nitrate removal to improve ecosystem services.

2.4.6. Pore water samplers

Pore water samplers supported the hypothesis that denitrification was a major driver of nitrate removal in this stream. Rusmana (2005) did a similar study to characterize nitrogen dynamics in sediments in an English estuary. Decreasing concentrations of N moving downward into the soil indicate a removal mechanism in the soil. Decreasing [NO_3] moving deeper into the sediment were observed in both Sand and Much sites. The [NO_3] gradient in Muck was much greater than in Sand. In nearly all samplers deployed in the Muck [NO_3] approached zero (< 0.1 mg/L) within the first 3 cm of the sediment surface. In some Muck trials NO_3^- approached zero above the sediment surface. The sediment surface elevation at the Muck site was more imprecise as the surface was a very loose, uncompact sediment with suspended organic matter making the surface hard to clearly define. There did not appear to be any clear seasonal trends in the downward gradient at the Muck site. We may have expected a steeper gradient or lower concentrations at lower depths during the warmer months, but this did not appear to be the case. In Jan-29 and Oct-1 trials there were sudden spikes in [NO_3] below the elevation at which [NO_3] had approached zero, possibly indicating oxygenated microzones within the sediment.

Several studies have observed the phenomenon of oxygen-rich or depleted microzones (Jensen et. al, 2005; Brandes & Devol, 1995); Svensson & Leonardson (1996) showed how microzones caused by bioturbation led to changes in denitrification and oxygen uptake, which was likely in

this stream as many burrowing invertebrates were seen. Nitrate penetrated deeper in Sand sediments, up to 12-18 cm in the Sep-18 trial. The lack of a carbon source restricting respiration would result in greater DO in the water; oxygen inhibits denitrification by being preferentially used as an electron acceptor, and by preventing activity of several denitrifying enzymes. Steeper [NO_3] gradients were seen in the Dec-17 samplers. This was likely the result of the accumulation of leaf litter in the stream where the samplers were deployed resulting in increased respiration, lower DO, and better conditions for denitrification to occur.

Ammonium profiles tended to follow an opposite trend. In surface waters oxidized NO_3 is the dominant form of inorganic nitrogen since adequate DO allows nitrification to occur. Low [NH_4] (<0.2 mg L^{-1}) were seen at elevations above the surface sediment, although some trials showed higher [NH_4] in the water column. In Muck sediment there was an increase in [NH_4] at nearly the same depths at which [NO_3] began to decrease. Increases in [NH_4] followed decreases in [NO_3]. These trends are expected to be related, but not causal. Denitrifiers would begin to use nitrate during respiration in the absence of oxygen. The respiration of OM would result in the production and extracellular release of NH_4 as byproduct. As NH_4 accumulates, the lack of oxygen prevents transformation to nitrate by nitrifiers. Thus, we would expect [NH_4] to be low where NO_3 is abundant, and vice versa. Samplers deployed in Sand did not as clearly exhibit this trend. Ammonium concentrations remained low throughout the profile, except in Profile 2 of the Sep-18 trial were some increases were seen at the point of near zero [NO_3]. Sediment cores at the Sand site showed low organic content in the sediment. With lower organic matter respiration would be diminished with less DO in the pore water being consumed. With more DO present it is likely that any NH_4 in the Sand was able to be nitrified in the presence of oxygen. Unfortunately this study was not able to directly measure [DO] in the sediment to validate this.

2.4.7. Temperature

While temperature clearly had an impact over seasonal changes, it did not appear to affect NO_3 removal kinetics at the daily time scale. Several [NO_3] time series showed noticeable decreases in NO_3 removal rates, although they did not appear to be in sync with falling temperatures during the night. This may be due to a time lag between the reduction of metabolism in the sediment as temperature dropped and the subsequent slowed downward flux of N into the sediment.

Alternatively, the temperature change over 24 hours may not have produced a detectable change in NO_3 flux. Denitrification occurring in the sediment would not have been exposed to temperature changes greater than 3° C in any of the trials.

The upstream (Muck1) trials were selected for additional analysis using Eq. 3.1 to observe effect of the daily temperature flux on uptake velocity. Mean temperatures from each mesocosms at the Muck1 site, for water column and soil profiles separately, were plotted against their respective calculated first-order ρ value. For the Muck1 trials a value of θ_{water}= 1.028 and $\rho_{20,water}$=0.062 m d^{-1} were calculated from water column temperatures, and θ_{water}= 1.020 and $\rho_{20,water}$=0.060 m d^{-1} were calculated from sediment temperatures. For each mesocosm, a first-order equation was applied in which uptake velocity, ρ_{temp}, was updated every 15 minutes using temperature data collected by the HOBO data loggers. The result was a first-order removal rate with non-constant ρ (ρ_{temp}). These time series were compared to the original first-order time series fitted to the spectrophotometer data with constant ρ value (ρ_C). Removal rates were alternately over or under predicted by non-constant uptake velocity depending on the relation between the original ρ_C value and the temperature adjusted ρ_{temp} predicted by ρ_{20} and θ. If $\rho_C > \rho_{temp}$ over the 24-period, the temperature-corrected method over-predicted [NO_3] and under-predicted removal rate; if $\rho_C < \rho_{temp}$, the temperature-corrected method under-predicted [NO_3] and over-predicted removal rate. This is not alarming since ρ_{20} and θ are both empirical, fitted parameters based on the full data set at that site. Errors in prediction would be expected and would be related to the residual between ρ_C and the linear regression between temperature and ρ_C.

What was interesting to note was the change in ρ_{temp} seen over the daily time step even at higher temperature fluctuations. Mesocosms in the Oct-1 trial had the greatest range of temperature over the 24 h period and should thus be expected to have greatest variation in ρ_{temp}. Temperature fluctuation of the water column in these mesocosms was roughly 6° C, while it was <3° C in the sediment. Considering the higher temperature flux in the water column, the variability in ρ_{temp} among mesocosms over 24 h was 0.00343-0.00398. Similarly, the standard error of prediction when fitting the first-order model to the concentrations predicted by the spectrophotometer and PLSR was 0.00147-0.00228. The variation of ρ_{temp} predicted by correcting ρ_{20} according to temperature was marginally outside the margin of error when fitting a ρ_{FO} to the [NO_3] time series. As the bulk of NO_3 removal is believed to occur in the sediment, sediment temperature

flux may be more accurate in adjusting ρ_{temp} values. Standard deviation of ρ_{temp} values corrected by the sediment temperature profiles was 0.00109-0.00136, falling within the margin of error of prediction for ρ_C. While it is widely accepted that temperature has an effect on microbial activity, it is not clear from this method that variability in metabolic rates are detectable at the daily scale. The data here illustrate that even with the advanced measurement capabilities of the s::can spectrophotometer it would be difficult to observe changes in reaction kinetics driven by temperature changes over the course of a day. Rather, this technology may be more suited to detecting short-term changes in NO_3 removal kinetics in a lab setting where temperature could be varied considerably and maintained for longer periods.

2.4.8. Nitrogen uptake kinetics

In this study there didn't appear to be any model preference for the zero or first-order model, when considering model residuals and R^2 values. The EL model was poorly suited to modeling. O'Brien & Dodds (2010) found non-linear kinetics of NO_3 uptake in three different Kansas streams that were well described by EL and Michaelis-Menten (MM) kinetics, although fits were not largely different from a simple linear model. O'Brien et. al (2007) found that EL models better described uptake rates in Kansas streams over first-order and MM kinetics, although concluded that EL models may apply better to streams with chronic nitrate loading rather than short-term pulses. Aguilera et al. (2013) also found support for the EL model with non-linear declines in uptake velocity at higher concentrations. These three studies were done on the reach-scale using tracer injections over a wide range of [NO_3] (0.1 – 12.0 mg N L^{-1}). A microcosm study performed by Fleming-Singer and Horne (2002) also found mixed-order kinetics that closely resembled first-order rate. Birgand et al. (2016) found in very similar laboratory mesocosms run over several days and with higher initial nitrate concentrations (~10 mg N L^{-1}), that the EL model was consistently the best model, although the MM model was a close second. The first order model was ruled out in most cases. While the literature supports a non-constant removal rate, our data supports that at the site scale and in streams with high ambient N (>2 mg N L^{-1}) NO_3 removal may be adequately modeled by a zero-order rate constant. The inability of the EL model to describe most of our data may have been the result of only sampling for 24 hours. At the daily time scale, we cannot see the decrease in concentration necessary to observe reduced efficiency or concentration-dependent uptake.

2.4.9. Selecting data intervals

The multiplexer technology used in this project provides high temporal resolution of data even with high number of replicates. Samples were drawn from a mesocosm every six minutes; with five mesocosms this gave 30 min. data intervals on each mesocosm. Over the 24-h trial this gave upwards of 48 data points for each mesocosm. Some trials ran slightly longer than 24 h and had greater number of data points in the time series. These data points, making up the full data set for a mesocosm, were used to make estimates of uptake velocity, ρ, in the first and zero-order kinetics models. While greater data resolution is favorable for predicting kinetics there is likely a point past which increased resolution doesn't provide additional benefits to parameter estimates. Lower data intervals may provide comparable estimates. Figures 2-10, 2-11, and 2-12 below illustrate this concept. For each full data set there is a degree of error in the calculation of ρ which can be characterized by a 95% C.I. for the calculation. To compare how a smaller sample size would affect calculation error, the full data (i.e. all 40 – 50 $[NO_3]$ measurements taken in a given trial) was subsampled without replacement with n= 3, 5, 8, 15, 20, 25, 30, 35, and 40 sample size. The same method for calculating ρ from the full data set was then applied to these reduced populations in 200 subsampling iterations. This method of subsampling comparison was applied to one mesocosm time series from the Aug-28, Jan-29, and Mar-18 trials. Three mesocosms were selected that had a range of zero order ρ values (Jan-29 ρ_{zo} =0.046; Mar-18 ρ_{zo} =0.245; Aug-28 ρ_{zo}=0.584) to determine if kinetic rates had an effect on acceptable subsample size.

From Figs. 2-10, 2-11, and 2-12 it is clear that an acceptable tradeoff occurs somewhere between 20-30 data points, with 25 data points over 24 hours giving acceptable results. At this sample size the 95% C.I. for the sample of ρ values generated by the smaller data set falls within the 95% C.I. of the ρ estimate. We would be 95% confident that the kinetic rate calculated by taking 25-30 samples from each mesocosm would give an estimate within the margin of error of a data set with more samples. On the daily time scale, this would be a sampling interval of 48-58 minutes. Some studies use hourly measurements to determine reaction rates, which may be acceptable, although these findings suggest less than hourly data is needed for making estimates of the true mean with 95% confidence. While the MPS is capable of sampling at smaller time intervals, it is intended for remote use in the field. Greater data intervals would extend battery

life, decrease wear on the system and pump, and require less memory of the spectrophotometer. The figures illustrate how sample size of n= 3 – 20 could produce estimates outside of the 95% C.I. of the full data set. These reduced sample intervals would equate to sampling every 1.5 – 8.0 h. The subsampling technique used in this analysis, however, did not require randomly selected data points to be at regular intervals of each other.

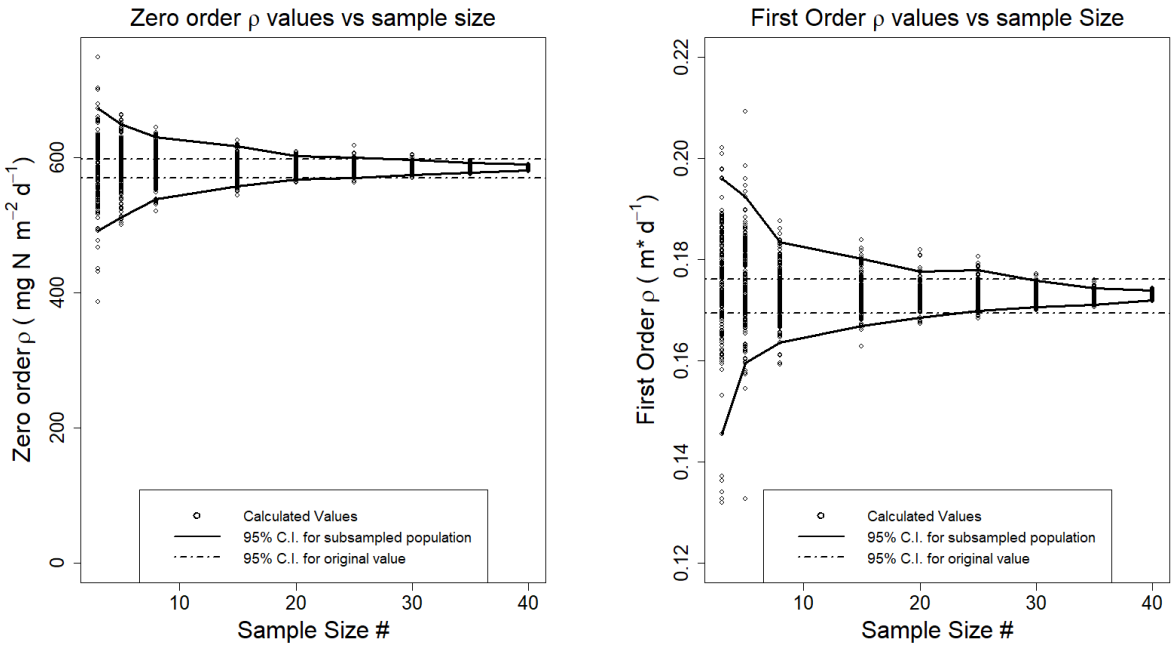

Figure 2-10. Results of analysis subsampling [NO_3] time series for the Aug-29 trial to determine how fewer sampling points would affect the prediction of uptake velocity. Results indicate that less than hourly sampling is needed to make an estimate of uptake velocity with 95% confidence.

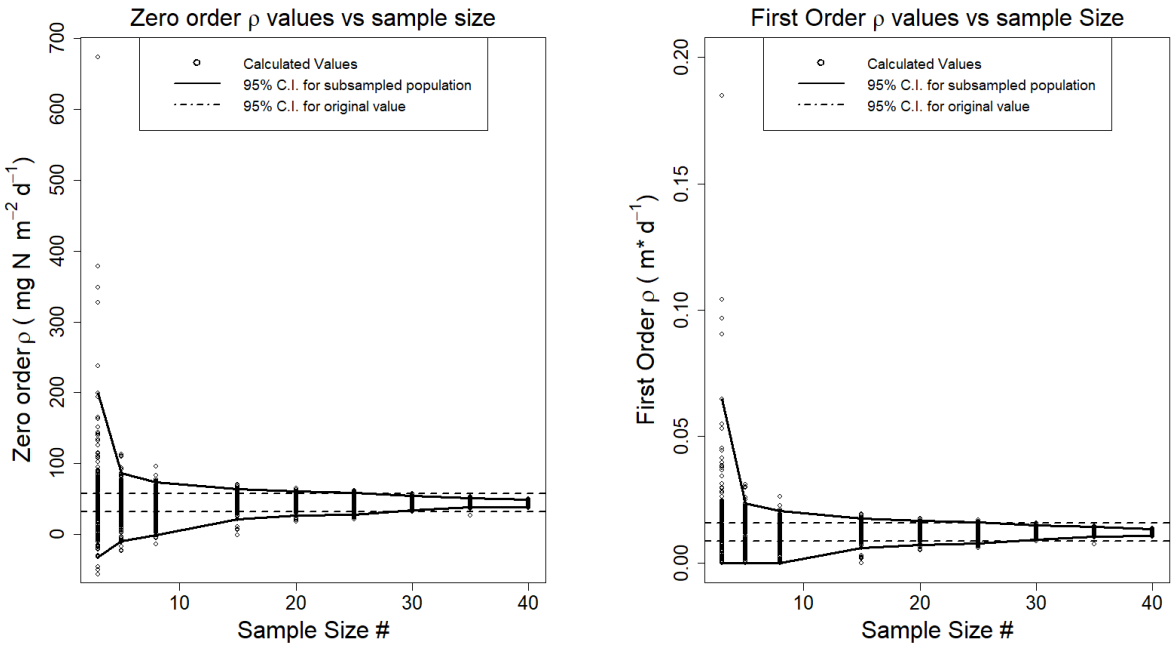

Figure 2-11. Results of analysis subsampling [NO_3] time series for the Jan-29 trial to determine how fewer sampling points would affect the prediction of uptake velocity. Results indicate that less than hourly sampling is needed to make an estimate of uptake velocity with 95% confidence.

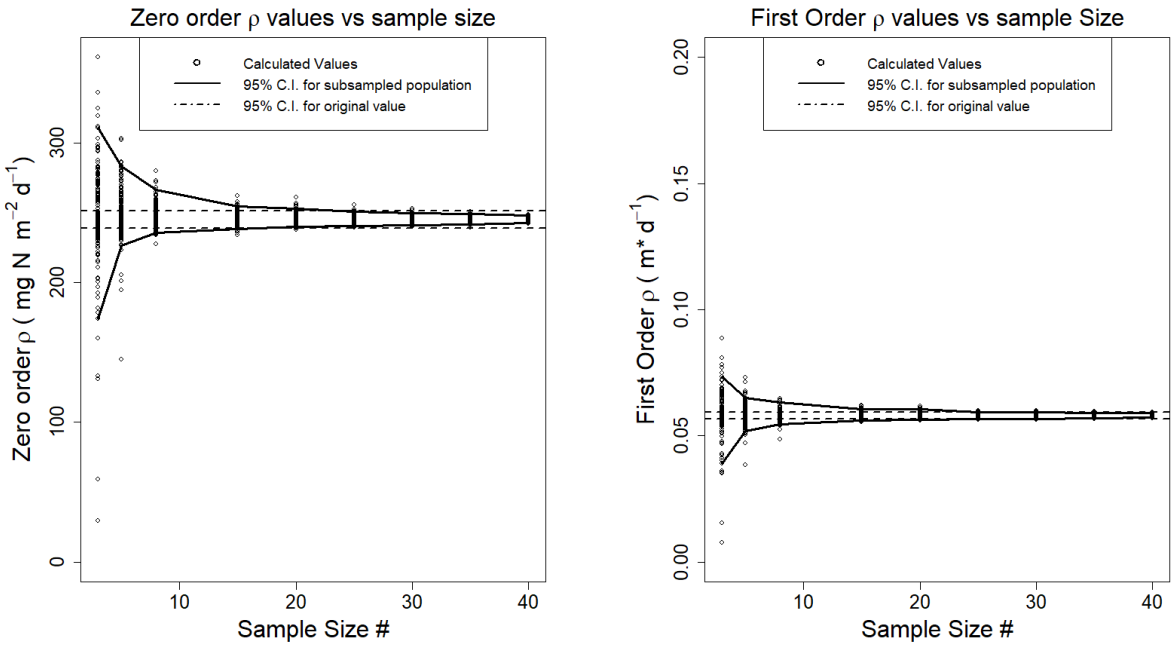

Figure 2-12. Results of analysis subsampling [NO_3^-] time series for the Mar-18 trial to determine how fewer sampling points would affect the prediction of uptake velocity. Results indicate that less than hourly sampling is needed to make an estimate of uptake velocity with 95% confidence.

2.5. Conclusions

The *in situ* mesocosm method using high-frequency, multi-point sampling successfully measured changes in nitrate concentrations in eleven 24-h experimental trials. The multiplexer was able to obtain data at <36 min intervals in four treatment replicates (Sediment) and one control mesocosm (Control). The method was able to observe high seasonality in nitrate removal rates, with the effect of season varying depending on sediment zone. Nitrate removal rates in Muck sediments were higher at warmer temperatures, while Sand sediments had higher removal during the winter likely attributed to leaf pack accumulation. The method provides an easily repeatable method for determining in situ nitrate removal using multiple replicates. Although the MPS was not specifically necessary for this experiment, subsetting data collected in several experiments showed that less than hourly samples would be required for more accurate estimates of uptake kinetics. It is possible that samples could be collected as frequently manually, but the MPS makes this significantly less labor intensive.

There are several limitations to the in situ mesocosm method presented. The method uses spectrophotometric measurement to track changes in nitrate concentration within each mesocosm. Unlike other methods such as acetylene-block and N_2 accumulation, it does not indicate what microbial process is responsible for nitrate removal or even if the process is microbially-driven. The method requires assuming that reductions in nitrate removal are caused by a removal mechanism within the sediment, with the most likely cause being microbial activity. It is not possible to determine which microbial process involving consumption of nitrate is responsible. Most of the discussion in this chapter suggests that nitrate removal is the product of denitrification. This is supported by higher nitrate removal in organic Muck sediments with available carbon as the electron donor. It is not impossible that nitrate removal was also driven by Annamox bacteria, especially since Muck pore water profiles showed high [NH_4] within the sediment. Nitrate removal through DNRA is less likely since negligible increase of [NH_4] was observed.

While the *in situ* mesocosm method is useful for observing sediment-driven nitrate flux, it is not suited for observing reach scale processes. The method does not capture nitrogen removal that occurs as stream water moves through the riparian zone, along extended hyporheic flow paths, or

through extrusive in stream features (e.g. woody debris, dams). The method is further limited to soft-bottom sediments where mesocosms can be easily inserted. The large *in situ* mesocosm method is best suited for quantifying nitrate removal at the site scale and comparing differences in removal across sediments and seasons, and as such serves as an acceptable benchmark method.

2.6. References

Aguilera, R., Marcé, R., & Sabater, S. (2013). Modeling nutrient retention at the watershed scale: Does small stream research apply to the whole river network? *Journal of Geophysical Research: Biogeosciences, 118*(2), 728-740.

An, S., & Gardner, W. S. (2002). Dissimilatory nitrate reduction to ammonium (DNRA) as a nitrogen link, versus denitrification as a sink in a shallow estuary (laguna Madre/Baffin bay, texas). *Marine Ecology Progress Series, 237*(4)

Arango, C. P., Tank, J. L., Schaller, J. L., Royer, T. V., Bernot, M. J., & David, M. B. (2007). Benthic organic carbon influences denitrification in streams with high nitrate concentration. *Freshwater Biology, 52*(7), 1210-1222.

Arango, C., & Tank, J. L. (2008). Land use influences the spatiotemporal controls on nitrification and denitrification in headwater streams. *Journal of the North American Benthological Society, 27*(1), 90-107.

Arnold, J., Corre, M. D., & Veldkamp, E. (2008). Cold storage and laboratory incubation of intact soil cores do not reflect in-situ nitrogen cycling rates of tropical forest soils. *Soil Biology and Biochemistry, 40*(9), 2480-2483.

Arthington, Á. H., Naiman, R. J., Mcclain, M. E., & Nilsson, C. (2010). Preserving the biodiversity and ecological services of rivers: New challenges and research opportunities. *Freshwater Biology, 55*(1), 1-16.

Ashkenas, L. R., Johnson, S. L., Gregory, S. V., Tank, J. L., & Wollheim, W. M. (2004). A stable isotope tracer study of nitrogen uptake and transformation in an old-growth forest stream. *Ecology, 85*(6), 1725-1739.

Aulakh, M., Doran, J., & Mosier, A. (1991). Field evaluation of four methods for measuring denitrification. *Soil Science Society of America Journal, 55*(5), 1332-1338.

Bernhardt, E. S., & Likens, G. E. (2002). Dissolved organic carbon enrichment alters nitrogen dynamics in a forest stream. *Ecology, 83*(6), 1689-1700.

Bernhardt, E. S., Palmer, M. A., Allan, J. D., Alexander, G., Barnas, K., Brooks, S., et al. (2005). Synthesizing U.S. river restoration efforts. *Science, 308*(5722), 636-637. Retrieved from http://www.jstor.org/stable/3841978

Birgand, F., Aveni-Deforge, K., Smith, B., Maxwell, B., Horstman, M., Gerling, A. B., et al. (2016). First report of a novel multiplexer pumping system coupled to a water quality probe to collect high temporal frequency in situ water chemistry measurements at multiple sites. *Limnology and Oceanography: Methods,*

Birgand, F., Skaggs, R. W., Chescheir, G. M., & Gilliam, J. W. (2007). Nitrogen removal in streams of agricultural Catchments—A literature review. *Critical Reviews in Environmental Science and Technology, 37*(5), 381-487. doi:10.1080/10643380600966426

Brandes, J. A., & Devol, A. H. (1995). Simultaneous nitrate and oxygen respiration in coastal sediments: Evidence for discrete diagenesis. *Journal of Marine Research, 53*(5), 771-797.

Burgin, A. J., & Hamilton, S. K. (2007). Have we overemphasized the role of denitrification in aquatic ecosystems? A review of nitrate removal pathways. *Frontiers in Ecology and the Environment, 5*(2), 89-96.

Christensen, P. B., Nielsen, L. P., Sørensen, J., & Revsbech, N. P. (1990). Denitrification in nitrate-rich streams: Diurnal and seasonal variation related to benthic oxygen metabolism. *Limnology and Oceanography, 35*(3), 640-651.

ERIKSSON, P., & WEISNER, S. (1996). Functional differences in epiphytic microbial communities in nutrient-rich freshwater ecosystems: An assay of denitrifying capacity. *Freshwater Biology, 36*(3), 555-562.

Etheridge, J. R., Birgand, F., Osborne, J. A., Osburn, C. L., Burchell, M. R., & Irving, J. (2014). Using in situ ultraviolet-visual spectroscopy to measure nitrogen, carbon, phosphorus, and suspended solids concentrations at a high frequency in a brackish tidal marsh. *Limnology and Oceanography: Methods, 12*(1), 10-22.

Fields, S. (2004). Global nitrogen: Cycling out of control. *Environmental Health Perspectives, 112*(10), A556-63.

Fleming-Singer, M. S., & Horne, A. J. (2002). Enhanced nitrate removal efficiency in wetland microcosms using an episediment layer for denitrification. *Environmental Science & Technology, 36*(6), 1231-1237.

Frumkin, H. (2001). Beyond toxicity: Human health and the natural environment. *American Journal of Preventive Medicine, 20*(3), 234-240.

Groffman, P. M., Altabet, M. A., Böhlke, J., Butterbach-Bahl, K., David, M. B., Firestone, M. K., et al. (2006). Methods for measuring denitrification: Diverse approaches to a difficult problem. *Ecological Applications, 16*(6), 2091-2122.

Groffmann, P. M., Zak, D. R., Christensen, S., Mosier, A., & Tiedje, J. M. (1993). Early spring nitrogen dynamics in a temperate forest landscape. *Ecology, ,* 1579-1585.

Hart, S., & Binkley, D. (1985). Correlations among indices of forest soil nutrient availability in fertilized and unfertilized loblolly pine plantations. *Plant and Soil, 85*(1), 11-21.

Hauck, R., & Bremner, J. (1976). Use of tracers for soil and fertilizer nitrogen research. *Advances in Agronomy, 28*, 219-266.

Healy, M. G., Rodgers, M., & Mulqueen, J. (2006). Denitrification of a nitrate-rich synthetic wastewater using various wood-based media materials. *Journal of Environmental Science and Health Part A, 41*(5), 779-788.

Ingemann Jensen, S., Kühl, M., Glud, R. N., Jørgensen, L. B., & Priemé, A. (2005). Oxic microzones and radial oxygen loss from roots of zostera marina. *Marine Ecology-Progress Series Online, 293*, 49-58.

Kaplan, S. (1995). The restorative benefits of nature: Toward an integrative framework. *Journal of Environmental Psychology, 15*(3), 169-182.

Kondolf, G. M. (1996). A cross section of stream channel restoration. *Journal of Soil and Water Conservation, 51*(2), 119-125.

Kuypers, M. M., Sliekers, A. O., Lavik, G., Schmid, M., Jørgensen, B. B., Kuenen, J. G., et al. (2003). Anaerobic ammonium oxidation by anammox bacteria in the black sea. *Nature, 422*(6932), 608-611.

Law, C., Rees, A., & Owens, N. (1993). Nitrous oxide production by estuarine epiphyton. *Limnology and Oceanography;(United States), 38*(2)

Lin, C. (2017). *Characterization of the solute dynamics signature of an agricultural coastal plain stream, north carolina, USA* North Carolina State University.

Messer, T. L., Burchell II, M. R., Birgand, F., Broome, S. W., & Chescheir, G. (2017). Nitrate removal potential of restored wetlands loaded with agricultural drainage water: A mesocosm scale experimental approach. *Ecological Engineering, 106*, 541-554.

Mevik, B., & Wehrens, R. (2007). The pls package: Principal component and partial least squares regression in R. *Journal of Statistical Software, 18*(2), 1-24.

Michotey, V., & Bonin, P. (1997). Evidence for anaerobic bacterial processes in the water column: Denitrification and dissimilatory nitrate ammonification in the northwestern mediterranean sea. *Marine Ecology Progress Series, 160*, 47-56.

Mulholland, P. J., Valett, H. M., Webster, J. R., Thomas, S. A., Cooper, L. W., Hamilton, S. K., et al. (2004). Stream denitrification and total nitrate uptake rates measured using a field^ 1^ 5N tracer addition approach. *Limnology and Oceanography, ,* 809-820.

O'Brien, J. M., & Dodds, W. K. (2010). Saturation of NO3-uptake in prairie streams as a function of acute and chronic N exposure. *Journal of the North American Benthological Society, 29*(2), 627-635.

O'Brien, J. M., Warburton, H. J., Graham, S. E., Franklin, H. M., Febria, C. M., Hogsden, K. L., et al. (2017). Leaf litter additions enhance stream metabolism, denitrification, and restoration prospects for agricultural catchments. *Ecosphere, 8*(11)

Parkin, T. B., Sexstone, A. J., & Tiedje, J. M. (1985). Comparison of field denitrification rates determined by acetylene-based soil core and nitrogen-15 methods. *Soil Science Society of America Journal, 49*(1), 94-99.

Payne, W. (1991). A review of methods for field measurements of denitrification. *Forest Ecology and Management, 44*(1), 5-14.

Postel, S., & Carpenter, S. (1997). Freshwater ecosystem services. *Nature's Services: Societal Dependence on Natural Ecosystems, 195*

Reddy, K. (1983). Fate of nitrogen and phosphorus in a waste-water retention reservoir containing aquatic macrophytes. *Journal of Environmental Quality, 12*(1), 137-141.

Reddy, K., & Tucker, J. (1985). Growth and nutrient uptake of pennywort (hydrocotyle umbellata L.), as influenced by the nitrogen concentration of the water. *J.Aquat.Plant Manage, 23*, 35-40.

Saliling, W. J. B., Westerman, P. W., & Losordo, T. M. (2007). Wood chips and wheat straw as alternative biofilter media for denitrification reactors treating aquaculture and other wastewaters with high nitrate concentrations. *Aquacultural Engineering, 37*(3), 222-233.

Sebok, E., Duque, C., Engesgaard, P., & Boegh, E. (2015). Spatial variability in streambed hydraulic conductivity of contrasting stream morphologies: Channel bend and straight channel. *Hydrological Processes, 29*(3), 458-472.

Sirivedhin, T., & Gray, K. A. (2006). Factors affecting denitrification rates in experimental wetlands: Field and laboratory studies. *Ecological Engineering, 26*(2), 167-181.

Sorensen, J. (1978). Denitrification rates in a marine sediment as measured by the acetylene inhibition technique. *Applied and Environmental Microbiology, 36*(1), 139-143.

Steingruber, S. M., Friedrich, J., Gachter, R., & Wehrli, B. (2001). Measurement of denitrification in sediments with the 15N isotope pairing technique. *Applied and Environmental Microbiology, 67*(9), 3771-3778.

SVENSSON, J., & Leonardson, L. (1996). Effects of bioturbation by tube-dwelling chironomid larvae on oxygen uptake and denitrification in eutrophic lake sediments. *Freshwater Biology, 35*(2), 289-300.

Vanderborght, J., & Billen, G. (1975). Vertical distribution of nitrate concentration in interstitial water of marine sediments with nitrification and denitrification. *Limnology and Oceanography, 20*(6), 953-961.

Waters, E. R., Morse, J. L., Bettez, N. D., & Groffman, P. M. (2014). Differential carbon and nitrogen controls of denitrification in riparian zones and streams along an urban to exurban gradient. *Journal of Environmental Quality, 43*(3), 955-963.

Wohl, E., Dwire, K., Sutfin, N., Polvi, L., & Bazan, R. (2012). Mechanisms of carbon storage in mountainous headwater rivers. *Nature Communications, 3*, 1263.

CHAPTER 3: Drying-rewetting Cycles Affect Nitrate Removal Rates in Woodchip Bioreactors. Maxwell, B. M., Birgand, F., Schipper, L. A., Christianson, L. E., Tian, S., Helmers, M. J., et al. (2018). *Journal of Environmental Quality.*

3.1. Introduction

Woodchip bioreactors (aka denitrifying bioreactors) are used as a conservation practice to treat nitrate-nitrogen (NO_3-N) in drainage water. Woodchips provide the electron donor for microbial denitrification to reduce aqueous nitrate to gaseous forms (N_2, N_2O) and remove nitrogen (N) from drainage water. Woodchip bioreactors are increasingly used in various applications which include poorly drained crop fields (Christianson et al., 2012; David et al., 2016; Woli et al., 2010), dairy (Schipper et al., 2010) and hog farms (Liu, 2017), aquaculture units (Lepine et al., 2016) , hydroponics operations (Warneke et al., 2011), urban bioretention cells (Chen et al., 2013; Kim et al., 2003) and regenerative stormwater conveyance (Brown et al., 2010). A number of factors affect the treatment efficiency of woodchip bioreactors including hydraulic residence time (HRT) (Greenan et al., 2009; Hoover et al., 2016), water temperature (David et al., 2016; Hoover et al., 2016), age of woodchips (David et al., 2016; Robertson, 2010), bed design (Cameron and Schipper, 2011; Christianson et al., 2011), influent concentration (Lepine et al., 2016), and carbon (C) source (Cameron and Schipper, 2010). One of the recurring challenges reported in the bioreactor literature is decreasing NO_3 removal efficiency over time, particularly after the first year of operation. Most woodchip bioreactors are currently not actively managed, and increasing removal efficiency may seem out of reach as it is controlled by environmental variables (temperature, water chemistry) or media characteristics (age, carbon source).

There is evidence, however, that post-installation management could increase denitrification rates within woodchip bioreactors. One such management option is drying-rewetting cycles. In the soil literature, a number of studies investigated the effect of drying-rewetting (DRW) cycles on the rates of soil metabolic processes (Beare et al., 2009; Borken and Matzner, 2009; Miller et al., 2005; Ruser et al., 2006; Palmer et al., 2016; Xiang et al., 2008). Drying-rewetting cycles in soils have been linked to increased nitrous oxide (N_2O) production (Ruser et al., 2006), increased C and N leaching (Miller et al., 2005), and changes in microbial and fungal communities (Gordon et al., 2008). Woodchip bioreactors are comparable to soil systems with an organic substrate degraded by microbes taking part in various biogeochemical processes.

The hypotheses for this work are that aerobic conditions provided during bioreactor drying cycles would 1) increase breakdown of organic matter (OM) and 2) stimulate NO_3 removal by increasing C availability. Literature suggests that increased breakdown of OM produces greater CO_2 and other byproducts of respiration including dissolved organic carbon (DOC). This DOC is generally lower molecular weight (MW) and more easily used as an electron donor, leading to an increase in denitrification rates (Dodla et al., 2008; Zarnetske et al., 2011; ÆsØy et al., 1998). Drying-rewetting cycles could potentially be used to increase NO_3 removal rates in woodchip bioreactors on-site. However, there is a lack of research investigating the impact of DRW cycles on C and N fluxes in engineered systems with high C content media (e.g. woodchip bioreactors). One exception includes Christianson et al. (2017) who found a 96 h DRW event increased NO_3 removal in woodchip columns from 48 to 90%, although the study was only able to observe the effects of a single DRW event. The objective of this study was to determine whether repeated, short-term DRW cycles could sustainably increase NO_3 removal in woodchip bioreactors.

The term 'drying-rewetting' in this article, consistent with previous literature on DRW cycles, refers to the process of draining previously saturated woodchips, allowing air to enter the pore space previously filled by water, and saturating the pores with water again. During the 'drying' part of the cycle, the woodchip porous medium is drained to equilibrium and is thus still moist and not 'dry' as the term might suggest.

3.2. Materials and methods

3.2.1. Experimental design

A 287-day column experiment was performed at the NCSU Biological and Agricultural Engineering facility from February to December 2017. Eight experimental units consisted of 15.2 cm diameter, 95 cm tall polyvinylchloride (PVC) columns filled with aged woodchips. Woodchips were collected from a 6-year-old field bioreactor treating drainage from a hog lagoon sprayfield in Plymouth, NC. Woodchips were analyzed for carbon, nitrogen and phosphorus content and pH (Table C-1). From bottom to top, each column was filled with a base gravel bed (6 cm depth, 5–10 mm diam. gravel) covered by plastic mesh (2 mm mesh size) to provide uniform, upward flow though the column. On top of the gravel layer, 50 cm of woodchips (4,650–5,086 g, wet weight) were packed in each column, leaving 39 cm of headspace above the

woodchips. The columns were capped to limit exchange with the atmosphere. The water inlet was installed at the gravel layer level, and the outlet even with the top of the woodchip layer. Inlet and outlet hose barb connections were installed on the column sidewall (Figure C-1). Upflow (0.68±0.14 L h^{-1}; mean±standard deviation) was provided by an 8-channel ISMATEC (IP series, ISMATEC, Wertheim, Germany) peristaltic pump for an 8±2 h HRT (Table C-2, Figure C-2) in each column.

Each of the eight columns was assigned one of two conditions (n=4). The control (SAT) consisted of continuous saturation provided by a constant and uninterrupted upflow during the entire experiment. Water level in the SAT columns remained constant at the level of the overflow. The treatment (DRW) consisted of exposing the woodchips to aerobic conditions for 8 h in weekly drying-rewetting cycles. Flow to DRW columns was stopped once a week by disconnecting the inflow lines. After stopping flow the DRW columns were drained rapidly (~15 min time to drain) and left unsaturated for 8 h, exposing the woodchips to aerobic conditions. Then, flow to DRW columns was reestablished by reconnecting the inflow line. The duration of unsaturated conditions was based on results from preliminary lab experiments and for practical experimental reasons in which columns could be drained and resaturated at the beginning and end of the day. Outflow from DRW columns occurred ~8 h after restarting flow. A single DRW cycle referred to each draining event and subsequent rewetting. All columns received constant upflow for 287 days, outside the 8 h drained times of the DRW columns, and DRW columns were exposed to 39 DRW cycles. Moisture content (MC) of woodchips within the columns after 8 h of unsaturated conditions, measured using the oven-dry method, was calculated as MC = 57 – 59%.

Columns were fed from a 1,200 L stock tank filled with decholorinated (Omnipure K5626-JJ filters) tap water spiked with KNO_3 (19.5±1.3 mg NO_3-N L^{-1}) such that inlet NO_3-N concentrations were similar to those seen in tile drainage (David et al., 2016; Christianson et al., 2012). Two stock tanks were used such that one tank could be mixed and degassed to lower dissolved oxygen (DO) levels in the stock tank (7.2±0.7 mg DO L^{-1}, Figure C-3) while still providing uninterrupted flow to columns from the other tank. Flow rates to each column were measured 2-3 times daily by collecting outflow in 9 L jugs for 5–12 hours and measuring outflow volume with a graduated cylinder.

During the first three weeks (Start-up Periods A, B, C) all columns received the SAT control (continuous saturation) to determine variability between columns prior to applying the DRW treatment. After the first three weeks, columns were ranked according to N removal rates and columns with the second, fourth, sixth, and eighth highest N removal rates were assigned the DRW treatment, and the others the SAT control. Collected data were given a Period number corresponding to the number of prior DRW cycles (e.g. Period 2 for data collected after the second and prior to the third DRW cycle, with one week between each DRW cycle).

3.2.2. High frequency water physico-chemistry analysis

Stock tank and column outflow water chemistry were measured using a small volume multiplexed pumping system (MPS) (Maxwell et al., unpublished data, 2018) coupled to a high frequency spectrophotometer. The MPS sequentially pumped 25 mL samples from each column for absorbance measurement by a field spectrophotometer (Spectro::lyser; manufactured by s::can, Type SP-1-035-p0-s-NO-075) fitted with a 4 mm pathlength, 1.1 mL flow through quartz cuvette (46-Q-4, Starna Cells, Inc.). The spectrophotometer and MPS measurement sequence was adjusted such that the stock tank and each column outflow concentrations were measured on 2 h intervals. Nitrate concentrations were calculated from the measured absorbance following methods previously described (Birgand et al. 2016; Etheridge et al., 2014; Vaughan et al., 2017).

During measurements, water was pumped via 0.9 mm diameter PFTE tubing (0.2 mL s^{-1}) through a 60 µm plankton mesh screened intake placed in the top 3 cm of the saturated media in each column. To minimize cross-contamination between columns the first 5 mL of sample volume were diverted to waste, after which 20 mL of sample volume (>18 times cuvette volume) were pumped for spectrophotometric analysis, according to validated sampling procedures for the small volume MPS (Maxwell et al., unpublished data, 2018). Low pump rate and sample volume (25 mL every 2 h) were used to limit impact of sampling on column hydraulics (sample volume <2% of cumulative flow volume over 2 h). Forty sample volumes analyzed by the spectrophotometer were submitted for lab analysis (EPA Method 353.2, BAE Environmental Analysis Lab, North Carolina State University) to calibrate the probe for NO_3 (Etheridge et al., 2014). Due to equipment and personnel limitations, column outflow was monitored using this

high-frequency sampling method during Days 0–98, 147–171, and 252–287, while columns received continuous upflow over the entire 287 days.

Temperature (Figure C-2) and DO (Figure C-3) of column outflow were measured hourly using Presens® temperature sensors and oxygen dipping probes (DP-PSt3, Presens Precision Sensing GmbH). Temperature and DO sensors were inserted through the top of the column and placed such that the sensor tips were at least 2 cm below the surface of woodchip media, per manufacturer's specifications. A manual two-point calibration for DO sensors was performed using 0 and 100% air saturation (a.s.) standards. A 0% a.s. standard was made by dissolving 1 g Na_2SO_3 and 1 mg $CoCl_2$ in 1 L DI water, mixing gently, and left to stand for 30 min. A 100% a.s. standard was made by vigorously bubbling tap water with an air stone and bubbler for 30 min and left to stand for 30 min.

3.2.3. Discrete composite water chemistry

During selected Periods, composite outflow samples were collected to quantify additional water chemistry parameters of interest. Composite samples were taken by collecting outflow from each column over 1.5 h (~1.0 L). Grab samples were collected from all columns immediately after rewetting of drained columns and again prior to subsequent drainage. Grab samples were analyzedfor NO_3, total ammonia nitrogen (TAN) (EPA Method 351.2), total Kjeldahl nitrogen (TKN) and total nitrogen (TN) (Standard Methods 4500-Norg B, Bran & Leubbe Autoanalyzer III), and DOC and total carbon (TC) (EPA415.1 with Teledyne Tekmar Apollo 9000, 0.45 µm filter). Composite samples were collected during Periods 2, 3, 4, 5, 36, and 39.

3.2.4. Nitrate removal rates

Volumetric NO_3 removal rates (R_{NO3}) for each column were calculated as the difference between column inlet NO_3-N concentrations ($[NO_3]_{in}$) and outlet NO_3-N concentrations ($[NO_3]_{out}$) times the flow rate over the woodchip-filled column volume (0.009 m^3), yielding units in g N m^{-3} d^{-1}.

3.2.5. Statistical analysis

Mixed linear model analysis was performed in SAS (SAS Proc MIXED, SAS 9.4) on data collected from all columns to determine the treatment effect on NO_3 removal rates, as well as the effect of Period number and Period Day, or the number of days since rewetting of DRW columns. Period number rather than time was used as a variable to reduce autocorrelation of high-frequency measurements. The statistical model in this analysis is described by Equation 3.1,

$$Y_{i,j} = \mu + \alpha_i + b_j + (\alpha b)_{i,j} + \varepsilon_{i,j,k} \qquad \text{(Equation 3.1)}$$

Where $Y_{i,j}$ = predicted nitrate removal rates for i^{th} treatment, j^{th} Period; μ = overall mean; α_i = fixed effect of i^{th} treatment; b_j = fixed effect of j^{th} Period; $(\alpha b)_{i,j}$ = i^{th} treatment- j^{th} Period interaction; $\varepsilon_{i,j,k}$ = error in k^{th} observation on a response variable at the i^{th} treatment, j^{th} Period.

The regression analysis accounted for repeated measurements for each column by specifying column as a subject with repeated measures over time (repeated Day/subject=Column) with the covariance structure selected by minimizing the model Akaike information criterion (AIC). An AR(1) model was selected using this criterion. Random effects were included for nested factors (Column within Treatment, and Column/Treatment within Period). Treatment effect within each Period was determined using least squares means with a Tukey correction for multiple comparisons. The full SAS code is included in the Supporting Information.

3.3. Results

3.3.1. High frequency water physico-chemistry

The multiplexed sampling system captured 13,100 data points for $[NO_3]_{out}$ over the experiment, or roughly 1,600–1,700 data points per column. The MPS was not used during the entire experiment, with high frequency water chemistry data collected over three separate experimental phases. The first phase included Start-up Periods A-C and Periods 1–11 (Days 0–98), the second phase included Periods 19–22 (Days 147–171), and the last phase included Periods 35–39 (Days 252–287. Column $[NO_3]_{out}$ varied considerably over the experiment from 0.0–19.5 mg NO_3-N L^{-1} (Figure 3-1), with much of the variation occurring during Periods 1–11.

Interestingly, during the first 11 days after initiating flow (Periods A & B), all columns showed very little NO_3 removal as $[NO_3]_{out}$ were less than 7% lower than $[NO_3]_{in}$. This was followed by a rapid decrease in $[NO_3]_{out}$ during Days 11–20, suggesting some microbial acclimation and distinct change in microbial activity during these first three weeks (Start-up Periods A-C). Much of the following increases and decreases in $[NO_3]_{out}$ (~2–17 mg NO_3-N L^{-1}) were associated with changes in flow rates (due to clogging of pump tubing from biofilm)and large temperature variations (due to lab facility heating-cooling issues).

Dissolved oxygen (DO) in the effluent was generally <0.1 mg L^{-1} for all columns over the entire experiment and did not exceed 0.25 mg L^{-1} (Figure C-3). During DRW cycles DO rose to 7–9 mg L^{-1} in DRW columns as the column was drained, suggesting that aerobic conditions prevailed in the water free pores at this time. Upon rewetting DO quickly fell below 0.25 mg L^{-1} within 1 h of flow at the outlet. Low DO concentrations at the column outlets indicate the majority of DO in the stock tank water was depleted before leaving the columns. Mean temperatures were 22.8, 19.6, and 22.4 °C in Periods 1-11, 19-22, and 35-39, respectively

3.3.2. Water chemistry from composite samples

Nitrate effluent concentrations in composite samples followed similar trends as those from the high frequency monitoring. Nitrate was lower in DRW columns, but not statistically lower until Period 4. There were significantly and consistently greater DOC and TC in DRW column effluent (Figure 3-2). Mean concentrations of DOC in the effluent immediately after rewetting (~1.5 h after) was consistently greater in DRW columns by 0.5-2.0 mg L^{-1}, although these differences decreased and were not significant prior to subsequent drainage (~1.5 h prior). Mean TC concentrations were greater in DRW columns by 2.3-3.3 mg C L^{-1} immediately after rewetting, with differences decreasing and, other than Periods 2 & 39, still significantly greater after 7 days prior to subsequent drainage. Total and dissolved organic carbon in effluent composite samples, both immediately after rewetting and prior to subsequent drainage, decreased over the experiment with the highest DOC/TC concentrations in Periods 2 & 3 (Figure 3-2). Total Kjeldahl and ammoniacal nitrogen concentrations in composite samples did not change significantly from column inlet to outlet or constitute a significant contribution to the nitrogen balance in the columns.

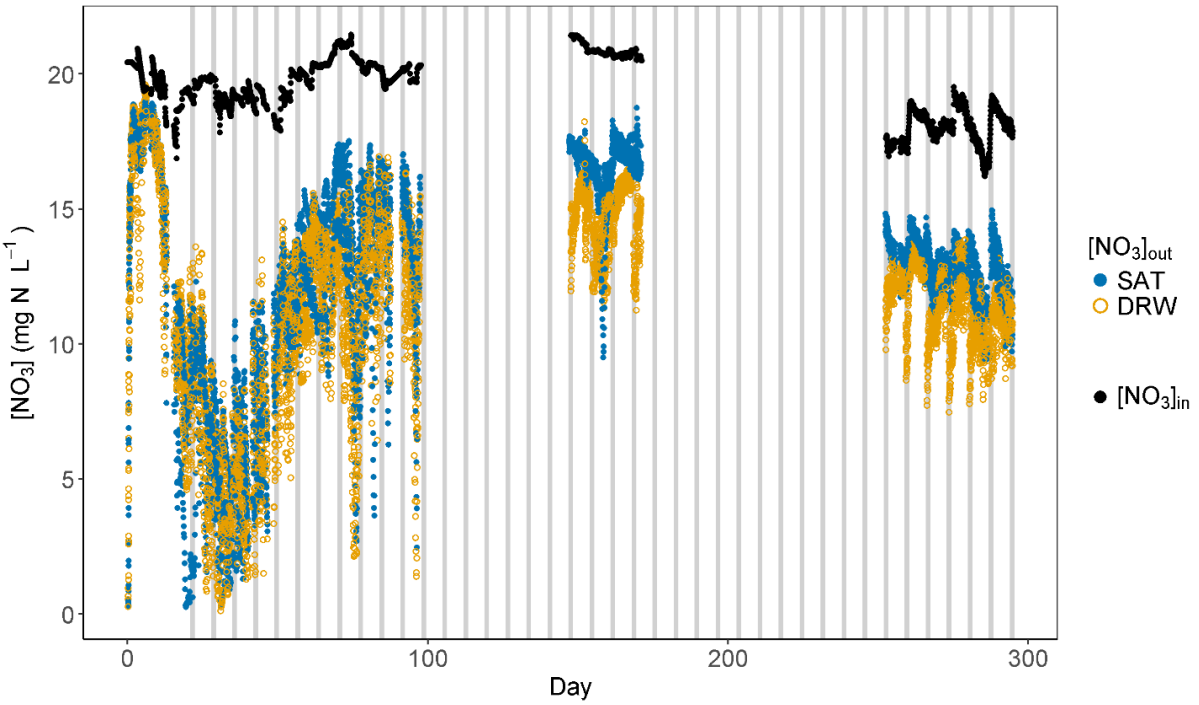

Figure 3-1. Nitrate concentrations in the stock tank $[NO_3]_{in}$ and outflow of all columns $[NO_3]_{out}$ over the experiment for saturated (SAT) and drying-rewetting (DRW) columns. Grey vertical bars denote DRW events. Flow was continuous though the entire 287 day experiment, with high-frequency water chemistry monitoring during Days 0–97, 147–171, and 252–287.

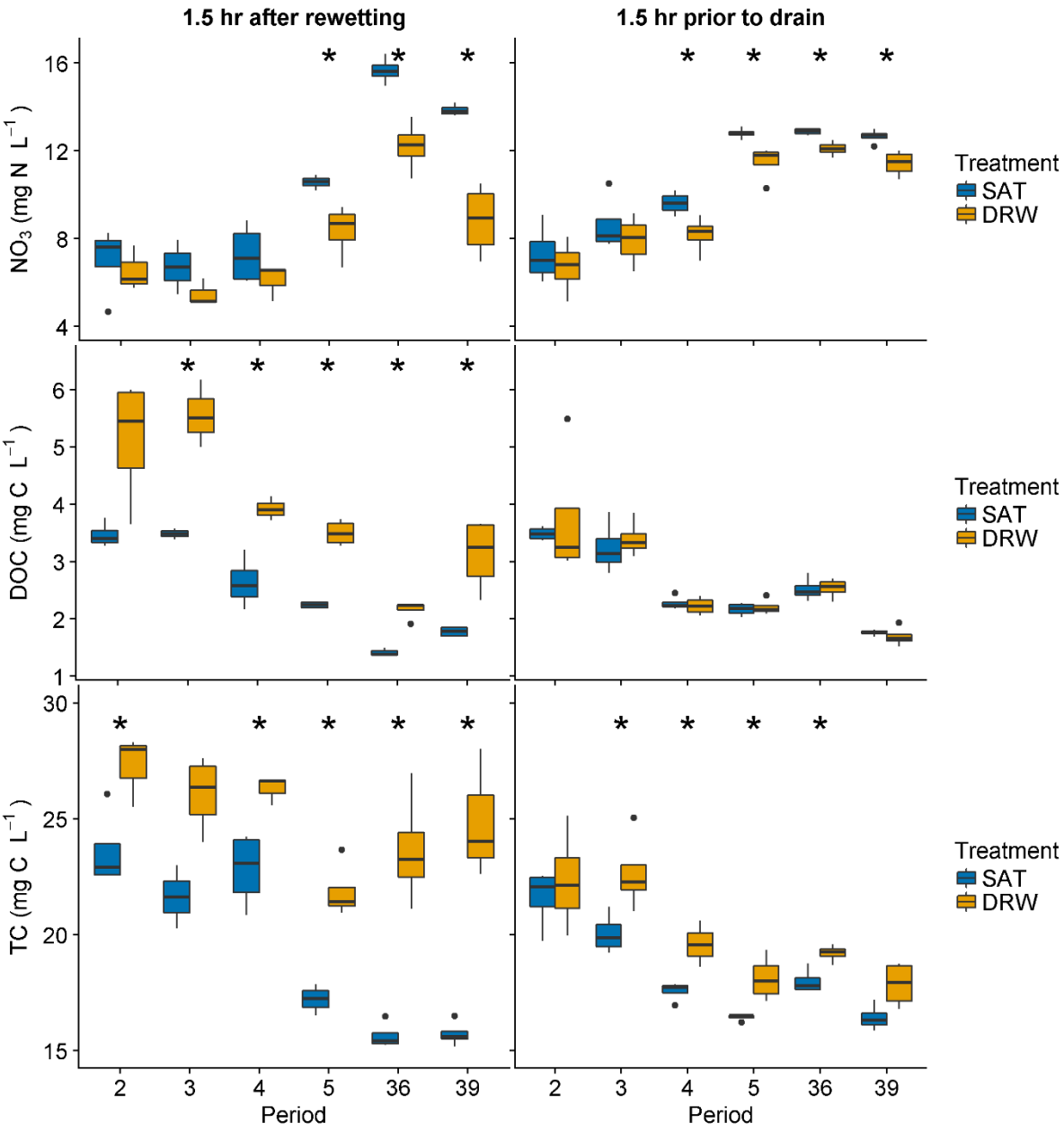

Figure 3-2. Outflow composite samples taken immediately after rewetting (1.5 h after outflow) and prior to subsequent drain (1.5 h prior to column draining). TKN and TAN results are not shown. Periods 2, 3, 4, 5, 36, and 39 began on Day 28, 35, 42, 49, 259, and 280. *denotes statistically significant difference between saturated (SAT) and drying-rewetting (DRW) group means for NO_3, DOC, and TC concentrations in outflow composite samples.

3.3.3. Nitrate removal rates

Volumetric NO_3 removal rates (R_{NO3}) were highly variable during, within and between DRW cycles, and ranged from 0.0–41.2 g N m^{-3} d^{-1} (Figure 3-3, Table C-3). During the first ten days, mean R_{NO3} for SAT and DRW groups were 4.5 and 4.4 g N m^{-3} d^{-1}, respectively. Column R_{NO3} increased and were highest during Days 20–50 (Periods 1–4) with mean R_{NO3} equal to 21.4 and 23.1 g N m^{-3} d^{-1} for SAT and DRW groups, respectively.. Overall, average R_{NO3} decreased to 13.6 and 18.5 g N m^{-3} d^{-1} during Periods 7-11, and to 8.3 and 12.1 g N m^{-3} d^{-1} during Periods 19-22, to finally stabilize at 8.9 and 12.3 g N m^{-3} d^{-1} during Periods 35-39, for SAT and DRW groups, respectively. Much of the variability in R_{NO3} during Periods 0–11 was due to greater variability in temperature and column flow rates, with considerably less R_{NO3} variability later in the experiment (Periods 19–22 and Periods 35–39) after temperature and flow issues were addressed.

While not as apparent during Periods 1–11 (likely due to temperature and flow variability during these weeks), a clear pattern of R_{NO3} appeared in DRW columns over the course of each week following a DRW cycle (Figure 3-4). While R_{NO3} in SAT columns remained stable, R_{NO3} in DRW columns were highest just after rewetting, steadily decreased for three days, and appeared mostly stable for the following four days during which R_{NO3} were still significantly higher than R_{NO3} in SAT columns.. Data from Periods 19–22 and 35–39 were selectively used to illustrate decreasing R_{NO3} after rewetting (Figure 3-4) since flow and temperature were most stable in these Periods. This trend was not clearly observed in data from Periods 1–11 (Figure C-4) when flow and temperature were less stable.

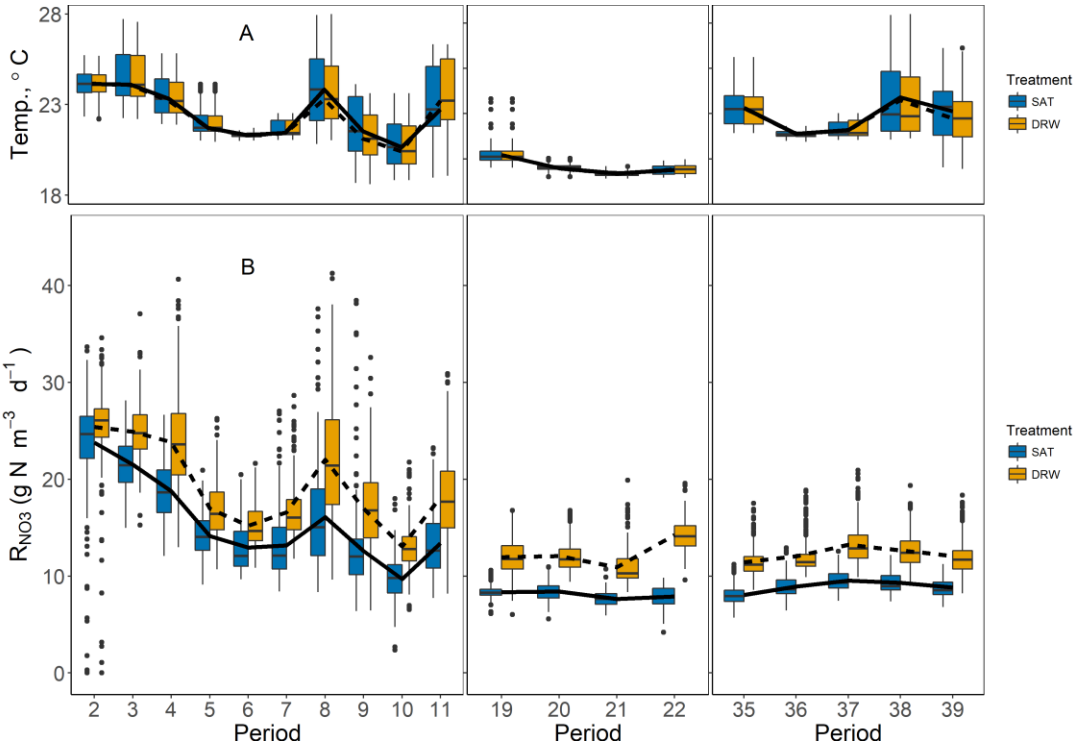

Figure 3-3. Box plots of temperature (A) and volumetric nitrate removal rates, R_{NO3}, (B) for both DRW and SAT columns from Periods 2–11, 19–22, and 35–39 (Days 28–287). Dashed and solid lines indicate weekly means for each Period for DRW and SAT groups, respectively.

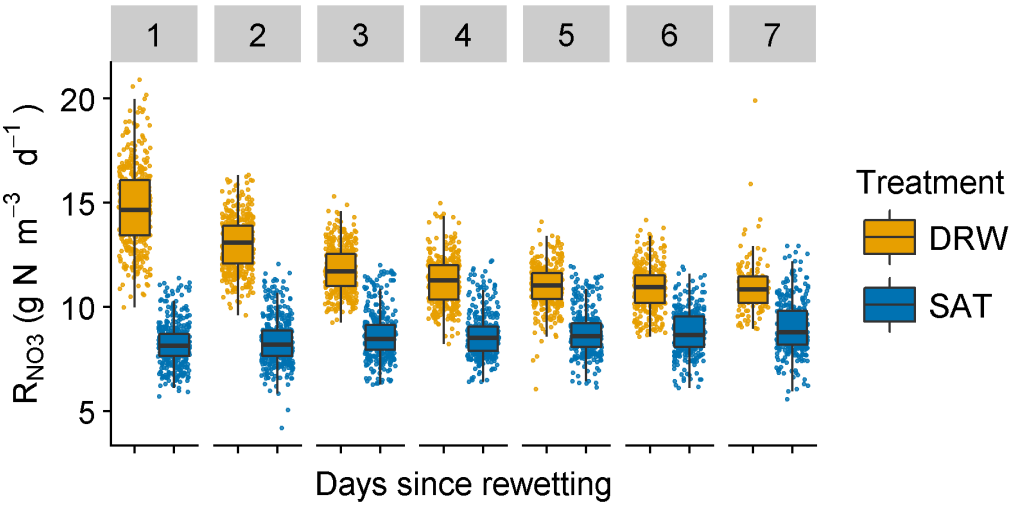

Figure 3-4. Boxplots of volumetric NO_3 removal rates (R_{NO3}) according to the number of days since the previous drying-rewetting (DRW) event (for Periods 19–22 & 35–39). Removal rates in DRW columns were ~80% greater than SAT columns on the first day after rewetting, with DRW R_{NO3} decreasing and eventually stabilizing ~4 days after rewetting.

3.3.4. ANOVA analysis

Data prior to Period 2 was not included in ANOVA analysis testing significance of DRW treatment to remove data possibly influenced by the early microbial acclimation. After the second DRW event (i.e. Period 2) R_{NO3} in DRW columns were greater, compared to SAT, in all subsequent Periods. The main effect of Treatment proved to be significant ($p=0.0017$, Table C-4), as well as main effect of Period ($p<0.0001$). The interaction of Period with Treatment was not significant ($p=0.2504$), indicating that R_{NO3} of both treatments changed with Period, however treatment effect did not significantly change with Period. When using the lsmeans slice option within the mixed model procedure, the DRW treatment was significant ($\alpha=0.05$) in all Periods 2–39 (Table C-5). The ANOVA estimate for Treatment effect (3.36 g N m^{-3} d^{-1}) was comparable to observed mean differences in R_{NO3} between treatments across Periods (Table C-3).

A separate ANOVA analysis was done on Periods 19–39 when flow and temperature conditions were more stable (Table C-6). In this model Treatment, Period Day, and their interaction were all significant, supporting observations that DRW R_{NO3} declined quickly in Days 1–3 and were relatively stable in Days 4–7. Model estimates for the fixed effect of Period Day were 3.5, 2.7, 1.7, 1.3, 0.7, 0.3 and -0.2 g N m^{-3} d^{-1} for Days 1–7, respectively, with Period Day effect not significant on Days 5–7, confirming that the effect of DRW was highest just after rewetting and declined afterwards.

3.4. Discussion

3.4.1. Nitrate removal rates increased by DRW cycles

After 39 DRW cycles over 287 days, data collected from this experiment provides convincing evidence that regular DRW cycles significantly improved NO_3 removal rates in woodchip columns. Low R_{NO3} in both treatment groups during the first ten days of the experiment (Start-Up Periods A & B) were most likely due to acclimation of the microbial community. Gungor-Demirci and Demirer (2004) reported microbial acclimation in an anaerobic digester of 3–5 days until gas production occurred, while Horiba et al. (2005) found that steady-state conditions for denitrifying bacteria in culture did not occur until 80 days after inoculation. While the woodchips were obtained from a field bioreactor, the water chemistry for the experiment was dramatically

different from the sprayfield drainage water and might be a reason for an adjustment by the microbial community. Significant differences in R_{NO3} between treatments did not occur until after the second DRW event (Period 2), indicating that the microbial community in DRW columns also took time to adjust to weekly DRW conditions.

After the initial microbial acclimation (Start-Up Periods A-C), R_{NO3} in both groups declined over the experiment. While some of the variability in R_{NO3} closely follows changes in temperature, it is unlikely temperature alone was responsible for the decrease in R_{NO3} over time. Mean temperature in Periods 2–11 and Periods 35–39 were 22.8 and 22.4 °C, but mean R_{NO3} in Periods 35–39 were lower by ~7 g N m^{-3} d^{-1} (Table C-3). It is possible that decreasing bioavailability of the woodchips over experiment led to lower R_{NO3}, since organic matter tends to become more recalcitrant as it decomposes (Berg, 2000; Cleveland et al., 2004; Girisha et al., 2003). Ghane et al. (2018) showed that the lignocellulose index (LCI) of woodchips in a four-year-old woodchip bioreactor increased over time, with a higher percentage of the woodchips composed of recalcitrant lignin. Declining NO_3 removal in aging woodchip bioreactors has been well-documented, although decreases in performance occur mostly within the first year (David et al., 2016; Robertson, 2010).

High resolution data clearly illustrated the decline in R_{NO3} within 3 days of rewetting, a process that would have been less clear based on infrequent data. This is a significant finding in that increased NO_3 removal via DRW cycles should not be overestimated. Columns receiving DRW treatment had R_{NO3} initially 79–81% greater on the first day after rewetting, but only 24–38% greater from the third to the seventh day, explaining the significant interaction effect between Treatment and Period Day (Table C-6). High resolution data was crucial in accounting for variability in $[NO_3]_{out}$ caused by temperature and flow, particularly in the first 100 days when R_{NO3} were highly variable. Increased difference in mean R_{NO3} between treatments during Periods 8 and 11 (5.93 and 4.75 g N m^{-3} d^{-1}, respectively) corresponded to substantial temperature increases, suggesting that DRW treatment had a greater effect on R_{NO3} at higher temperatures (Figure 3-3).

Observed R_{NO3} were on the intermediate to high end of those reported in a review of 12 different field denitrification beds (2–22 g N m^{-3} d^{-1}; reviewed by Schipper et al. 2010), likely due to the

higher temperature range in this experiment. Volumetric NO_3 removal rates were substantially higher than those reported in a column study (Greenan et al., 2009) with temperature maintained at 10 °C (2.9–4.5 g N m^{-3} d^{-1}), and comparable to rates reported in a separate woodchip column study (Hoover et al., 2016) at 20–21.5 °C (10–21 g N m^{-3} d^{-1}). Rates were lower than those reported at similar temperature range (32–39 g N m^{-3} d^{-1} at 14.6–23.5°C), although in that experiment N loading rates were significantly higher and influent had high DOC:NO_3 ratios (Lepine et al., 2016). In our experiment, R_{NO3} during brief temperature increases (up to 41.2 g N m^{-3} d^{-1} at 27.4°C) were much greater than the 95% confidence interval reported in a meta-analysis (Addy et al., 2016) of bioreactor removal rates seen at temperature >16.9°C (3.7–14.9 g N m^{-3} d^{-1}).

3.4.2. Total and dissolved organic carbon production linked to NO_3 removal

Results of the composite samples indicate that columns were a net source of dissolved organic carbon (Figure 3-2). Differences in composite samples between treatment groups were much higher immediately after rewetting than prior to the subsequent drain seven days later. Greater TC and DOC concentrations in DRW columns immediately after rewetting support previous findings that respiration and C mineralization increase after drying-rewetting cycles (Beare et al., 2009; Borken and Matzner, 2009; Fierer and Schimel, 2003; Gordon et al., 2008). DOC made up 27–53% of the differences in TC between groups after rewetting. The fact that differences in DOC became insignificant after seven days may explain why R_{NO3} declined with the number of days since rewetting. Organic breakdown during aerobic conditions likely increased the availability of carbon to fuel denitrification in DRW columns, with R_{NO3} decreasing as DOC was leached from the columns. Leaching of DOC over the week in DRW columns showed similar trends to DOC leaching in upflow columns from fresh OM (McLaughlan and Al-Mashaqbeh, 2009; Schmidt and Clark, 2013). Increased treatment effect during Periods 8 and 11 when temperature increased dramatically would be explained by higher rates of aerobic OM breakdown under elevated temperatures, subsequently leading to greater DOC leaching. These findings contrast with Halaburka et al. (2017) where DOC production rates in woodchip columns receiving continuous flow were not correlated with NO_3 removal rates.

Although it is clear from the composite samples that more DOC was leached from DRW columns, it is not clear whether the primary driver of increased R_{NO3} is differences in quantity of available carbon, its quality, or both. Several studies have shown that bioavailability of the electron donor influences denitrification rates (Cameron and Schipper, 2011; Dodla et al., 2008; Zarnetske et al., 20011; Schmidt and Clark, 2013). While the most immediate suspect for this increased DOC is aerobic breakdown of the woodchips, it is possible that the DOC comes from the biofilm on and within the woodchips. Several studies have observed the release of microbial C following DRW cycles in soils, either from mineralized biofilm or from extracellular release of C molecules following change in osmotic pressure (Gordon et al., 2008; Kieft, 1987; Halverson et al., 2000).

3.4.3. Design implications

Increased NO_3 removal via DRW cycling could decrease the volume required to achieve a target NO_3 removal. For example, using mean R_{NO3} seen in SAT columns in Periods 19-22 and 35–39 (8.8 g N m^{-3} d^{-1}), a 57 m^3 bioreactor would be required to treat 50% of tile drainage (20 mg NO_3-N L^{-1}) at a flow rate of 50 m^3 d^{-1}. Mean R_{NO3} in DRW columns during this same time were 12.3 g N m^{-3} d^{-1}, requiring a 41 m^3 bioreactor (28% reduction in volume) to achieve the same percent reduction. Whether or not this size reduction would result in a net cost reduction is unclear. Christianson et al. (2012) put the unit cost for two bioreactors in Iowa at \$40–80 m^{-3}. It is uncertain whether manually controlling flow to achieve DRW cycles would result cost savings when factoring in labor costs or that regular bioreactor management would be feasible for farmers. An automated system to manage flow is possible, but may not be cost-effective for smaller bioreactors where size reduction does not reduce costs below the capital cost of an automated control system. Application of DRW cycles may be more useful in controlled systems (e.g. tertiary wastewater treatment, constructed treatment wetlands).

3.4.4. Management considerations

Should DRW cycles become implemented in the field, it is useful to calculate the DRW frequency that would provide the optimum NO_3 removal. As R_{NO3} are much higher just after rewetting, increasing DRW frequency may be advantageous (Figure 3-5). During the 8 h of aerobiosis of the DRW cycles, however, drained woodchips would provide no NO_3 removal.

Using daily average R_{NO3} values when rates were most stable (Periods 19-22 and 35-39; Figure 3-4) it is possible to calculate the total mass NO_3 removed as a function of DRW frequency, taking into account treatment lost while woodchips are drained. The results of this simple analysis show that draining the columns for 8 h every 2–3 days would theoretically produce the greatest net increase in total NO_3 removed (41–43%; Figure 3-5), while weekly DRW only provide a 33% increase in total NO_3 removed (average weekly removal of 83.6 g N m^{-3} and 59.6 g N m^{-3} for DRW and SAT columns, respectively). This analysis assumes the average daily R_{NO3} would not change with increased DRW frequency. In field bioreactors under managed DRW cycles, untreated flow would be discharged though the bypass manifold designed to prevent flooding of crop fields.

Percent NO_3 mass reduction ($100\%*([NO_3]_{in} - [NO_3]_{out}) /[NO_3]_{in}$) is commonly reported and is a useful metric for water quality planners to quantify removal efficiency of treatment systems. While NO_3 removal rates, R_{NO3}, were increased by 24–81%, this translated to a more modest increase in percent NO_3 mass reduction of <10 percentage points for our experimental settings ($[NO_3]_{in}$=19.5±1.3 mg NO_3-N L^{-1}; HRT=8±2 h HRT). Percent mass reduction, however, depends on the HRT and $[NO_3]_{in}$ and would increase with higher HRT and lower $[NO_3]_{in}$. For example, using average R_{NO3} during later Periods (Figure 3-4) at the mean 8±2 h HRT, the percent NO_3 mass reduction for SAT and DRW columns would have been 28 and 40% at $[NO_3]_{in}$ = 15 mg NO_3-N L^{-1} (increase of 12 percentage points), or 42 and 61% at $[NO_3]_{in}$ = 10 mg NO_3-N L^{-1} (increase of 19 percentage points). Managers who will use DRW cycling to improve bioreactor performance should keep in mind that increases in the rate of NO_3 removal may not equal increases in percent NO_3 reduction, depending on site conditions.

Woodchips with regular DRW cycles would be broken down faster than constantly saturated woodchips, however, resulting in an expected shorter bioreactor lifespan or decreased time before new woodchips would need to be added. Lifetime of the woodchips would depend on how long and how often woodchips were unsaturated. Moorman et al. (2010) saw that wood loss in more frequently unsaturated, shallow woodchips was 62% greater over 9 years than deeper woodchips. The study predicted that the half-life for shallow woodchips was only 13% (4.6 years) of that for deeper woodchips. Ghane et al. (2018) also found significantly higher LCI and lower C:N ratios for woodchips located close to the inlet of a field bioreactor, a zone more

frequently exposed to high DO and aerobic breakdown of OM. Carbon loss from woodchips would depend on the duration and frequency of DRW cycles.

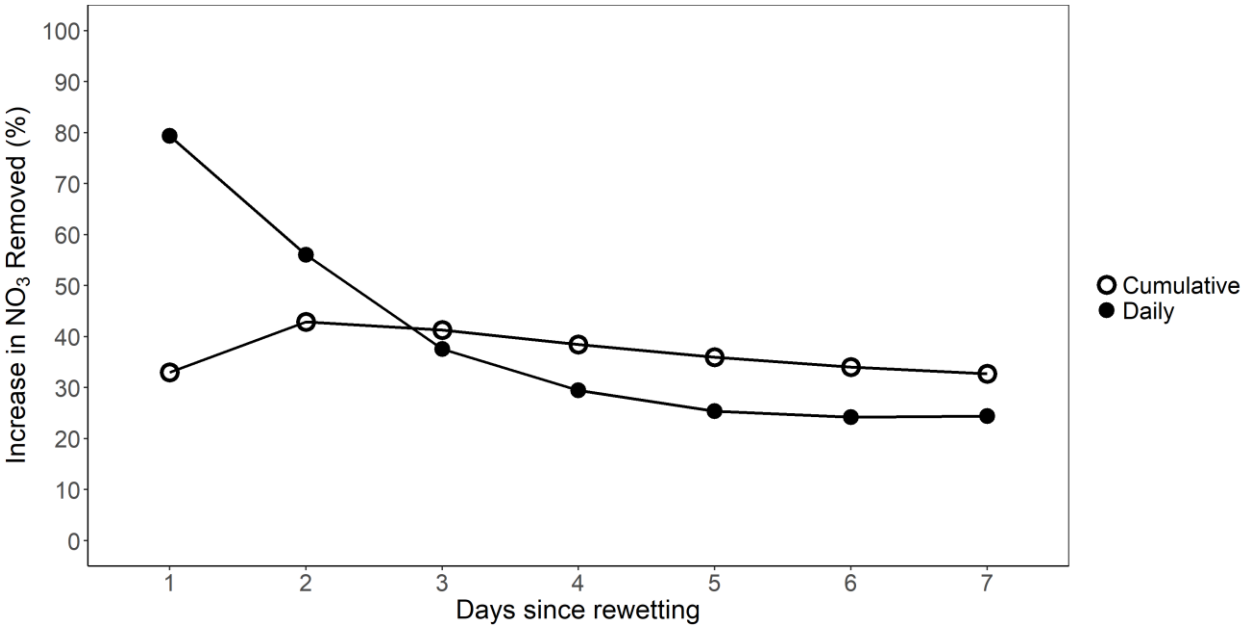

Figure 3-5. Increases in total NO_3 removed in DRW columns, relative to SAT columns, based on differences in daily mean R_{NO3} (solid) and cumulative NO_3 removed when considering untreated bypass while DRW columns were drained (hollow). The results indicate that increasing the DRW frequency to one drain every 2–3 days would provide the greatest overall improvement (41–43%) in total NO_3 removed.

3.5. Conclusions

This study showed N removal in woodchip bioreactors could be enhanced by DRW cycles with unsaturated periods as short as 8 hours. Increases in NO_3 removal rates were as high as 81% the first day after rewetting with weekly mean removal rates increased by 36-43%, although managers of bioreactors may see lower increases in percent NO_3 reduction. DRW cycles in field bioreactors can be made possible through water level management or other innovative design. Field studies of DRW effects on removal rates are necessary since biogeochemical conditions in unsaturated woodchips buried under soil are likely to be different than those seen in this column study. Limited analysis was given to quantifying the effects of temperature, flow, and DOC on NO_3 removal. The substantial amount of data collected in this experiment makes a clear answer to the hypothesis and a deeper analysis difficult to address in a single paper. A subsequent paper

will look at primary drivers of nitrate removal in DRW columns. Aerobic processes during the 8 h drained period are likely responsible for improved performance, with increased organic breakdown the primary cause of increased NO_3 removal rates.

3.6. References

Addy, K., Gold, A. J., Christianson, L. E., David, M. B., Schipper, L. A., & Ratigan, N. A. (2016). Denitrifying bioreactors for nitrate removal: A meta-analysis. *Journal of Environmental Quality, 45*(3), 873-881.

ÆsØy, A., Ødegaard, H., Bach, K., Pujol, R., & Hamon, M. (1998). Denitrification in a packed bed biofilm reactor (BIOFOR)—experiments with different carbon sources. *Water Research, 32*(5), 1463-1470.

Beare, M., Gregorich, E., & St-Georges, P. (2009). Compaction effects on CO_2 and N_2O production during drying and rewetting of soil. *Soil Biology and Biochemistry, 41*(3), 611-621.

Berg, B. (2000). Litter decomposition and organic matter turnover in northern forest soils. *Forest Ecology and Management, 133*(1-2), 13-22.

Borken, W., & Matzner, E. (2009). Reappraisal of drying and wetting effects on C and N mineralization and fluxes in soils. *Global Change Biology, 15*(4), 808-824.

Brown, T., Berg, J., & Underwood, K. (2010). Replacing incised headwater channels and failing stormwater infrastructure with regenerative stormwater conveyance. *Low impact development 2010: Redefining water in the city* (pp. 207-217)

Cameron, S. G., & Schipper, L. A. (2010). Nitrate removal and hydraulic performance of organic carbon for use in denitrification beds. *Ecological Engineering, 36*(11), 1588-1595.

Cameron, S. G., & Schipper, L. A. (2011). Evaluation of passive solar heating and alternative flow regimes on nitrate removal in denitrification beds. *Ecological Engineering, 37*(8), 1195-1204.

Chen, X., Peltier, E., Sturm, B. S., & Young, C. B. (2013). Nitrogen removal and nitrifying and denitrifying bacteria quantification in a stormwater bioretention system. *Water Research, 47*(4), 1691-1700.

Christianson, L. E., Bhandari, A., & Helmers, M. J. (2011). Pilot-scale evaluation of denitrification drainage bioreactors: Reactor geometry and performance. *Journal of Environmental Engineering, 137*(4), 213-220.

Christianson, L. E., Bhandari, A., Helmers, M. J., Kult, K. J., Sutphin, T., & Wolf, R. (2012). Performance evaluation of four field-scale agricultural drainage denitrification bioreactors in iowa. *Transactions of the ASABE, 55*(6), 2163.

Christianson, L. E., Lepine, C., Sibrell, P. L., Penn, C., & Summerfelt, S. T. (2017). Denitrifying woodchip bioreactor and phosphorus filter pairing to minimize pollution swapping. *Water Research, 121*, 129-139.

Cleveland, C. C., Neff, J. C., Townsend, A. R., & Hood, E. (2004). Composition, dynamics, and fate of leached dissolved organic matter in terrestrial ecosystems: Results from a decomposition experiment. *Ecosystems, 7*(3), 175-285.

David, M. B., Gentry, L. E., Cooke, R. A., & Herbstritt, S. M. (2016). Temperature and substrate control woodchip bioreactor performance in reducing tile nitrate loads in east-central illinois. *Journal of Environmental Quality, 45*(3), 822-829.

Dodla, S. K., Wang, J. J., DeLaune, R. D., & Cook, R. L. (2008). Denitrification potential and its relation to organic carbon quality in three coastal wetland soils. *Science of the Total Environment, 407*(1), 471-480.

Etheridge, J. R., Birgand, F., Osborne, J. A., Osburn, C. L., Burchell, M. R., & Irving, J. (2014). Using in situ ultraviolet-visual spectroscopy to measure nitrogen, carbon, phosphorus, and suspended solids concentrations at a high frequency in a brackish tidal marsh. *Limnology and Oceanography: Methods, 12*(1), 10-22.

Fierer, N., & Schimel, J. P. (2003). A proposed mechanism for the pulse in carbon dioxide production commonly observed following the rapid rewetting of a dry soil. *Soil Science Society of America Journal, 67*(3), 798-805.

Ghane, E., Fausey, N. R., & Brown, L. C. (2015). Modeling nitrate removal in a denitrification bed. *Water Research, 71*, 294-305.

Ghane, E., Feyereisen, G. W., Rosen, C. J., & Tschirner, U. W. (2018). Carbon quality of four-year-old woodchips in a denitrification bed treating agricultural drainage water.

Girisha, G., Condron, L., Clinton, P., & Davis, M. (2003). Decomposition and nutrient dynamics of green and freshly fallen radiata pine (pinus radiata) needles. *Forest Ecology and Management, 179*(1), 169-181.

Gordon, H., Haygarth, P. M., & Bardgett, R. D. (2008). Drying and rewetting effects on soil microbial community composition and nutrient leaching. *Soil Biology and Biochemistry, 40*(2), 302-311.

Greenan, C. M., Moorman, T. B., Parkin, T. B., Kaspar, T. C., & Jaynes, D. B. (2009). Denitrification in wood chip bioreactors at different water flows. *Journal of Environmental Quality, 38*(4), 1664-1671.

Güngör-Demirci, G., & Demirer, G. N. (2004). Effect of initial COD concentration, nutrient addition, temperature and microbial acclimation on anaerobic treatability of broiler and cattle manure. *Bioresource Technology, 93*(2), 109-117.

Halaburka, B. J., LeFevre, G. H., & Luthy, R. G. (2017). Evaluation of mechanistic models for nitrate removal in woodchip bioreactors. *Environmental Science & Technology, 51*(9), 5156-5164.

Halverson, L. J., Jones, T. M., & Firestone, M. K. (2000). Release of intracellular solutes by four soil bacteria exposed to dilution stress. *Soil Science Society of America Journal, 64*(5), 1630-1637.

Hoover, N. L., Bhandari, A., Soupir, M. L., & Moorman, T. B. (2016). Woodchip denitrification bioreactors: Impact of temperature and hydraulic retention time on nitrate removal. *Journal of Environmental Quality, 45*(3), 803-812.

Horiba, Y., Khan, S. T., & Hiraishi, A. (2005). Characterization of the microbial community and culturable denitrifying bacteria in a solid-phase denitrification process using poly (ε-caprolactone) as the carbon and energy source. *Microbes and Environments, 20*(1), 25-33.

Kieft, T. L. (1987). Microbial biomass response to a rapid increase in water potential when dry soil is wetted. *Soil Biology and Biochemistry, 19*(2), 119-126.

Kim, H., Seagren, E. A., & Davis, A. P. (2003). Engineered bioretention for removal of nitrate from stormwater runoff. *Water Environment Research, 75*(4), 355-367.

Lepine, C., Christianson, L., Sharrer, K., & Summerfelt, S. (2016). Optimizing hydraulic retention times in denitrifying woodchip bioreactors treating recirculating aquaculture system wastewater. *Journal of Environmental Quality, 45*(3), 813-821.

Liu, Y. (2017). The performance of controlled drainage and inline denitrifying woodchip bioreactor for reducing nutrient losses from subsurface drained grassland receiving liquid swine lagoon effluent. (Doctoral Dissertation, NCSU). (http://www.lib.ncsu.edu/resolver/1840.20/34529)

McLaughlan, R. G., & Al-Mashaqbeh, O. (2009). Simple models for the release kinetics of dissolved organic carbon from woody filtration media. *Bioresource Technology, 100*(9), 2588-2593.

Miller, A. E., Schimel, J. P., Meixner, T., Sickman, J. O., & Melack, J. M. (2005). Episodic rewetting enhances carbon and nitrogen release from chaparral soils. *Soil Biology and Biochemistry, 37*(12), 2195-2204.

Moorman, T. B., Parkin, T. B., Kaspar, T. C., & Jaynes, D. B. (2010). Denitrification activity, wood loss, and N 2 O emissions over 9 years from a wood chip bioreactor. *Ecological Engineering, 36*(11), 1567-1574.

Palmer, K., Kopp, J., Gebauer, G., & Horn, M. A. (2016). Drying-rewetting and flooding impact denitrifier activity rather than community structure in a moderately acidic fen. *Frontiers in Microbiology, 7*, 727. doi:10.3389/fmicb.2016.00727 [doi]

Robertson, W. (2010). Nitrate removal rates in woodchip media of varying age. *Ecological Engineering, 36*(11), 1581-1587.

Ruser, R., Flessa, H., Russow, R., Schmidt, G., Buegger, F., & Munch, J. (2006). Emission of N_2O, N_2 and CO_2 from soil fertilized with nitrate: Effect of compaction, soil moisture and rewetting. *Soil Biology and Biochemistry, 38*(2), 263-274.

SAS Institute Inc. (2011). *Base SAS® 9.4 procedures guide.* Cary, NC: SAS Institute.

Schipper, L. A., Cameron, S., & Warneke, S. (2010). Nitrate removal from three different effluents using large-scale denitrification beds. *Ecological Engineering, 36*(11), 1552-1557.

Schmidt, C. A., & Clark, M. W. (2013). Deciphering and modeling the physicochemical drivers of denitrification rates in bioreactors. *Ecological Engineering, 60,* 276-288.

Vaughan, M. C., Bowden, W. B., Shanley, J. B., Vermilyea, A., Sleeper, R., Gold, A. J., et al. High-frequency dissolved organic carbon and nitrate measurements reveal differences in storm hysteresis and loading in relation to land cover and seasonality. *Water Resources Research,*

Warneke, S., Schipper, L. A., Bruesewitz, D. A., McDonald, I., & Cameron, S. (2011). Rates, controls and potential adverse effects of nitrate removal in a denitrification bed. *Ecological Engineering, 37*(3), 511-522.

Woli, K. P., David, M. B., Cooke, R. A., McIsaac, G. F., & Mitchell, C. A. (2010). Nitrogen balance in and export from agricultural fields associated with controlled drainage systems and denitrifying bioreactors. *Ecological Engineering, 36*(11), 1558-1566.

Xiang, S., Doyle, A., Holden, P. A., & Schimel, J. P. (2008). Drying and rewetting effects on C and N mineralization and microbial activity in surface and subsurface california grassland soils. *Soil Biology and Biochemistry, 40*(9), 2281-2289.

Zarnetske, J. P., Haggerty, R., Wondzell, S. M., & Baker, M. A. (2011). Labile dissolved organic carbon supply limits hyporheic denitrification. *Journal of Geophysical Research: Biogeosciences, 116*(G4)

Drying-rewetting Cycles Affect Nitrate Removal Rates in Woodchip Bioreactors. Maxwell, B. M., Birgand, F., Schipper, L. A., Christianson, L. E., Tian, S., Helmers, M. J., et al. (2018). *Journal of Environmental Quality.*

Role in Authorship of Paper : Primary author and contributor of research described herein.

Published online November 15, 2018

Journal of Environmental Quality TECHNICAL REPORTS
SURFACE WATER QUALITY

Drying–Rewetting Cycles Affect Nitrate Removal Rates in Woodchip Bioreactors

Bryan M. Maxwell, François Birgand,* Louis A. Schipper, Laura E. Christianson, Shiying Tian, Matthew J. Helmers, David J. Williams, George M. Chescheir, and Mohamed A. Youssef

Abstract

Woodchip bioreactors are widely used to control nitrogen export from agriculture using denitrification. There is abundant evidence that drying–rewetting (DRW) cycles can promote enhanced metabolic rates in soils. A 287-d experiment investigated the effects of weekly DRW cycles on nitrate (NO_3) removal in woodchip columns in the laboratory receiving constant flow of nitrated water. Columns were exposed to continuous saturation (SAT) or to weekly, 8-h drying-rewetting (8 h of aerobiosis followed by saturation) cycles (DRW). Nitrate concentrations were measured at the column outlets every 2 h using novel multiplexed sampling methods coupled to spectrophotometric analysis. Drying–rewetting columns showed greater export of total and dissolved organic carbon and increased NO_3 removal rates. Nitrate removal rates in DRW columns increased by up to 80%, relative to SAT columns, although DRW removal rates decreased quickly within 3 d after rewetting. Increased NO_3 removal in DRW columns continued even after 39 DRW cycles, with −33% higher total NO_3 mass removed over each weekly DRW cycle. Data collected in this experiment provide strong evidence that DRW cycles can dramatically improve NO_3 removal in woodchip bioreactors, with carbon availability being a likely driver of improved efficiency. These results have implications for hydraulic management of woodchip bioreactors and other denitrification practices.

Core Ideas

- Weekly, 8-h drying–rewetting (DRW) cycles increased nitrate removal in woodchip columns.
- Increased nitrate removal in DRW columns declined with number of days since rewetting.
- Nitrate removal corresponded to greater leaching of dissolved organic C in DRW columns.
- Effect of DRW was significant even after 39 weekly DRW cycles.

J. Environ. Qual.
doi:10.2134/jeq2018.05.0199
Supplemental material is available online for this article.
Received 22 May 2018.
Accepted 22 Oct. 2018.
*Corresponding author (birgand@ncsu.edu).

WOODCHIP BIOREACTORS (denitrifying bioreactors) are used as a conservation practice to treat nitrate-nitrogen (NO_3–N) in drainage water. Woodchips provide the electron donor for microbial denitrification to reduce aqueous nitrate to gaseous forms (N_2, N_2O) and remove N from drainage water. Woodchip bioreactors are increasingly used in various applications, which include poorly drained crop fields (Christianson et al., 2012; David et al., 2016; Woli et al., 2010), dairy (Schipper et al., 2010) and hog farms (Liu, 2017), aquaculture units (Lepine et al., 2016), hydroponics operations (Warneke et al., 2011), urban bioretention cells (Chen et al., 2013; Kim et al., 2003), and regenerative stormwater conveyance (Brown et al., 2010). A number of factors affect the treatment efficiency of woodchip bioreactors, including hydraulic residence time (HRT) (Greenan et al., 2009; Hoover et al., 2016), water temperature (David et al., 2016; Hoover et al., 2016), age of woodchips (David et al., 2016; Robertson, 2010), bed design (Cameron and Schipper, 2011; Christianson et al., 2011), influent concentration (Lepine et al., 2016), and carbon (C) source (Cameron and Schipper, 2010). One of the recurring challenges reported in the bioreactor literature is decreasing NO_3 removal efficiency over time, particularly after the first year of operation. Most woodchip bioreactors are currently not actively managed, and increasing removal efficiency may seem out of reach as it is controlled by environmental variables (temperature, water chemistry) or media characteristics (age, C source).

There is evidence, however, that post-installation management could increase denitrification rates within woodchip bioreactors. One such management option is drying–rewetting (DRW) cycles. In the soil literature, a number of studies investigated the effect of DRW cycles on the rates of soil metabolic processes (Beare et al., 2009; Borken and Matzner, 2009; Miller et al., 2005; Ruser et al., 2006; Palmer et al., 2016; Xiang et al., 2008). Drying–rewetting cycles in soils have been linked to increased nitrous oxide (N_2O) production (Ruser et al., 2006),

B.M. Maxwell, F. Birgand, S. Tian, G.M. Chescheir, and M.A. Youssef, Dep. of Biological and Agricultural Engineering, North Carolina State Univ., Raleigh, NC, USA 27695-7625; L.A. Schipper, Biogeochemistry and Ecohydrology Research, Univ. of Waikato, New Zealand 3216; L.E. Christianson, Dep. of Crop Sciences, Univ. of Illinois, Champaign, IL, USA 61820; M.J. Helmers, Dep. of Agricultural and Biosystems Engineering, Iowa State Univ., Ames, IA, USA 50011; D.J Williams, USEPA, Durham, NC, USA 27709. Assigned to Associate Editor Mussie Habteselassie.

Abbreviations: DO, dissolved oxygen; DOC, dissolved organic carbon; DRW, drying–rewetting; HRT, hydraulic residence time; MPS, multiplexed pumping system; SAT, saturation; TC, total carbon.

increased C and N leaching (Miller et al., 2005), and changes in microbial and fungal communities (Gordon et al., 2008). Woodchip bioreactors are comparable to soil systems, with an organic substrate degraded by microbes taking part in various biogeochemical processes.

The hypotheses for this work are that aerobic conditions provided during bioreactor drying cycles would (i) increase breakdown of organic matter and (ii) stimulate NO_3 removal by increasing C availability. Literature suggests that increased breakdown of organic matter produces greater CO_2 and other byproducts of respiration, including dissolved organic C (DOC). This DOC is generally lower molecular weight and more easily used as an electron donor, leading to an increase in denitrification rates (ÆsØy et al., 1998; Dodla et al., 2008; Zarnetske et al., 2011). Drying–rewetting cycles could potentially be used to increase NO_3 removal rates in woodchip bioreactors on-site. However, there is a lack of research investigating the impact of DRW cycles on C and N fluxes in engineered and normally saturated systems with high C content media (e.g., woodchip bioreactors). One exception is Christianson et al. (2017), who found a 96-h DRW event increased NO_3 removal in woodchip columns from 48 to 90%, although the study was only able to observe the effects of a single DRW event. The objective of the present study was to determine whether repeated, short-term DRW cycles could sustainably increase NO_3 removal in woodchip bioreactors.

The term *drying–rewetting* in this article, consistent with previous literature on DRW cycles, refers to the process of draining previously saturated woodchips, allowing air to enter the pore space previously filled by water, and saturating the pores with water again. During the "drying" part of the cycle, the woodchip porous medium is drained to equilibrium and is thus still moist and not dry, as the term might suggest.

Materials and Methods

Experimental Design

A 287-d column experiment was performed at the North Carolina State University Biological and Agricultural Engineering facility from February to December 2017. Eight experimental units consisted of 15.2-cm-diam., 95-cm-tall polyvinylchloride columns filled with aged woodchips. Woodchips were collected from a 6-yr-old field bioreactor treating drainage from a hog lagoon sprayfield in Plymouth, NC. Woodchips were analyzed for C, N, and P content and pH (Supplemental Table S1). From bottom to top, each column was filled with a base gravel bed (6 cm depth, 5- to 10-mm-diam. gravel) covered by plastic mesh (2-mm mesh size) to provide uniform, upward flow though the column. On top of the gravel layer, 50 cm of woodchips (4650–5086 g wet weight) were packed in each column, leaving 39 cm of headspace above the woodchips. The columns were capped to limit exchange with the atmosphere. The water inlet was installed at the gravel layer level, and the outlet was even with the top of the woodchip layer. Inlet and outlet hose barb connections were installed on the column sidewall (Supplemental Fig. S1). Upflow (0.68 ± 0.14 L h^{-1}; mean ± SD) was provided by an eight-channel ISMATEC peristaltic pump for an 8 ± 2 h HRT (Supplemental Table S2) in each column.

Each of the eight columns was assigned one of two conditions ($n = 4$). The control (SAT) consisted of continuous saturation provided by a constant and uninterrupted upflow during the entire experiment. Water level in the SAT columns remained constant at the level of the overflow. The treatment (DRW) consisted of exposing the woodchips to aerobic conditions for 8 h in weekly DRW cycles. Flow to DRW columns was stopped once a week by disconnecting the inflow lines. After stopping flow, the DRW columns were drained rapidly (~15 min time to drain) and left unsaturated for 8 h, exposing the woodchips to aerobic conditions. Then, flow to DRW columns was reestablished by reconnecting the inflow line. The duration of unsaturated conditions was based on results from preliminary laboratory experiments and for practical experimental reasons in which columns could be drained and resaturated at the beginning and end of the day. Outflow from DRW columns occurred ~8 h after restarting flow. A single DRW cycle referred to each draining event and subsequent rewetting. All columns received constant upflow for 287 d, outside the 8-h drained times of the DRW columns, and DRW columns were exposed to 39 DRW cycles. Moisture content of woodchips within the columns after 8 h of unsaturated conditions, measured using the oven-dry method (European Committee for Standardization, 2009), was calculated as 57 to 59%.

Columns were fed from a 1200-L stock tank filled with dechlorinated (Omnipure K5626-JJ filters) tap water spiked with KNO_3 (19.5 ± 1.3 mg NO_3–N L^{-1}) such that inlet NO_3–N concentrations were similar to those seen in tile drainage (e.g., Christianson et al., 2012; David et al., 2016). Two stock tanks were used such that one tank could be mixed and degassed to lower dissolved oxygen (DO) levels in the stock tank (7.2 ± 0.7 mg DO L^{-1}) while still providing uninterrupted flow to columns from the other tank. Flow rates to each column were measured two to three times daily by collecting outflow in 9-L jugs for 5 to 12 h and measuring outflow volume with a graduated cylinder.

During the first 3 wk (Start-up Periods A, B, C), all columns received the SAT control (continuous saturation) to determine variability between columns before applying the DRW treatment. After the first 3 wk, columns were ranked according to N removal rates, and columns with the second-, fourth-, sixth-, and eighth-highest N removal rates were assigned the DRW treatment, and the others were assigned the SAT control. Collected data were given a period number corresponding to the number of prior DRW cycles (e.g., Period 2 for data collected after the second and prior to the third DRW cycle, with 1 wk between each DRW cycle).

High-Frequency Water Physico-Chemistry Analysis

Stock tank and column outflow water chemistry were measured using a small volume multiplexed pumping system (MPS) (Maxwell et al., 2018) coupled to a high frequency spectrophotometer. The MPS sequentially pumped 25-mL samples from each column for absorbance measurement by a field spectrophotometer (Spectro::lyser Type SP-1-035-p0-s-NO-075; s::can) fitted with a 4-mm path length, 1.1-mL flow through quartz cuvette (46-Q-4, Starna Cells, Inc.). The spectrophotometer and MPS measurement sequence was adjusted such that the stock tank and each column outflow concentrations were measured at 2-h intervals. Nitrate concentrations were calculated from the measured absorbance following methods previously described

(Birgand et al., 2016; Etheridge et al., 2014; Vaughan et al., 2017).

During measurements, water was pumped via 0.9-mm-diam. polytetrafluoroethylene tubing (0.2 mL s^{-1}) through a 60-µm plankton mesh screened intake placed in the top 3 cm of the saturated media in each column. To minimize cross-contamination between columns, the first 5 mL of sample volume were diverted to waste, after which 20 mL of sample volume (>18 times cuvette volume) were pumped for spectrophotometric analysis, according to validated sampling procedures for the small volume MPS (Maxwell et al., 2018). Low pump rate and sample volume (25 mL every 2 h) were used to limit impact of sampling on column hydraulics (sample volume <2% of cumulative flow volume over 2 h). Forty sample volumes analyzed by the spectrophotometer were submitted for laboratory analysis (USEPA Method 353.2, BAE Environmental Analysis Laboratory, North Carolina State University) to calibrate the probe for NO_3 (Etheridge et al., 2014). Due to equipment and personnel limitations, column outflow was monitored using this high-frequency sampling method during Days 0 to 98, 147 to 171, and 252 to 287, while columns received continuous upflow over the entire 287 d.

Temperature (Supplemental Fig. S2) and DO (Supplemental Fig. S3) of column outflow were measured hourly using Presens temperature sensors and oxygen dipping probes (DP-PSt3, Presens Precision Sensing GmbH). Temperature and DO sensors were inserted through the top of the column and placed such that the sensor tips were at least 2 cm below the surface of woodchip media, per manufacturer's specifications. A manual two-point calibration for DO sensors was performed using 0 and 100% air saturation standards. A 0% air saturation standard was made by dissolving 1 g Na_2SO_3 and 1 mg $CoCl_2$ in 1 L deionized water, mixing gently, and leaving to stand for 30 min. A 100% air saturation standard was made by vigorously bubbling tap water with an air stone and bubbler for 30 min and leaving to stand for 30 min.

Discrete Composite Water Chemistry

During selected periods, composite outflow samples were collected to quantify additional water chemistry parameters of interest. Composite samples were taken by collecting outflow from each column over 1.5 h (~1.0 L). Grab samples were collected from all columns immediately after rewetting of drained columns and again before subsequent drainage. Grab samples were analyzed for NO_3 (EPA standard 353.2; USEPA, 1993b), total ammonia N (standard method 4500-NH_3 G; Rice et al., 2017a), total Kjeldahl N (EPA standard 351.2; USEPA, 1993a) and total N (standard method 4500-N_{org} B, Bran & Leubbe Autoanalyzer III; Rice et al., 2017b), and DOC and total C (TC) (EPA standard 415.1, Teledyne Tekmar Apollo 9000; 0.45-µm filter; USEPA, 1999). Composite samples were collected during Periods 2, 3, 4, 5, 36, and 39.

Nitrate Removal Rates

Volumetric NO_3 removal rates (R_{NO3}) for each column were calculated as the difference between column inlet NO_3–N concentrations ($[NO_3]_{in}$) and outlet NO_3–N concentrations ($[NO_3]_{out}$) times the flow rate over the woodchip-filled column volume (0.009 m^3), yielding units in grams N per cubic meter per day.

Statistical Analysis

Mixed linear model analysis was performed in SAS (SAS Proc MIXED, SAS 9.4 [SAS Institute, 2011]) on data collected from all columns to determine the treatment effect on NO_3 removal rates, as well as the effect of period number and period day, or the number of days since rewetting of DRW columns. Period number rather than time was used as a variable to reduce autocorrelation of high-frequency measurements. The statistical model in this analysis is described by Eq. [1]:

$$Y_{ij} = \mu + \alpha_i + b_j + (\alpha b)_{ij} + \varepsilon_{ijk} \quad [1]$$

where Y_{ij} = predicted nitrate removal rates for ith treatment, jth period; μ = overall mean; α_i = fixed effect of ith treatment; b_j = fixed effect of jth period; $(\alpha b)_{ij}$ = ith treatment–jth period interaction; and ε_{ijk} = error in kth observation on a response variable at the ith treatment, jth period.

The regression analysis accounted for repeated measurements for each column by specifying column as a subject with repeated measures over time (repeated day/subject = column) with the covariance structure selected by minimizing the model Akaike information criterion. Random effects were included for nested factors (column within treatment, and column/treatment within period). Treatment effect within each period was determined using least squares means with a Tukey correction for multiple comparisons. The full SAS code is included in the Supplemental Material.

Results

High-Frequency Water Physico-Chemistry

The multiplexed sampling system captured 13,100 data points for $[NO_3]_{out}$ over the experiment, or approximately 1600 to 1700 data points per column. The MPS was not used during the entire experiment, with high-frequency water chemistry data collected over three separate experimental phases. The first phase included Start-up Periods A to C and Periods 1 to 11 (Days 0–98), the second phase included Periods 19 to 22 (Days 147–171), and the last phase included Periods 35 to 39 (Days 252–287. Column $[NO_3]_{out}$ varied considerably over the experiment, from 0.0 to 19.5 mg NO_3–N L^{-1} (Fig. 1), with much of the variation occurring during Periods 1 to 11.

Interestingly, during the first 11 d after initiating flow (Periods A and B), all columns showed very little NO_3 removal as $[NO_3]_{out}$ was <7% lower than $[NO_3]_{in}$. This was followed by a rapid decrease in $[NO_3]_{out}$ during Days 11 to 20, suggesting some microbial acclimation and distinct change in microbial activity during these first 3 wk (Start-up Periods A–C). Much of the following increases and decreases in $[NO_3]_{out}$ (~2–17 mg NO_3–N L^{-1}) were associated with changes in flow rates (due to clogging of pump tubing from biofilm) and large temperature variations (due to laboratory facility heating–cooling issues).

Dissolved oxygen in the effluent was generally <0.1 mg L^{-1} for all columns over the entire experiment and did not exceed 0.25 mg L^{-1} (Supplemental Fig. S3). During DRW cycles, DO rose to 7 to 9 mg L^{-1} in DRW columns as the column was drained, suggesting that aerobic conditions prevailed in the water free pores at this time. Upon rewetting, DO quickly fell below 0.25 mg L^{-1} within 1 h of flow at the outlet. Low DO concentrations at the

column outlets indicate the majority of DO in the stock tank water was depleted before leaving the columns. Mean temperatures were 22.8, 19.6, and 22.4°C in Periods 1 to 11, 19 to 22, and 35 to 39, respectively.

Water Chemistry from Composite Samples

Nitrate effluent concentrations in composite samples followed similar trends as those from the high-frequency monitoring. Nitrate was lower in DRW columns, but not statistically lower until Period 4. There were significantly and consistently greater DOC and TC in DRW column effluent (Fig. 2). Mean concentrations of DOC in the effluent immediately after rewetting (~1.5 h after) was consistently greater in DRW columns by 0.5 to 2.0 mg L^{-1}, although these differences decreased and were not significant before subsequent drainage (~1.5 h prior). Mean TC concentrations were greater in DRW columns by 2.3 to 3.3 mg C L^{-1} immediately after rewetting, with differences decreasing and, other than Periods 2 and 39, still significantly greater after 7 d prior to subsequent drainage. Total C and DOC in effluent composite samples, both immediately after rewetting

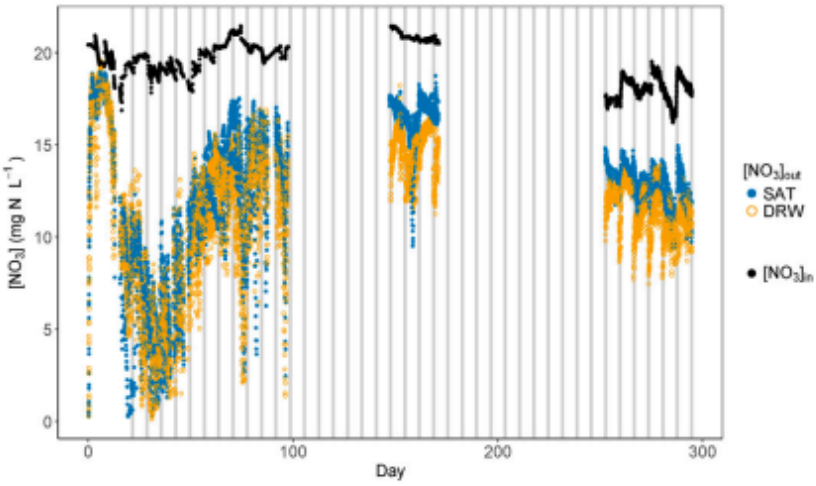

Fig. 1. Nitrate concentrations in the stock tank $[NO_3]_{in}$ and outflow of all columns $[NO_3]_{out}$ over the experiment for saturated (SAT) and drying–rewetting (DRW) columns. Gray vertical bars denote DRW events. Flow was continuous though the entire 287-d experiment, with high-frequency water chemistry monitoring during Days 0–97, 147–171, and 252–287.

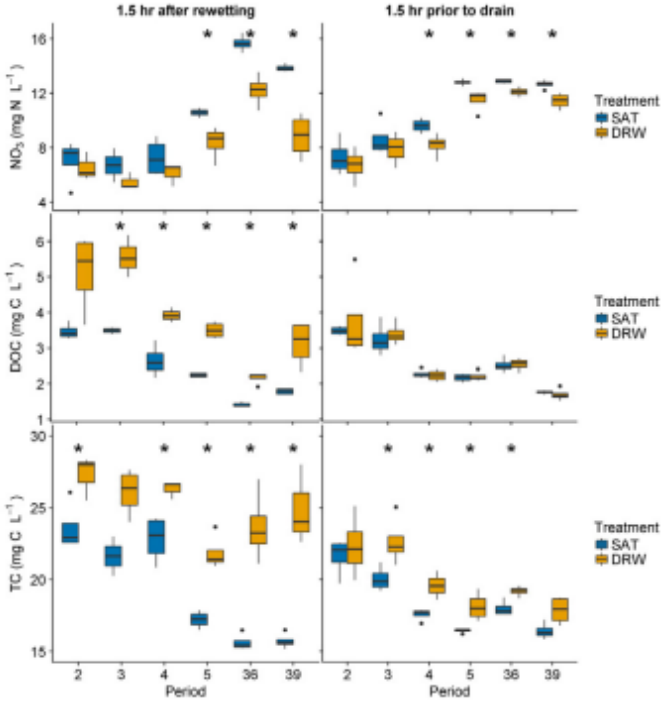

Fig. 2. Outflow composite samples taken immediately after rewetting (1.5 h after outflow) and prior to subsequent drain (1.5 h prior to column draining). Total Kjeldahl nitrogen and total ammonia nitrogen results are not shown. Periods 2, 3, 4, 5, 36, and 39 began on Day 28, 35, 42, 49, 259, and 280. *denotes statistically significant difference between saturated (SAT) and drying–rewetting (DRW) group means for NO_3, dissolved organic C (DOC), and total C (TC) concentrations in outflow composite samples.

and before subsequent drainage, decreased over the experiment, with the highest DOC and TC concentrations in Periods 2 and 3 (Fig. 2). Total Kjeldahl and ammoniacal N concentrations in composite samples did not change significantly from column inlet to outlet or constitute a significant contribution to the nitrogen balance in the columns.

Nitrate Removal Rates

Volumetric NO_3 removal rates (R_{NO3}) were highly variable within and between DRW cycles and ranged from 0.0 to 41.2 g N m^{-3} d^{-1} (Fig. 3, Supplemental Table S3). During the first 10 d, mean R_{NO3} for SAT and DRW groups were 4.5 and 4.4 g N m^{-3} d^{-1}, respectively. Column R_{NO3} increased and were highest during Days 20 to 50 (Periods 1–4), with mean R_{NO3} equal to 21.4 and 23.1 g N m^{-3} d^{-1} for SAT and DRW groups, respectively. Overall, average R_{NO3} decreased to 13.6 and 18.5 g N m^{-3} d^{-1} during Periods 7 and 11 and to 8.3 and 12.1 g N m^{-3} d^{-1} during Periods 19 to 22, to finally stabilize at 8.9 and 12.3 g N m^{-3} d^{-1} during Periods 35 to 39, for SAT and DRW groups, respectively. Much of the variability in R_{NO3} during Periods 0 to 11 was due to greater variability in temperature and column flow rates, with considerably less R_{NO3} variability later in the experiment (Periods 19–22 and Periods 35–39) after temperature and flow issues were addressed.

Although not as apparent during Periods 1 to 11 (likely due to temperature and flow variability during these weeks), a clear pattern of R_{NO3} appeared in DRW columns over the course of each week following a DRW cycle (Fig. 4). While R_{NO3} in SAT columns remained stable, R_{NO3} in DRW columns were highest just after rewetting, steadily decreased for 3 d, and appeared mostly stable for the following 4 d during which R_{NO3} were still significantly higher than R_{NO3} in SAT columns. Data from Periods 19 to 22 and 35 to 39 were selectively used to illustrate decreasing R_{NO3} after rewetting (Fig. 4) since flow and temperature were most stable in these periods. This trend was not clearly observed in data from Periods 1 to 11 (Supplemental Fig. S4) when flow and temperature were less stable.

Analysis of Variance

Data prior to Period 2 were not included in ANOVA analysis testing significance of DRW treatment to remove data possibly influenced by the early microbial acclimation. After the second DRW event (i.e., Period 2), R_{NO3} in DRW columns were greater, compared with SAT, in all subsequent periods. The main effect of treatment proved to be significant ($p = 0.0017$, Supplemental Table S4), as was the main effect of period ($p < 0.0001$). The interaction of period with treatment was not significant ($p = 0.2504$), indicating that R_{NO3} of both treatments changed with period; however, treatment effect did not significantly change with period. When using the lsmeans slice option within the mixed model procedure, the DRW treatment was significant ($\alpha = 0.05$) in all Periods 2 to 39 (Supplemental Table S5). The ANOVA estimate for Treatment effect (3.36 g N m^{-3} d^{-1}) was

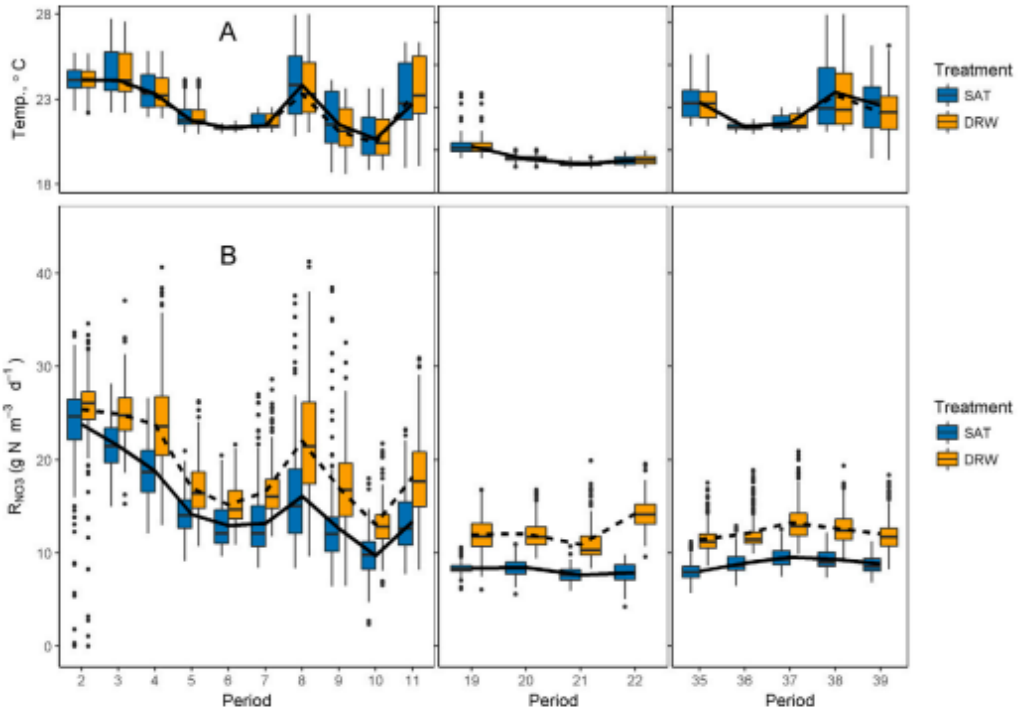

Fig. 3. Box plots of (A) temperature and (B) volumetric nitrate removal rates, R_{NO3}, for both drying–rewetting (DRW) and saturated (SAT) columns from Periods 2–11, 19–22, and 35–39 (Days 28–287). Dashed and solid lines indicate weekly means for each period for DRW and SAT groups, respectively.

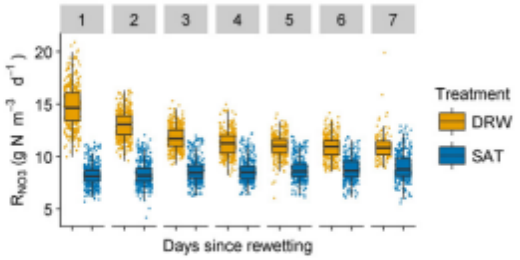

Fig. 4. Boxplots of volumetric NO_3 removal rates (R_{NO3}) according to the number of days since the previous drying–rewetting (DRW) event (for Periods 19–22 and 35–39). Removal rates in DRW columns were ~80% greater than saturated (SAT) columns on the first day after rewetting, with DRW R_{NO3} decreasing and eventually stabilizing ~4 d after rewetting.

comparable to observed mean differences in R_{NO3} between treatments across periods (Supplemental Table S3).

A separate ANOVA analysis was done on Periods 19 to 39 when flow and temperature conditions were more stable (Supplemental Table S6). In this model, treatment, period day, and their interaction were all significant, supporting observations that DRW R_{NO3} declined quickly in Days 1 to 3 and were relatively stable in Days 4 to 7. Model estimates for the fixed effect of period day were 3.5, 2.7, 1.7, 1.3, 0.7, 0.3, and –0.2 g N m^{-3} d^{-1} for Days 1 to 7, respectively, with period day effect not significant on Days 5 to 7, confirming that the effect of DRW was highest just after rewetting and declined afterward.

Discussion

Nitrate Removal Rates Increased by Drying–Rewetting Cycles

After 39 DRW cycles over 287 d, data collected from this experiment provide convincing evidence that regular DRW cycles significantly improved NO_3 removal rates in woodchip columns. Low R_{NO3} in both treatment groups during the first 10 d of the experiment (Start-up Periods A and B) were most likely due to acclimation of the microbial community. Güngör-Demirci and Demirer (2004) reported microbial acclimation in an anaerobic digester of 3 to 5 d until gas production occurred, while Horiba et al. (2005) found that steady-state conditions for denitrifying bacteria in culture did not occur until 80 d after inoculation. While the woodchips were obtained from a field bioreactor, the water chemistry for the experiment was dramatically different from the sprayfield drainage water and could be a reason for an adjustment by the microbial community. Significant differences in R_{NO3} between treatments did not occur until after the second DRW event (Period 2), indicating that the microbial community in DRW columns also took time to adjust to weekly DRW conditions.

After the initial microbial acclimation (Start-up Periods A–C), R_{NO3} in both groups declined over the experiment. While some of the variability in R_{NO3} closely follows changes in temperature, it is unlikely temperature alone was responsible for the decrease in R_{NO3} over time. Mean temperature in Periods 2 to 11 and Periods 35 to 39 were 22.8 and 22.4°C, but mean R_{NO3} in Periods 35 to 39 were lower by ~7 g N m^{-3} d^{-1} (Supplemental Table S3). It is possible that decreasing bioavailability of the woodchips over experiment led to lower R_{NO3}, since organic matter tends to become more recalcitrant as it decomposes (Berg, 2000; Cleveland et al., 2004; Girisha et al., 2003). Ghane et al. (2018) showed that the lignocellulose index of woodchips in a 4-yr-old woodchip bioreactor increased over time, with a higher percentage of the woodchips composed of recalcitrant lignin. Declining NO_3 removal in aging woodchip bioreactors has been well documented, although decreases in performance occur mostly within the first year (David et al., 2016; Robertson, 2010).

High resolution data clearly illustrated the decline in R_{NO3} within 3 d of rewetting, a process that would have been less clear using infrequent data. This is a significant finding in that increased NO_3 removal via DRW cycles should not be overestimated. Columns receiving DRW treatment had R_{NO3} initially 79 to 81% greater on the first day after rewetting, but only 24 to 38% greater from the third to the seventh day, explaining the significant interaction effect between treatment and period day (Supplemental Table S6). High resolution data were crucial in accounting for variability in $[NO_3]_{out}$ caused by temperature and flow, particularly in the first 100 d when R_{NO3} were highly variable. Increased difference in mean R_{NO3} between treatments during Periods 8 and 11 (5.93 and 4.75 g N m^{-3} d^{-1}, respectively) corresponded to substantial temperature increases, suggesting that DRW treatment had a greater effect on R_{NO3} at higher temperatures (Fig. 3).

Observed R_{NO3} were on the intermediate to high end of those reported in a review of 12 different field denitrification beds (2–22 g N m^{-3} d^{-1}; reviewed by Schipper et al., 2010), likely due to the higher temperature range in this experiment. Volumetric NO_3 removal rates were substantially higher than those reported in a column study (Greenan et al., 2009) with temperature maintained at 10°C (2.9–4.5 g N m^{-3} d^{-1}), and comparable to rates reported in a separate woodchip column study (Hoover et al., 2016) at 20 to 21.5°C (10–21 g N m^{-3} d^{-1}). Rates were lower than those reported at similar temperature range (32–39 g N m^{-3} d^{-1} at 14.6–23.5°C), although in that experiment N loading rates were significantly higher and influent had high DOC/NO_3 ratios (Lepine et al., 2016). In our experiment, R_{NO3} during brief temperature increases (up to 41.2 g N m^{-3} d^{-1} at 27.4°C) were much greater than the 95% confidence interval reported in a meta-analysis (Addy et al., 2016) of bioreactor removal rates seen at temperature >16.9°C (3.7–14.9 g N m^{-3} d^{-1}).

Total Carbon and Dissolved Organic Carbon Production Linked to NO_3 Removal

Results of the composite samples indicate that columns were a net source of DOC (Fig. 2). Differences in composite samples between treatment groups were much higher immediately after rewetting than before the subsequent drain 7 d later. Greater TC and DOC concentrations in DRW columns immediately after rewetting support previous findings that respiration and C mineralization increase after DRW cycles (Beare et al., 2009; Borken and Matzner, 2009; Fierer and Schimel, 2003; Gordon et al., 2008). Dissolved organic C made up 27 to 53% of the differences in TC between groups after rewetting. That differences in DOC became insignificant after 7 d may explain why R_{NO3} declined

with the number of days since rewetting. Organic breakdown during aerobic conditions likely increased the availability of C to fuel denitrification in DRW columns, with R_{NO3} decreasing as DOC was leached from the columns. Leaching of DOC over the week in DRW columns showed similar trends to DOC leaching in upflow columns from fresh organic matter (McLaughlan and Al-Mashaqbeh, 2009; Schmidt and Clark, 2013). Increased treatment effect during Periods 8 and 11 when temperature increased dramatically would be explained by higher rates of aerobic organic matter breakdown under elevated temperatures, subsequently leading to greater DOC leaching. These findings contrast with Halaburka et al. (2017), where DOC production rates in woodchip columns receiving continuous flow were not correlated with NO_3 removal rates, although these results were obtained on relatively short (1-wk) experiments using 2-d interval sampling.

Although it is clear from the composite samples that more DOC was leached from DRW columns, it is not clear whether the primary driver of increased R_{NO3} is differences in quantity of available C, its quality, or both. Several studies have shown that bioavailability of the electron donor influences denitrification rates (Cameron and Schipper, 2011; Dodla et al., 2008; Zarnetske et al., 2011; Schmidt and Clark, 2013). While the most immediate suspect for this increased DOC is aerobic breakdown of the woodchips, it is possible that the DOC comes from the biofilm on and within the woodchips. Several studies have observed the release of microbial C following DRW cycles in soils, either from mineralized biofilm or from extracellular release of C molecules following change in osmotic pressure (Gordon et al., 2008; Halverson et al., 2000; Kieft, 1987).

Design Implications

Increased NO_3 removal via DRW cycling could decrease the volume required to achieve a target NO_3 removal. For example, using mean R_{NO3} seen in SAT columns in Periods 19 to 22 and Periods 35 to 39 (8.8 g N m^{-3} d^{-1}), a 57-m^3 bioreactor would be required to treat 50% of tile drainage (20 mg NO_3–N L^{-1}) at a flow rate of 50 m^3 d^{-1}. Mean R_{NO3} in DRW columns during this same time were 12.3 g N m^{-3} d^{-1}, requiring a 41-m^3 bioreactor (28% reduction in volume) to achieve the same percentage reduction. Whether this size reduction would result in a net cost reduction is unclear. Christianson et al. (2012) put the unit cost for two bioreactors in Iowa at $40 to $80 m^{-3}. It is uncertain whether manually controlling flow to achieve DRW cycles would result in cost savings when factoring in labor costs or that regular bioreactor management would be feasible for farmers. An automated system to manage flow is possible but may not be cost-effective for smaller bioreactors where size reduction does not reduce costs below the capital cost of an automated control system. Application of DRW cycles may be more useful in controlled systems (e.g., tertiary wastewater treatment, constructed treatment wetlands).

Management Considerations

Should DRW cycles become implemented in the field, it is useful to calculate the DRW frequency that would provide the optimum NO_3 removal. As R_{NO3} are much higher just after rewetting, increasing DRW frequency may be advantageous (Fig. 5). During the 8 h of aerobiosis of the DRW cycles, however, drained woodchips would provide no NO_3 removal. Using daily average R_{NO3} values when rates were most stable (Periods 19–22 and 35–39; Fig. 4) it is possible to calculate the total mass NO_3 removed as a function of DRW frequency, taking into account treatment lost while woodchips are drained. The results of this simple analysis show that draining the columns for 8 h every 2 to 3 d would theoretically produce the greatest net increase in total NO_3 removed (41–43%; Fig. 5), while weekly DRW only provides a 33% increase in total NO_3 removed (average weekly removal of 83.6 and 59.6 g N m^{-3} for DRW and SAT columns, respectively). This analysis assumes the average daily R_{NO3} would not change with increased DRW frequency. In field bioreactors under managed DRW cycles, untreated flow would be discharged though the bypass manifold designed to prevent flooding of crop fields.

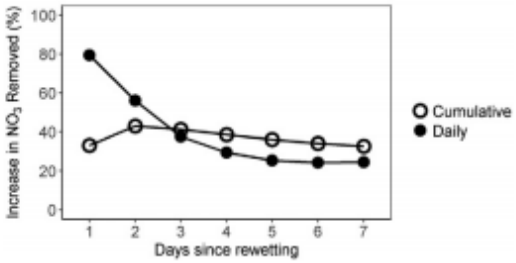

Fig. 5. Increases in total NO_3 removed in drying–rewetting (DRW) columns, relative to saturated (SAT) columns, based on differences in daily mean removal rates (R_{NO3}) (solid) and cumulative NO_3 removed when considering untreated bypass while DRW columns were drained (hollow). The results indicate that increasing the DRW frequency to one drain every 2–3 d would provide the greatest overall improvement (41–43%) in total NO_3 removed.

Percentage NO_3 mass reduction ($100\% \times ([NO_3]_{in} - [NO_3]_{out})/[NO_3]_{in}$) is commonly reported and is a useful metric for water quality planners to quantify removal efficiency of treatment systems. While NO_3 removal rates, R_{NO3}, were increased by 24 to 81%, this translated to a more modest increase in percentage NO_3 mass reduction of <10% points for our experimental settings ($[NO_3]_{in}$ = 19.5 ± 1.3 mg NO_3–N L^{-1}; HRT = 8 ± 2 h). Percentage mass reduction, however, depends on the HRT, and $[NO_3]_{in}$ and would increase with higher HRT and lower $[NO_3]_{in}$. For example, using average R_{NO3} during later periods (Fig. 4) at the mean 8 ± 2 h HRT, the percentage NO_3 mass reduction for SAT and DRW columns would have been 28 and 40% at $[NO_3]_{in}$ = 15 mg NO_3–N L^{-1} (increase of 12% points), or 42 and 61% at $[NO_3]_{in}$ = 10 mg NO_3–N L^{-1} (increase of 19% points). Managers who will use DRW cycling to improve bioreactor performance should keep in mind that increases in the rate of NO_3 removal may not equal increases in percentage NO_3 reduction, depending on site conditions.

Woodchips with regular DRW cycles would be broken down faster than constantly saturated woodchips, however, resulting in an expected shorter bioreactor lifespan or decreased time before new woodchips would need to be added. Lifetime of the woodchips would depend on how long and how often woodchips were unsaturated. Moorman et al. (2010) saw that wood loss in more frequently unsaturated, shallow woodchips was 62% greater over 9 yr than deeper woodchips. The study predicted that the half-life for shallow woodchips was only 13% (4.6 yr) of that

for deeper woodchips. Ghane et al. (2018) also found significantly higher lignocellulose index and lower C-to-N ratios for woodchips located close to the inlet of a field bioreactor, a zone more frequently exposed to high DO and aerobic breakdown of organic matter. Carbon loss from woodchips would depend on the duration and frequency of DRW cycles.

Conclusions

This study showed N removal in woodchip bioreactors could be enhanced by DRW cycles with unsaturated periods as short as 8 h. Increases in NO_3 removal rates were as high as 81% the first day after rewetting with weekly mean removal rates increased by 36 to 43%, although managers of bioreactors may see lower increases in percentage NO_3 reduction. Drying–rewetting cycles in field bioreactors can be made possible through water level management or other innovative design. Field studies of DRW effects on removal rates are necessary since biogeochemical conditions in unsaturated woodchips buried under soil are likely to be different than those seen in this column study. Limited analysis was given to quantifying the effects of temperature, flow, and DOC on NO_3 removal. The substantial amount of data collected in this experiment makes a clear answer to the hypothesis and a deeper analysis difficult to address in a single paper. A subsequent paper will look at primary drivers of NO_3 removal in DRW columns. Aerobic processes during the 8-h drained period are likely responsible for improved performance, with increased organic breakdown the primary cause of increased NO_3 removal rates.

Supplemental Material

The supplemental material includes additional information on column flow, temperature, and dissolved oxygen; ANOVA slice analysis results; mean volumetric nitrate removal rates; SAS code; ANOVA proc mixed results; and a photograph of the laboratory experiment set-up. All data collected from this experiment and R code used to produce figures can be downloaded from a public Github repository at https://github.com/bmmaxwel/Maxwell.et.al.2018_WettingDrying.

Acknowledgments

This work was financially supported by USDA NIFA [#S1063 and #2016-67019-25279] as part of an international collaboration between researchers at NCSU, Iowa State University, University of Illinois Champaign-Urbana, USEPA, and University of Waikato in New Zealand The authors would like to thank the Environmental Analysis Laboratory at NCSU for water chemistry analysis, Dr. Consuello Arellano of the NCSU Statistics Department for statistical consulting, and J.A. Yount for help with data collection.

References

Addy, K., A.J. Gold, L.E. Christianson, M.B. David, L.A. Schipper, and N.A. Ratigan. 2016. Denitrifying bioreactors for nitrate removal: A meta-analysis. J. Environ. Qual. 45(3):873–881. doi:10.2134/jeq2015.07.0399

ÆsØy, A., H. Ødegaard, K. Bach, R. Pujol, and M. Hamon. 1998. Denitrification in a packed bed biofilm reactor (BIOFOR): Experiments with different carbon sources. Water Res. 32(5):1463–1470. doi:10.1016/S0043-1354(97)00358-8

Beare, M., E. Gregorich, and P. St-Georges. 2009. Compaction effects on CO_2 and N_2O production during drying and rewetting of soil. Soil Biol. Biochem. 41(3):611–621. doi:10.1016/j.soilbio.2008.12.024

Berg, B. 2000. Litter decomposition and organic matter turnover in northern forest soils. For. Ecol. Manage. 133(1-2):13–22. doi:10.1016/S0378-1127(99)00294-7

Birgand, F., K. Aveni-Deforge, B. Smith, B.M. Maxwell, M. Horstman, A.B. Gerling, and C.C. Carey. 2016. First report of a novel multiplexer pumping system coupled to a water quality probe to collect high temporal frequency in situ water chemistry measurements at multiple sites. Limnol. Oceanogr. Methods 14(12):767–783. doi:10.1002/lom3.10122

Borken, W., and E. Matzner. 2009. Reappraisal of drying and wetting effects on C and N mineralization and fluxes in soils. Glob. Change Biol. 15(4):808–824. doi:10.1111/j.1365-2486.2008.01681.x

Brown, T., J. Berg, and K. Underwood. 2010. Replacing incised headwater channels and failing stormwater infrastructure with regenerative stormwater conveyance. In: S. Struck and K. Lichten, editors, Low impact development 2010: Redefining water in the city. American Society of Civil Engineers, Reston, VA. p. 207–217. doi:10.1061/41099(367)19

Cameron, S.G., and L.A. Schipper. 2010. Nitrate removal and hydraulic performance of organic carbon for use in denitrification beds. Ecol. Eng. 36(11):1588–1595. doi:10.1016/j.ecoleng.2010.03.010

Cameron, S.G., and L.A. Schipper. 2011. Evaluation of passive solar heating and alternative flow regimes on nitrate removal in denitrification beds. Ecol. Eng. 37(8):1195–1204. doi:10.1016/j.ecoleng.2011.02.020

European Committee for Standardization. 2009. Solid biofuels—methods for determination of moisture content—oven dry method—Part 2: Total moisture—simplified method. CEN/TC 335. European Committee for Standardization (CEN).

Chen, X., E. Peltier, B.S. Sturm, and C.B. Young. 2013. Nitrogen removal and nitrifying and denitrifying bacteria quantification in a stormwater bioretention system. Water Res. 47(4):1691–1700. doi:10.1016/j.watres.2012.12.033

Christianson, L.E., A. Bhandari, and M.J. Helmers. 2011. Pilot-scale evaluation of denitrification drainage bioreactors: Reactor geometry and performance. J. Environ. Eng. 137(4):213–220. doi:10.1061/(ASCE)EE.1943-7870.0000316

Christianson, L.E., A. Bhandari, M.J. Helmers, K.J. Kult, T. Sutphin, and R. Wolf. 2012. Performance evaluation of four field-scale agricultural drainage denitrification bioreactors in Iowa. Trans. ASABE 55(6):2163–2174. doi:10.13031/2013.42508

Christianson, L.E., C. Lepine, P.L. Sibrell, C. Penn, and S.T. Summerfelt. 2017. Denitrifying woodchip bioreactor and phosphorus filter pairing to minimize pollution swapping. Water Res. 121:129–139. doi:10.1016/j.watres.2017.05.026

Cleveland, C.C., J.C. Neff, A.R. Townsend, and E. Hood. 2004. Composition, dynamics, and fate of leached dissolved organic matter in terrestrial ecosystems: Results from a decomposition experiment. Ecosystems 7(3):175–285. doi:10.1007/s10021-003-0236-7

David, M.B., L.E. Gentry, R.A. Cooke, and S.M. Herbstritt. 2016. Temperature and substrate control woodchip bioreactor performance in reducing tile nitrate loads in east-central Illinois. J. Environ. Qual. 45(3):822–829. doi:10.2134/jeq2015.06.0296

Dodla, S.K., J.J. Wang, R.D. DeLaune, and R.L. Cook. 2008. Denitrification potential and its relation to organic carbon quality in three coastal wetland soils. Sci. Total Environ. 407(1):471–480. doi:10.1016/j.scitotenv.2008.08.022

Etheridge, J.R., F. Birgand, J.A. Osborne, C.L. Osburn, M.R. Burchell, and J. Irving. 2014. Using in situ ultraviolet-visual spectroscopy to measure nitrogen, carbon, phosphorus, and suspended solids concentrations at a high frequency in a brackish tidal marsh. Limnol. Oceanogr. Methods 12(1):10–22. doi:10.4319/lom.2014.12.10

Fierer, N., and J.P. Schimel. 2003. A proposed mechanism for the pulse in carbon dioxide production commonly observed following the rapid rewetting of a dry soil. Soil Sci. Soc. Am. J. 67(3):798–805. doi:10.2136/sssaj2003.0798

Ghane, E., G.W. Feyereisen, C.J. Rosen, and U.W. Tschirner. 2018. Carbon quality of four-year-old woodchips in a denitrification bed treating agricultural drainage water. Trans. ASABE 61:995–1000. doi:10.13031/trans.12642

Girisha, G., L. Condron, P. Clinton, and M. Davis. 2003. Decomposition and nutrient dynamics of green and freshly fallen radiata pine (*Pinus radiata*) needles. For. Ecol. Manage. 179(1–3):169–181. doi:10.1016/S0378-1127(02)00518-2

Gordon, H., P.M. Haygarth, and R.D. Bardgett. 2008. Drying and rewetting effects on soil microbial community composition and nutrient leaching. Soil Biol. Biochem. 40(2):302–311. doi:10.1016/j.soilbio.2007.08.008

Greenan, C.M., T.B. Moorman, T.B. Parkin, T.C. Kaspar, and D.B. Jaynes. 2009. Denitrification in wood chip bioreactors at different water flows. J. Environ. Qual. 38(4):1664–1671. doi:10.2134/jeq2008.0413

Güngör-Demirci, G., and G.N. Demirer. 2004. Effect of initial COD concentration, nutrient addition, temperature and microbial acclimation on anaerobic treatability of broiler and cattle manure. Bioresour. Technol. 93(2):109–117. doi:10.1016/j.biortech.2003.10.019

Halaburka, B.J., G.H. LeFevre, and R.G. Luthy. 2017. Evaluation of mechanistic models for nitrate removal in woodchip bioreactors. Environ. Sci. Technol. 51(9):5156–5164. doi:10.1021/acs.est.7b01025

Halverson, L.J., T.M. Jones, and M.K. Firestone. 2000. Release of intracellular solutes by four soil bacteria exposed to dilution stress. Soil Sci. Soc. Am. J. 64(5):1630–1637. doi:10.2136/sssaj2000.6451630x

Hoover, N.L., A. Bhandari, M.L. Soupir, and T.B. Moorman. 2016. Woodchip denitrification bioreactors: Impact of temperature and hydraulic retention time on nitrate removal. J. Environ. Qual. 45(3):803–812. doi:10.2134/jeq2015.03.0161

Horiba, Y., S.T. Khan, and A. Hiraishi. 2005. Characterization of the microbial community and culturable denitrifying bacteria in a solid-phase denitrification process using poly (ε-caprolactone) as the carbon and energy source. Microbes Environ. 20(1):25–33. doi:10.1264/jsme2.20.25

Kieft, T.L. 1987. Microbial biomass response to a rapid increase in water potential when dry soil is wetted. Soil Biol. Biochem. 19(2):119–126. doi:10.1016/0038-0717(87)90070-8

Kim, H., E.A. Seagren, and A.P. Davis. 2003. Engineered bioretention for removal of nitrate from stormwater runoff. Water Environ. Res. 75(4):355–367. doi:10.2175/106143003X141169

Lepine, C., L. Christianson, K. Sharrer, and S. Summerfelt. 2016. Optimizing hydraulic retention times in denitrifying woodchip bioreactors treating recirculating aquaculture system wastewater. J. Environ. Qual. 45(3):813–821. doi:10.2134/jeq2015.05.0242

Liu, Y. 2017. The performance of controlled drainage and inline denitrifying woodchip bioreactor for reducing nutrient losses from subsurface drained grassland receiving liquid swine lagoon effluent. Ph.D. diss., North Carolina State University.

Maxwell, B.M., F. Birgand, B. Smith, and K. Aveni-Deforge. 2018. A small-volume multiplexed pumping system for automated, high-frequency water chemistry measurements in volume-limited applications. Hydrol. Earth Syst. Sci. 22(11):5615–5628. doi:10.5194/hess-22-5615-2018

McLaughlan, R.G., and O. Al-Mashaqbeh. 2009. Simple models for the release kinetics of dissolved organic carbon from woody filteration media. Bioresour. Technol. 100(9):2588–2593. doi:10.1016/j.biortech.2008.12.002

Miller, A.E., J.P. Schimel, T. Meixner, J.O. Sickman, and J.M. Melack. 2005. Episodic rewetting enhances carbon and nitrogen release from chaparral soils. Soil Biol. Biochem. 37(12):2195–2204. doi:10.1016/j.soilbio.2005.03.021

Moorman, T.B., T.B. Parkin, T.C. Kaspar, and D.B. Jaynes. 2010. Denitrification activity, wood loss, and N_2O emissions over 9 years from a wood chip bioreactor. Ecol. Eng. 36(11):1567–1574. doi:10.1016/j.ecoleng.2010.03.012

Palmer, K., J. Kopp, G. Gebauer, and M.A. Horn. 2016. Drying-rewetting and flooding impact denitrifier activity rather than community structure in a moderately acidic fen. Front. Microbiol. 7:727. doi:10.3389/fmicb.2016.00727

Robertson, W. 2010. Nitrate removal rates in woodchip media of varying age. Ecol. Eng. 36(11):1581–1587. doi:10.1016/j.ecoleng.2010.01.008

Ruser, R., H. Flessa, R. Russow, G. Schmidt, F. Buegger, and J. Munch. 2006. Emission of N_2O, N_2, and CO_2 from soil fertilized with nitrate: Effect of compaction, soil moisture, and rewetting. Soil Biol. Biochem. 38(2):263–274. doi:10.1016/j.soilbio.2005.05.005

SAS Institute. 2011. Base SAS 9.4 procedures guide. SAS Inst., Cary, NC.

Schipper, L.A., S. Cameron, and S. Warneke. 2010. Nitrate removal from three different effluents using large-scale denitrification beds. Ecol. Eng. 36(11):1552–1557. doi:10.1016/j.ecoleng.2010.02.007

Schmidt, C.A., and M.W. Clark. 2013. Deciphering and modeling the physicochemical drivers of denitrification rates in bioreactors. Ecol. Eng. 60:276–288. doi:10.1016/j.ecoleng.2013.07.041

Rice, E.W., R.B. Baird, and A.D. Eaton, editors. 2017a. 4500-NH_3 nitrogen (ammonia) G. In: Standard methods for examination of water and wastewater. American Public Health Association, American Water Works Association, and Water Environment Federation, Washington, DC.

Rice, E.W., R.B. Baird, and A.D. Eaton, editors. 2017b. 4500-N_{org} B. In: Standard methods for examination of water and wastewater. American Public Health Association, American Water Works Association, and Water Environment Federation, Washington, DC.

USEPA. 1993a. Standard 351.2, Revision 2.0: Determination of total Kjeldahl nitrogen by semi-automated colorimetry. USEPA, Cincinnati, OH.

USEPA. 1993b. Standard 353.2, Revision 2.0: Determination of nitrate-nitrite nitrogen by automated colorimetry. USEPA, Cincinnati, OH.

USEPA. 1999. EPA Standard 415.1. Total organic carbon in water. USEPA, Cincinnati, OH.

Vaughan, M.C., W.B. Bowden, J.B. Shanley, A. Vermilyea, R. Sleeper, A.J. Gold, S. Pradhanang , S.P. Inamdar, D.F. Levia, and A.S. Andres. 2017. High-frequency dissolved organic carbon and nitrate measurements reveal differences in storm hysteresis and loading in relation to land cover and seasonality. Water Resour. Res. 53(7):5345–5363.

Warneke, S., L.A. Schipper, D.A. Bruesewitz, I. McDonald, and S. Cameron. 2011. Rates, controls and potential adverse effects of nitrate removal in a denitrification bed. Ecol. Eng. 37(3):511–522. doi:10.1016/j.ecoleng.2010.12.006

Woli, K.P., M.B. David, R.A. Cooke, G.F. Mclsaac, and C.A. Mitchell. 2010. Nitrogen balance in and export from agricultural fields associated with controlled drainage systems and denitrifying bioreactors. Ecol. Eng. 36(11):1558–1566. doi:10.1016/j.ecoleng.2010.04.024

Xiang, S., A. Doyle, P.A. Holden, and J.P. Schimel. 2008. Drying and rewetting effects on C and N mineralization and microbial activity in surface and subsurface California grassland soils. Soil Biol. Biochem. 40(9):2281–2289. doi:10.1016/j.soilbio.2008.05.004

Zarnetske, J.P., R. Haggerty, S.M. Wondzell, and M.A. Baker. 2011. Labile dissolved organic carbon supply limits hyporheic denitrification. J. Geophys. Res. Biogeosci. 116:G04036. doi:10.1029/2011JG001730

CHAPTER 4: Drivers of Nitrate Removal in Woodchip Bioreactors Exposed to Drying-rewetting Cycles

4.1. Introduction

Woodchip bioreactors (also referred to as denitrification beds) are an agricultural BMP used for the removal of nitrate (NO_3) in water discharged at the edge of farm fields. The removal process is denitrification where nitrogen in the aqueous nitrate anion form is reduced into gaseous dinitrogen and nitrous oxide, and thus leaves the aquatic environment. Woodchip bioreactors (WB) installed as large pits in the ground (e.g., ~1 to 1.5 m deep, 1 to 6 m wide, and 3 to 30 m long) are designed to promote denitrifying conditions in that 1) a carbon substrate is added to serve as an electron donor for denitrifying microbes and 2) such that anoxic conditions persist favoring the use of NO_3 as the electron acceptor. Anaerobic denitrification is achieved by either managing the water table with control structures or placing the WB below the water table. Woodchip bioreactor applications for removing NO_3, include subsurface drainage water from crop (Christianson et al., 2012; David et al., 2016; Woli et al., 2010), dairy (Schipper et al., 2010) and hog farm fields (Liu, 2017), aquaculture units (Lepine et al., 2016; von Ahnen et al., 2016), and hydroponics operations (Warneke et al., 2011).

Volumetric nitrate removal rates (g N m^{-3} woodchip-filled volume d^{-1}) in woodchip bioreactors have been shown to be variable over time and as environmental factors change. Schipper et al. (2010) reported rates in a number of lab and field studies of 2 – 22 g N m^{-3} d^{-1}, and Lepine et al. (2016) saw rates as high as 32 – 39 g N m^{-3} d^{-1} in a bioreactor treating aquaculture effluent. Nitrate removal rates in field bioreactors treating tile drainage water are typically much lower. In four field bioreactors in Iowa, Christianson et al. (2012) saw mean removal rates of 0.4 – 7.8 g N m^{-3} d^{-1}. A more recent meta-analysis of 26 woodchip bioreactor studies gave a 95% confidence interval of 2.9 – 7.3 and 1.4 – 5.4 for field bioreactors and bioreactors >13 months old (Addy et al., 2016). Mean nitrate removal rates >10 g N m^{-3} d^{-1} are typically not seen in studies of field bioreactors unless the woodchips are <1 yr in age or temperature is high (>20 – 22 °C). Higher total treatment can overcome low volumetric rates by increasing hydraulic residence time (HRT) via lower design flow rate (Greenan et al., 2009; Hoover et al., 2016; Lepine et al., 2016).

Low volumetric NO_3 removal rates are linked to the need for bioreactor longevity. Coarse woodchips, most commonly used as the fill media and electron donor for denitrification, provide a carbon source with low bioavailability that is broken down slowly over time. Woodchips have a high carbon content (~50%; Greenan et al., 2009; Moorman et al., 2010), although their high percentage of recalcitrant lignin (17 -22 %, Feyereisen et al, 2016; Christianson et al., 2016) limits anaerobic respiration rates. Because woodchip bioreactors are designed for a long lifespan (10 – 20 yr), low NO_3 removal rates are inherent to their design. Nitrate removal is highest in young woodchips when a higher percentage of biomass is made up of more easily degraded C compounds (e.g. cellulose, hemicellulose) relative to rates seen in older woodchips with higher content of recalcitrant lignin (Ghane et al., 2018). Several methods have been proposed for improving in situ NO_3 removal rates in woodchip bioreactors including more degradable carbon sources (Cameron and Schipper, 2010; Feyereisen et al., 2016), heating (Cameron and Schipper, 2011), electrical stimulation (Law et al., 2018), methanol or acetate dosing (Saliling et al., 2017; Roser et al., 2018), and drying-rewetting cycles (Christianson et al., 2017; Maxwell et al., 2018).

A previous 10 month column study conclusively showed that drying-rewetting (DRW) cycles as short as 8 h on a weekly basis could improve NO_3 removal rates relative to constantly saturated conditions (Maxwell et al., 2018). Increases in NO_3 removal rates were highest immediately after rewetting (79 – 81%), with mean ~33% increase in total mass N removed over each week. Higher dissolved organic carbon (DOC) in composite outflow samples supported the hypothesis that increased NO_3 removal rates were linked to higher leaching of more bioavailable organics released during aerobic respiration. Other studies have similarly reported greater C leaching following DRW cycles (Groffman and Tiedje, 1988; Gordon et al., 2008; Beare et al., 2009). Although DOC concentration ([DOC]) was also measured at high-frequency, the paper was limited in scope to addressing the basic hypothesis of increased NO_3 removal caused by DRW cycles.

It is important to understand the underlying mechanisms driving increased NO_3 removal in woodchips exposed to DRW cycles. If aerobic respiration during unsaturated aerobic conditions is responsible for greater NO_3 removal, one hypothesis is that duration or longer periods of aerobic conditions might provide greater increases. Other factors (e.g. HRT, temperature) are also likely to influence the effect of DRW cycles on NO_3 removal. This study was conducted to

evaluate 1) whether shorter or longer duration of unsaturated conditions provides lesser or greater NO_3 removal after subsequent rewetting, 2) the quantitative effect of [DOC] on NO_3 removal rates and 3) the interaction of HRT and temperature on NO_3 removal in woodchips exposed to DRW cycles.

4.2. Methods

4.2.1. Experimental design

A 105-day column experiment was performed at the NCSU Biological and Agricultural Engineering facility from May to August 2018. Eight experimental units consisted of 15.2 cm diameter, 96 cm tall polyvinylchloride (PVC) columns filled with aged woodchips collected from a 6-year-old field bioreactor. Previous analysis of the aged woodchips reported total C content of 34 – 45% and C:N ratio of 48 – 54 (Maxwell et al., 2018). The upflow columns consisted of woodchips above a gravel underbed with water entering the base of the column fed by an 8-channel ISMATEC peristaltic pump (0.68±0.11 L h^{-1}, mean±standard deviation, Figure D-1). Columns received inflow from a 1,200 L stock tank of dechlorinated tap water spiked with KNO_3 (17.3±0.6 mg N L^{-1}). A complete description of the columns, sampling equipment, and facilities are described in Maxwell et al. (2018).

The previous DRW experiment consisted of two treatments (n=4). Columns were either exposed to continuous flow, constant saturation (SAT) or continuous flow outside of weekly 8 h aerobic periods where columns were drained then refilled once flow was restarted (DRW). In the present study columns were assigned one of four treatments (n=2). Two columns received the same SAT treatment. The remaining six columns received a weekly DRW event where unsaturated conditions lasted for 2 h, 8 h, or 24 h. The SAT and 8 h DRW treatments were repeated to compare results of this study to the previous study. Columns that received the SAT and 8 h DRW treatment in the previous experiment also received the same SAT and 8 h DRW treatment, respectively, in the current study. The 2 h and 24 h DRW treatments were selected to compare the effects of DRW events of much shorter or longer duration than the previous study. A single DRW cycle refers to each draining and subsequent refilling of columns with KNO_3 water. Over the 105-d experiment, a baseline period of 33 d was used to compare variability of columns, after which 11 DRW cycles were applied to the three DRW treatments. Although all DRW columns

were given ‘weekly’ treatments, columns were drained simultaneously. As such, 24 h DRW columns had 22 or 16 h less saturated time between consecutive draining events, relative to the 2 h and 8 h DRW treatments, respectively.

The term ‘drying-rewetting’ in this article, consistent with previous literature on DRW cycles, refers to the process of draining previously saturated woodchips, allowing air to enter the pore space previously filled by water, and saturating the pores with water again. During the ‘drying’ part of the cycle, the woodchip porous medium is drained to equilibrium and is thus still moist and not ‘dry’ as the term might suggest. Collected data were given a Period number corresponding to the number of prior DRW cycles (e.g. Period 2 for data collected after the second and prior to the third DRW cycle, with one week between each DRW cycle). In this paper, the data from the current experiment and the previous experiment (Maxwell et al., 2018) are presented for comparison and are referred to as DRW 2018 and DRW 2017, respectively.

4.2.2. High frequency water physico-chemistry analysis

Stock tank and column outflow water chemistry were measured using a small volume multiplexed pumping system (MPS) coupled to a high frequency spectrophotometer (S::CAN, Austria). The full sampling sequence and methods for sequentially sampling water chemistry in each column is described in Maxwell et al. (2018). In short, upon a 12V pulse generated by the spectrophotometer (which normally triggers a wiper), the MPS pumped water from column n to a flow-through 10-mm pathlength quartz cuvette attached to the S::CAN. Pumping stopped for probe reading, then reversed the peristaltic pump to purge water back to waste. The system then switched the valve manifold to pump column n+1 and waited for the next signal. Each column was sampled every 2 h continuously over the entire 105-d experiment. Lab samples (n=28) were collected and analyzed for [NO_3] (EPA Method 353.2, BAE Environmental Analysis Lab, North Carolina State University) and [DOC] (EPA 415.1,Teledyne Tekmar Apollo 9000, Mason, OH; 0.45 µm filter). Temperature (Figure D-1) and DO (Figure D-2) of column outflow were measured hourly using Presens® temperature sensors and oxygen dipping probes (DP-PSt3, Presens Precision Sensing GmbH, Regensburg, Germany).

4.2.3. Nitrate removal rates

Volumetric NO_3 removal rates (R_{NO3}) for each column were calculated as the difference between column inlet NO_3-N concentrations ($[NO_3]_{in}$) and outlet NO_3-N concentrations ($[NO_3]_{out}$) times the flow rate over the woodchip-filled column volume (0.009 m^3), yielding units in g N m^{-3} d^{-1}. Leaching rates of DOC (L_{DOC}) were calculated using the same method, using differences in inlet and outlet [DOC].

4.2.4. Statistical analysis

Mixed linear model analysis was performed in SAS (SAS Proc MIXED, SAS 9.4) on data collected from all columns to determine the effect of treatment, temperature, HRT, and DOC leaching rate (L_{DOC}). Three models were developed for both the DRW 2018 and the DRW 2017 experiment. The first model tested for the significance of the treatment main effect only. In the DRW 2018 experiment with three treatments and one control, treatment effect was determined using least squares means with a Tukey correction for multiple comparisons. The second model tested the significance of main effects of temperature, HRT, and L_{DOC} and calculated the coefficients of each main effect. The third model tested the significance of each of the three main effects as well as all two-way interaction between the three effects, and calculated the coefficients of each interaction effect.

The regression analysis accounted for repeated measurements for each column by specifying column as a subject with repeated measures over time (repeated Day/subject=Column) with the covariance structure selected by minimizing the model Akaike information criterion (AIC). Random effects were included for nested factors (Column within Treatment). The full SAS code for all three models is included in the Supporting Information.

4.3. Results

4.3.1. High frequency water physico-chemistry

In the 2018 study (DRW 2018), the multiplexed sampling system successfully captured 9,940 measurements for $[NO_3]_{out}$ and $[DOC]_{out}$ over the 105-d period, or ~1,240 measurements per column (Figure D-3 and Figure D-4). Unlike the previous 287-d study (DRW 2017), $[NO_3]_{out}$

was measured every 2 h over the entire experiment rather than only select periods. Columns receiving drying-rewetting cycles underwent 11 DRW cycles (Periods 1 – 11) following a 33 d period (Period 0) in which all columns had continuous flow, constant saturation. Approximately 53 and 17 h of data were removed on Day 17 and Day 75, respectively, after electrical issues with the 8-channel pump caused flow rates to drop rapidly in all columns. In several other instances data were removed on a column-by-column basis when clogging or wear of the peristaltic pump tubing caused flow to be dramatically reduced over a short period of time.

Inlet $[NO]_3$, measured at the tank, was more stable and slightly lower (17.3±1.1 mg N L^{-1}) in the DRW 2018 experiment relative to DRW 2017 (19.5±1.3 mg N L^{-1}). After the initial start-up of flow to columns, $[NO_3]_{out}$ in all columns ranged from 0.3 – 15.7 mg N L^{-1} and varied largely with flow rate. Mean $[DOC]_{in}$ from the tank was 0.9±0.1 mg C L^{-1}, roughly half $[DOC]_{in}$ from the previous DRW 2017 experiment (1.9±0.6 mg C L^{-1}), likely due to the shorter duration of the experiment and cleaning of the KNO_3 stock tank prior to the experiment. Column $[DOC]_{out}$ ranged from 1.0 – 3.9 mg C L^{-1}.

Temperatures were also more stable in the 2018 experiment relative to DRW 2017 (Figure D-1). Temperatures during DRW 2018 cycles (Period 1 – 11) ranged from 20.5 – 24.7 °C (22.7±0.9 °C), compared with more variable temperatures during the 2017 experiment (18.6 – 29.0 °C, 22.0±2.0 °C). A diurnal signal was seen in the temperature data at Day>31, with decreased daytime temperatures caused by greater cooling in the lab during the day. Diurnal variation of temperatures was <0.5°C. Outside of periods when columns were drained, [DO] in column outflow was generally <0.1 mg L^{-1} in all columns (Figure D-2) and $[DO]_{in}$ from the tank was 6.50±0.8 mg L^{-1}.

4.3.2. Nitrate removal rates in the DRW 2018 experiment

Volumetric nitrate removal rates, R_{NO3}, were lowest in SAT and 2 h DRW treatments and highest in the 24 h DRW treatment (Figure 4-1, Table D-1). Removal rates were most similar between treatment groups during the 33 d baseline period in which all columns received the SAT treatment, although there were differences between groups. Mean R_{NO3} during the baseline Period 0 were 16.5, 12.1, 15.8, 18.8 g N m^{-3} d^{-1} for SAT, 2 h, 8 h, and 24 h DRW groups, respectively, indicating differences between groups prior to initiating DRW cycles. Mean R_{NO3}

during Period 0 for 24 h DRW treatment was higher due to increased R_{NO3} in one of the replicates. Differences in mean R_{NO3} between columns within the same treatment group during Period 0 were <2.7 g N m^{-3} d^{-1}, other than the 24 h DRW group where mean R_{NO3} of the two columns differed by 6 g N m^{-3} d^{-1}.

After the initiation period, R_{NO3} diverged quickly among DRW 2018 treatment groups. For clarity, Figure 4-2 shows mean R_{NO3} over each weekly DRW cycle (Periods 1-11). Removal rates in 24 h DRW columns were immediately higher than all other treatment groups after the first DRW cycle (Period 1). Removal rates in SAT columns were higher than 2 h DRW columns until the fourth DRW cycle, after which rates were comparable between the two groups. Removal rates in SAT and 8 h DRW columns were similar until the third DRW cycle, after which R_{NO3} in 8 h DRW columns were higher in all Periods. Differences between treatment groups appeared to be most stable after the third DRW cycle. Mean R_{NO3} from Periods 3-11 were 11.8±2.7, 12.3±2.9, 16.8±3.1, and 24.4±4.0 g N m^{-3} d^{-1} for SAT, 2 h, 8 h, and 24 h DRW groups, respectively. Relative to the SAT treatment group, weekly mean R_{NO3} were greater by 6±10, 45±13, and 114±29% in 2 h, 8 h, and 24 h DRW groups.

Removal rates in SAT and 8 h DRW columns for Periods 3-11 in the present study were comparable to those seen in DRW 2017 in Periods 5 - 20 (Days 49 – 161). In DRW 2017 SAT and 8 h DRW, weekly mean R_{NO3} in these periods ranged from 8.4 – 14.1 and 12.0 – 18.1 g N m^{-3} d^{-1} for SAT and 8 h DRW columns. Differences between SAT and 8 h DRW weekly mean R_{NO3} in DRW 2017 ranged from 2.2 – 5.9 g N m^{-3} d^{-1}, with an average difference in R_{NO3} of 3.5 g N m^{-3} d^{-1}. In the present study, differences in weekly mean R_{NO3} between SAT and 8 h DRW from Periods 4 – 11 ranged from 3.2 – 6.0, with a higher average difference of 5.0 g N m^{-3} d^{-1}. Percent increase in weekly mean R_{NO3} in the 8 h DRW group, relative to the SAT treatment, in the current study was comparable to that seen in DRW 2017 (34±8% increase).

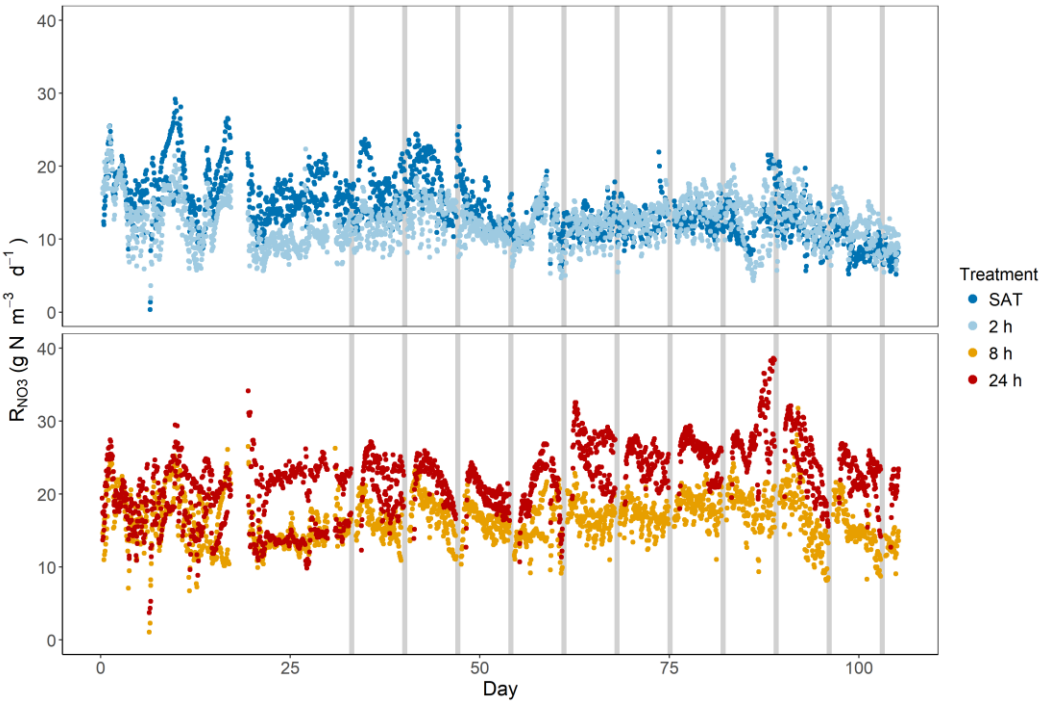

Figure 4-1. Volumetric nitrate removal rates (R_{NO3}) for all columns from each group. Variability between groups during the 33 d baseline period indicated pre-treatment differences, particularly in one column of the 24 h DRW group.

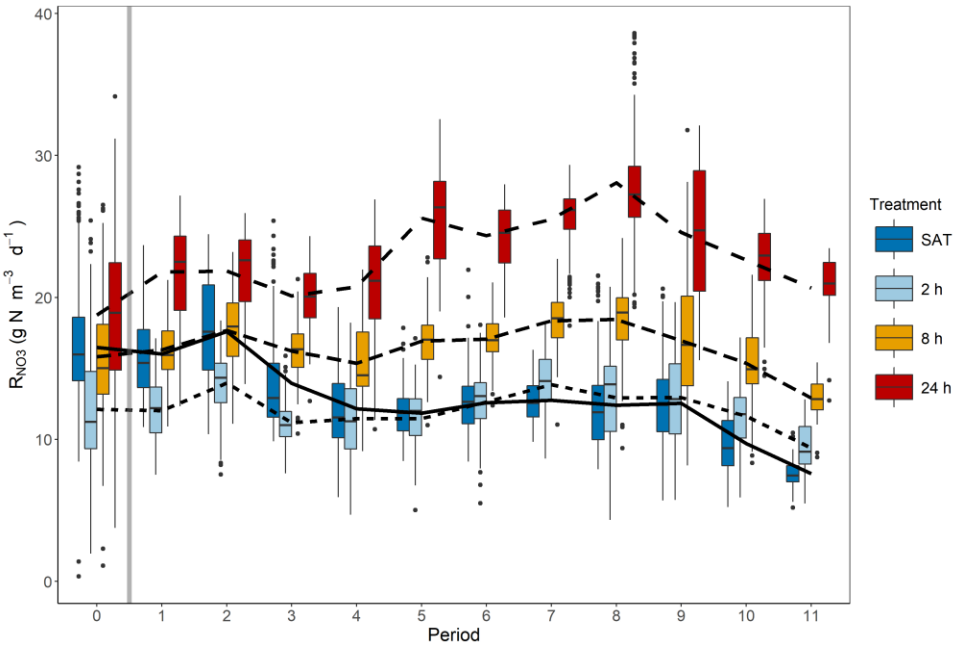

Figure 4-2. Box plots of volumetric NO_3 removal rates (R_{NO3}) during each weekly period, with Period 0 being the 33 d baseline period where all columns received the SAT treatment. The grey vertical bar indicates the beginning of DRW cycles.

4.3.3. Dissolved organic carbon leaching in the DRW 2018 experiment

Leaching rates of DOC, L_{DOC}, among treatment groups followed similar trends to R_{NO3} (Figure 4-3 and Figure 4-4). Leaching was highest in 24 h DRW columns and lowest in SAT and 2 h DRW columns. Clear differences in SAT and 8 h DRW columns did not appear until after the third DRW cycle, and differences between SAT and 2 h columns were not significant for most of the experiment. Mean L_{DOC} from Periods 3 – 11 were 1.2±0.3, 1.2±0.3, 1.8±0.4, and 3.1±0.9 g C m^{-3} d^{-1} for SAT, 2 h, 8 h, and 24 h DRW groups, respectively. Relative to the SAT treatment group, weekly mean L_{DOC} were greater by 8±12, 56±16, and 176±32% in 2 h, 8 h, and 24 h DRW groups.

4.3.4. Comparison of organic carbon leaching between the 2017 and 2018 study

In the DRW 2018 experiment, leaching in SAT and 8 h DRW groups was comparable to rates seen in the DRW 2017 study (Figure D-5). In the DRW 2017 experiment, high initial leaching of DOC at the beginning of the experiment (Periods 2 – 11), led to mean L_{DOC} of 1.5±0.8 and 1.9±0.9 g C m^{-3} d^{-1} for SAT and 8 h DRW columns. Differences in L_{DOC} became more distinct in later periods when flow and temperature conditions were more stable. Mean L_{DOC} in Periods 19 – 21 were 0.6±0.1 and 0.9±0.1 g C m^{-3} d^{-1} for SAT and 8 h DRW columns, and 0.9±0.1 and 1.3±0.3 g C m^{-3} d^{-1} for SAT and 8 h DRW columns in Periods 35 – 39 of the DRW 2017 study.

In the 2018 study, L_{DOC} in 24 h DRW columns were initially low immediately after columns were rewetted (Figure 4-5). Low initial L_{DOC} were followed by increasing L_{DOC} until 1.8 – 2.0 days after rewetting, after which L_{DOC} was either stable or gradually declined. The 8 h DRW columns exhibited a similar pattern, although changes in L_{DOC} over days since rewetting were lower. This same trend was seen in DRW 2017 in 8 h DRW columns during Days 147 – 172, where low initial L_{DOC} was followed by peak L_{DOC} 1 – 2 d after rewetting and a subsequent gradual decrease in L_{DOC} until the next DRW cycle. This trend was not seen in later Days 252 – 287 in DRW 2017, where L_{DOC} was highest immediately after rewetting and decreased until the next DRW cycle. The delay in DOC leaching seen in less than 150 days of both 2017 and 2018 experiments might therefore be temporary.

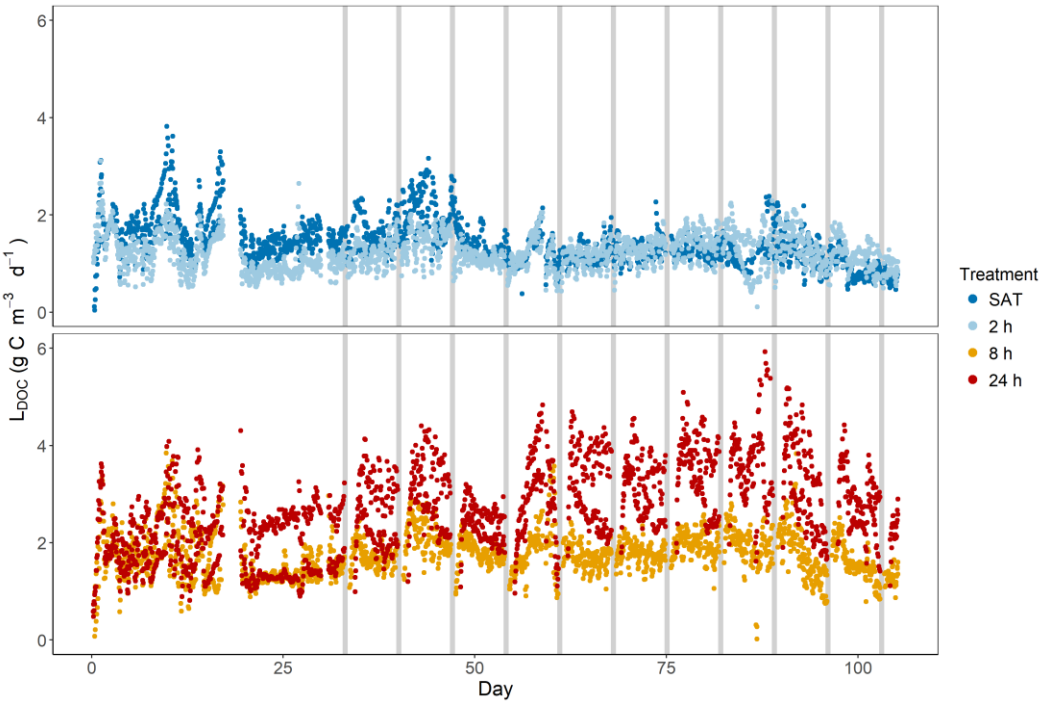

Figure 4-3. Leaching rates of DOC (L_{DOC}) for all columns from each group. Variability between groups during the 33 d baseline period indicated pre-treatment differences, particularly in one column of the 24 h DRW group.

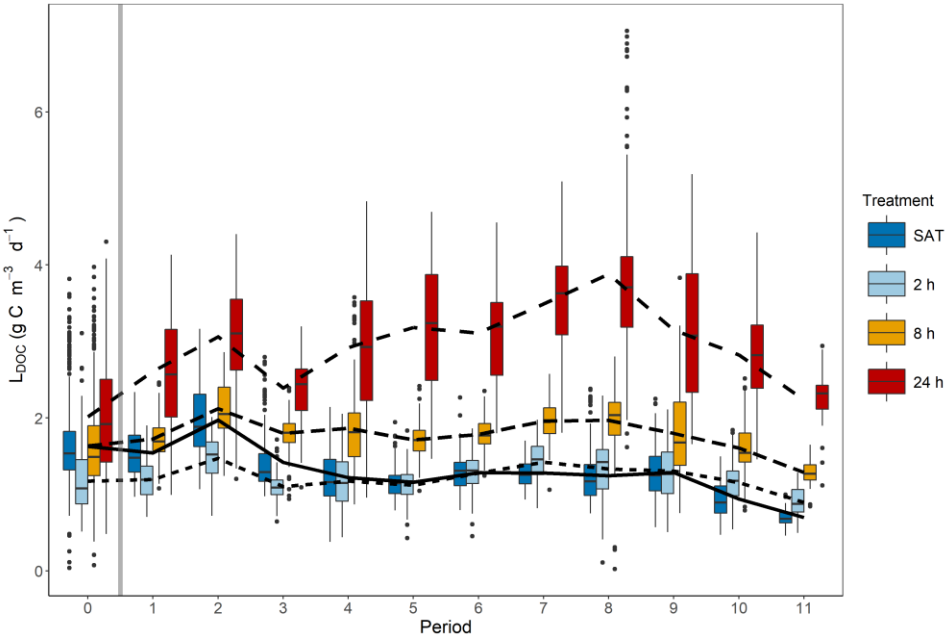

Figure 4-4. Box plots of DOC leaching rates (L_{DOC}) during each weekly period, with Period 0 being the 33 d baseline period where all columns received the SAT treatment. The grey vertical bar indicates the beginning of DRW cycles.

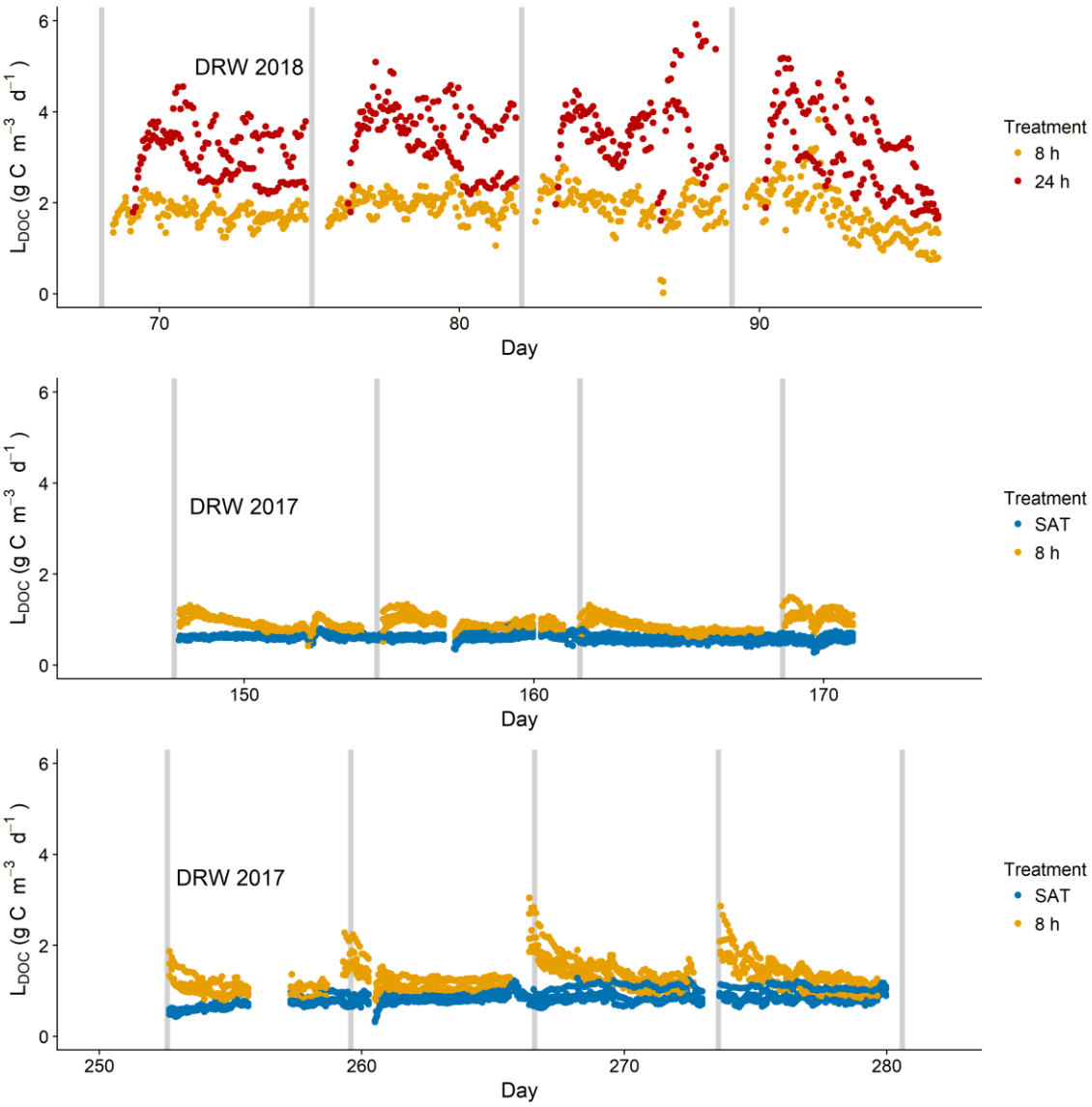

Figure 4-5. Leaching rates of DOC in the DRW 2017 and DRW 2018 studies. In the DRW 2018 study, peak L_{DOC} did not occur until 1.8 – 2.0 d after rewetting. This same trend was seen in Days 147 – 172 of the DRW 2017 experiment in 8 h DRW columns, but not in later Days 252 – 287 where L_{DOC} was highest immediately after rewetting and declined over week.

4.3.5. Effect of temperature

In both 2017 and 2018 experiments, increases in temperature were correlated with increased R_{NO3} in all treatments (Figure 4-6). Following the first DRW cycle in 2018, temperatures ranged from 20.5 – 24.7 °C. Lab temperature decreases at the end of the experiment corresponded to a decrease in R_{NO3} in all treatment groups. Similar temperature trends were seen in the DRW 2017

data (Figure 4-3). Values of Q_{10} for NO_3 removal rates were calculated for each group separately. Values of Q_{10} for SAT and 8 h DRW groups in DRW 2017 (2.68 and 2.41) were comparable to those in DRW 2018 (2.20 and 2.62). In the DRW 2018 experiment, Q_{10} was highest in the 24 h DRW column and lowest in the SAT columns. This is counter to results from DRW 2017 in which Q_{10} was higher in SAT columns relative to 8 h DRW. The largest absolute increase of weekly mean R_{NO3} in 8 h and 24 h DRW columns, relative to SAT columns, occurred during Period 8 when temperatures were highest. Similar results were seen in DRW 2017 when the largest absolute increase in weekly mean R_{NO3} in 8 h DRW columns occurred during Periods 8 and 11 when temperature was highest. Rates of DOC leaching increased with temperature (Figure D-6). Calculated Q_{10} for L_{DOC} were generally higher than Q_{10} for R_{NO3}, with the highest L_{DOC} Q_{10} (4.33) seen in 24 h DRW columns.

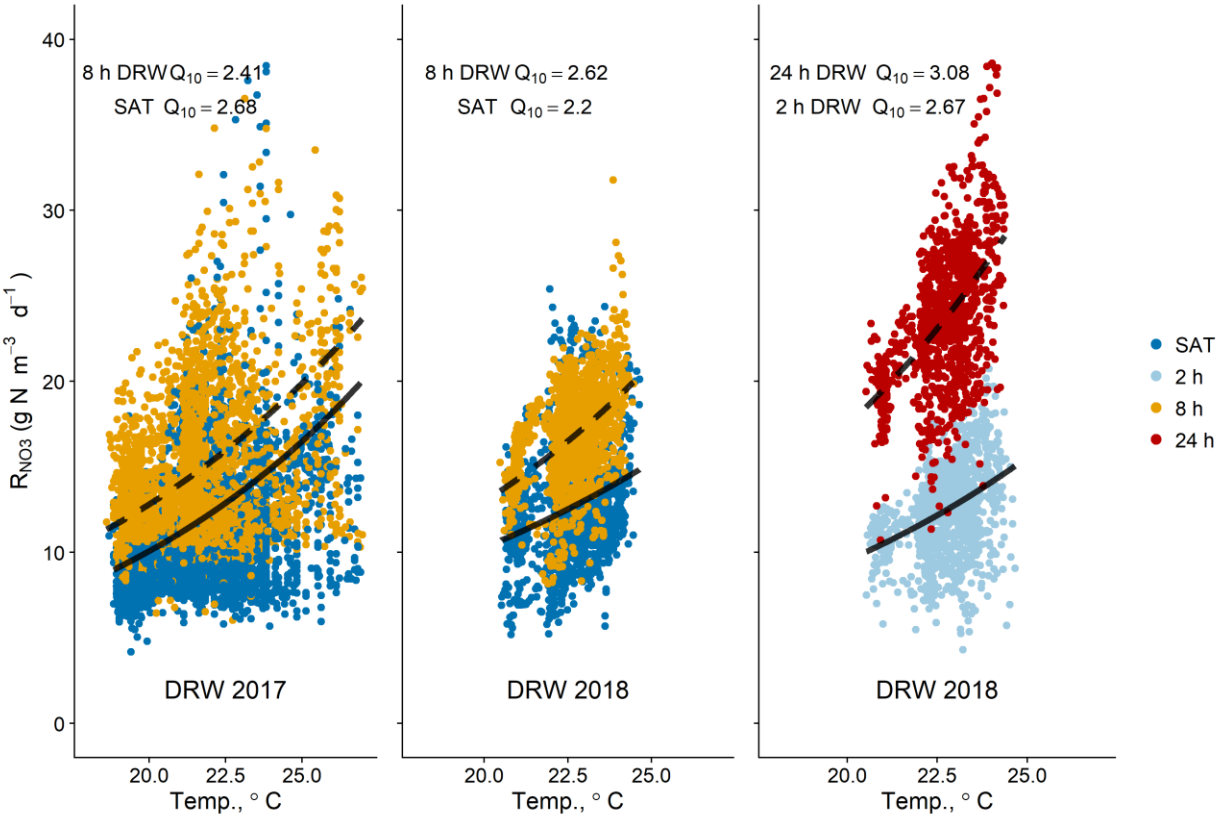

Figure 4-6. Volumetric nitrate removal rates plotted against temperature in the DRW 2017 and DRW 2018 experiments. Nitrate removal was positively correlated with temperature in all treatment groups, with Q_{10} of 2.20 – 3.08. Calculated R_{NO3} Q_{10} was highest in the 24 h DRW group.

4.3.6. Effect of HRT

Hydraulic residence time was not correlated with with R_{NO3} ($R^2 < 0.01$) in SAT and 2 h DRW in the DRW 2018 experiments and both groups of the DRW 2017 experiment (Figure 4-7). There was a moderate negative correlation with HRT in 8 h ($R^2 = 0.13$) and 24 h DRW (0.27) groups. The relationship appeared to be non-linear. In the DRW 2018 experiment increases in HRT had the most dramatic effect on R_{NO3} in 24 h DRW columns. At longer HRT (> 12 h) higher values of R_{NO3} were less common. In the DRW 2017 experiment R_{NO3} > 20 g N m^{-3} d^{-1} in SAT and 8 h DRW columns was not observed when HRT > 12.5 h. The same was true in the DRW 2018 when HRT > 11.5 h. Hydraulic residence time was not correlated ($R^2 < 0.05$) with L_{DOC} in all treatment groups in both experiments (Fig. S10).

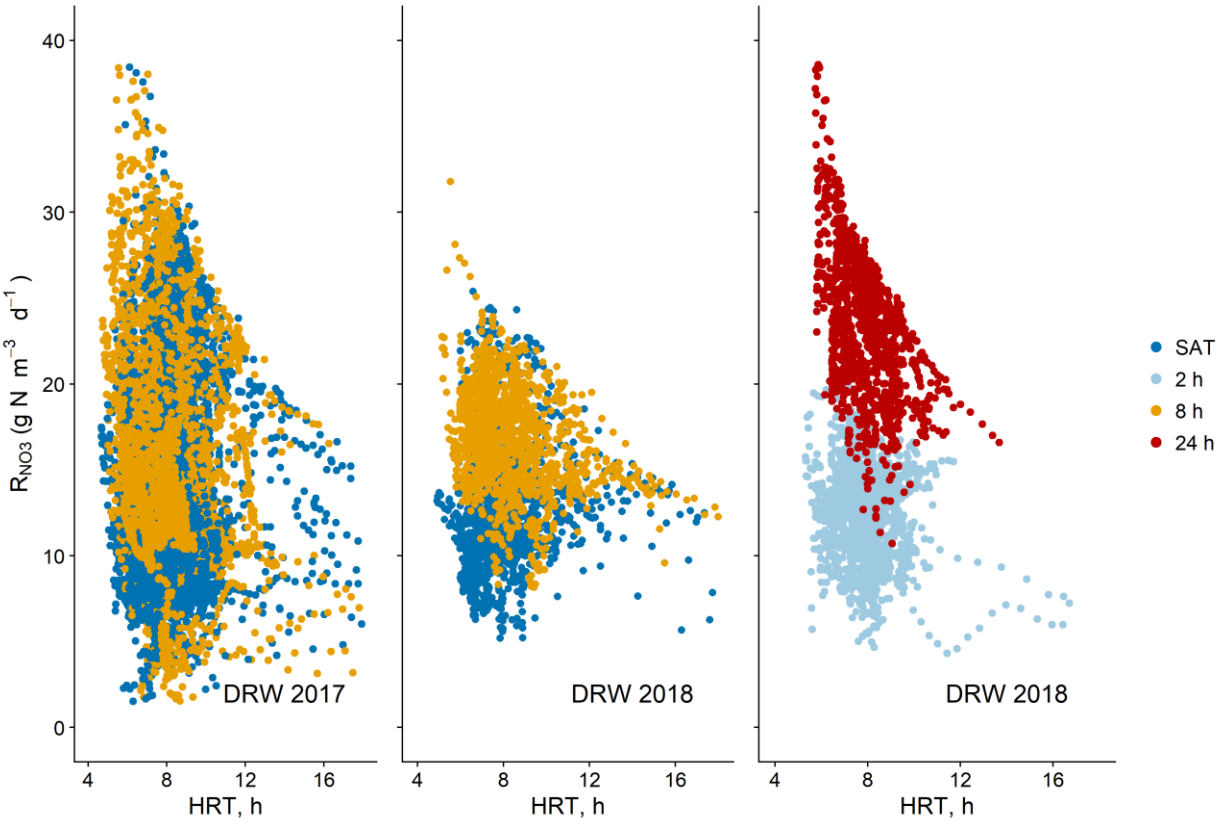

Figure 4-7. Volumetric nitrate removal rates plotted against hydraulic residence time (HRT) in the DRW 2017 and DRW 2018 experiments. R_{NO3} was weakly negatively correlated with HRT, with R_{NO3} < 20 g N m^{-3} d^{-1} when HRT > 12.5 h.

4.3.7. Results of ANOVA

Similar to the DRW 2017 experiment, the DRW 2018 columns took several weeks to adjust to the DRW treatment likely due to microbial acclimation. For the ANOVA analysis, only data collected after the fourth DRW cycle was used (Period > 3). For both experiments an AR(1) model was selected for considering the repeated measurements.

In the DRW 2018 experiment, all treatments were significantly different from each other with the exception of 2 h DRW relative to SAT (Table 4-1). Relative to the SAT control, the DRW treatment effect was 0.8, 5.0, and 12.4 g N m^{-3} d^{-1} additional nitrate removed for 2 h DRW, 8 h DRW, and 24 h DRW, respectively. The 8 h DRW treatment was also significant in the DRW 2017 experiment with an 3.8 g N m^{-3} d^{-1} additional nitrate removed. The main effects of temperature, HRT, and L_{DOC} were also significant in both experiments. The coefficients of temperature and L_{DOC} were positive and the coefficient for HRT negative for both experiments (Table 4-2). All two-way interactions between the three main effects (temperature, HRT, and L_{DOC}) were also significant (Table D-2). Coefficients for all three two-way interactions were negative for both experiments.

Table 4-1. Results of ANOVA analysis showing significance of the main effect of Treatment only on nitrate removal rates and coefficient of effect size for the DRW 2018 and DRW 2017 experiments. All comparisons were significantly different in DRW 2018 with the exception of 2 h DRW vs SAT. The 8 h DRW group was significantly different from SAT in DRW 2017.

DRW 2018 results – model 1						
Effect	**Estimate of Treatment Effect g N m^{-3} d^{-1}**	**Std Error**	**DF**	**t Value**	**Pr > |t|**	**Adj P**
2 h DRW vs SAT	0.76	0.42	4	-1.8	0.1459	0.3889
8 h DRW vs SAT	4.98	0.41	4	-12.0	0.0003	0.001
24 h DRW vs SAT	12.35	0.42	4	-29.3	<.0001	<.0001
8 h DRW vs 2 h DRW	4.21	0.42	4	-9.9	0.0006	0.002
24 h DRW vs 2 h DRW	11.59	0.43	4	-26.9	<.0001	<.0001
24 h DRW vs 8 h DRW	7.38	0.42	4	-17.5	<.0001	0.0002
DRW 2017 results – model 1						
8 h DRW vs SAT	3.84	0.70	6	-5.5	0.0015	0.0015

Table 4-2. Results of ANOVA analysis showing significance of the main effects of Temperature, HRT, and L_{DOC} on nitrate removal rates and coefficient of effect size for the DRW 2018 and DRW 2017 experiments. All main effects were significant in both experiments. Coefficients for temperature and L_{DOC} were positive and coefficients for HRT were negative in both experiments.

DRW 2018 results – model 2					
Effect	**Estimate of Effect g N m^{-3} d^{-1}**	**Std Error**	**DF**	**t Value**	**Pr > |t|**
L_{DOC}	5.76	0.04	3442	132.93	<.0001
HRT	-0.35	0.02	3442	-14.77	<.0001
Temperature	0.33	0.04	3442	7.86	<.0001
DRW 2017 results – model 2					
L_{DOC}	6.06	0.04	9531	142.38	<.0001
HRT	-0.36	0.01	9531	-27.08	<.0001
Temperature	0.04	0.01	9531	2.86	0.0042

4.4. Discussion

4.4.1. Duration of drying-rewetting increases NO_3 removal

The 2017 DRW experiment conclusively showed that weekly, 8 h DRW cycles could increase R_{NO3} (Maxwell et al., 2018). The study was unable to determine the effect of duration of the DRW cycle (i.e. length of time woodchips are length unsaturated prior to rewetting) since only one level was tested. The current 2018 DRW experiment clearly shows duration of the DRW cycle is positively correlated with R_{NO3}. There were small differences in R_{NO3} during the 33-d baseline Period 0, indicating that pre-treatment variability between groups. Once drying-rewetting cycles were initiated in the three DRW treatment groups, however, R_{NO3} quickly diverged and remained consistently and significantly higher in 8 h and 24 h DRW groups, relative to SAT columns. Treatment effect for 8 h DRW columns was consistent after the third DRW cycle indicating some period of acclimation, although R_{NO3} for the 24 h DRW columns increased immediately after the first DRW cycle. Although mean R_{NO3} for 2 h DRW columns was greater in most periods than SAT columns, in many periods this difference was not significant and in some cases R_{NO3} was lower than SAT columns. The results indicate that a 2 h

DRW cycle may not be sufficient to substantially increase R_{NO3} relative to constantly saturated woodchips.

TheDRW 2017 experiment showed that weekly mean R_{NO3} increased by 34±8% in 8 h DRW columns. The results of the 2018 experiment showed that this may be a consistent range of increase for this DRW duration, with R_{NO3} increased by 45±13% relative to SAT columns. Tripling the DRW duration in 24 h columns increased R_{NO3} by a similar order, with mean R_{NO3} more than double that of SAT columns. The effect of DRW duration on absolute R_{NO3} was roughly linear ($R^2 = 0.70$) and followed the equation $R_{NO3,inc} = 0.54 * T_{DRW} + 11.74$, where $R_{NO3,inc}$ is the increase in removal rates (g N m^{-3} d^{-1}) relative to SAT columns, and T_{DRW} is the length of the unsaturated period in hours (Figure 4-8).

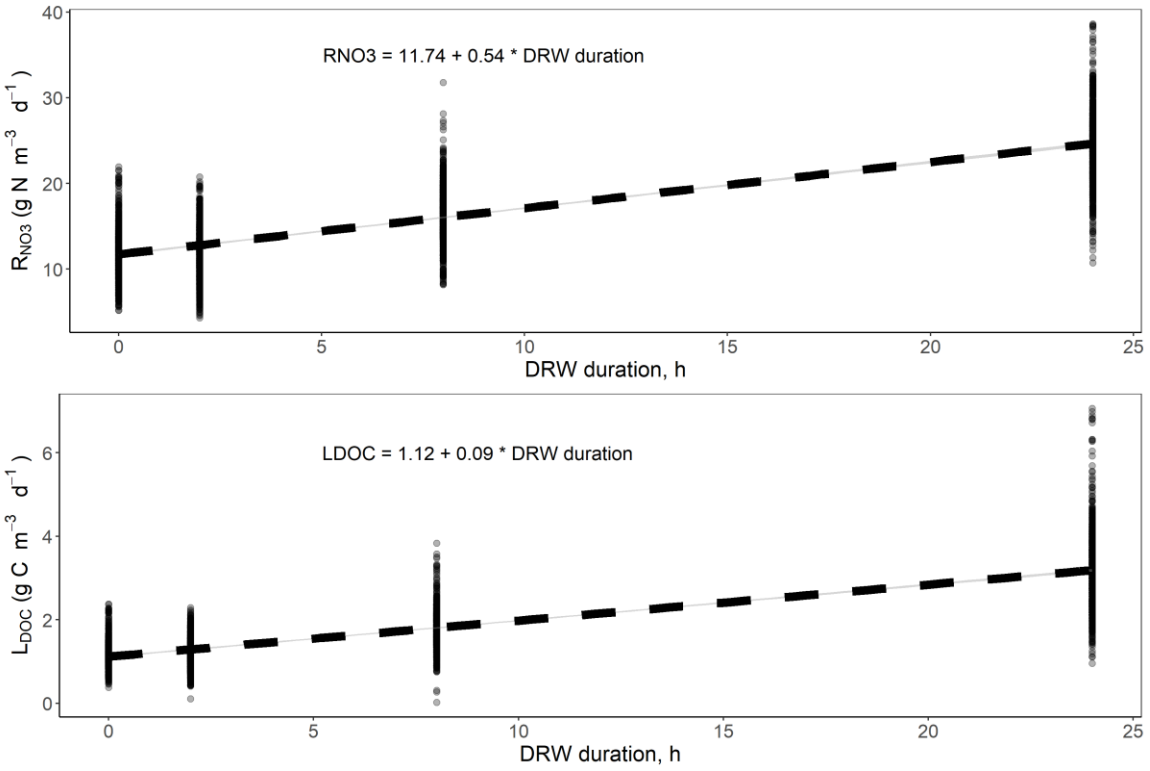

Figure 4-8. Increase in R_{NO3} and L_{DOC} was mostly linear with increase in duration of the drained period during DRW cycle. Points plotted represent data collected during Periods 4 – 11 from SAT and DRW treatment columsn.

An increasing effect of the DRW treatment was seen in the DRW experiment as Period number increased. The ratio of weekly mean R_{NO3} for DRW treatment columns to SAT columns increased with time in all treatment groups (Figure 4-9) and appeared to still be increasing at the end of the experiment after 11 DRW cycles. In the linear regression of the weekly mean R_{NO3} ratio versus Period number, the slope of the regression was significantly greater than zero for all three treatment groups. Ratio of 8 h DRW weekly mean R_{NO3} to SAT weekly mean R_{NO3} was also increasing until Period 10 – 11 in the DRW 2017 experiment, but was relatively stable from Periods 19 – 39 (Figure 4-10). This suggests that the shorter 105-d DRW 2018 experiment may not have had sufficient time to reach stable conditions. By the end of the 2018 experiment, ratios for DRW:SAT columns were 1.2, 1.7, and 2.7 for 2 h, 8 h, and 24 h DRW groups, respectively.

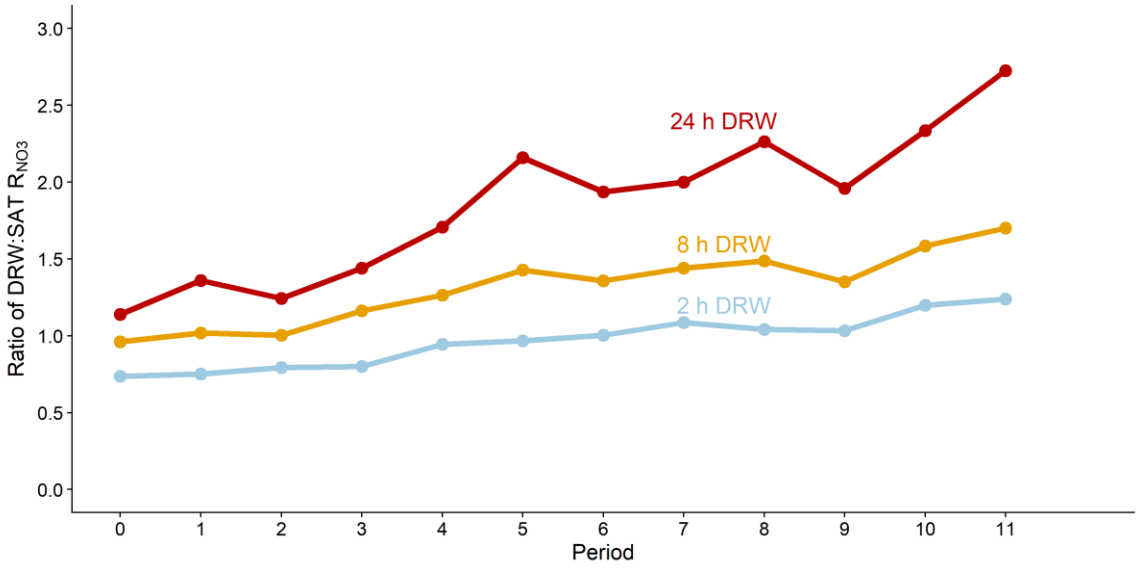

Figure 4-9. Ratio of DRW weekly mean R_{NO3} to SAT weekly mean R_{NO3} in DRW 2018 experiment. In all treatment groups, the effect of the DRW treatment increased with increasing number of DRW cycles.

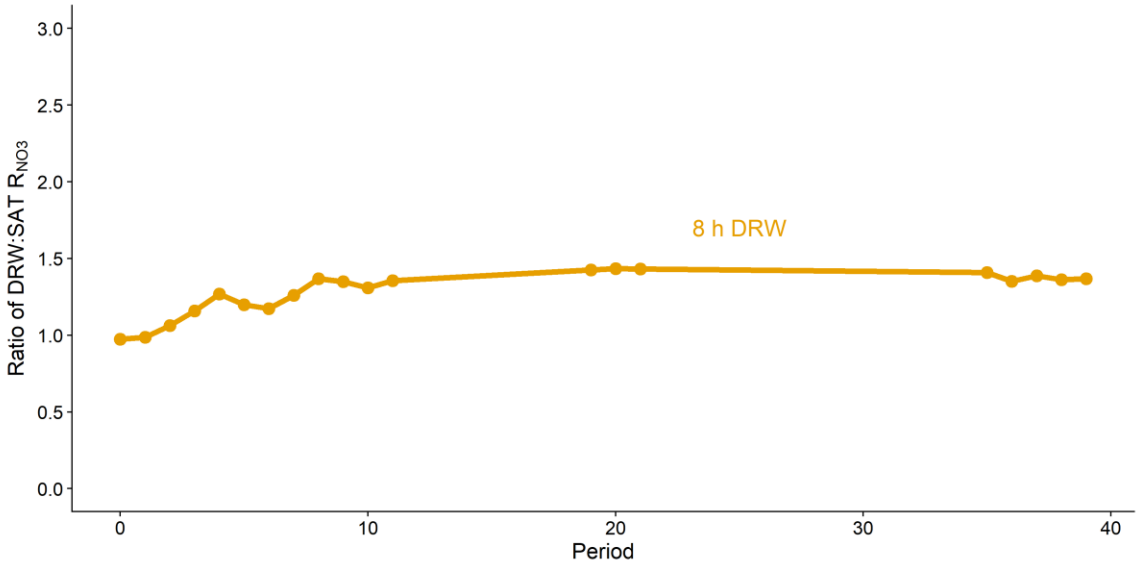

Figure 4-10. Ratio of DRW weekly mean R_{NO3} to SAT weekly mean R_{NO3} in DRW 2017 experiment. The effect of the DRW treatment increased with increasing number of DRW cycles up until Period 10 – 11, after which the ratio was relatively constant for the remainder of the experiment (Periods 19 – 39).

4.4.2. Duration of drying-rewetting increases DOC leaching

The 2 h DRW treatment led to a modest but significant increase in L_{DOC} of <0.1 g C m^{-3} d^{-1}, relative to SAT columns. Increases in L_{DOC} were more substantial in the 8 h DRW group in both DRW 2017 and DRW 2018 experiments. In Periods 19 – 39 of the DRW 2017 experiment, mean L_{DOC} was significantly greater in 8 h DRW columns by 0.4 g C m^{-3} d^{-1}. In Periods 4 – 11 of the DRW 2018 experiment, mean L_{DOC} was significantly greater in 8 h DRW columns by 0.6 g C m^{-3} d^{-1}. Leaching of DOC was further increased in 24 h DRW columns, where L_{DOC} was greater by 2.0 g C m^{-3} d^{-1}, relative to SAT columns. Considering the weekly mean L_{DOC} during each period (Figure 4-2), absolute L_{DOC} were roughly linear (R^2 = 0.69) and followed the equation L_{DOC} = 0.09*T_{DRW} + 1.12, where T_{DRW} is the DRW duration in hours.

These results support the hypothesis that the duration of aerobic periods have a direct effect on the leaching of DOC. As time of aerobiosis increased, additional DOC was made available during aerobic breakdown and subsequently leached from the columns upon rewetting. Gordon et al. (2008) found that [DOC] in leachate of grassland soil cores following a DRW cycle were

double those of a constantly saturated control, with leachate [DOC] decreasing quickly Days 1 – 9 after rewetting and not significantly different from Days 9 – 50 after rewetting. Miller et al. (2005) found similar results in chaparral soil exposed to DRW cycles, with leachate [DOC] 2 – 5x greater than constantly saturated soils. Limited attention, however, has been given to effect of DRW duration on subsequent C losses from unsaturated, moist media. The findings in this study are counter to those discussed by Schimel et al. (1999) and Hentschel et al. (2007), although these studies observed DRW effects on soils. Research on C release following DRW cycles has mostly focused on soils dried to a low enough moisture content (MC) to limit microbial activity. Our 2017 experiment showed that woodchips in the 8 h DRW columns still retained MC of 50%. The aerobic respiration was most likely not water-limited, which may explain the linear increases in DOC leaching in response to increased DRW duration.

4.4.3. Aerobically-induced DOC production stimulates NO_3 removal rates

In all treatments in both studies, R_{NO3} was strongly correlated with L_{DOC}, and L_{DOC} had a significant effect for both studies in the ANOVA analysis. In nearly all cases this relationship was highly linear (Figure 4-11). In the DRW 2018 study, linear regressions of R_{NO3} against L_{DOC} for Periods 4 – 11 had R^2 of 0.97, 0.99, 0.84, and 0.83 for SAT, 2 h, 8 h, and 24 h DRW columns, respectively. In the DRW 2017, linear regressions for SAT and 8 h DRW were 0.85 and 0.78. The strong linear relationship even in SAT treatment groups shows that the influence of DOC on R_{NO3} was not limited to DOC produced while woodchips were unsaturated from DRW cycles. Further examination of the DRW 2017 data shows that the slope of the linear regression in both SAT and 8 h DRW groups changed over the experiment (Figure D-8),

indicating that the nature of the DOC/R_{NO3} relationship may change over time.

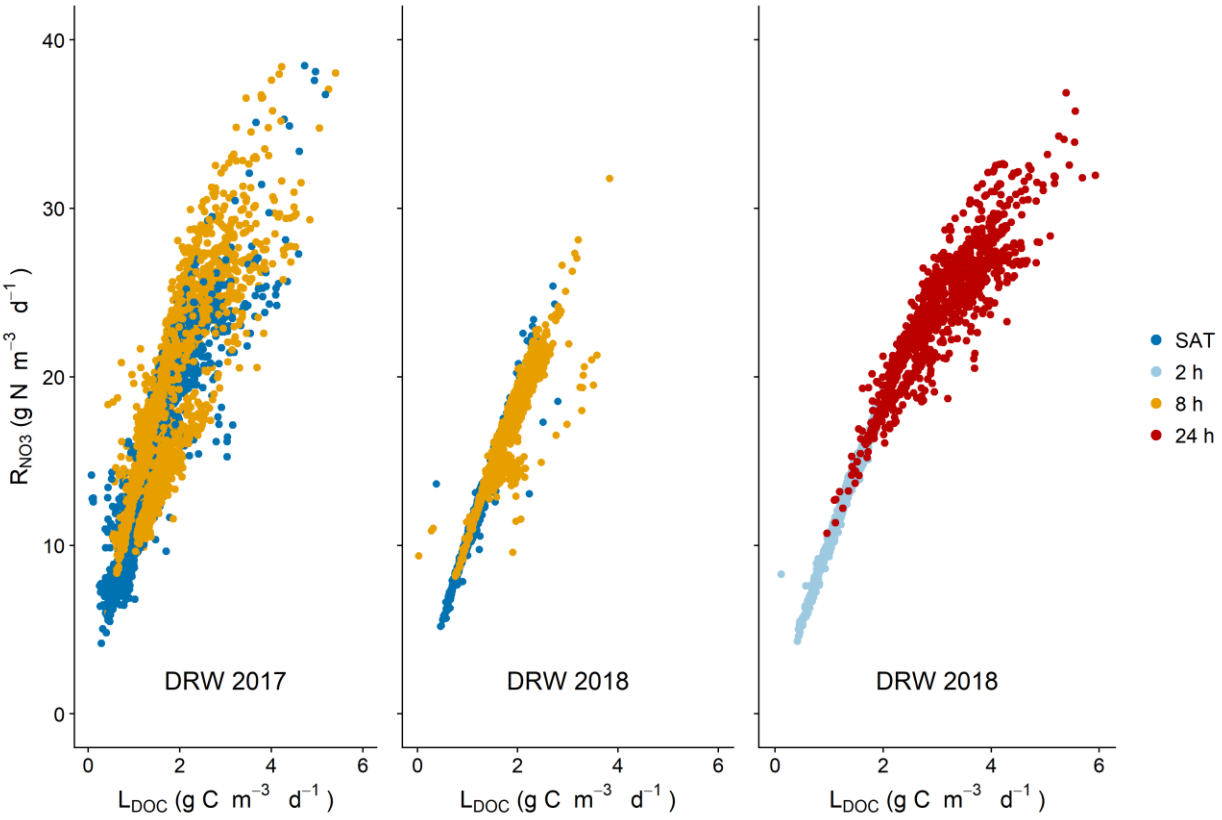

Figure 4-11. Nitrate removal rates plotted against DOC leaching rates. Nitrate removal was strongly correlated with L_{DOC}, even in SAT columns not undergoing DRW cycles.

The fact that R_{NO3} were stimulated by increased L_{DOC} indicates that NO_3 removal in the columns was strongly carbon-limited. Several studies have previously alluded to or shown C-limited denitrification in woodchip bioreactors (Cameron and Schipper, 2010; Feyereisen et al., 2016; Saliling et al., 2017; Roser et al., 2018), with denitrifiers limited by the rate at which they can metabolize 'recalcitrant', lignin-heavy woodchips. Byproducts of organic matter breakdown (e.g. DOC) are typically lower molecular weight electron donors (Fox and Comerford, 1990; van Hees et al., 2005; Lützow et al., 2006). Lower molecular weight organic compounds are more bioavailable and rapidly used by certain microbes (Cleveland and Townsend, 2006; Cleveland et al., 2007; Eilers et al., 2010). The less linear trend of R_{NO3} versus L_{DOC} in the 24 h DRW group, where L_{DOC} was highest, suggests there is possibly an upper limit of [DOC] to linear increases in R_{NO3} beyond which NO_3 removal is no longer C-limited. This saturation of [DOC], however, may only be occurring in woodchips closer to the column outlet immediately after rewetting,

where there is not sufficient time to consume the DOC produced when columns were drained before it is discharged from the column. Leached DOC was highest immediately after rewetting and the rate of DOC leaching may have exceeded denitrifiers' ability to consume it. Looking at the ratio of R_{NO3}:L_{DOC} plotted against days since rewetting and $[DOC]_{out}$ (Figure 4-12), the former may explain more of the departure from linearity. The highest values of R_{NO3}:L_{DOC} were seen immediately after rewetting, however the lowest R_{NO3}:L_{DOC} values were seen at the highest $[DOC]_{out}$.

Rate of DOC leaching also increased over the experimental time scale, considering both DRW 2017 and DRW 2018 experiments. These increases were seen even in SAT columns. In DRW 2017, mean L_{DOC} from Days 147 – 172 were 0.6 and 0.9 g C m^{-3} d^{-1} in SAT and 8 h DRW columns, respectively, increasing to 0.9 and 1.3 g C m^{-3} d^{-1} in Days 252 – 287. In DRW 2018, during Days 54 – 105 (or 504 – 554 days since the beginning of the previous experiment) mean L_{DOC} increased to 1.2 and 1.8 g C m^{-3} d^{-1}. The results run counter to previous discussions that DOC leaching in woodchip bioreactors decreases over time (Lepine et al., 2016; David et al., 2016), although much of the attention has been given to the large decreases in L_{DOC} after the first year.

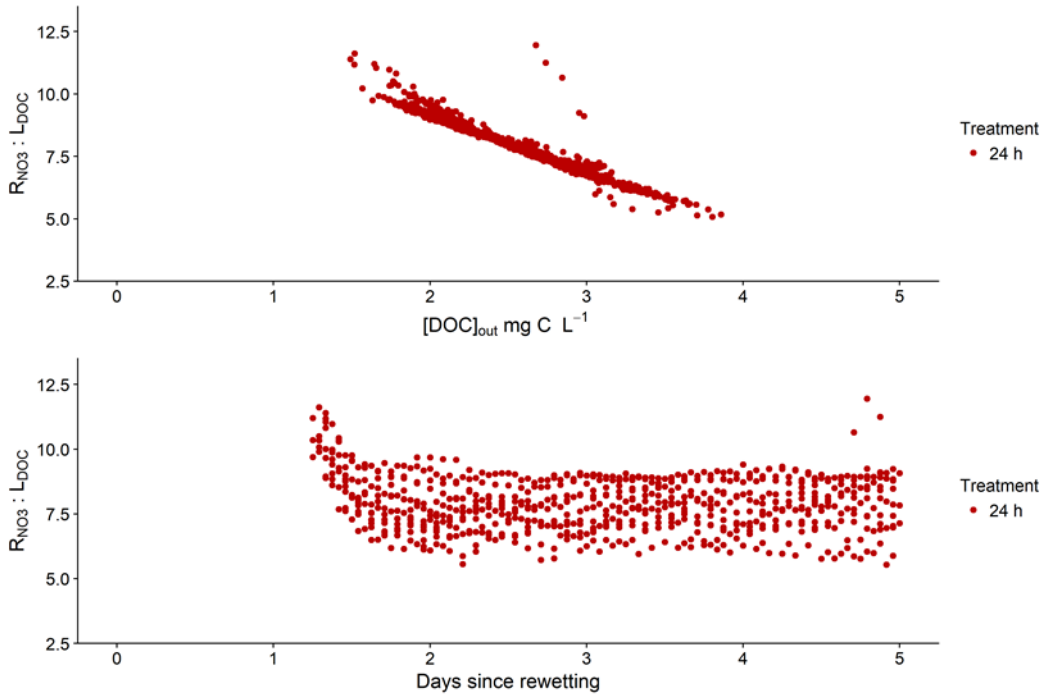

Figure 4-12. Ratio of R_{NO3}:L_{DOC} for 24 h DRW columns in the DRW 2018 experiment. Lower values of the ratio at higher $[DOC]_{out}$ may explain the non-linearity of the relationship between the two variables in 24 h DRW columns, rather than the R_{NO3}:L_{DOC} relationship immediately after rewetting.

It is not immediately clear why L_{DOC} increased over time in our column experiments, particularly since woodchips are thought to become less easily degraded with age. It is possible there is a stage in the life of the woodchip at which changes in woodchip structure may allow increased DOC leaching. Previous research has shown that degradation by fungi and microbes can increase the specific surface area of woody debris, exposing more of the overall volume to mineralization (Sutherland et al., 1979). In woodchips exposed to DRW cycles, aerobic periods are likely to expose portions of the woodchip that might otherwise remain inaccessible. Lignin prevents hydrolysis of more labile cell components through covalent bonds with cellulose, hemicellulose, and proteins (Koshijima and Watanabe, 2003; Talbot et al., 2011), forming a protective "sheath" that is resistant to enzymatic attack (Adani et al., 2011). Degradation of lignin by anaerobic respiration is negligible (Zeikus et al., 1982; Holt and Jones, 1983; Odier and Monties, 1983), and lignin breakdown is primarily accomplished through aerobic microbes or fungi (Kirk and Farrell, 1987). Byproducts of aerobic breakdown of lignin (e.g. oligolignols) are able to be more readily used during anaerobic respiration (Healy and Young, 1978; Colberg and Young, 1985).

Regular exposure of woodchips to aerobic conditions both exposes previously unavailable carbon molecules and releases lignin byproducts able to be used in anaerobic respiration, possibly creating more complex 3D structures and more exchange surface areas.

Given the knowledge of woodchip composition and low ability of anaerobic microbes to degrade lignin, it is important to consider the carbon source for denitrification in constantly saturated woodchip bioreactors. Either denitrifiers are able to successfully access and hydrolyze the cellulose and hemicellulose fraction of woodchips, or denitrifiers in bioreactors do not directly obtain their carbon source from the woodchips. Dissolved oxygen entering at the inlet can provide aerobic conditions ([DO] > 2 mg L^{-1}) that penetrate anywhere from 10 – 40% of the bioreactor length (Warneke et al., 2011; Christianson et al., 2013; Halaburka et al., 2017). The byproducts of aerobic decomposition of the woodchips would serve as more readily used fuel for downstream denitrification. While the presence of [DO] in woodchip bioreactors is considered an inhibitory factor, its inhibition on denitrification may be offset or even outweighed by its contribution to the increase in labile carbon pool.

4.4.4. Dissolved organic carbon and NO_3 dynamics after rewetting

The 2017 data showed that R_{NO3} increases in 8 h DRW columns were greatest immediately after rewetting (Maxwell et al., 2018), particularly for periods 34-40. Daily mean R_{NO3} increased by 79 – 81% on Day 1 after rewetting, gradually falling to 24 – 38% increase in R_{NO3} Day 3 – 7 after rewetting. Although R_{NO3} increases for 8 h and 24 h DRW column similarly decreased over the week after rewetting in 2018, this decline was not as large as the 2017 experiment (Figure 4-13). For 8 h DRW columns in Periods 4 - 11, mean daily R_{NO3} increased by 40±18 and 61±15% on Days 1 & 2 after rewetting, and greater by 44±16% on Days 3 – 7, respectively. For 24 h DRW columns, mean daily R_{NO3} increased by 102±30 and 128±38% on Days 1 & 2 after rewetting, and only greater by 105±27% on Days 3 – 7. Data collected from 8 h DRW columns in the 2017 experiment show that the percent increase R_{NO3} immediately after rewetting was lower in the 2018 experiment. This may be the result of woodchips being degraded during the previous 297 d experiment. Woodchips in the 2018 experiment would have had a lower proportion of easily degradable cellulose and hemicellulose, as was previously shown to be the case in aged woodchips in bioreactors (Ghane et al., 2018). Don and Kalbitz (2005) showed that

DOC leached from aged leaf litter was 34% less mineralizable than DOC from fresh litter. Lower percent increases of R_{NO3} in the DRW 2018 experiment immediately after rewetting may have been due to metabolized byproducts of the lignin-dominated, aged woodchips being less bioavailable for anaerobic denitrifiers.

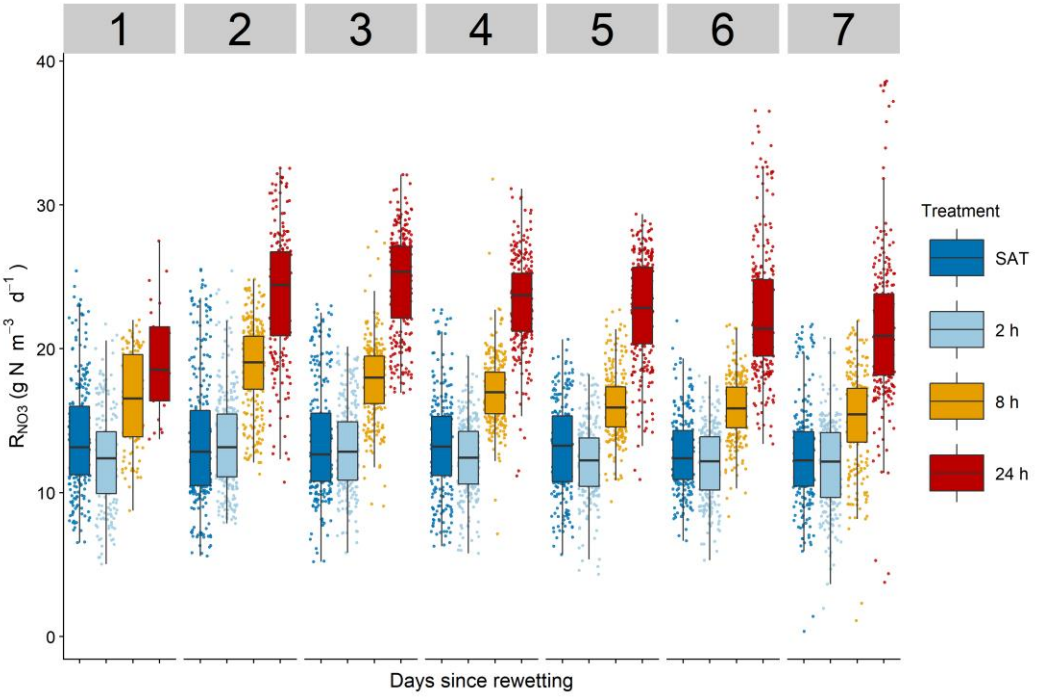

Figure 4-13. Box plots of R_{NO3} for each treatment group according to the number of days since rewetting. Nitrate removal peaked on the second day after rewetting, although subsequent declines in R_{NO3} were not as high as the previous DRW 2017 experiment.

Further supporting the hypothesis that DOC was the primary driver of R_{NO3} increases, L_{DOC} followed a similar decreasing trend as days since rewetting increased (Figure D-9). These findings are comparable with previously observed behavior of DOC leaching from media containing mineralized organic matter (Chow et al., 2006; Hansson et al., 2010). Gordon et al. (2008) showed that, in soil cores exposed to DRW cycles, leachate [DOC] was greatest during Days 1 – 3 following rewetting, and that [DOC] did not significantly decrease from Days 9 – 50. It is also likely that the most bioavailable DOC was rapidly consumed, leading to subsequently lower R_{NO3} and L_{DOC} as number of days since rewetting increased. Chow et al. (2006) showed that C mineralization rates decreased quickly following DRW cycles. Cleveland et al. (2004) showed that 50% of DOC leached from litter was consumed in the first 4 days. Both processes,

R_{NO3} and L_{DOC}, likely influenced each other as columns were flushed following rewetting. Less labile DOC was available for denitrification as columns were flushed, and the large pulse of R_{NO3} led to a rapid consumption of DOC resulting in decreasing $[DOC]_{out}$.

In Periods 19 – 21 (Days 147 – 172) of the DRW 2017 experiment, R_{NO3} and L_{DOC} were initially low immediately after rewetting (Figure 4-5 and 4-14). Both rates then peaked ~2 d after rewetting before gradually decreasing through the remainder of the week. This trend was not observed in later Periods 35 – 39 (Days 252 – 287), where R_{NO3} and L_{DOC} were highest immediately after rewetting and then only decreased. In the DRW 2018 in 24 h DRW columns, R_{NO3} and L_{DOC} trends after rewetting were more similar to Days 147 – 172 of the previous experiment. It is not clear what could be the cause of this change in behavior after rewetting. Both experiments used the same media so woodchip aging is not a likely cause, since the lagged peak appeared in the much later DRW 2018 experiment. Preferential flow of inlet water could explain these time series, however it does not explain the lack of a lagged peak during Days 252 – 287 in DRW 2017. A possible explanation could be microbial acclimation to DRW cycles. Previous studies have shown that rapid changes in water potential can lead to the lysis of microbes or release of extracellular enzymes (Fierer and Schimel, 2003; Mihka et al., 2005; Borken and Matzner, 2009), with subsequent leaching of microbial biomass. This release of low MW biomass would increase L_{DOC} and be rapidly consumed during increased R_{NO3}. It is possible that only after many DRW cycles over a long period (39 DRW cycles over 287 d, in DRW 2017) that the microbial community was more resistant to biomass loss. This is more likely than a change in the ability of microbes to mineralize woodchips during aerobiosis, which would change the size of the L_{DOC} peak following rewetting, not the presence of a lag in this peak. Microbial acclimation to sudden aerobic and anaerobic conditions also relate to results from 2 h DRW column. There was a measurable difference of mean R_{NO3} and L_{DOC} between 2 h DRW and SAT groups, but in most periods this difference was very small or not significant. A 2 h unsaturated period was not a sufficient amount of time for aerobic processes to significantly increase subsequent L_{DOC}, although the ratio of 2 h DRW to SAT was increasing over the experiment. After keeping microbes under anaerobic conditions for 74 h, Harrison et al. (1971) found that aerobic respiration peaked after 2 – 8 h with steady state being achieved after 8 h. Conversely, anaerobic respiration after previous aeration did not increase until 8 h after anaerobic conditions began, and steady-state was not reached until 14 h. Baumann et al. (1996)

found that time until anaerobic respiration reached steady-state was closer to 30 h. The time lag for steady-state anaerobic respiration following rewetting may be longer than the lag for steady-state aerobic respiration following draining.

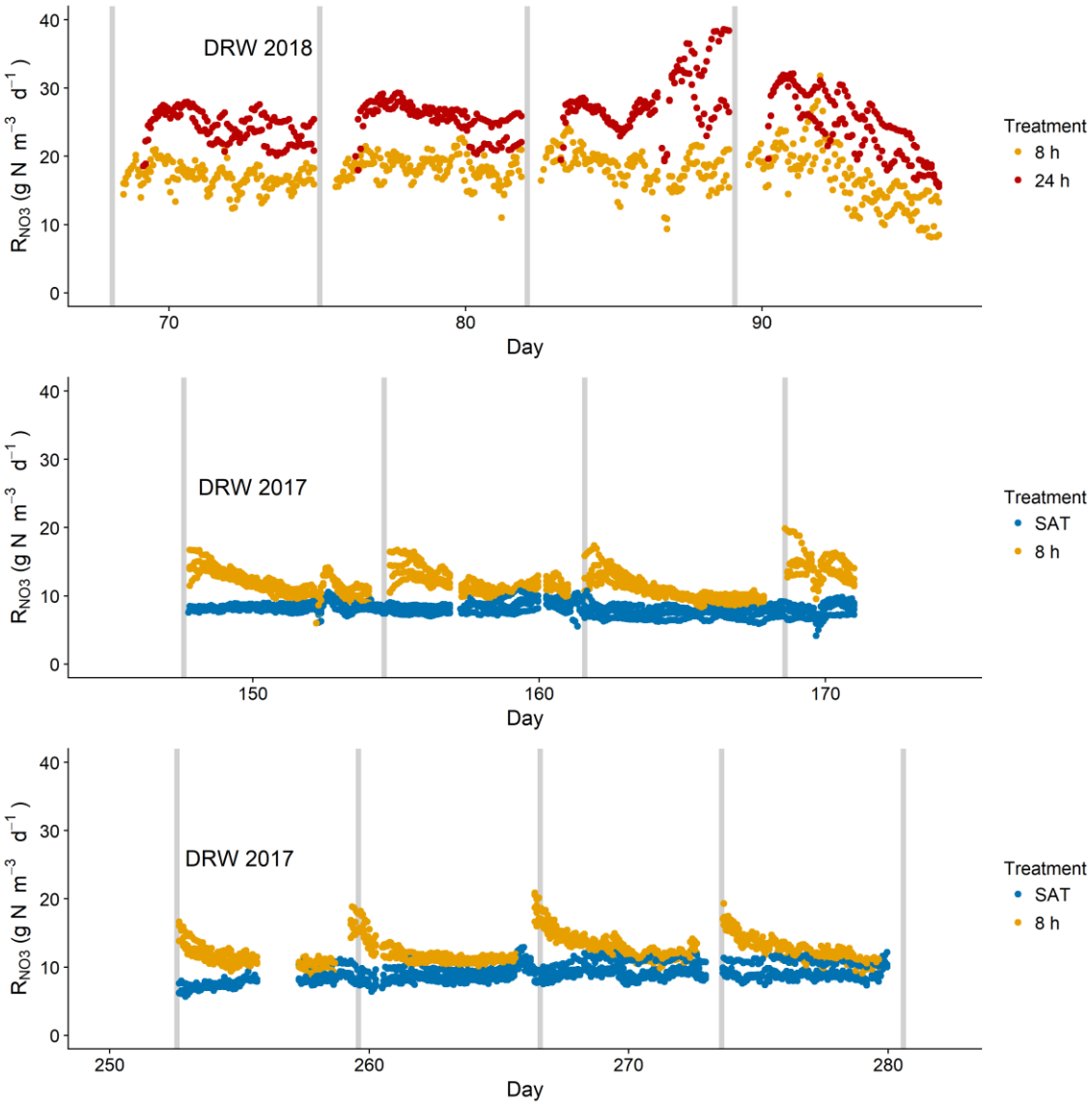

Figure 4-14. Nitrate removal rates in the DRW 2017 and DRW 2018 studies during selected period showing R_{NO3} dynamics after rewetting. In the DRW 2018 study, peak R_{NO3} did not occur until 1.8 – 2.0 d after rewetting. This same trend was seen in Days 147 – 172 of the DRW 2017 experiment in 8 h DRW columns, but not in later Days 252 – 287 where R_{NO3} was highest immediately after rewetting and declined over week.

4.4.5. Temperature effects on R_{NO3}

Values for R_{NO3} Q_{10} were relatively similar between treatment groups. In both DRW 2017 and DRW 2018 experiments, R_{NO3} Q_{10} ranged from 2.2 – 3.08, with the highest Q_{10} seen in the 24 h DRW group. These values are comparable with Q_{10} values of 1.6 – 2.9 reported in the literature (Cameron and Schipper, 2010; Warneke et al., 2011; Hoover et al., 2016; Lepine et al., 2016).). Reporting Q_{10} for a given microbial process is based on the premise that, as temperature increases, the increase in that reaction's rate is caused by the increase in temperature. The data collected in this study, however, shows that separate microbial processes having an effect on R_{NO3} were also temperature-dependent. Values of Q_{10} for L_{DOC} were higher than R_{NO3} Q_{10}. Increasing temperature led to higher production and leaching of DOC. This was true even in SAT columns (L_{DOC} Q_{10} : 2.60 – 3.47). Although this might suggest DOC released from anaerobic breakdown was stimulated by temperature, the temperature-dependence of L_{DOC} in saturated columns may also be higher productivity of aerobic breakdown occurring near the column inlet. Dissolved oxygen entered the columns between 5.0 – 7.5 mg L^{-1} and would have resulted in some aerobic respiration even in SAT columns until DO was fully consumed. The highest L_{DOC} Q_{10} in the 24 h DRW group (4.33) was likely the cause for the same group having the highest R_{NO3} Q_{10} (3.08). Temperature increases had a large effect on DOC release which interacted with the effect on R_{NO3}. In the end the Q_{10} values reported here lump several factors together. They are comparable to other values reported for woodchip bioreactors but should not be used in modeling exercises that consider other driving factors.

The interaction between temperature and L_{DOC} is an important consideration for understanding temperature-dependence of denitrification, especially when it is occurring temporally or spatially adjacent to aerobic processes. The highest 24 h DRW increase in mean R_{NO3} occurred during the period when temperatures were highest. This was also observed in Periods 8 and 11 of DRW 2017, with difference in mean R_{NO3} between 8 h DRW and SAT columns reaching 4.8 and 5.9 g N m^{-3} d^{-1} (compared with an average difference of 3.5 g N m^{-3} d^{-1}). Increased temperature would stimulate not only aerobic respiration in saturated woodchips with high [DO] near the inlet, but also aerobic respiration when woodchips are unsaturated. Greater DOC release during unsaturated period at higher temperatures would lead to subsequent higher R_{NO3} upon rewetting. This is an important consideration for future work of DRW cycles in woodchip bioreactors under

cold conditions. The absolute or percent increase in R_{NO3} from DRW cycles is likely to decrease with temperature decrease.

4.4.6. Effect of HRT on R_{NO3}

A significant negative effect of HRT on R_{NO3} was seen in both DRW 2017 and DRW 2018 experiments. Residence time in woodchip bioreactors is known to have an effect on percent NO_3 reduction, but previous studies have found no significant effect of HRT on R_{NO3} (Christianson et al., 2012; Healy et al., 2012; Hoover et al., 2016; Lepine et al., 2016). Greenan et al. (2009) found a positive correlation between HRT and R_{NO3}, while David et al. (2016) found a negative correlation. There are supporting arguments for both negative and positive correlations. At sufficiently low HRT, high flow rate into the bioreactor would cause DO to penetrate further along the bioreactor length as mass flow rate exceeds the rate at which microbes can consume DO. Higher [DO] in internal sampling wells at greater flows was previously shown (Christianson et al., 2013; Halaburka et al., 2017). Denitrification is inhibited by [DO] > 1 – 2 mg L^{-1} (Oh and Silverstein, 1999; Gomez et al., 2002). Higher proportion of the bioreactor experiencing DO-inhibition would result in reduction in overall volumetric N removal rates. Hydraulic residence times in these upflow columns were apparently not low enough (HRT > 4 h) to induce a reduction in R_{NO3}.

There is also a corresponding argument for lower R_{NO3} at higher HRT. One of the byproducts during the mineralization of organics is phenolics, which at sufficient concentrations can inhibit rates of denitrification (Okolo et al., 2007; Dodla et al., 2008). As HRT increases, the concentration of phenolics would increase, as would the likelihood of any given denitrification micro-site experiencing phenolic-inhibition, although $[DOC]_{out}$ was relatively low throughout the experiment (1.9±0.5 mg C L^{-1}). There is also the increasing likelihood of NO_3-limitation at higher HRT. As residence time is increased, $[NO_3]$ will continue to decrease along the bioreactor. The $[NO_3]$ at which denitrification is believed to be N-limited is 1 – 2 mg N L^{-1} (Warneke et al., 2011; Halaburka et al., 2017). Although $[NO_3]$ may be higher in bulk flow moving through inter-woodchip pores (i.e. gravitational porosity), it is likely to be lower at denitrification sites on the surface of and within woodchips (i.e. secondary porosity). This secondary porosity in woodchips has been shown to make up 30 – 36% of total porosity (Hoover

et al., 2016). Therefore, it is likely that NO_3-limiting conditions are occurring in a sizable portion of the woodchips, particularly in secondary porosity.

4.4.7. Management considerations

Exposing woodchips to DRW cycles results in faster degradation of the woodchips. In field bioreactors using DRW cycles a shorter life expectancy would occur. Only the aqueous emissions are considered in this chapter, although gaseous emissions have been concurrently measures in 2017 and 2018. No attempt to accurately quantify the rate of total carbon loss caused by DRW cycles is given here. Although [DOC] was measured continuously, DOC made up a variable 27 – 53% of total C in outflow (shown in the 2017 experiment). The measurements made also do not account for C lost as CO_2 when DRW columns were drained or flowing. A subsequent study should focus on total mass loss and changes in C:N ratio for woodchips exposed to DRW cycles for varying duration and frequency, using a similar methodology of Moorman et al. (2010). Woodchips exposed to DRW cycles might be expected to degrade similarly to woodchips in shallow zones of bioreactors that are less frequently saturated. Woodchips at 90-100 cm depth of a field bioreactor had 62% greater mass loss than woodchips at 155 – 170 cm, and estimated to have a half-life shorter by 32 years (Moorman et al., 2010). Decrease in lifespan of the woodchips would depend on DRW cycle duration and frequency.

In the DRW 2017 study, an analysis was done to determine the net N mass reduction for SAT and 8 h DRW treatment given that DRW columns did not treat any NO_3 while drained. This would simulate bypass flow while field bioreactors are subjected to DRW cycles, although in some applications flow could simply be stopped while columns are drained. Figure 4-15 shows the percent increase in daily mean R_{NO3} and percent increase in net N mass reduction at the given number of days since rewetting, based on data collected in Periods 4 - 11. Percent increase in cumulative NO_3 removed was lowest in the 2 h DRW columns, with a maximum increase of <6% six days after rewetting. Cumulative increase was highest (40%) in 8 h DRW columns 5 – 6 days after rewetting, comparable to findings from DRW 2017 (41 – 43%). Cumulative increase was also highest on Day 6 for 24 h DRW columns, although data was only collected for six days after rewetting due to the 24 h drained period. Increase in daily mean R_{NO3} was 109 – 130%, however cumulative increase was only 80%. The fact that maximum cumulative removal was

highest on Day 6 after rewetting is counter to results from DRW 2017 in which removal was highest 2 – 3 days after rewetting. This was due to the fact that, in the current study, percent difference in daily R_{NO3} did not substantially decrease over the week. Optimum frequency of DRW cycles may depend on age of the woodchips.

A management strategy that could increase the value of DRW cycles would be to drain field bioreactors prior to expected rainfall events. During storm events overall N reduction can be reduced dramatically when bypass flow occurs, offsetting any N removed by the bioreactor with proportionally large volumes of untreated bypass flow. Draining the bioreactor prior to storm events would not only increase storage capacity, thereby preventing some portion of bypass flow, but also increase overall N reduction via increased R_{NO3}. Increased NO_3 removal would continue as the flow event moved through the system, based on results from the 2017 and 2018 studies showing that R_{NO3} was still higher one week after the DRW event. Net increase in overall N reduction by draining the bioreactor would depend on the size of the bioreactor, event flow duration and magnitude, and DRW duration.

4.5. Conclusions

Increased duration of unsaturated conditions in DRW cycles increased subsequent NO_3 removal rates upon rewetting. This increase was greatest in 24 h DRW columns where R_{NO3} was more than doubled, while unsaturated conditions of only 2 h did not substantially increase R_{NO3}. Duration of unsaturated conditions increased subsequent DOC leaching rates, with R_{NO3} and L_{DOC} strongly correlated during the DRW 2018 and DRW 2017 experiments——. Both variables were also stimulated by temperature increases, with a greater effect of DRW cycles at higher temperatures. Hydraulic residence time had a significant and negative effect on R_{NO3} in both experiments. Although R_{NO3} time series differed slightly in their trends between the DRW 2017 and DRW 2018, the percent increase in cumulative NO_3 removed in 8 h DRW versus SAT columns over the week was comparable between both studies (40 – 43%).

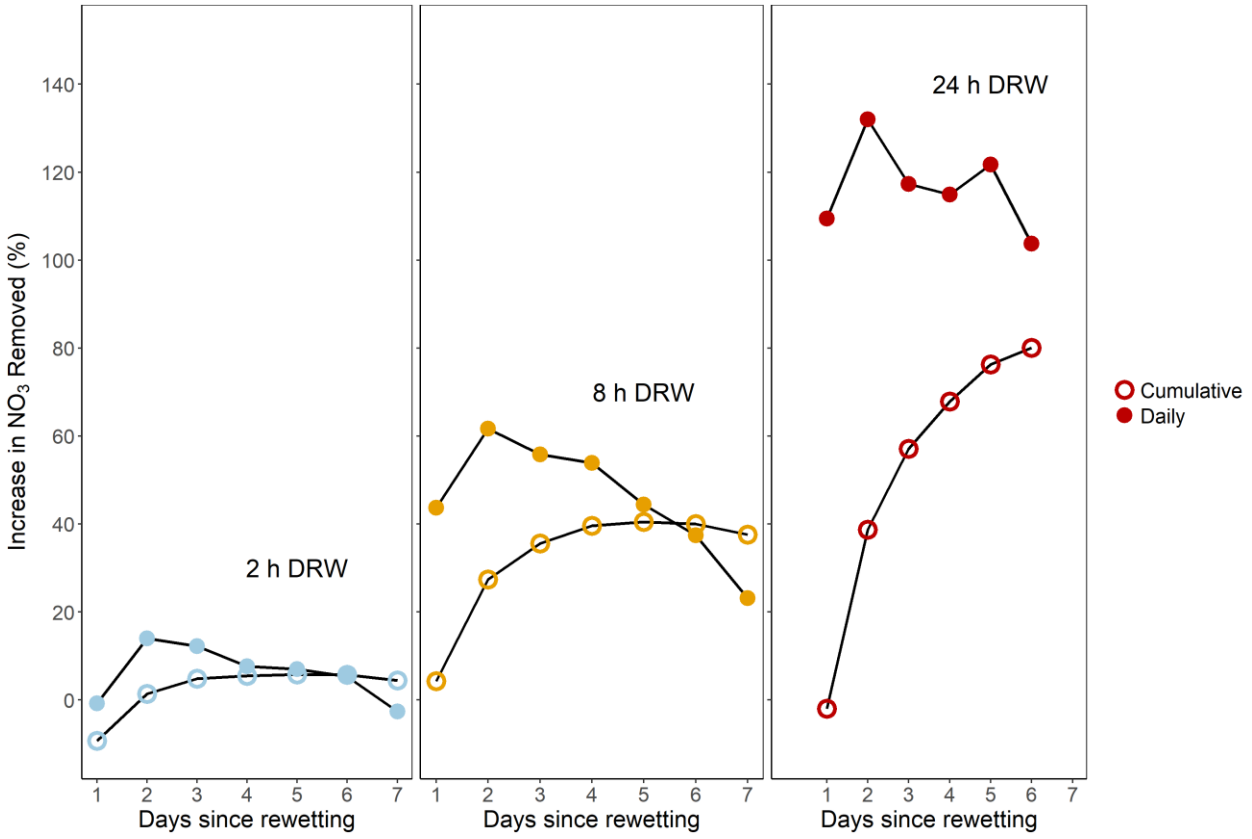

Figure 4-15. Increases in total NO_3 removed in DRW columns, relative to SAT columns, based on differences in daily mean R_{NO3} (solid) and cumulative NO_3 removed when considering untreated bypass while DRW columns were drained (hollow). Percent increase in cumulative NO_3 removal was highest after 6 d in all DRW groups, with increases of 6, 40, and 80% in 2 h, 8 h, and 24 h DRW groups, respectively.

The DRW 2017 and DRW 2018 studies conclusively show that DRW cycles can be used to stimulate NO_3 removal in woodchip bioreactors and that the percent increase in NO_3 removal is affected by DRW duration. The next phase of research for DRW cycles in woodchip bioreactors will be observing percent increases in R_{NO3} under variable frequencies and field conditions. Because most woodchip bioreactors are covered with soil, woodchips may not be as susceptible to aerobic breakdown underground as they were in this lab column experiment. It is possible that unsaturated duration may need to be much longer to produce the same R_{NO3} and L_{DOC} response seen in these studies.

4.6. References

Adani, F., Spagnol, M., & Nierop, K. G. (2007). Biochemical origin and refractory properties of humic acid extracted from maize plants: The contribution of lignin. *Biogeochemistry, 82*(1), 55-65.

Addy, K., Gold, A. J., Christianson, L. E., David, M. B., Schipper, L. A., & Ratigan, N. A. (2016). Denitrifying bioreactors for nitrate removal: A meta-analysis. *Journal of Environmental Quality, 45*(3), 873-881.

Baumann, B., Snozzi, M., Zehnder, A. J., & Van Der Meer, J. R. (1996). Dynamics of denitrification activity of paracoccus denitrificans in continuous culture during aerobic-anaerobic changes. *Journal of Bacteriology, 178*(15), 4367-4374.

Beare, M., Gregorich, E., & St-Georges, P. (2009). Compaction effects on CO 2 and N 2 O production during drying and rewetting of soil. *Soil Biology and Biochemistry, 41*(3), 611-621.

Borken, W., & Matzner, E. (2009). Reappraisal of drying and wetting effects on C and N mineralization and fluxes in soils. *Global Change Biology, 15*(4), 808-824.

Cameron, S. G., & Schipper, L. A. (2010). Nitrate removal and hydraulic performance of organic carbon for use in denitrification beds. *Ecological Engineering, 36*(11), 1588-1595.

Cameron, S. G., & Schipper, L. A. (2011). Evaluation of passive solar heating and alternative flow regimes on nitrate removal in denitrification beds. *Ecological Engineering, 37*(8), 1195-1204.

Chow, A. T., Tanji, K. K., Gao, S., & Dahlgren, R. A. (2006). Temperature, water content and wet–dry cycle effects on DOC production and carbon mineralization in agricultural peat soils. *Soil Biology and Biochemistry, 38*(3), 477-488.

Christianson, L. E., Bhandari, A., Helmers, M. J., Kult, K. J., Sutphin, T., & Wolf, R. (2012). Performance evaluation of four field-scale agricultural drainage denitrification bioreactors in iowa. *Transactions of the ASABE, 55*(6), 2163.

Christianson, L. E., Lepine, C., Sharrer, K. L., & Summerfelt, S. T. (2016). Denitrifying bioreactor clogging potential during wastewater treatment. *Water Research, 105*, 147-156.

Christianson, L. E., Lepine, C., Sibrell, P. L., Penn, C., & Summerfelt, S. T. (2017). Denitrifying woodchip bioreactor and phosphorus filter pairing to minimize pollution swapping. *Water Research, 121*, 129-139.

Cleveland, C. C., Neff, J. C., Townsend, A. R., & Hood, E. (2004). Composition, dynamics, and fate of leached dissolved organic matter in terrestrial ecosystems: Results from a decomposition experiment. *Ecosystems, 7*(3), 175-285.

Cleveland, C. C., Nemergut, D. R., Schmidt, S. K., & Townsend, A. R. (2007). Increases in soil respiration following labile carbon additions linked to rapid shifts in soil microbial community composition. *Biogeochemistry, 82*(3), 229-240.

Cleveland, C. C., & Townsend, A. R. (2006). Nutrient additions to a tropical rain forest drive substantial soil carbon dioxide losses to the atmosphere. *Proceedings of the National Academy of Sciences of the United States of America, 103*(27), 10316-10321. doi:10.1073/pnas.0600989103 [doi]

Colberg, P. J., & Young, L. Y. (1985). Anaerobic degradation of soluble fractions of [C-lignin]lignocellulose. *Applied and Environmental Microbiology, 49*(2), 345-349.

David, M. B., Gentry, L. E., Cooke, R. A., & Herbstritt, S. M. (2016). Temperature and substrate control woodchip bioreactor performance in reducing tile nitrate loads in east-central illinois. *Journal of Environmental Quality, 45*(3), 822-829.

Dodla, S. K., Wang, J. J., DeLaune, R. D., & Cook, R. L. (2008). Denitrification potential and its relation to organic carbon quality in three coastal wetland soils. *Science of the Total Environment, 407*(1), 471-480.

Don, A., & Kalbitz, K. (2005). Amounts and degradability of dissolved organic carbon from foliar litter at different decomposition stages. *Soil Biology and Biochemistry, 37*(12), 2171-2179.

Eilers, K. G., Lauber, C. L., Knight, R., & Fierer, N. (2010). Shifts in bacterial community structure associated with inputs of low molecular weight carbon compounds to soil. *Soil Biology and Biochemistry, 42*(6), 896-903.

Feyereisen, G. W., Moorman, T. B., Christianson, L. E., Venterea, R. T., Coulter, J. A., & Tschirner, U. W. (2016). Performance of agricultural residue media in laboratory denitrifying bioreactors at low temperatures. *Journal of Environmental Quality, 45*(3), 779-787.

Fierer, N., & Schimel, J. P. (2003). A proposed mechanism for the pulse in carbon dioxide production commonly observed following the rapid rewetting of a dry soil. *Soil Science Society of America Journal, 67*(3), 798-805.

Fox, T., & Comerford, N. (1990). Low-molecular-weight organic acids in selected forest soils of the southeastern USA. *Soil Science Society of America Journal, 54*(4), 1139-1144.

Gómez, M., Hontoria, E., & González-López, J. (2002). Effect of dissolved oxygen concentration on nitrate removal from groundwater using a denitrifying submerged filter. *Journal of Hazardous Materials, 90*(3), 267-278.

Gordon, H., Haygarth, P. M., & Bardgett, R. D. (2008). Drying and rewetting effects on soil microbial community composition and nutrient leaching. *Soil Biology and Biochemistry, 40*(2), 302-311.

Greenan, C. M., Moorman, T. B., Parkin, T. B., Kaspar, T. C., & Jaynes, D. B. (2009). Denitrification in wood chip bioreactors at different water flows. *Journal of Environmental Quality, 38*(4), 1664-1671.

Groffman, P. M., & Tiedje, J. M. (1988). Denitrification hysteresis during wetting and drying cycles in soil. *Soil Science Society of America Journal, 52*(6), 1626-1629.

Halaburka, B. J., LeFevre, G. H., & Luthy, R. G. (2017). Evaluation of mechanistic models for nitrate removal in woodchip bioreactors. *Environmental Science & Technology, 51*(9), 5156-5164.

Hansson, K., Kleja, D. B., Kalbitz, K., & Larsson, H. (2010). Amounts of carbon mineralised and leached as DOC during decomposition of norway spruce needles and fine roots. *Soil Biology and Biochemistry, 42*(2), 178-185.

Harrison, D., & Loveless, J. (1971). Transient responses of facultatively anaerobic bacteria growing in chemostat culture to a change from anaerobic to aerobic conditions. *Microbiology, 68*(1), 45-52.

Healy, J. B., & Young, L. Y. (1979). Anaerobic biodegradation of eleven aromatic compounds to methane. *Applied and Environmental Microbiology, 38*(1), 84-89.

Hentschel, K., Borken, W., & Matzner, E. (2007). Leaching losses of inorganic N and DOC following repeated drying and wetting of a spruce forest soil. *Plant and Soil, 300*(1-2), 21-34.

Holt, D. M., & Jones, E. B. (1983). Bacterial degradation of lignified wood cell walls in anaerobic aquatic habitats. *Applied and Environmental Microbiology, 46*(3), 722-727.

Hoover, N. L., Bhandari, A., Soupir, M. L., & Moorman, T. B. (2016). Woodchip denitrification bioreactors: Impact of temperature and hydraulic retention time on nitrate removal. *Journal of Environmental Quality, 45*(3), 803-812.

Kirk, T. K., & Farrell, R. L. (1987). Enzymatic" combustion": The microbial degradation of lignin. *Annual Reviews in Microbiology, 41*(1), 465-501.

Koshijima, T., & Watanabe, T. (2013). *Association between lignin and carbohydrates in wood and other plant tissues* Springer Science & Business Media.

Krul, J. (1976). The relationship between dissimilatory nitrate reduction and oxygen uptake by cells of anAlcaligenesstrain in floes and and in suspension and by activated sludge floes. *Wat.Res, 8*

Law, J. Y., Soupir, M. L., Raman, D. R., Moorman, T., & Ong, S. K. (2018). Electrical stimulation for enhanced denitrification in woodchip bioreactors: Opportunities and challenges. *Ecological Engineering, 110*, 38-47.

Lepine, C., Christianson, L., Sharrer, K., & Summerfelt, S. (2016). Optimizing hydraulic retention times in denitrifying woodchip bioreactors treating recirculating aquaculture system wastewater. *Journal of Environmental Quality, 45*(3), 813-821.

Liu, Y. (2017). The performance of controlled drainage and inline denitrifying woodchip bioreactor for reducing nutrient losses from subsurface drained grassland receiving liquid swine lagoon effluent. (Doctoral Dissertation, NCSU). (http://www.lib.ncsu.edu/resolver/1840.20/34529)

Lützow, M. v., Kögel-Knabner, I., Ekschmitt, K., Matzner, E., Guggenberger, G., Marschner, B., et al. (2006). Stabilization of organic matter in temperate soils: Mechanisms and their relevance under different soil conditions–a review. *European Journal of Soil Science, 57*(4), 426-445.

Maxwell, B. M., Birgand, F., Schipper, L. A., Christianson, L. E., Tian, S., Helmers, M. J., et al. (2018). Drying-rewetting Cycles Affect Nitrate Removal Rates in Woodchip Bioreactors. *Journal of Environmental Quality.*

Mikha, M. M., Rice, C. W., & Milliken, G. A. (2005). Carbon and nitrogen mineralization as affected by drying and wetting cycles. *Soil Biology and Biochemistry, 37*(2), 339-347.

Moorman, T. B., Parkin, T. B., Kaspar, T. C., & Jaynes, D. B. (2010). Denitrification activity, wood loss, and N2O emissions over 9 years from a wood chip bioreactor. *Ecological Engineering, 36*(11), 1567-1574.

Odier, E., & Monties, B. (1983). Absence of microbial mineralization of lignin in anaerobic enrichment cultures. *Applied and Environmental Microbiology, 46*(3), 661-665.

Oh, J., & Silverstein, J. (1999). Oxygen inhibition of activated sludge denitrification. *Water Research, 33*(8), 1925-1937.

Okolo, J., Nweke, C., Nwabueze, R., Dike, C., & Nwanyanwu, C. (2007). Toxicity of phenolic compounds to oxidoreductases of acinetobacter species isolated from a tropical soil. *Scientific Research and Essays, 2*(7), 244-250.

Roser, M. B., Feyereisen, G. W., Spokas, K. A., Mulla, D. J., Strock, J. S., & Gutknecht, J. (2018). Carbon dosing increases nitrate removal rates in denitrifying bioreactors at low-temperature high-flow conditions. *Journal of Environmental Quality, 47*(4), 856-864.

Saliling, W. J. B., Westerman, P. W., & Losordo, T. M. (2007). Wood chips and wheat straw as alternative biofilter media for denitrification reactors treating aquaculture and other wastewaters with high nitrate concentrations. *Aquacultural Engineering, 37*(3), 222-233.

Schimel, J. P., Gulledge, J. M., Clein-Curley, J. S., Lindstrom, J. E., & Braddock, J. F. (1999). Moisture effects on microbial activity and community structure in decomposing birch litter in the alaskan taiga. *Soil Biology and Biochemistry, 31*(6), 831-838.

Schipper, L. A., Robertson, W. D., Gold, A. J., Jaynes, D. B., & Cameron, S. C. (2010). Denitrifying bioreactors—an approach for reducing nitrate loads to receiving waters. *Ecological Engineering, 36*(11), 1532-1543.

Sutherland, J. B., Blanchette, R. A., Crawford, D. L., & Pometto, A. L. (1979). Breakdown of douglas-fir phloem by a lignocellulose-degradingStreptomyces. *Current Microbiology, 2*(2), 123-126.

Talbot, J. M., Yelle, D. J., Nowick, J., & Treseder, K. K. (2012). Litter decay rates are determined by lignin chemistry. *Biogeochemistry, 108*(1-3), 279-295.

van Hees, P. A., Jones, D. L., Finlay, R., Godbold, D. L., & Lundström, U. S. (2005). The carbon we do not see—the impact of low molecular weight compounds on carbon dynamics and respiration in forest soils: A review. *Soil Biology and Biochemistry, 37*(1), 1-13.

Warneke, S., Schipper, L. A., Bruesewitz, D. A., McDonald, I., & Cameron, S. (2011). Rates, controls and potential adverse effects of nitrate removal in a denitrification bed. *Ecological Engineering, 37*(3), 511-522.

Warneke, S., Schipper, L. A., Matiasek, M. G., Scow, K. M., Cameron, S., Bruesewitz, D. A., et al. (2011). Nitrate removal, communities of denitrifiers and adverse effects in different carbon substrates for use in denitrification beds. *Water Research, 45*(17), 5463-5475.

Woli, K. P., David, M. B., Cooke, R. A., McIsaac, G. F., & Mitchell, C. A. (2010). Nitrogen balance in and export from agricultural fields associated with controlled drainage systems and denitrifying bioreactors. *Ecological Engineering, 36*(11), 1558-1566.

Zeikus, J., Wellstein, A., & Kirk, T. (1982). Molecular basis for the biodegradative recalcitrance of lignin in anaerobic environments. *FEMS Microbiology Letters, 15*(3), 193-197.

CHAPTER 5: High-frequency, Multi-point Sampling of Field Woodchip Bioreactors in Iowa and New Zealand

5.1. Introduction

Woodchip bioreactors (also referred to as denitrification beds) are an agricultural Beneficial Management Practice (BMP) used for the removal of nitrate (NO_3) in water discharged at the edge of farm fields. The removal process is denitrification where nitrogen in the aqueous nitrate anion form is reduced into gaseous dinitrogen and nitrous oxide, and thus leaves the aquatic environment. Woodchip bioreactors (WB) installed as large pits in the ground (e.g., ~1 to 1.5 m deep, 1 to 6 m wide, and 3 to 30 m long) are designed to promote denitrifying conditions in that 1) a carbon substrate is present to serve as an electron donor for denitrifying microbes and 2) anoxic conditions persist favoring the use of NO_3 as the electron acceptor. Bioreactors typically use coarse chipped wood (chip size ~3-50 mm) as the carbon substrate based on its ability to be broken down slowly and high pore volume when compacted (40-60%). Anaerobic conditions are achieved by either managing the water table with control structures or placing the WB below the local water table. Woodchip bioreactors applications for removing NO_3 include subsurface drainage water from crop fields (Christianson et al., 2012; David et al., 2016; Woli et al., 2010), effluent from dairy (Schipper et al., 2010) and hog farms (Liu, 2017), aquaculture units (Lepine et al., 2016; von Ahnen et al., 2016), and hydroponics operations (Warneke et al., 2011).

Over twenty years of research on woodchip bioreactors have improved understanding of their performance and the factors affecting it, providing data on their performance in short- and long-term experiments in the lab and field. Results of this research, however, has shown there is still considerable uncertainty in how well these systems reduce nitrogen loads. Volumetric nitrate removal rates (i.e., the mass of nitrogen removed per unit time and unit bioreactor volume; reported here as R_{NO3}) are highly variable across studies and even within the same bioreactor over time. Shipper et al. (2010) reported NO_3 removal rates of 0.01 – 3.6 and 2 – 22 g N m^{-3} d^{-1} in a review of denitrification walls and beds, respectively. Christianson et al. (2012) measured R_{NO3} of 0.4 – 7.8 g N m^{-3} d^{-1} in four Iowa bioreactors, with rates in two bioreactors decreasing by an order of magnitude in their second and third year of operation. In their meta-analysis Addy et al. (2016) reported R_{NO3} 95% confidence interval (CI) of 2.9 – 7.3 g N m^{-3} d^{-1} for 27 denitrification beds and 3.7 – 14.9 g N m^{-3} d^{-1} when water temperature was >16.9 °C. Lepine et

al. (2016), however, measured R_{NO3} of 32 – 39 g N m^{-3} d^{-1} at 19 °C, well outside the 95% CI reported in the meta-analysis.

While the range in reported R_{NO3} can, in part, be attributed to variability in bioreactor performance, some variability may also depend on uncertainty in measurement methods. Bioreactor monitoring has primarily relied on grab samples at the inlet and outlet, with R_{NO3} calculated from differences in inlet and outlet nitrate concentrations ($[NO_3]$), bed volume, and flow rate. Frequency of grab sampling is typically as low as weekly or monthly or based on flow-weighted composite samples (e.g., Liu, 2017). When variability of $[NO_3]$ at the inlet and outlet is low (e.g., large drainage area treated or base flow conditions), calculated rates based on grab samples may be less sensitive to sample timing. When $[NO_3]$ are more variable, errors may be significant since R_{NO3} is typically calculated from instantaneous flow and water chemistry values. Uncertainty produced by sampling infrequency can be significant when calculating total load or nutrient removal (e.g., Johnes 2007; Birgand et al., 2010; Williams et al., 2015).

Current woodchip bioreactor knowledge is limited by their study as "black box" systems. In nearly all studies, bioreactor water chemistry and flow are monitored at the inlet and outlet only. Internal processes are inferred from these data. Several studies have used breakthrough curves of a conservative tracer (typically bromide) at the outlet to quantify dispersion indices and hydraulic inefficiencies (Cameron and Schipper, 2011; Christianson et al., 2011; Christianson et al., 2013). These studies showed that hydraulic short-circuiting or flow inefficiencies occur, but the method is unable to provide understanding of where or how they are occurring. More recent studies have used internal porewater wells to observe biogeochemical kinetics along the bioreactor length (Christianson et al, 2013; Halaburka et al., 2017), but low frequency grab sampling methods over short durations yield few observations over a small range of conditions. In order to improve understanding and design of woodchip bioreactors, more robust and intensive methods for monitoring must be used.

This paper presents a novel method for high-frequency, multi-point monitoring of woodchip bioreactors. A large volume Multi-Point Sampling system (MPS, Birgand et al., 2016) was used for *in situ* measurements of NO_3 and dissolved organic carbon (DOC) in the inlet, outlet, and porewater sampling wells of two field bioreactors in the U.S. and in New Zealand. It was

hypothesized that the MPS method could 1) provide more robust measures of nitrate removal efficiency, 2) produce better data sets for establishing relationship between nitrate removal and other factors (e.g. flow, temperature) and 3) improve insights into where and why hydraulic efficiencies are occurring.

5.2. Materials and methods

5.2.1. Site description

Woodchip bioreactors in the U.S. and in New Zealand were selected. In the U.S., a woodchip bioreactor at the Northeast Research Farm in Nashua, Iowa (42.9° N, 92.6° W) was monitored during 2 – 13 June in 2017 and during 1 – 17 April in 2018. This field bioreactor (referred to as IA herein) receives tile drainage from a 14.2 ha corn-soybean rotation and was constructed in April 2009, i.e., about 9 years old at the time of monitoring. The unlined bioreactor (128.1 m^3) has a trapezoidal geometry (36.6 m *L* x 4.6 m top *W* x 2.4 m bottom *W* x 1.0 m *D,* Figure E-1). Tile drainage water enters and leaves the bioreactor through distributors made of perforated tile drainage pipe placed at the bioreactor bottom at the inlet and outlet. Additional site information and performance of this bioreactor was reported previously (Christianson et al., 2012; Christianson et al., 2013). The original bed depth for the IA bioreactor was reported as 1.0 m, although considerable subsidence (0.4-0.6 m) has occurred near the inlet and outlet since installation.

The second bioreactor located in Morrinsville, NZ (37.6° S, 175.6° E) was monitored from 8 August – 8 September in 2018. This bioreactor was constructed in 2016 and receives tile drainage from a pasture grazed by dairy and. This bioreactor (referred to as NZ) has a rectangular pyramidal geometry (11 m top *L* x 9 m bottom *L* x 7 m top *W* x 5 m bottom *W* x 1.2 m *D,* Figure E-2 & E-3). It is lined on the bottom and sides with an impermeable liner (Firestone EPDM 1.14 mm membrane) with a permeable geotextile over the woodchip bed. Flow enters the bioreactor through a perforated tile drainage distributor near the top of the bioreactor (0.78 m above bottom) at the inlet, and exits the bioreactor through a distributor at the bioreactor bottom at the outlet. This bioreactor is permanently saturated below the water table with 0.92 m water depth during periods of no flow. Both bioreactors were filled with coarse woodchips and covered with soil after installation.

5.2.2. Well layout

Porewater sampling wells in both bioreactors were installed in order to measure water chemistry differences within the bioreactor profile. Sampling wells in the IA bioreactor were installed during its construction in 2009 (Fig 1A). Well pairs (4 cm diameter PVC) were placed at 5.2, 11.6, 17.7, 24.1, 29.3, 35.7 m from the bioreactor inlet. To measure water chemistry differences along the vertical profile, each well pair consisted of shallow and deep wells screened to 46 - 61 and 15 - 30 cm from bottom, respectively, with wells at each pair spaced 30 cm apart. Wells at the IA bioreactor were labeled according to their screen depth (S for shallow, D for deep), and according to the location of its well pair (i.e. S1 and D1 for shallow and deep wells at the first well pair 5.2 m from inlet).

Nineteen sampling wells (5 cm diameter PVC) in the NZ bioreactor were installed in June 2018 along the bioreactor centerline and two longitudinal transects (Fig. 1B). Three sampling wells were placed along the centerline at 2.2, 4.3, and 6.7 m from the inlet manifold and fully screened to bed depth. Two separate longitudinal transects for observing water chemistry differences along the horizontal profile were placed 1.25 m on either side of the centerline. Each transect consisted of a well pair 0.5, 3.2, 5.9, and 8.5 m from the inlet manifold. Well pairs consisted of shallow and deep wells screened to 59 – 69 and 28 – 38 cm from the bottom, respectively, with wells at each pair spaced 50 cm apart. Wells at the NZ bioreactor were labeled according to their screen depth (S for shallow, D for deep), the position of their transect (L for left side, looking from the inlet to the outlet; C for center wells) and according to the location of its well pair (i.e. LS1 and LD1 for shallow and deep wells along the left transect at the first well pair 0.5 m from inlet, and so on). Sampling wells at both bioreactors were kept covered with PVC caps during monitoring.

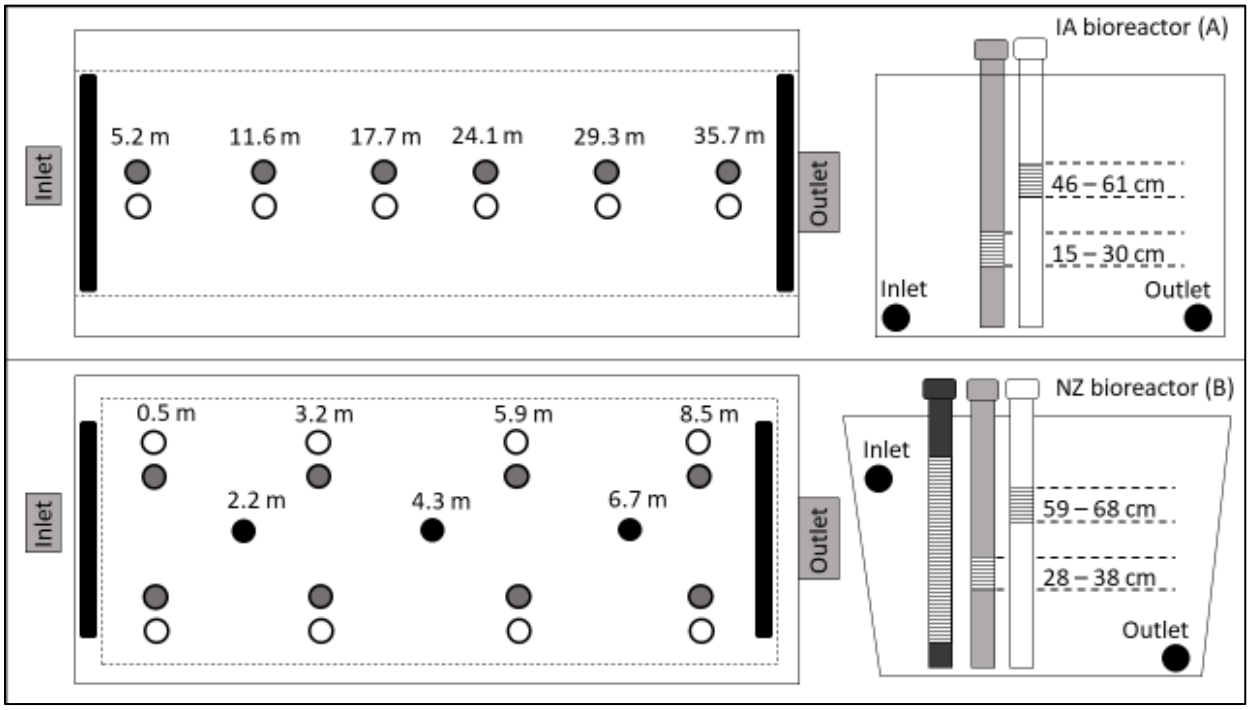

Figure 5-1A & 5-1B. Plan and side view diagram of IA and NZ bioreactor showing layout of internal sampling wells. Grey, white, and black circles on the plan view indicate deep, shallow or fully screened wells, respectively. Drawings are not to scale.

5.2.3. High frequency multi-point sampling

A multi-point sampler (MPS) was used for high frequency sampling of water chemistry at multiple locations. The MPS allows water samples from multiple locations to be pumped to a common probe using a 12-valve manifold (Model WTB-3R(K), Takasago Fluidic Systems, Nagoya, Japan), peristaltic pump (Boxer 15KS, Boxer GmbH, Ottobeuren, Germany), and a programmable printed circuit board (Advanced Circuits, Aurora, Colorado). The operation and design of the MPS is fully described in Birgand et al. (2016) and not covered further here.

The MPS pumped water from each well to a spectrophotometer (spectro::lyser, s::can, Vienna, Austria) for absorbance measurement. Estimates of [NO_3] and [DOC] were derived from the absorbance fingerprint, a method previously shown to be accurate and reliable for measuring concentrations of both nutrients (Rieger et al., 2004; Strohmeier et al., 2013; Etheridge et al., 2014; Birgand et al., 2016). The spectrophotometer was fitted with a 4 mL, 10-mm pathlength

quartz cuvette (Starnacells® 1-Q-10/SBTX2-8/10X20; Birgand et al., 2016). The small-volume quartz cuvette insert allowed the cuvette to be easily rinsed with >10x cuvette volume prior to each measurement to prevent cross-contamination between consecutive samples (Birgand et al., 2016; Maxwell et al., 2018). The quartz cuvette also allowed for a periodic rinse of the cuvette with a low-strength acid, if needed, to minimize fouling of the optical path by metals or organics.

Two MPS were used to monitor 14 and 21 sampling locations at the IA and NZ bioreactor, respectively. One MPS sampled the inlet and six wells within the first 17.7 m at the IA bioreactor, the second MPS sampling the outlet and final six wells. At the NZ bioreactor, one MPS sampled the inlet and ten wells within the first 4.3 m, the second MPS sampling the outlet and final nine wells. Wells were sampled moving from inlet to outlet, and shallow wells sampled before deep wells at the same well pair (Table E-1).

A single 'sample sequence' consisted of the MPS pumping water to the spectrophotometer from the current sample location, a measurement by the spectrophotometer, and finally purging the sample back to the current sample location. Each 'sample cycle' consisted of sampling each location before returning to the initial valve. Each sample sequence lasted 5-6 min, with data resolution at each location equal to a sample cycle (40 - 60 min). Length of sample tubing was 3-9 m, depending on the distance from the MPS to the sampling location. Sample tubing (3.18 mm ID, vinyl) was covered with 60 μm plankton mesh at the intake to prevent clogging of tubing. Sample tubing intake was located at 1-2 cm from the bottom of each well.

5.2.4. Probe calibration

The s::can spectrophotometer provides a global calibration for estimating [NO_3] and [DOC], although the manufacturer recommends a local calibration for greater accuracy. Probes were calibrated during each monitoring period using previously described PLSR calibration methods (Etheridge et al., 2014; Birgand et al. 2016), resulting in six separate calibrations for [NO_3] and [DOC] (two probes in three monitoring periods). Selected water samples were collected after absorbance measurements for later lab analysis. At least 10 samples were collected for each probe's calibration (Table E-2). The PLSR model selected for predicting [NO_3] and [DOC] was based on the number of components providing the lowest root mean squared error of prediction (RMSEP). In the case of poor fits of the PLSR model, a linear regression was used using lab

values and the probe's estimates for [NO_3] and [DOC]. Lab samples were analyzed at the NC State University BAE Environmental Analysis Lab for NO_3 (EPA Method 353.2) and DOC (EPA415.1 with Teledyne Tekmar Apollo 9000, 0.45 µm filter). Samples collected from the NZ bioreactor were analyzed using cadmium reduction flow injection (APHA 4500-NO_3 I, Hill Laboratories, Hamilton, NZ).

5.2.5. Flow and depth measurements

Flow at the IA bioreactor passed through Agri Drain control structures at the inlet and outlet. Bypass and outlet flow were calculated by measuring stage over a 45° v-notch weir. Water level was recorded every 1 - 5 minutes (Solinist Model 3001 Levelogger Junior). Previously published weir equations for this site were used (Christianson et al., 2012). Flow at the NZ bioreactor passed through similar control structures at the inlet and outlet, with only bypass and outlet flow measured. In both cases flow calculations considered the height of water below the weir v and assumed conservation of water mass entering and exiting the bioreactor (i.e. $Q_{in} = Q_{out}$). This assumption was best for the NZ bioreactor as the internal saturated volume did not change over time.

Because of its relatively recent installation, volume of the NZ bioreactor was assumed as the design volume (72.3 m^3). A porosity of 0.484 was measured onsite (Lincoln Agritech, personal comm.) Bed volume of the IA bioreactor was assumed as ten percent reduction from original volume (115.3 m^3), based on visual observations of subsidence. Christianson et al. (2013) assumed a porosity of 0.65 at this site, however for this study a porosity of 0.5 was assumed based on expected settling and measured porosity at the NZ bioreactor. Saturated depth of both bioreactors was based on well tape measurements in sampling wells (IA bioreactor) or depth measurements in the control structures (NZ bioreactor). Theoretical hydraulic residence time (HRT) was calculated based on the saturated volume of the bed (i.e., HRT = bioreactor Volume/flow rate).

5.2.6. Dissolved oxygen and temperature

Temperature and dissolved oxygen (DO) were measured using a ProODO Optical DO Instrument (YSI, Yellow Springs, Ohio) calibrated prior to and once a week during each

monitoring period using a one-point calibration per the manufacturer's specifications. Temperature and DO were measured at the inlet and outlet of the IA bioreactor in 2017, while both parameters were also measured at each sampling well during April 2018 and in August 2018 at the NZ bioreactor. The DO probe was suspended 1-2 cm above the bottom of the control structures or sampling wells during measurements.

5.2.7. Removal rate and percent reduction

Volumetric NO_3 removal rates, R_{NO3}, were calculated based on instantaneous conditions, similar to methods used the literature (e.g., Christianson et al., 2013; Hoover et al., 2016; David et al., 2016). Volumetric removal rates were calculated using Equation 1. For each measurement of outlet [NO_3] ($[NO_3]_{out}$), the corresponding value for inlet [NO_3] ($[NO_3]_{in}$) was selected as the inlet [NO_3] measurement closest in time. Flow measurements at 5 to 15-min intervals were interpolated to provide minutely data, and the flow rate, *Q*, at the time of $[NO_3]_{out}$ measurement was selected as the flow rate. Values of R_{NO3} represent volumetric removal rates based on instantaneous values. Calculations for percent reduction (Equation 2) similarly used instantaneous values of $[NO_3]_{in}$ and $[NO_3]_{out}$ that were closest in time. Cumulative volumetric removal rates, CR_{NO3}, were also calculated by integrating the time series of instantaneous in- and outlet loads i.e., flow times concentrations at the in- and outlets, respectively over the monitoring period using the trapezoidal-method for integration. Data gaps >24 h were removed when calculating CR_{NO3} and intervals of cumulative removal summed. Saturated woodchip-filled volume, *V*, of the bioreactor was used for calculating both volumetric rates, rather than the design woodchip-filled volume. Saturated volume was determined using water depth measurements.

$$R_{NO3} = \frac{([NO_3]_{in} - [NO_3]_{out}) * Q}{V} \qquad \text{Equation 5-1}$$

$$\text{Percent reduction} = \frac{([NO_3]_{in} - [NO_3]_{out}) * 100\%}{[NO_3]_{in}} \qquad \text{Equation 5-2}$$

Uncertainty of the cumulative load was calculated by creating separate calibrations from subsampled lab values. During subsampling of the lab values, 80% of the lab values were randomly selected to produce a new probe NO_3 calibration used to predict the [NO_3] time series, with each time series used to calculate a different cumulative load. This resampling and

recalibration was done 100 times, with the lowest and highest five values of cumulative load in and out removed to produce a 90% confidence interval for uncertainty. Maximum uncertainty in CR_{NO3} were calculated using the highest and lowest values of cumulative load in and out, respectively.

5.3. Results

5.3.1. Flow and [NO_3] time series at bioreactor inlets and outlets

From June 2 - 3, 2017, the MPS collected data at 5-min intervals, resulting in 40-min data intervals at each point including the inlet and outlet of the IA bioreactor (Figure 5-2A). Water chemistry was continuously measured over the 12-d period, with 24 h of data lost on June 5 due to fouling of the quartz cuvette. This issue was resolved by adding a tap water rinse at the end of each sampling cycle, purging back to the tap water reservoir and not the bioreactor. Higher variability was seen in $[NO_3]_{in}$ relative to $[NO_3]_{out}$, particularly at the beginning of the monitoring period when $[NO_3]_{in}$ decreased by as much as 0.8 mg N L^{-1} between consecutive measurements. This higher variability of $[NO_3]_{in}$ was most likely caused by the periodic additions of drainage water into the monitored inlet drain tile from a separate field causing some apparently erratic inlet nitrate concentration dips. Flow was highest from June 2 - 4 (215±16 mL s^{-1}, mean ± standard deviation), then relatively stable at a lower level from June 5 – 10 (170±16 mL s^{-1}), and showing a diurnal pattern with flow highest between 6:00 and 7:00 AM. Flow decreased further between June 11 – 13 (125±7 mL s^{-1}). During the June 2 – 10, $[NO_3]_{in}$ and $[NO_3]_{out}$ were relatively stable at 16.4±0.3 and 11.3 ±0.2 mg N L^{-1}, respectively. Decreases in $[NO_3]_{out}$ followed the decrease in flow beginning on June 11, with $[NO_3]_{out}$ lowest on June 13 (9.5±0.1 mg N L^{-1}). Average water depth in the bioreactor was 0.31 m for a saturated volume of 31.0 m^3, only 27% of the total bed volume (assuming 10% reduction of original volume due to subsidence). Theoretical HRT was 20.1±1.5 h during June 2 – 4, increasing to 34.4±2.1 h from June 11 – 13. No precipitation occurred over the 12-d period with bioreactor inflow driven by tile drainage "base flow".

High-frequency measurements were less successful at the IA bioreactor in April 2018 (Figure 5-2B). Unseasonably low air temperatures and snow caused water in the MPS sampling lines to freeze. Multi-point sampling was limited to the day time hours on most days, and overnight

sampling was only possible from April 11 – 14. Only 360 measurements were made at the inlet and outlet over the 15-d monitoring period, compared to 316 measurements made over 12-d in June 2017. From April 1 – 16, $[NO_3]_{in}$ and $[NO_3]_{out}$ were 13.4±0.7 and 11.9 ±0.5 mg N L^{-1}, respectively. Flow was more variable at the IA bioreactor in 2018 and was largely affected by snow and subsequent snow melt. From April 1 – 10, flow was 413±78 mL s^{-1}. On April 10 at 19:00 the inlet weir was lowered to reduce flow to the bioreactor, and flow from April 11 – 13 was 233±42 mL s^{-1}. A stop log failure at the inlet overnight on April 13 caused flow rates to dramatically increase up to 1,560 mL s^{-1}, followed by peaks in $[NO_3]_{in}$ and $[NO_3]_{out}$ of 15.5 and 13.0 mg N L^{-1}, respectively. From April 14 – 17 flow rates increased to 352±27 mL s^{-1}. Average water depth in the bioreactor was 0.37 m. Theoretical HRT was 13.3±3.0 h from April 1 – 10 and 24.5.3±2.7 h from April 11 – 13.

The most extensive data set was collected over 30 d at the NZ bioreactor (Figure 5-2C), with minor issues causing some data loss over the monitoring period. Two marine batteries powering both MPS and respective probes caused power loss overnight for two days (August 8 – 10), after which a total of four marine batteries were used to provide sufficient power. An oxalic acid rinse was tested on August 15 to reduce fouling of the quartz cuvette, however the acid solution exacerbated the fouling causing data loss on August 15 – 16. Condensation on the surface of the quartz cuvette interfered with the probe's measurements resulting in data loss during the hours when condensation occurred, typically between 10:00 AM and 4:00 PM. Of all three monitoring periods data loss from condensation was most significant during the NZ monitoring caused by higher humidity and temperature differences between air and drainage water.

Over the one month monitoring period (August 8 to September 8, 2018), $[NO_3]_{in}$ and $[NO_3]_{out}$ were 7.8±0.8 and 1.9 ±1.2 mg N L^{-1}, respectively. Increases in $[NO_3]_{in}$ immediately followed increases in flow associated with rainfall. Increases in $[NO_3]_{in}$ were followed much later by increases in $[NO_3]_{out}$. Average depth of water in the bioreactor was 0.97 m. Flow during periods of low flow was 53±42 mL s^{-1} at an HRT of 147±33 h, and high flow following rain events of 101±16 mL s^{-1} at an HRT of 75±11 h. At peak flows of 128 – 146 mL s^{-1} following rain events HRT decreased to 51 – 58 h.

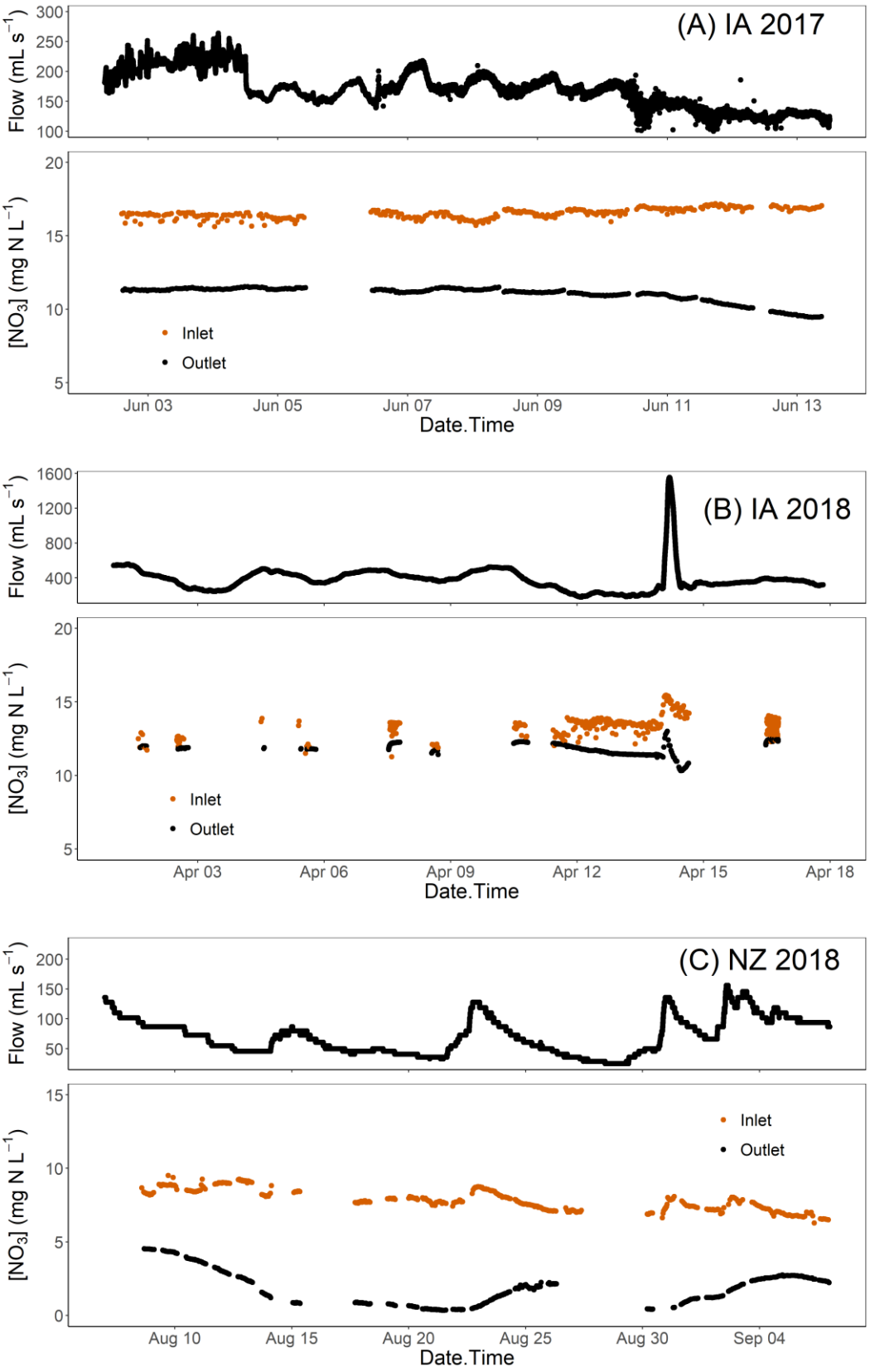

Figure 5-2A – C. Time series of flow and inlet and outlet [NO_3] for the IA and NZ bioreactors

5.3.2. Dissolved oxygen and temperature

During June 1 – 13 2017 at the IA bioreactor, DO at the inlet and outlet ($[DO]_{in}$ and $[DO]_{out}$, respectively) were relatively constant at 8.5±0.2 and 0.2±0.1 mg DO L^{-1}. Water temperature decreased by <0.3 °C from inlet to outlet. Inlet water temperature increased over 12 d from 11.2 °C on June 1 to 13.6 °C on June 13.

In April 2018 $[DO]_{in}$ at the IA bioreactor was higher (12.1±0.5 mg DO L^{-1}) at lower water temperatures (2.9 °C). Dissolved oxygen decreased gradually from inlet to outlet, with mean [DO] 2.5 mg L^{-1} in deep wells 11.6 m from the inlet (Figure 5-3A). Besides measurements on April 2, [DO] was <1 mg L^{-1} in shallow and deep wells >11.6 m from the inlet. Dissolved oxygen in deep wells at 5.2 and 11.6 m was significantly greater (α=0.01) than [DO] in shallow wells. At >11.6 m from inlet there were no significant differences in [DO] between shallow and deep wells. Increases in [DO] at 5.2 and 11.6 m were seen at greater flow. From April 1 – 10 (flow = 413±78 mL s^{-1}) mean [DO] in deep wells at 5.2 and 11.6 m was 10.2 and 2.7 mg L^{-1}, respectively. From April 11 – 13 (233±42 mL s^{-1}), mean DO in deep wells at both locations fell to 8.3 and 1.8 mg L^{-1}.

Dissolved oxygen at the NZ bioreactor inlet (4.1±0.3 mg L^{-1}) was much lower at water temperatures (12.2 °C) comparable to June 2017 at the IA bioreactor (Figure 5-3B). Dissolved oxygen decreased below 2 mg L^{-1} within 0.5 m of the inlet and did not exceed 1 mg L^{-1} after 3.2 m. Similar to the IA bioreactor, [DO] in shallow wells was significantly higher than deep wells at 0.5 m (α=0.01) and 3.2 m (α=0.05). Dissolved oxygen was not significantly correlated with flow rates at any wells.

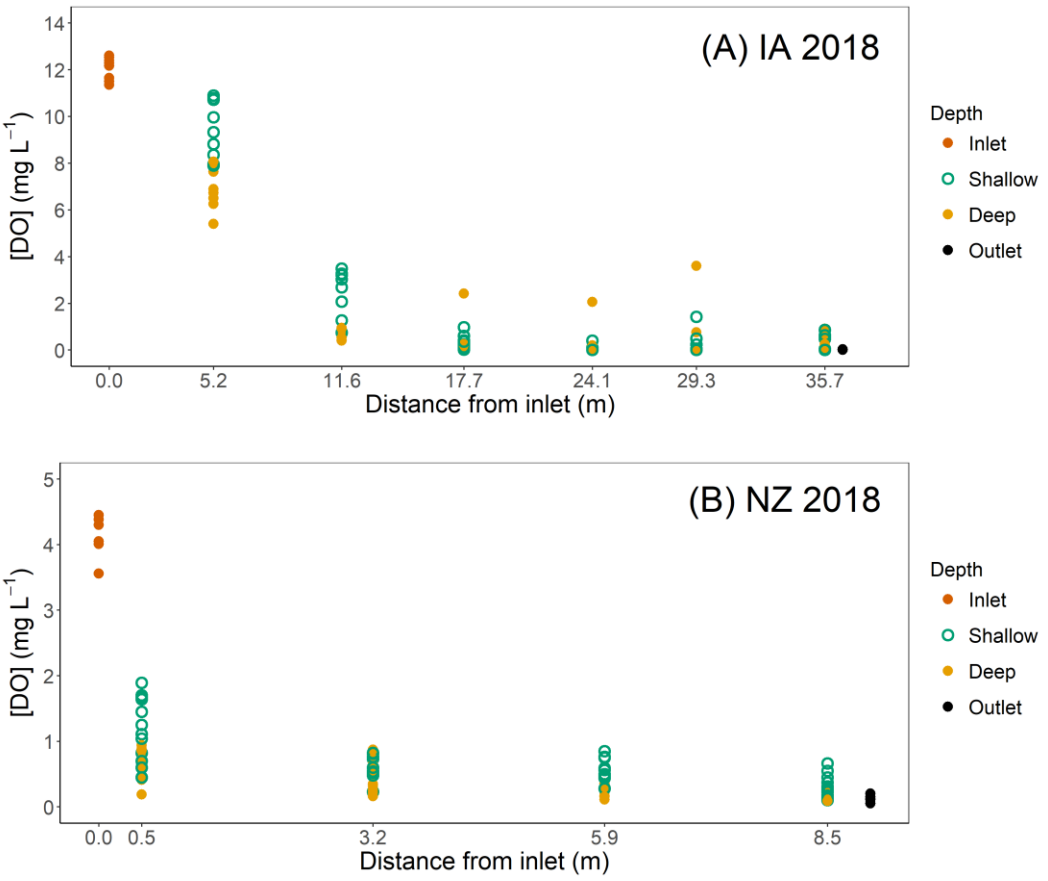

Figure 5-3A & 5-3B. Dissolved oxygen concentrations at (A) the IA bioreactor in April 2018 and (B) NZ bioreactor in August 2018. Shallow wells had higher [DO] than deep wells at both bioreactors, with significantly lower inlet [DO] at the NZ bioreactor.

5.3.3. Nitrate removal efficiency

Using Equation 5-1, the highest apparent R_{NO3} were measured in June 2017 at the IA bioreactor (Figure 5-4), while the lowest R_{NO3} were seen during 2018 at the NZ bioreactor. In several instances in April 2018 measured $[NO_3]_{in}$ was lower than $[NO_3]_{out}$ and resulted in negative R_{NO3} values. Data collected in April 2018 during high flow after stop log malfunction were removed for calculating R_{NO3} for this period. Mean R_{NO3} during the 2017 and 2018 IA and 2018 NZ monitoring periods were 2.49±0.30, 0.92±0.47, and 0.67±0.29 g N m^{-3} d^{-1}, respectively. Volumetric removal rates were based on saturated, woodchip-filled volume of the bioreactors, calculated to be 32.2, 36.8, and 55.4 m^3. The highest R_{NO3} at the NZ bioreactor occurred during

high flow events, when flow and $[NO_3]_{in}$ increased quickly while $[NO_3]_{out}$ remained low and lagged $[NO_3]_{in}$.

Using Equation 5-2, mean percent reduction during the IA 2018 and 2018 experiments and NZ 2018 experiment were 33.2±4.2, 9.2±4.7, and 76±4.7 %, respectively (Figure 5-4). The apparent percent reduction at each site varied by as much as 17.8, 25.0, and 50.5 percentage points. High variability in percent reduction at the NZ bioreactor was mostly due to increases in $[NO_3]_{out}$ lagging $[NO_3]_{in}$ during high flow. The highest percent reduction of NO_3 was measured at the NZ bioreactor, although lower $[NO_3]_{in}$ at this site biased percent reduction values. Highest percent reduction contrasted with low R_{NO3} at the NZ bioreactor and was caused by high HRT.

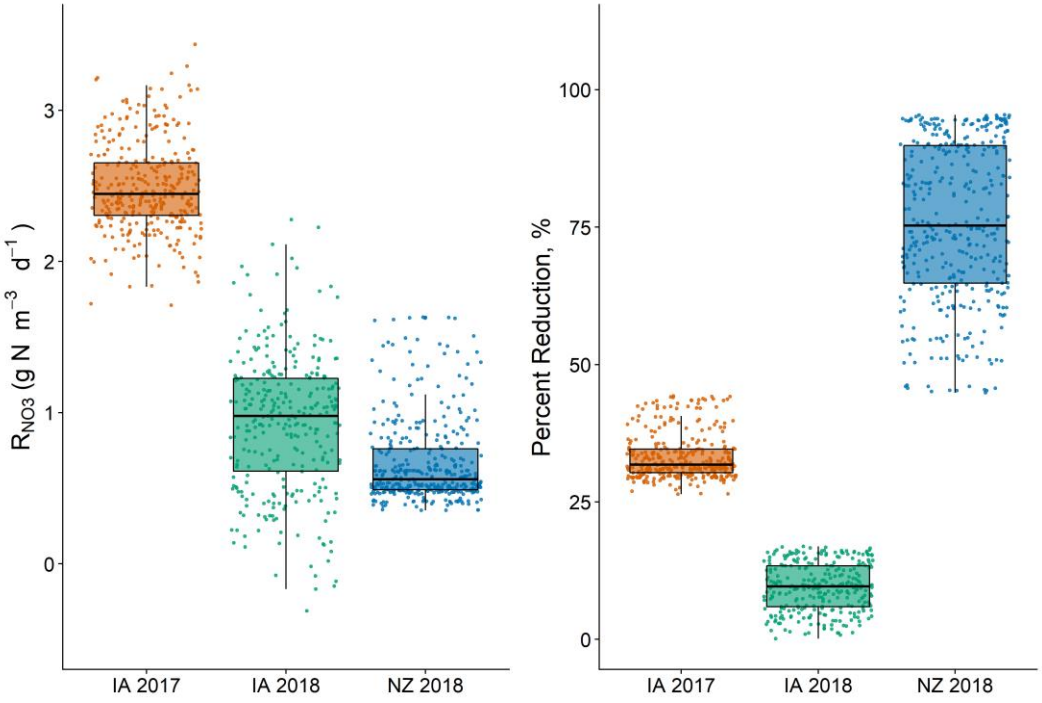

Figure 5-4. Volumetric nitrate removal rates, R_{NO3}, and percent reduction for the IA and NZ bioreactors. The highest R_{NO3} were seen in 2017 at the IA bioreactor, while the greatest percent reduction was seen at the NZ bioreactor.

5.3.4. Cumulative NO_3 removal

Cumulative nitrate removal was not calculated for the April 2018 monitoring period in IA due to limited amount of data collected. Cumulative nitrate removal was calculated for the June 2017

(IA) and August 2018 (NZ) monitoring periods only. Over the 10.8 d monitoring period at the IA bioreactor in 2017, cumulative loads using available data at the inlet and outlet were calculated to be 2,614 and 1,748 g N (Figure 5A). The cumulative load curve was broken into two curves due to data loss from 5 -6 June, 2017. Both flow and $[NO_3]_{in}$ were too variable to assume a linear interpolation over the 24.8 h gap in data. Based on the net difference in mass NO_3 entering and leaving the bioreactor over the 9.8 d period of complete data (792 g N), CR_{NO3} was calculated as 2.52 g N m^{-3} d^{-1}, in close agreement with the mean R_{NO3} values over the same period (2.49 g N m^3 d^{-1}). Total mass reduction of N over the sampling period was 33%, also in close agreement with mean percent reduction (Figure 5-4).

Two periods of data loss >1 d (15 - 16 and 26 – 30 of Aug) occurred over 30.8 d while monitoring the NZ bioreactor. The cumulative load curve for the NZ bioreactor (Fig. 5B) represents three periods in which $[NO_3]$ was successfully measured at both the inlet and outlet. During these periods several data gaps of 3 – 9 h caused by cuvette condensation required linear interpolation of $[NO_3]$. Cumulative NO_3 load at the inlet and outlet was computed to be 1,249 and 304 g N. Lower flows and $[NO_3]_{in}$ at the NZ bioreactor corresponded to a lower daily N load received by the bioreactor (51 g N d^{-1}), relative to daily load received by the IA bioreactor in 2017 (242 g N d^{-1}). Over the 24.5 d period in which cumulative load curves were used 945 g N were removed resulting in CR_{NO3} over the period of 0.70 g N m^3 d^{-1}, comparable to mean R_{NO3} over the same period (0.67 g N m^3 d^{-1}). Total mass reduction of N over the sampling period was 76%.

Uncertainty of cumulative NO_3 load for both IA and NZ was relatively small. Uncertainties of cumulative NO_3 loads for the IA 2017 experiment were estimated to be 0.6 – 1.5%. The resulting Uncertainty on CR_{NO3}, based on these recalculated cumulative loads, was 4.8 – 6.2%. Uncertainty in the NZ 2018 experiment was higher, likely due to the smaller amount of lab samples analyzed for $[NO_3]$. Uncertainty of cumulative NO_3 loads were 2.9 – 9.8%, with CR_{NO3} uncertainty of 8.5 – 13.8%.

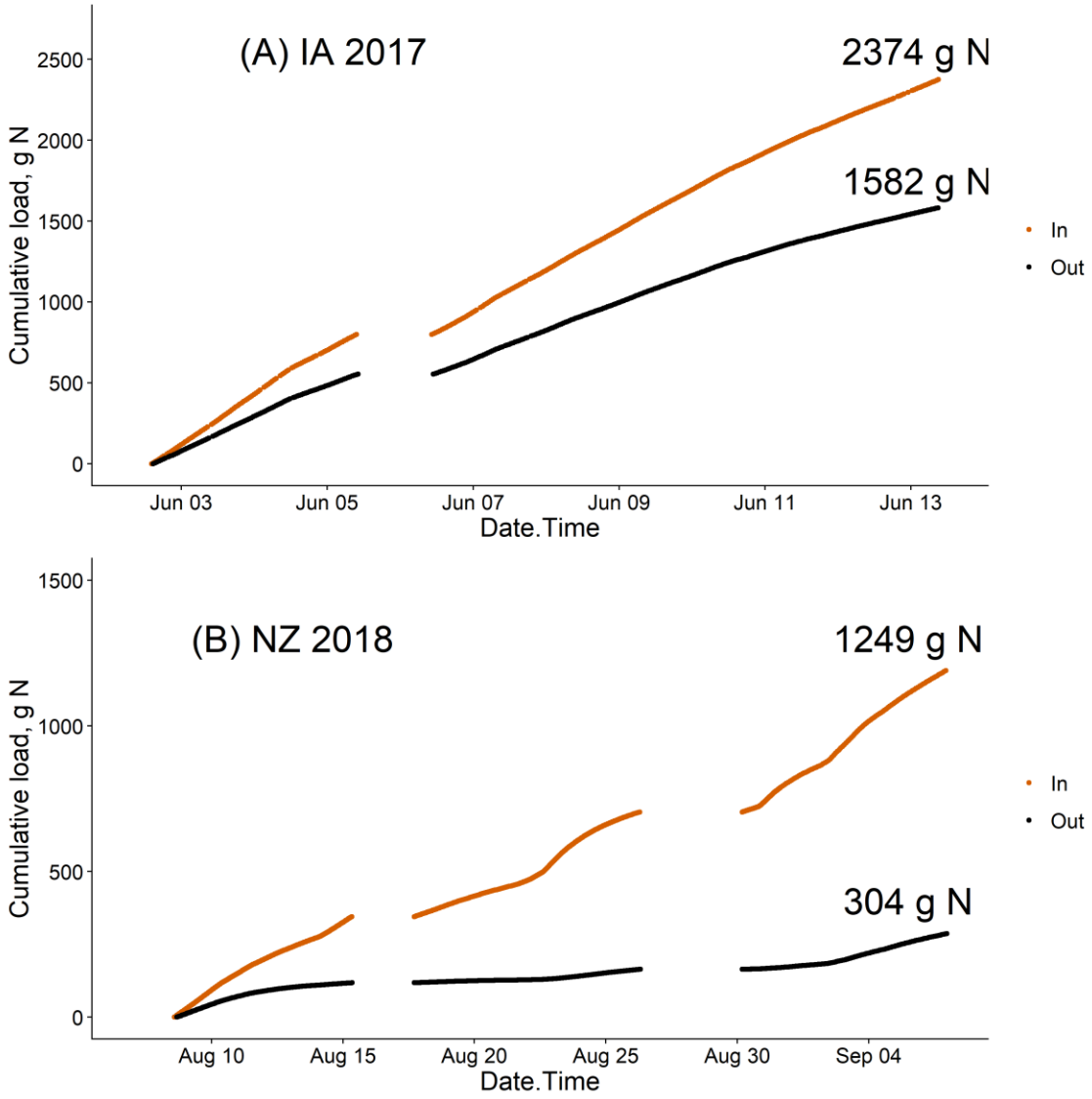

Figure 5-5A & 5-B. Calculated cumulative loads for IA 2017 and NZ 2018 data. Data gaps > 24 h were removed and cumulative load calculated over remaining intervals with high frequency data. Cumulative removal rates (CR_{NO3}) were in close agreement to mean R_{NO3} over the same period, with higher daily N loading at the IA bioreactor.

5.3.5. Vertical NO_3 profiles

Nitrate concentrations in sampling wells at the IA bioreactor varied according to well depth. In both 2017 (Figure 5-6) and 2018 (Figure E-4) [NO_3] was significantly and consistently higher in shallow wells compared to deep wells. For the 2017 and 2018 data only, the first 7 and 12 days of data are shown when flow rates were most stable. In 2018, too few measurements were made

at 17.7 and 24.1 m to make meaningful comparisons between wells. Differences in [NO_3] between shallow and deep wells were lowest (in 2017) or not significantly different (in 2018) 5.2 m from the inlet. In 2017 differences between shallow and deep wells increased with distance from the inlet up to 29.3 m. Differences in mean [NO_3] between shallow and deep wells in 2017 were <0.1, 0.3, 0.6, 1.3, 1.3, and 0.8 mg N L^{-1} at 5.2, 11.6, 17.7, 24.1, 29.3, and 35.7 m, respectively. Decreases in mean [NO_3] from one well pair to the next were 0.6, 0.9, 2.6, 0.4, and 0.3 mg N L^{-1} for deep wells and 0.3, 0.6, 1.9, 1.4, and 0.8 mg N L^{-1} for shallow wells, with the largest [NO_3] decreases occurring between 17.7 and 24.1 m. In 2018 differences in [NO_3] between shallow and deep wells were smaller but still significant (α=0.001) at wells >5.2 m from the inlet.

Differences between shallow and deep wells at the NZ bioreactor were less significant, with no consistent trends across the bioreactor length (Figure 5-7). Differences in [NO_3] between wells were only consistently significant (α=0.001) at the first well pair 0.5 m from the inlet, with mean [NO_3] in deep wells lower by 0.4 – 0.5 mg N L^{-1}. Nitrate was generally lower in deep wells at 3.2 m relative to shallow wells. The opposite was true at 5.9 m, where [NO_3] was generally higher or not significantly different compared to shallow wells. Mean [NO_3] in deep wells at 3.2 m from inlet were lower by <0.3 mg N L^{-1} and greater by <0.4 mg N L^{-1} at 5.9 m, relative to shallow wells on the same side of the bioreactor. Differences in [NO_3] between wells were generally not significant at 8.5 m from the inlet. Differences in mean [NO_3] between adjacent wells were 2.2, 1.8, and 1.0 mg N L^{-1} in deep wells, and 2.4, 2.2, and 0.8 mg N L^{-1} in shallow wells, with the greatest decreases occurring between 0.5 and 3.2 m.

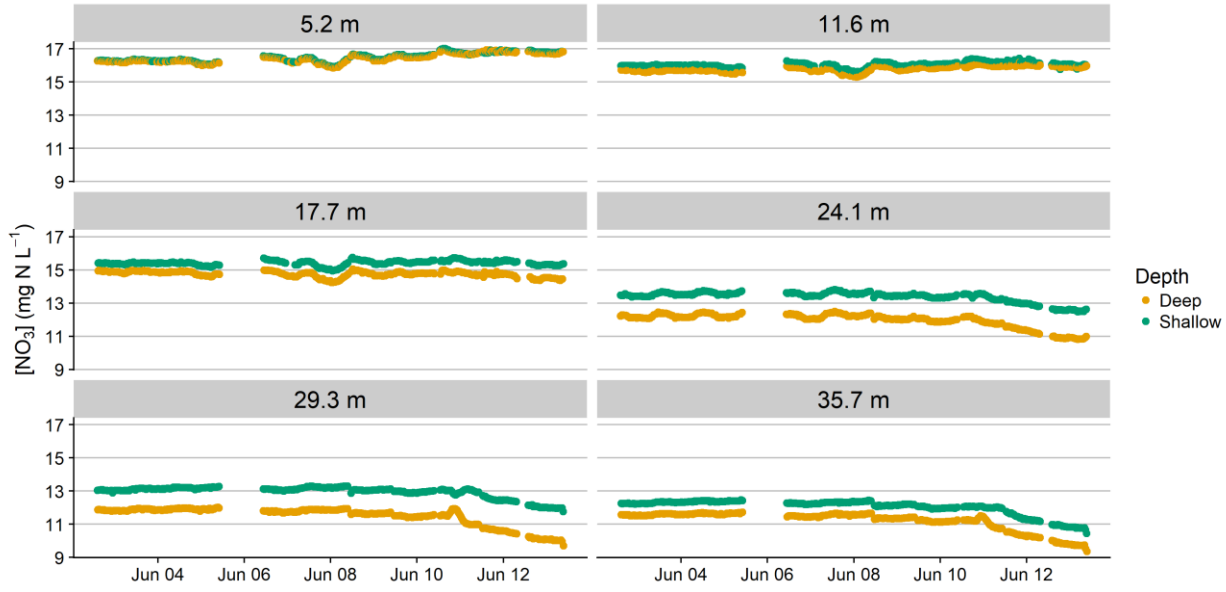

Figure 5-6. Times series of IA 2017 [NO_3] in shallow and deep wells, according to distance from the bioreactor inlet. Shallow wells had consistently higher [NO_3], and differences between shallow and deep wells increased with increasing distance from the inlet.

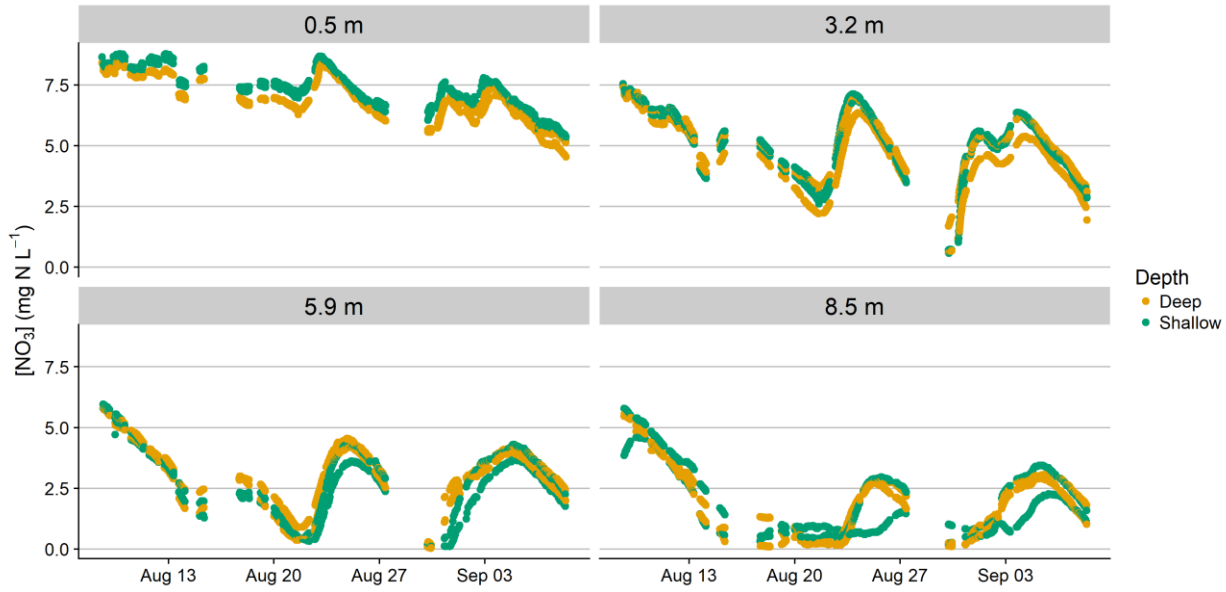

Figure 5-7. Times series of NZ 2018 [NO_3] in shallow and deep wells, according to distance from the bioreactor inlet. Shallow wells had consistently higher [NO_3], and differences between shallow and deep wells increased with increasing distance from the inlet.

5.3.6. Horizontal NO_3 profiles

Horizontal differences in [NO_3] profiles were measured only in the NZ bioreactor, with well transects 1.25 m either side of the centerline (Figure5- 8). Unlike vertical differences in [NO_3] at 0.5 m, horizontal differences at 0.5 m between left and right transect wells at shallow or deep locations was small (<0.1 mg N L^{-1}) and not significant. Mean [NO_3] was significantly higher in deep wells along the right transect by 0.7 and 0.4 mg N L^{-1} at 3.2 and 5.9 m, respectively, compared to the left transect. Mean [NO_3] was significantly higher in shallow wells along the left transect by 0.4 mg N L^{-1} at 5.9 m, relative to the right transect. The shallow well in the right transect at 8.5 m had consistently lower [NO_3] than the left transect and exhibited hydraulic inefficiencies. In two high flow events on August 24 and 31 [NO_3] in this well was less responsive and did not increase with all three other wells at 8.5 m. Mean [NO_3] differences between right and left transects were not significant at other locations.

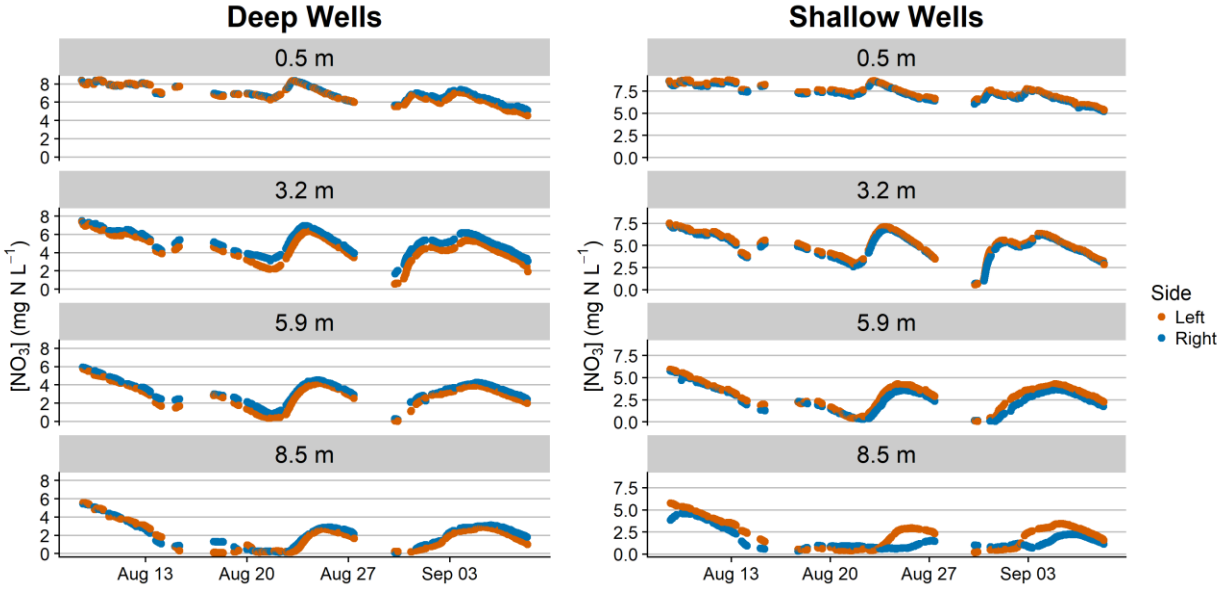

Figure 5-8. Time series of [NO_3] at the NZ bioreactor illustrating differences between left and right transects. Differences were mostly not significant and did not show any apparent horizontal gradients in [NO_3].

5.3.7. Longitudinal profiles of NO_3 and DOC

Dissolved organic carbon was successfully monitored at the IA bioreactor during 2017 only. Lab samples submitted for [DOC] in 2017 to calibrate both probes ranged from 0.58 – 1.29 mg C L^{-1} for the inlet probe and 0.99 – 1.25 mg C L^{-1} for the outlet probe and the PLSR calibration was used for the predictive model. While [NO_3] decreased from inlet to 17.7 m, [DOC] increased slightly over this length (Figure 5-9). Mean [DOC] was slightly higher in deep wells over this same length. Between 24.1 m and the outlet [DOC] did not increase or decrease significantly. Mean outlet [DOC] was significantly higher than mean inlet [DOC] by 0.3 m C L^{-1}, indicating the bioreactor was a net source of DOC, although difference between inlet and outlet as small relative to RMSEP of the predictive model (0.06 – 0.12 mg C L^{-1}).

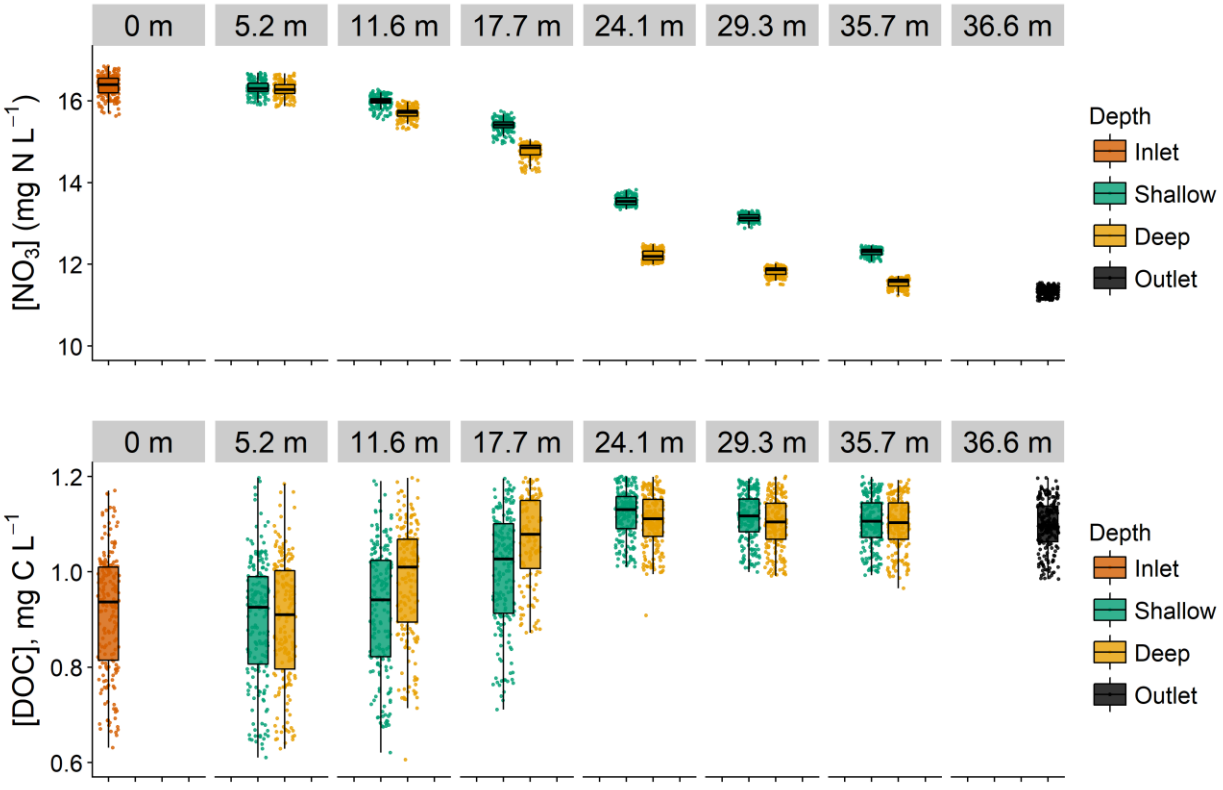

Figure 5-9. Longitudinal profiles of [NO_3] and [DOC] at shallow and deep wells. Nitrate decreased across the bioreactor with significant [NO_3] differences between shallow and deep wells. There were slight increases in [DOC] from 0 to 24.1 m, after which [DOC] was relatively constant.

5.3.8. Longitudinal profiles of removal rates

Similar to cumulative NO_3 load at the inlet and outlet, cumulative load at each well was calculated to calculate CR_{NO3} along the longitudinal profile of both bioreactors. Cumulative loads at each well were calculated (Figure D-5 and D-6) similar to inlet and outlet loads. The assumption of uniform flow through the bioreactor profile was assumed. Although this assumption may not be valid, especially considering previously shown non-uniform flow through bioreactors (Cameron and Schipper, 2011; Christianson et al., 2011; Christianson et al., 2013), the calculation can provide an approximation for incremental CR_{NO3} along the bioreactor length.

Removal rates over distance from inlet at the IA bioreactor followed a bell-shaped trend (Figure 5-10), with rates lowest at <11.6 m and >29.3 m. Removal rates peaked between 17.7 and 24.1 m at 0.35 and 0.48 mg L^{-1} m^{-3} at shallow and deep wells, respectively. These results are consistent with the largest change in mean [NO_3] occurring between 17.7 and 24.1 m. At all wells pairs apparent removal rates were higher in deep wells, with the exception of wells at 35.7 m. The lowest rates (0.01-0.08 mg L^{-1} m^{-3}) occurred within the first 5.2 m.

In the NZ bioreactor removal rates gradually decreased over the length of the bioreactor (Figure 5-11). The highest apparent removal rates of 0.6 – 0.7 and 1.4 – 1.7 g N m^{-3} d^{-1} were within 0.5 m of the inlet in shallow and deep wells, respectively. Removal rates in shallow wells followed a bell-shaped trend, with rates highest (1.0 – 1.1 g N m^{-3} d^{-1}) at 3.2 – 5.9 m. Contrasting with the IA bioreactor, there was no clear difference in apparent removal rates between shallow and deep wells. Rates across depths were comparable other than at 0.5 m where rates were higher in deep wells. Mean removal rates along the bioreactor were 1.1, 0.9, 0.9, and 0.4 mg L^{-1} m^{-3} at 0.5, 3.2, 5.9, and 8.5 m, with the largest decrease in rates occurring between 5.9 and 8.5 m.

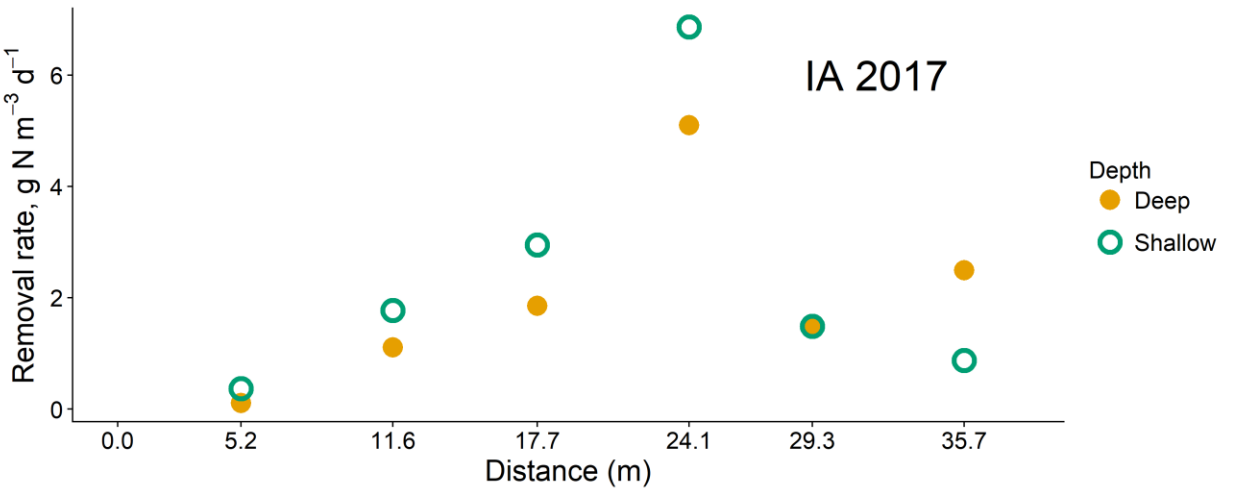

Figure 5-10. Apparent NO_3 removal rates in shallow and deep wells at the IA bioreactor in 2017. Calculations were made based on cumulative [NO_3] load at each well over the monitoring period. Removal rates follow a bell-shaped curve, with the lowest removal rates near the bioreactor inlet and outlet.

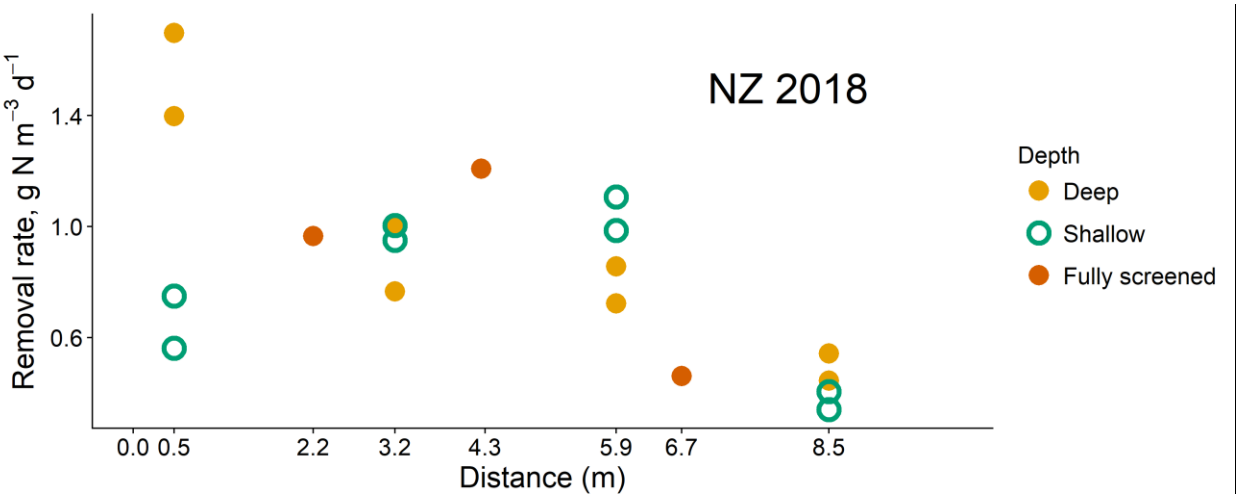

Figure 5-11. Apparent NO_3 removal rates in shallow, deep, and fully screened wells at the NZ bioreactor in 2018. Calculations were made based on cumulative [NO_3] concentration at each well over the monitoring period. Removal rates were highest near the inlet, gradually decreasing with increasing distance from the inlet.

5.4. Discussion

5.4.1. Methodological considerations for calculating NO_3 removal rates

Before discussing the biogeochemical significance of the results, it is important to first discuss methodological considerations, as the NO_3 removal rates calculated and reported here are highly dependent and possibly biased by the calculation methods. High-frequency measurements of $[NO_3]_{in}$ and $[NO_3]_{out}$ provided a large number of data points for R_{NO3} and percent reduction. These calculated removal rates are comparable to traditional discrete sampling methods in that reported removal rates are based on instantaneous flow and water chemistry, where the change in $[NO_3]$ is compared to the flow rate at the time when discrete samples are collected. The high-frequency data collected illustrates the potential for error in reporting these instantaneous rates when variability in R_{NO3} and percent reduction over short durations is high. Calculated R_{NO3} at the IA bioreactor in 2017 and 2018 ranged from 1.71 – 3.44 and 0.02 – 2.28 g N m^{-3} d^{-1}, respectively, while percent reduction varied by 18 and 17 percentage points. Calculated R_{NO3} at the NZ bioreactor were also highly variable (0.35 – 1.63 g N m^{-3} d^{-1}) with percent reduction varying by 50 percentage points.

While some of the variability in R_{NO3} and percent reduction may reflect true changes in performance, time series during the NZ monitoring period (Figure 5-2C) best illustrate methodical errors in using instantaneous values for determining performance. During the rainfall event on August 22, 2018, $[NO_3]_{in}$ and flow increased quickly from 7.8 mg N L^{-1} and 66 mL s^{-1} to peaks of 8.8 mg N L^{-1} and 128 mL s^{-1}, respectively, between 19:00 – 23:00. Increases in $[NO_3]_{out}$, however, arrived later and more gradually as inflow water took time to reach the outlet. Although the full time series of this event is incomplete due to data loss, the peak in $[NO_3]_{out}$ can be visually approximated where the data is interrupted. Peak outlet flow (128 mL s^{-1}) occurred on August 22 at 19:00 while peak $[NO_3]_{out}$ (2.2 mg N L^{-1}) did not occur until August 26, at 4:00, i.e., ~80 h after peak $[NO_3]_{in}$.

If measuring performance based on instantaneous values, removal rates and percent reduction would be biased on either end of the rainfall event. At the beginning of the event, peak flows and $[NO_3]_{in}$ along with low $[NO_3]_{out}$ would produce high apparent removal rates due to the lagging $[NO_3]_{out}$. Similarly, as flow and $[NO_3]_{in}$ decrease following the rainfall event and peak $[NO_3]_{out}$

finally arrives, the lowest apparent removal rates would be reported. Percent reduction at the beginning and end of this rainfall event would be calculated as 94 and 69%, respectively, varying by 25 percentage points within a single event. The same trend can be seen in the events on August 31 and September 2. A closer approximation of percent reduction for this event might be considered as the difference in peak $[NO_3]_{in}$ and peak $[NO_3]_{out}$, a reduction of 75%. This long lag between $[NO_3]_{in}$ and $[NO_3]_{out}$ is not only problematic for reporting bioreactor performance, it produces misleading relationships between HRT and R_{NO3}, where apparent R_{NO3} decreases with increasing HRT (or decreasing flow).

Reported removal rates or percent reduction may be less prone to error when flow and water chemistry are less variable. At the IA bioreactor in 2017, $[NO_3]_{in}$ and $[NO_3]_{out}$ were more stable over time compared to the NZ bioreactor, and HRT (~20 – 35 h) was much shorter than for NZ (~100 – 150 h). Lagged peaks in $[NO_3]$ at the inlet and outlet were not observed. Even though there was certainly still lag between NO_3 arriving at the inlet and leaving the outlet, its impact on calculated removal was diminished since $[NO_3]_{in}$ and $[NO_3]_{out}$ were more stable over time. This resulted in less variable percent reduction for the IA bioreactor (Figure 5-4). Percent reduction varied by only 9 percentage points from June 2 to 6 before flow started to decline. Calculated R_{NO3} in 2017 was still highly variable over time, which was more directly caused by changes in measured flow. The IA bioreactor used a much narrower weir causing flow measurements to be much more susceptible to small variations which propagated into R_{NO3}. Errors in relationships between flow and R_{NO3} over this period would be less biased due to the lack of lagging peaks. Calculated R_{NO3} as flow decreased from June 10 – 13, however, would still be underestimated since $[NO_3]_{out}$ would be a result of higher flow rates over the last 20 – 35 h, rather than the lower flow at the time $[NO_3]_{out}$ was measured.

Calculating removal rate using cumulative mass removal over the monitoring period is a more robust indicator of the overall performance. This calculation does not rely on instantaneous values which, depending on conditions, can be highly variable and biased. Cumulative removal compensates for variability by integrating over time, looking instead at the total mass NO_3 entering and leaving the bioreactor over the period. The tendency of cumulative removal to average incremental removal rates is supported by the results in Figure 5-4 and 5-5. Mean R_{NO3} and CR_{NO3} (g N m^{-3} d^{-1}) in the IA 2017 and NZ 2018 bioreactors differed by 1 and 4%,

respectively. While there may be high uncertainty in individual measurements of R_{NO3}, averaging measurements over time can offset errors and give a closer approximation to true NO_3 removal rates.

Accurate estimates of either metric may not require as high-frequency of data as was collected in this study. For the IA 2017 and NZ 2018 data, 69 and 86% of R_{NO3} values fell within one standard deviation of mean R_{NO3}. Randomly subsampling these data sets produce R_{NO3} values outside this confidence interval 31 and 14% of the time. If, however, this data is randomly subsampled (n=1000) by taking one value of R_{NO3} per day (i.e. simulating daily sampling), then calculating a mean for the IA 2017 and NZ 2018 periods by averaging these daily R_{NO3} measurements, mean R_{NO3} is within one standard deviation of the true mean R_{NO3} 100% of the time (Figure 5-12). Average of subsampled daily R_{NO3} varied from the "true mean" of hourly R_{NO3} by <8% for IA 2017 and NZ 2018 data. This suggests that daily measurements of removal rates, when averaged over the same period of time, may be adequate for accurately reporting performance. Further analysis can determine the effect of sampling frequency on errors in reported CR_{NO3}. Johnes (2007) showed that weekly or monthly subsampling of daily flow and phosphorus measurements produced significant errors in calculated cumulative load, and that uncertainty was higher for watersheds with more variable flow or water chemistry. Williams et al. (2015) found similar results calculating annual NO_3 load leaving four tile-drained fields (8 – 13 ha), with uncertainty of ±10% at weekly sampling intervals. While an error in a single cumulative load 10% may be tolerable, cumulative removal requires accurately reporting two cumulative loads. A 10% error in cumulative load in and out of the bioreactor could result in an error in cumulative removal of up to 20%.

The disadvantage of cumulative removal and mean R_{NO3} is that a single value is reported over a range of conditions, diminishing the value of high-frequency measurements for observing trends in removal over short periods. For field experiments with highly variable flow and water chemistry, more long-term monitoring would be required to assess relationships between R_{NO3} and temperature or flow with confidence. These methodological considerations are essential for

the interpretation of the results herein.

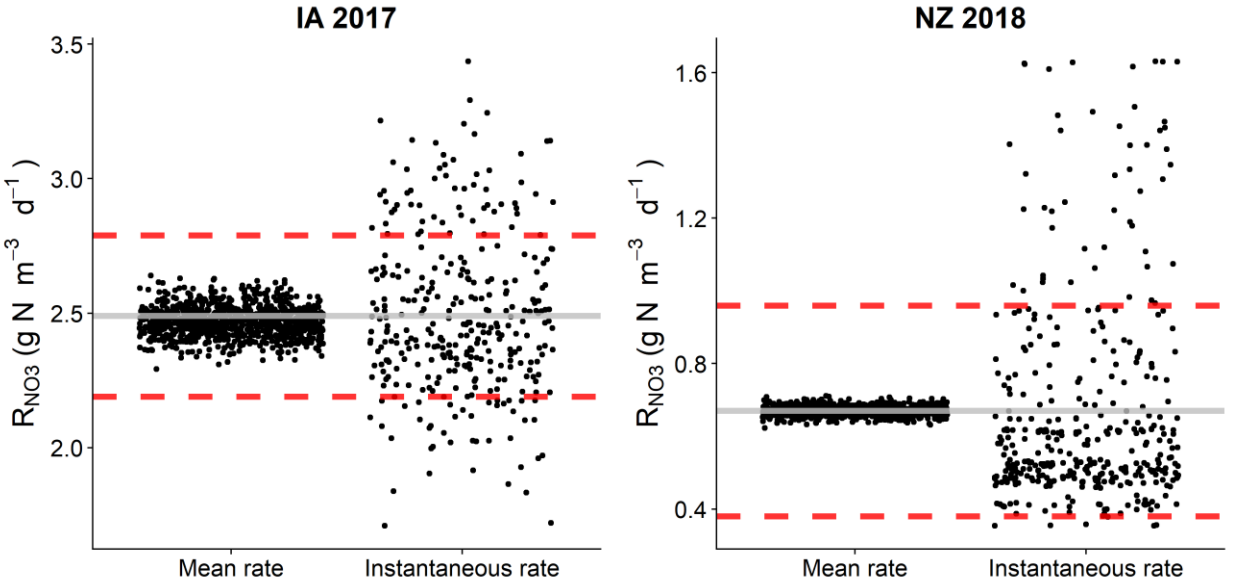

Figure 5-12. Mean and instantaneous R_{NO3} during the IA 2017 and NZ 2018 monitoring period. Mean R_{NO3} was calculated by repeatedly subsampling the complete data set (n=1000) to simulate daily measurements then averaging the daily R_{NO3} values. When reducing sample frequency to daily intervals, calculated mean R_{NO3} over each period varied <8% from the true mean.

5.4.2. Removal rates and percent reduction

Nitrate removal efficiency was variable between bioreactors. In the IA bioreactor, mean R_{NO3} ranged from 2.49 g N m^{-3} d^{-1} in June 2017 to 0.92 g N m^{-3} d^{-1} in April 2018. Christianson et al. (2012) previously reported annual removal rates of 1.56 and 0.86 g N m^{-3} d^{-1} for 2009 and 2010, respectively, in the first and second year after installation. Higher removal rates are expected at warmer temperatures and would explain the higher removal rates in June 2017 relative to annually-summed removal rates based on flow composite samples at the site in its first year of operation when removal rates are highest. Range of water temperature recorded in 2009 & 2010 (2 – 20 °C) at the IA bioreactor show that, while April 2018 monitoring at 2.9 °C may accurately reflect the lowest removal seen at cold conditions, R_{NO3} in June 2017 may not reflect the highest rates when drainage water temperature is highest. Annual percent reduction for 2009 and 2010 (14.6 and 11.7%, Christianson et al., 2012) fell within the range of percent reduction seen from June 2017 to April 2018. Mean R_{NO3} in April 2018 were slightly greater than rates at much

warmer temperatures in 2011 (0.38 – 0.71 g N m^{-3} d^{-1}; 9 – 17 °C) at the same site (Christianson et al., 2013), and mean R_{NO3} in June 2017 were 2-4x greater than rates at comparable temperatures in 2011.

Nitrate removal rates at the IA bioreactor in June 2017 were comparable to mean rates for bioreactors >24 months in age (1.4 – 4.3 g N m^{-3} d^{-1}) reported in a meta-analysis of bioreactor studies (Addy et al., 2016). Removal rates in June and April were outside or at the low end of 95% confidence intervals reported for bioreactors at 6 – 16.9 °C (3.3 – 8.8 g N m^{-3} d^{-1}) and <6 °C (0.9 – 3.8 g N m^{-3} d^{-1}). Removal rates in 2017 and 2018 showed performance of the IA bioreactor may be greater than previously reported (Christianson et al., 2013), especially considering monitoring in this study took place in its ninth and tenth year of operation. The IA bioreactor's performance, however, is low when comparing removal rates seen in other field bioreactors (2.9 – 7.3 g N m^{-3} d^{-1}) at similar temperatures, but may be within the observed range of performance when considering age (Addy et al., 2016). Lower removal rates could be explained by hydraulic inefficiencies shown through bromide tracer tests performed at the site, where breakthrough curves indicated a large to moderate sized dead zone and short-circuiting of flow (Christianson et al., 2013). Low NO_3 removal in the IA bioreactor could also be explained by inflow of groundwater along the length of the bioreactor due to the lack of an impermeable liner. Removal rates were calculated based on the assumption of conservation of water mass and that seepage into the bioreactor was negligible compared to tile flow in. This assumption was not validated, however, since only outflow of the IA bioreactor is monitored.

Accurately determining the saturated bed depth of the IA bioreactor was important since R_{NO3} are normalized by bed volume. This was done by manually measuring water depth within the bioreactor, and considering the saturated volume only. While the design depth of the bioreactor is 1 m, water depth in 2017 and 2018 was 0.32 – 0.37 m. Had the design volume of the bioreactor been used, mean R_{NO3} in 2017 and 2018 would have been 0.72 and 0.31 g N m^{-3} d^{-1}, more comparable to rates previously reported for this bioreactor (Christianson et al., 2013).

Removal rates in the NZ bioreactor were significantly lower compared to the IA bioreactor. Mean R_{NO3} for the NZ bioreactor (0.67 g N m^{-3} d^{-1}) at 12.0 – 12.4 °C was significantly lower than 2017 R_{NO3} at the IA bioreactor at comparable temperatures (11.2 – 13.6 °C) and even lower

than 2018 R_{NO3} at the IA bioreactor at 2.8 – 2.9 °C. Removal rates in NZ were well outside the range of rates reported for field bioreactors or bioreactors at comparable temperatures (Addy et al., 2016). Nitrate-limiting conditions could partially explain low R_{NO3}, since NO_3 removal tends to follow first-order or Michaelis-Menten kinetics at $[NO_3] < 1$-2 mg N L^{-1} (Robertson, 2010; Warneke et al., 2011; Halaburka et al., 2017). Over the 30-d monitoring period, $[NO_3]_{out}$ was <2 mg N L^{-1} 56% of the time and <1 mg N L^{-1} 32% of the time. As $[NO_3]$ became limiting closer to the outlet it is likely that each cubic meter of woodchips became less efficient in removing NO_3, decreasing the cumulative volumetric removal of the entire bioreactor. This is supported by decreasing apparent R_{NO3} with increasing distance from the inlet (Figure 12). Mean R_{NO3} was still well outside the 95% confidence interval (1.7 – 6.7 g N m^{-3} d^{-1}) reported for N-limited bioreactors (Addy et al., 2016).

5.4.3. Temperature effect

Effect of temperature on R_{NO3} was assessed at the IA bioreactor by comparing data from June 2017 to April 2018. Range of inlet water temperatures at the NZ bioreactor (0.4 °C) was not high enough produce observable temperature-driven changes in R_{NO3}. Although IA R_{NO3} were highly variable in 2017 and 2018, R_{NO3} in June were significantly higher and mean R_{NO3} greater by 1.57 g N m^{-3} d^{-1} relative to April. Values of mean R_{NO3} and mean temperature from each period were used to calculate Q_{10} for nitrate removal in this bioreactor using the equation given by Hoover et al. (2016), yielding a Q_{10} of 2.9. This value is higher than Q_{10} values of 1.6 – 2.0 previously reported in woodchip bioreactors (Cameron and Schipper, 2010; Warneke et al., 2011; Lepine et al., 2016). The Q_{10} of the IA bioreactor in this study is more comparable to Q_{10} values (2.3 – 2.9) seen by Hoover et al. (2016), which found increasing Q_{10} as temperature increased. In all studies sample collection was done on an infrequent (e.g. weekly, monthly) or composite basis. Although partial information may contribute to the variability in reported Q_{10} values for nitrate removal in bioreactors, it is just as likely that experimental variability is a major contributor. Table E-5 summarizes several studies that looked at the effect of temperature on nitrate removal in woodchip bioreactors. Hoover et al. (2016) reported the highest observed Q_{10}, but only saw this value at higher temperatures when dividing results across the range of temperatures tested. Cameron and Schipper (2010) saw Q_{10} decline in different C media after aging from 1-10 months to 10-24 months. Warneke et al. (2011) saw rates decline even further in the same media

aged >2.5 yr, although $[NO_3]_{in}$ was an order of magnitude lower in the follow-up study. Nordström and Herbert (2019) showed that the temperature-dependence of NO_3 removal in woodchip bioreactors decreases over time, and related this to the changes in quality of carbon available for denitrifiers. Across the same temperature range, NO_3 removal rates can be limited by conditions other than temperature (e.g. $[NO_3]_{in}$, carbon quality, [DO], HRT). Davidson et al. (2006) speculated that respiration Q_{10} >2.5 indicated an unidentified process confounding the effect of temperature. Schmidt and Clark (2013) suggested R_{NO3} Q_{10} >2.0 in woodchip bioreactors may be caused by greater C availability. In other words, the Q_{10} indicator is a parameter that lumps all factors, including temperature, when considering effect of temperature on R_{NO3}. It is likely the that reported decrease of Q_{10} with bioreactor age corresponds to a decrease in quantity/quality of carbon over time; Schmidt and Clark (2013) further confirm this. Although changing conditions across experiments introduces variability, the high-frequency methods presented here can theoretically reduce measurement uncertainty to better quantify temperature-R_{NO3} relationships and co-occurring processes that interact with this relationship (e.g. DOC production, DO consumption).

Although temperature increased by 2.4 °C during the June 2017 monitoring period, fitting a Q_{10} relationship would have suggested a negative effect of temperature on R_{NO3}. Decreased flow over the 10 d period corresponded to lower R_{NO3}, even as temperature increased from 11.2 to 13.6 °C. The ability of high-frequency methods to quantify relationships between temperature and NO_3 removal may be of limited use over short-term monitoring periods where 1) temperature changes are small and 2) other factors, such as flow, are highly variable. The high-frequency data set was instrumental, however, in increasing the confidence of calculated R_{NO3} in period and the resulting Q_{10}. Additional monitoring over the temperature range not observed during these periods (3 – 11 °C) is necessary to confirm the shape of the temperature/removal rate relationship, although evidence supports that this is an exponential relationship for most microbial processes (Janssens and Pilegaard, 2003; Davidson et al., 2006; Bonnet et al., 2013, Schmidt and Clark, 2013).

5.4.4. Apparent flow effect

In all three monitoring periods there was an apparent positive relationship between flow rate and R_{NO3} (5-14A & 5-14B). Fitting the data to a simple linear model, the strongest correlation between flow (Q, L h^{-1}) and R_{NO3} (g N m^{-3} d^{-1}) occurred at the IA bioreactor in 2017 (R_{NO3} = 0.002 * Q + 1.3, r^2=0.55) and the NZ bioreactor (R_{NO3} = 0.002 * Q + 0.0, r^2=0.66), with the lowest correlation at the IA bioreactor in 2018 (R_{NO3} = 0.0002 * Q + 0.6, r^2=0.04). The weak correlation between flow and R_{NO3} during April 2018 may have been due to the extremely low temperatures where R_{NO3} was mainly constrained by temperature and not largely affect by changes in flow. Although hydraulic residence time is positively correlated with percent reduction (Robertson, 2010; Christianson et al., 2012; Hoover et al., 2016; Lepine et al., 2016), most studies have reported no significant correlation between HRT and NO_3 volumetric removal rates in woodchip bioreactors (Christianson et al., 2012; Healy et al., 2012; Hoover et al., 2016; Lepine et al., 2016). Greenan et al. (2009) found a positive correlation between HRT and NO_3 removal efficiency, and suggested increasing penetration of DO might be the cause. David et al. (2016) found that R_{NO3} in a field bioreactor decreased with increasing HRT, although the study used infrequent, instantaneous measurements to calculate R_{NO3}. Jaynes et al. (2013) also found decreased R_{NO3} with increasing HRT in a woodchip column experiment.

For the NZ data, it is important to consider the times series for $[NO_3]_{in}$ and $[NO_3]_{out}$ when correlating flow and R_{NO3} (Figure 5-2C). Flow and $[NO_3]$ during this monitoring period were highly variable and, due to the long HRT of this system, peak $[NO_3]_{out}$ lagged $[NO_3]_{in}$ in by 1-3 days. Consider the rainfall event on August 23. Peaks in flow and $[NO_3]_{in}$ occur within hours of each other, while $[NO_3]_{out}$ remains low as new water takes time to move to the outlet. Based on the conditions around peak flow, calculated R_{NO3} is highest when flow is greatest and the difference in $[NO_3]$ highest. Similarly, after flow has receded and peak $[NO_3]_{out}$ finally arrives, calculated R_{NO3} would be lowest when flow and difference in $[NO_3]$ are lowest. The strong correlation shown in Figure 5-14B, therefore, is misleading and shows the error of calculating performance based on instantaneous conditions. Instantaneous R_{NO3} fails to acknowledge that water at the inlet and outlet are disconnected by time. Although the IA 2017 data also shows a positive correlation between the two variables, this temporal disconnection may introduce less bias since conditions were more stable. In order to truly ascertain the impact of flow on R_{NO3} it

would be better to observe N removal over a range of flows held at "steady-state", where the necessary monitoring period depends on HRT. A suggested period of steady-state monitoring for accurately measuring R_{NO3} at a given flow could be >10x HRT.

There are several justifications for the hypothesis that removal rates are positively correlated with flow rates. It is possible hydraulic inefficiencies in highly porous media (e.g. woodchips) are reduced at higher flows. This may occur when pressure head is high leading to increased macro-porewater velocity and possibly turbulent flow. Greater pressure head would overcome pores blocked by clogging from biofilms. Preferential flowpaths through which majority of water travels at low flows may be overwhelmed at higher flows, causing higher and greater dispersion and more uniform mixing. High flows would theoretically reduce the likelihood or size of "dead zones", or areas of the woodchip matrix with lower flow relative to bulk flow. Herbert (2011) showed higher dispersion coefficients in sawdust columns at higher flows. A likely source of decreased permeability around dead zones is bioclogging of pores. Bioclogging in porous media has been well-documented (Vandevivere and Baveye, 1992; Suchomel et al., 1998; Rockhold et al., 2002; Seifert and Engesgaard, 2007), at times reducing hydraulic conductivity by orders of magnitude. High flows producing greater shear forces within pores could scour biofilms clogging these pores, reducing impermeability of dead zones. Shearing of pore-clogging biofilms has been observed (Dupin and McCarty, 2000; Kim and Fogler, 2000; Stewart and Fogler, 2001). David et al. (2016) speculated that bioclogging was the cause of observed patterns in conductivity versus hydraulic gradient in a field bioreactor, and that reduced biofilm growth at higher flows led to higher conductivity.

Another explanation could be the existence of NO_3-limited denitrification occurring at woodchip microsites. This concept has been previously theorized to explain observed data (Parkin, 1987; Holmes et al., 1996; Schipper, 2005). Despite [NO_3] leaving the bioreactor being higher than the range where NO_3-limitation occurs (1 – 2 mg N L^{-1}), [NO_3] closest to the sites where denitrification is occurring (e.g. woodchip surface, woodchip internal pores) may fall into this range, particularly since flow through internal pores is slower (Herbert, 2011; Jaynes et al., 2016). This relates directly to the concept of the Damköhler number, Da_{hz}, the dimensionless ratio (R_R / R_T) of reaction rate over transport, or loading, rate (Harvey et al., 2013; Oldham et al., 2013; Pinay et al., 2018). It is likely that at the microsite scale, particularly at denitrification

sites within woodchip pores where residence time is longer, the likelihood of R_{NO3} being transport limited is increased at greater HRT.

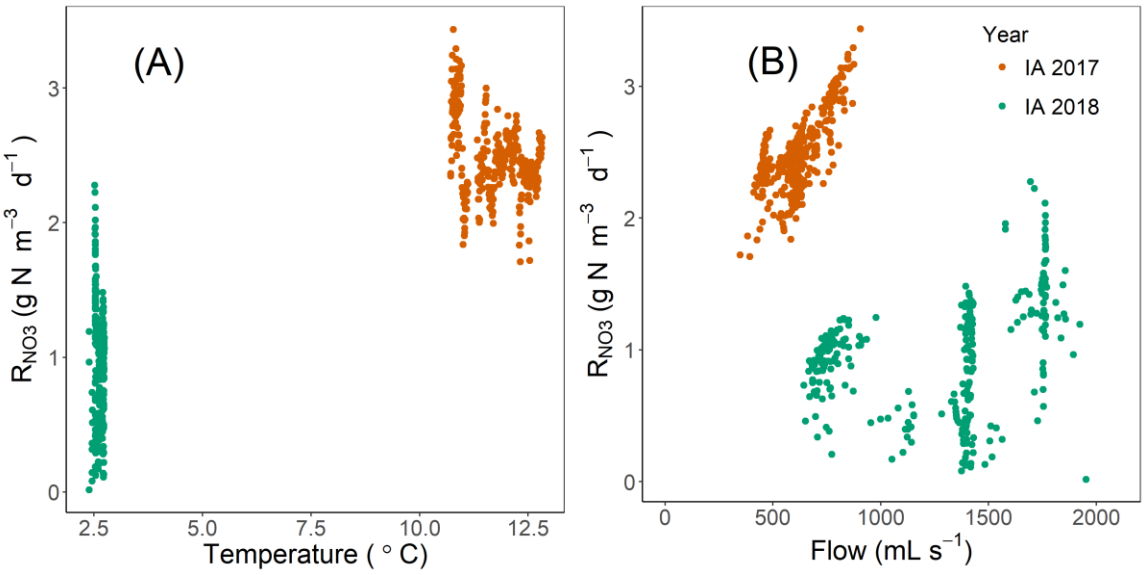

Figure 5-13A & 5-13B. Volumetric nitrate removal rates, R_{NO3}, plotted against temperature (A) and flow (B) for the IA 2017 and 2018 data sets. Nitrate removal rates appeared to be positively correlated with both temperature and flow.

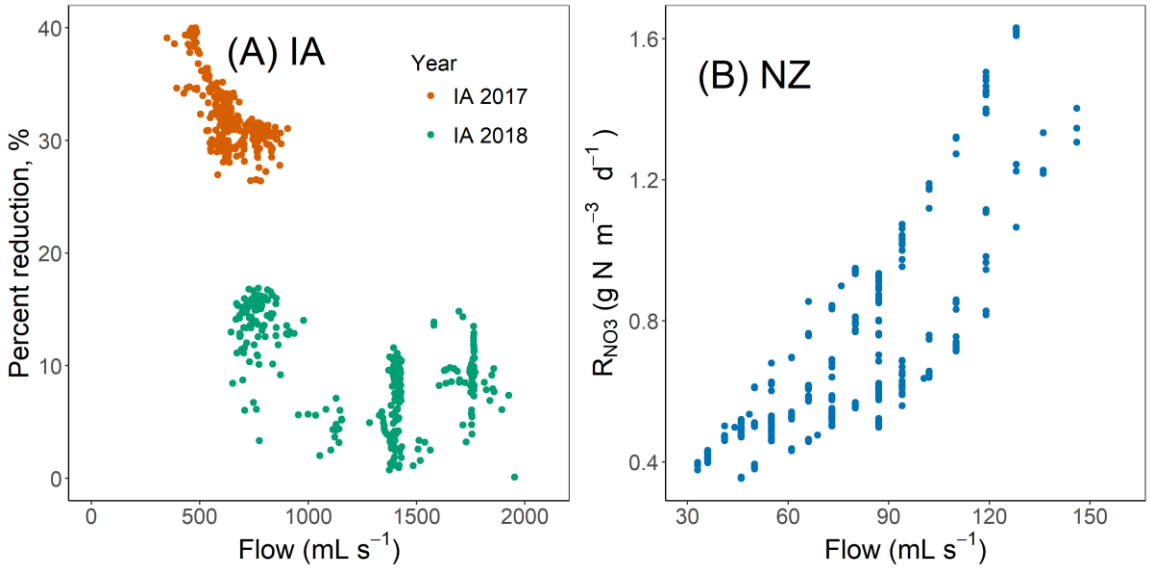

Figure 5-14A & 5-14B. Percent reduction of NO_3 plotted against flow for the IA 2017 and 2018 data (A) and R_{NO3} plotted against flow for the NZ 2018 data (B).

A third possible explanation could the inhibition of microbial activities in prolonged anaerobic conditions. Freeman et al. (2001a, 2001b) suggest that respiration in saturated peat soils may be

limited by a multi-step process which they refer to as an 'enzymic latch'. They hypothesized, confirmed in later studies (Fenner et al., 2005; Fenner et al., 2011; Saraswati et al., 2016), that microbial respiration in prolonged anaerobic conditions may be limited by the accumulation of phenolic compounds which (1) directly inhibit microbial metabolism and (2) inhibit extracellular hydrolase enzyme activities, the latter helping breakdown organic matter to become available for microbes. This with the other factors described above could also contribute the lower volumetric removal rate for higher HRT, although confirmation is needed that these observations apply in woodchip bioreactors.

5.4.5. Vertical and longitudinal NO_3 gradients

Shallow and deep wells at the IA bioreactor showed a clear pattern of lower [NO_3] in deeper wells. Vertical differences in [NO_3] were largest in June 2017, although differences between shallow and deep wells were still significant in April 2018. Differences were lowest closest to the inlet and increased with increasing distance from the inlet manifold (Figure 5-6). Consistently lower [NO_3] in deep wells was not observed in the NZ bioreactors, other than at the first well pair 0.5 m from the inlet.

A number of factors could be responsible for the observed vertical and longitudinal gradient of [NO_3] at the IA bioreactor. In Chapters 3 & 4 it was previously shown that [DOC] greatly stimulated NO_3 removal. The zone in which [NO_3] decreased most rapidly (17.7 – 24.1 m) aligned with the zone in which [DOC] stopped increasing (Figure 5-9). Mean [DOC] in deep wells was also slightly higher relative to shallow wells up to 17.7 m. Incremental [NO_3] removal rates (Figure 5-10) increased along with [DOC]. It is possible that [DOC] produced aerobically in zones near the inlet, where [DO] was still present, explains the dramatic increase in [NO_3] reduction from 17.7 – 24.4 m. The effect of [DOC] may have been highest at these locations since this is also the zone where [DO] was depleted. Beyond 17.7 m, rate of [NO_3] reduction declined as [DOC] stopped increasing. Beyond the point of DO depletion DOC would have been anaerobically-produced and would appear to be less useful for denitrifiers, considering the declining NO_3 removal rates from 24.4 m to outlet. The zone in which DO is depleted but aerobically-produced DOC is present, although small, appears to be a highly productive zone in terms of NO_3 removal rates.

Flow regime, determined by the distributor design at the inlet and outlet, could potentially impact vertical NO_3 gradients. The IA bioreactor used a bottom-to-bottom flow regime where the NZ bioreactor had a diagonal downflow design, with the inlet and outlet distributor 0.79 and 0 m from bioreactor bottom. Clear [NO_3] differences between shallow and deep wells in the IA bioreactor could suggest that the NZ distributor design produced more uniform flow. Cameron and Schipper (2011) showed that bioreactors with horizontal-diffuse flow regime had higher hydraulic efficiency than horizontal-point flow, and vertical upflow or downflow design had the highest hydraulic efficiencies. The age difference between bioreactors (NZ ~ 2 yr; IA ~ 9 yr) makes this assumption unreliable, however, since differences in flow uniformity could be the result of differences in the woodchip matrix (e.g. clogging, compaction, degradation of woodchips). Cameron and Schipper (2010) found conductivity of woodchips declined over 22 months, and Ghane et al. (2014) saw lower permeability in old woodchips (aged 26 months) relative to fresh woodchips. Lower [NO_3] in deep wells at the IA bioreactor are counter-intuitive to how water should be moving through a bottom-to-bottom manifold design. Using theoretical flowpaths and assuming a homogenous media, water should move fastest between the shortest flowpath, or directly from inlet to outlet through the deep zone. Residence time would be lowest along the direct flowpath and result in greater [NO_3], not supported by the IA 2017 data. Our observations suggest the hydraulic conductivity at the deep well depths of the IA bioreactor was lower than that at the shallower wells. This could have resulted in less flow, higher residence time, and explain lower [NO_3] in the deep wells. This does not necessarily equate to higher $R_{NO3.}$

In April 2018 [DO] did not decrease to non-inhibiting levels for denitrification until 11.6 – 17.7 m from the inlet, or 31 – 48% of the total bioreactor length. Although these same measurements were not available in June 2017 when $[DO]_{in}$ was lower (8 – 9 mg DO L^{-1}), it is reasonable to assume that [DO] could have similarly been high enough near the inlet to inhibit denitrification. Higher [DO] near the inlet would explain low apparent NO_3 removal in this zone (Figure 5-11), and why the largest decreases in [NO_3] did not occur until 17.7 – 24.1 m once [DO] had been reduced further. Higher [DO] in shallow wells could higher [NO_3], since denitrification in this zone would be less efficient from DO inhibition. This could explain why differences between shallow and deep wells in the NZ bioreactor were relatively small, considering low $[DO]_{in}$ combined with long HRT that quickly reduced [DO] within 0.5 – 3.2 m of inlet. This justification, however, fails to explain why [DO] is higher in shallow wells in IA. Higher [DO] in

shallow wells could be explained by shallow wells being closer to the air-water interface over which new oxygen is diffusing into the water. It is unlikely, however, that this rate of diffusion is sufficiently high to produce the observed [DO] profiles. This diffusion would be occurring along the entire bed length. Beyond 17.7 m there were no significant vertical differences in [DO] and DO almost completely removed. It is assumed that nearly all of the O_2 entering the system is in water entering through the inlet and being consumed more rapidly in shallow wells.

Inlet [DO] was much lower for the NZ bioreactor compared to the IA bioreactor. Although it could be expected that low $[DO]_{in}$ should increase overall R_{NO3}, it is worth considering aerobic breakdown of woodchips when $[DO]_{in}$ is high. The previous two chapters showed that DOC released from aerobic breakdown of woodchips increased R_{NO3}. Woodchips near the inlet undergo mineralization by aerobic microbes until DO is sufficiently depleted. At higher $[DO]_{in,}$ the amount of aerobically-produced DOC would increase. Anaerobic breakdown of lignin-heavy compounds is negligible (Zeikus et al., 1982; Holt and Jones, 1983; Odier and Monties, 1983). It is possible that lower $[DO]_{in,}$ while shrinking the zone where DO inhibition is occurring, may also have a net decrease in R_{NO3} due to less available DOC for denitrification. It is not clear, however, whether this was the major cause of low R_{NO3} seen in the NZ bioreactor since NO_3 limiting conditions were also likely.

5.4.6. Evidence of non-uniform flow

An alternative explanation for vertical $[NO_3]$ gradients in the IA bioreactor is non-uniform flow. Indirect evidence of non-uniform flow was previously discussed. Slower flow in dead zones increase HRT relative to bulk flow resulting in lower $[NO_3]$. This hypothesis was tested using $[NO_3]$ time series following rainfall events and by using short-term additions of KNO_3 at the inlet at the NZ and IA bioreactors

Consider two events in April 2018 at the IA bioreactor. During the high flow event (~1600 mL s^{-1}) on April 14, $[NO_3]_{in}$ increased quickly with high flow (Figure 5-2B). Increases in $[NO_3]$ in both shallow and deep wells at 5.2 m were observed within < 1 h of increasing $[NO_3]_{in}$. Time series at 5.2 m shallow and deep wells are similar with nearly simultaneous $[NO_3]$ increases, suggesting relatively uniform flow in the first 5.2 m (Figure 5-15). Time series of $[NO_3]$ at 11.7 m suggest less uniform flow, with $[NO_3]$ in the shallow well increasing gradually as $[NO_3]$ in the

deep well is unresponsive. This suggests that at 11.7 m new water is moving more slowly through deeper wells.

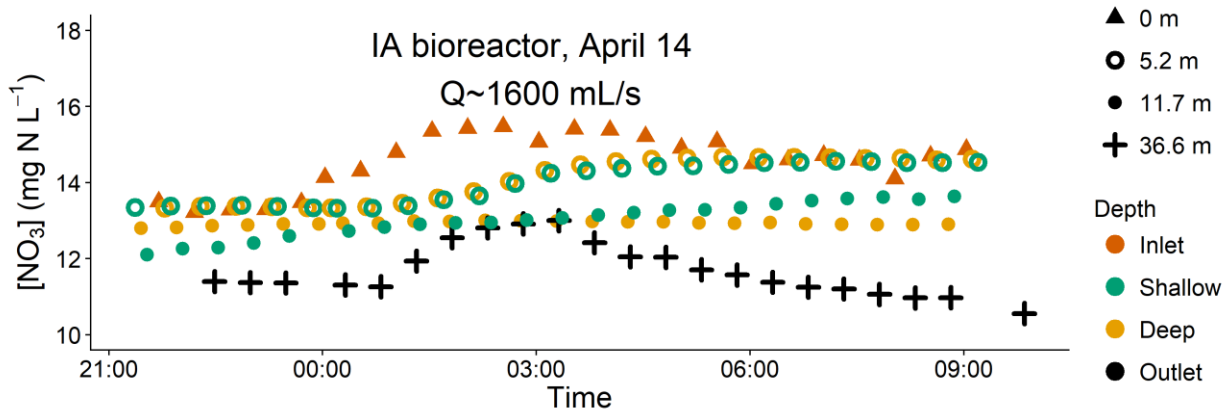

Figure 5-15. Time series of [NO_3] in the IA bioreactor during a high flow event. Increased [NO_3] at the inlet was followed by uniform increases in shallow and deep wells at 5.2 m. An increase in [NO_3] in the shallow well at 11.7 m was seen, while an increase in corresponding deep well was not. Nitrate time series indicate solute dispersion was uniform at 5.2 m.

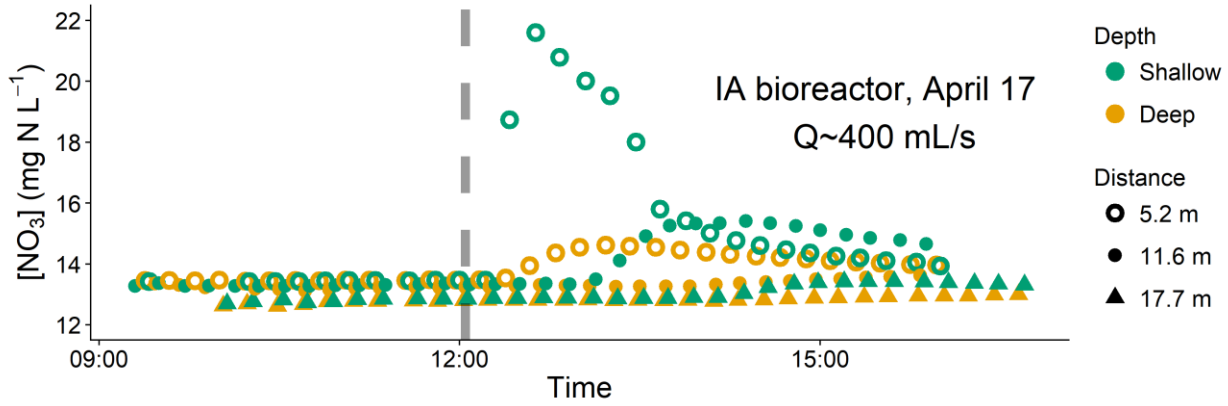

Figure 5-16. Time series of [NO_3] in the IA bioreactor following a KNO_3 injection (dashed grey line) at low flow. Increased [NO_3] at the inlet was followed by non-uniform increases in shallow and deep wells at 5.2 m. Increases in [NO_3] in the shallow wells at 11.7 and 17.7 m was seen were greater and arrived sooner than [NO_3] increases at the corresponding deep wells.

Similar trends were seen during a tracer injection on April 17 (Figure 5-16). At 12:03 120 g of KNO_3 was dissolved in 20 L of water and injected into the inlet manifold downstream of the inlet control structure. Shallow and deep wells had significantly different peak [NO_3] concentrations of 21.6 and 14.6 mg N L^{-1}, respectively, with peaks arriving within 35 and 70 min of tracer injection. Peak [NO_3] at the 5.2 m deep well was lower and decreased slower in the deep well, showing more of the tracer moved through the shallow well and passed more quickly

through it. Peak [NO_3] in the shallow well at 11.6 m occurred ~2.3 h after tracer injection. Nitrate in the deep well at 11.6 m was less responsive with a small [NO_3] increase beginning ~2.2 h after injection. Shorter time of arrival and higher magnitude of [NO_3] peaks occurred in all shallow wells 5.2 – 17.7 m, relative to deep wells. These results are counter-intuitive to theoretical flowpaths of a bottom-to-bottom manifold design. These time series could be explained, however, when considering lower hydraulic conductivity in deeper woodchips caused by silting, clogging, or compaction of the woodchip media over time. This explanation is supported by results from porosity measurements at the NZ bioreactor (Lincoln Agri-tech, personal communication, September 2018) where porosity in the bottom ~10 cm of the bioreactor was 10-30% lower than the rest of the bioreactor. The older IA bioreactor would be expected to have even greater porosity decreases in deeper zones, if silting/compaction are the cause. Most of the [NO_3] from the tracer arrived at shallow wells as more flow was directed through the shallow zone where conductivity was highest. Time series of [NO_3] in these wells also support previous findings showing moderate to large dead zones in this bioreactor (Christianson et al., 2013). This would suggest that lower conductivity in deeper woodchips, rather than distributor design, is responsible for observed hydraulic inefficiencies.

Flow at the NZ bioreactor was more uniform with some evidence of preferential flow and dead zones. A rain event on August 23 showed $[NO_3]_{in}$ increasing quickly with flow (Fig 5-17). Times series at the 0.5 m well pair showed lower [NO_3] in deeper wells, although [NO_3] in deep wells were lower prior to the storm and approached values closer to shallow wells during and after rainfall. Peak [NO_3] in deep wells at 0.5 m lagged shallow wells by 4-5 h. At 3.2 m peak [NO_3] at the left deep well lagged other wells at this location by 3-5 h. At all well pairs [NO_3] in deep wells was lower before and during than event than shallow wells. The opposite trend occurred in the second half of the bioreactor, where [NO_3] was generally lower at shallow wells. The right shallow well at 8.5 m was mostly unresponsive and did not significantly increase until [NO_3] peaked in the adjacent deep well. Similar trends were seen in the rainfall event on September 1 (Figure E-7).

The slower [NO_3] arrival in 0.5 m deep wells and apparent dead zone at the 8.5 m shallow well support the hypothesis that areas of low flow occur directly below the inlet distributor and above the outlet distributor. Because the most direct flow path in this bioreactor is diagonal downwards,

the points of lowest flow are furthest from this line. This is similar to results from Maxwell et al. (2018) which observed a dead zone in shallow wells above an outlet manifold placed at the bottom of a lab bioreactor. Differences in [NO_3] among shallow and deep wells throughout the NZ bioreactor could be explained by theoretical flow lines. Deep wells at 0.5 and 3.2 m would be further from the most direct flow path relative to shallow wells, and explain the slightly lower [NO_3] in deep wells at these locations. Shallow wells at 5.9 m and 8.5 m would be further from the most direct flow path, and explain the lower [NO_3] in shallow wells at these locations (Figure 5-17).

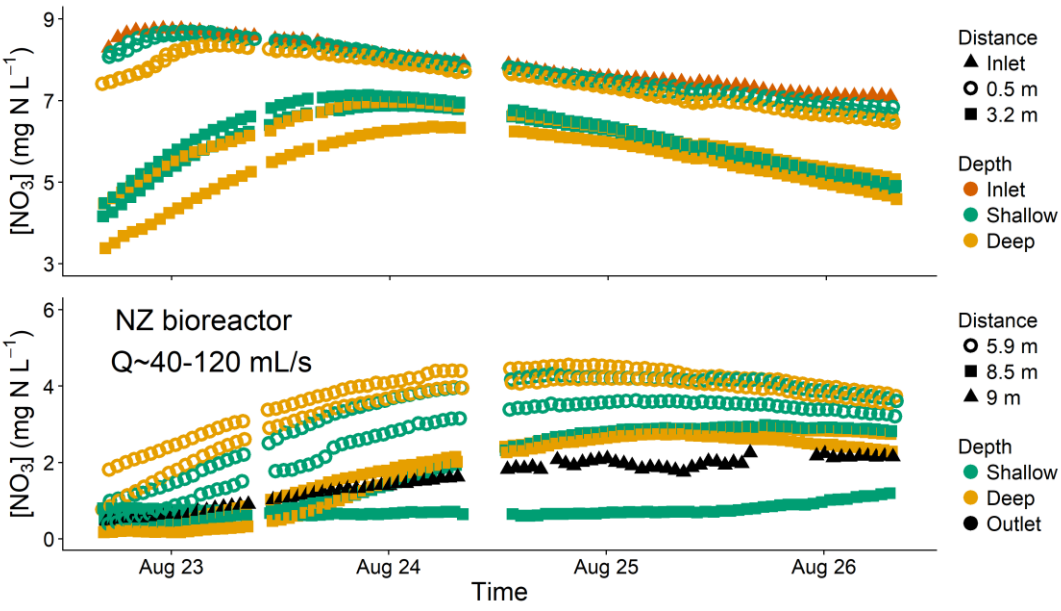

Figure 5-17. Time series of [NO_3] in the NZ bioreactor following a rain event. Increased [NO_3] at the inlet was followed by relatively uniform [NO_3] increases throughout the bioreactor. Nitrate was generally higher in shallow ≤3.2 m and higher in deep wells ≥5.9 m. One shallow well closest to the outlet showed a significant dead zone above the outlet distributor.

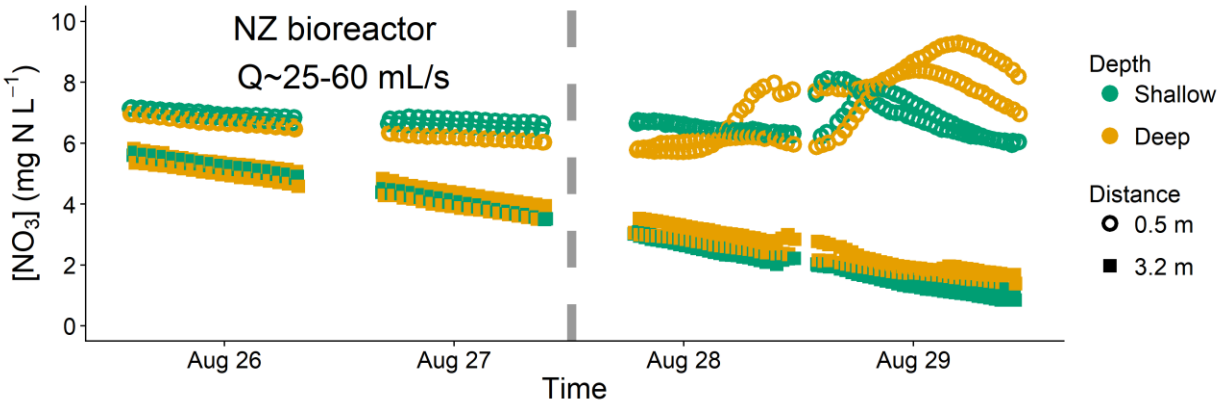

Figure 5-18. Time series of [NO_3] in the NZ bioreactor following a KNO_3 injection (dashed grey line) at low flow. Nitrate arrived at the 0.5 m right deep well prior to the shallow well at the same location, and arrived at the 0.5 m left shallow well prior to the deep well at the same location. Peak [NO_3] at 0.5 m deep wells arrived 13 h apart.

Time series of [NO_3] were less uniform after KNO_3 injection (205 g) at low flow on August 17 at 12:18 (Figure 5-18). Nitrate first arrived at the right deep well 0.5 m from inlet 21 h after injection. Incomplete mixing of the tracer in the inlet structure caused a second [NO_3] peak to arrive 41 h after injection. Peak [NO_3] in the right shallow well arrived 31 h after injection, 10 h after peak [NO_3] in the deep well at the same well pair. At the 0.5 m well pair along the left side of the bioreactor, peak [NO_3] arrived at the shallow and deep wells 27 and 34 h after injection, respectively. Nitrate arrival at 0.5 m wells 0.5 m was less uniform during the tracer injection than during observed rainfall events, suggesting that hydraulic efficiency and mixing within the bioreactor may be less uniform under low flows. This is consistent with IA 2018 data (Figure 5-15 & 5-16) where arrival of NO_3 at the first well nest was more uniform at higher flow.

Decreasing porosity in lower woodchips has practical design implications. The IA bioreactor used inlet and outlet distributors placed at the bioreactor bottom. Placing distributors in the zone where porosity decreases the fastest could reduce flow capacity of the bioreactor, since lower porosity decreases hydraulic conductivity. Decreased porosity may not be the result of silting and compaction alone. Ghane et al. (2018) showed that woodchips closet to the inlet in a 5-year-old bioreactor were most degraded. This is likely due to aerobic breakdown of woodchips near the inlet where [DO] is highest. Distributors placed at the top of the woodchips may help limit conductivity losses near the inlet. A manifold design that provides distributed flow, such as those

proposed in Cameron and Schipper (2011), could also limit the influence of dead zones by providing more uniform flowpaths.

5.4.7. Preferential flow and NO_3 removal kinetics

If R_{NO3} are negatively correlated with hydraulic residence time, the observed [NO_3] time series in internal sampling wells provide a mechanism for why this may occur. Nitrate removal rates decrease and follow substrate-dependent kinetics at sufficiently low [NO_3]. Several studies have reported an N-limitation threshold (K_N) of 1 – 2 mg N L^{-1} (Robertson, 2010; Halaburka et al., 2017). While [NO_3] in the bulk flow is often used to determine whether NO_3-limiting conditions are occurring, it is necessary to consider that NO_3 limiting conditions are most likely occurring at denitrifying micro-sites on the surface of or within woodchips. Internal or secondary porewater is less mobile than water moving between woodchips in the drainable pore volume (Healy, 2011; Jaynes et al., 2016). New [NO_3] in the internal pore space enters primarily through diffusion (Genuchten and Wierenga, 1977; Jaynes et al., 2016). This internal pore volume is not negligible, and can constitute 30-36% of total pore volume in packed woodchips (Hoover et al., 2016). At lower flow rates the transport rate of [NO_3] is reduced, increasing the likelihood of conditions predicted by the Damköhler number (Da_{hz}>1) where NO_3 removal rates are limited by transport. At higher flows, NO_3 turnover is higher, decreasing the probability of NO_3-limitations at the woodchip surface and increasing diffusion into internal pore spaces by increasing the concentration gradient.

Hydraulic inefficiencies also increase the likelihood that NO_3 removal becomes transport limited. One shallow well near the outlet of the NZ bioreactor was generally unresponsive to new nitrate (Figure 5-17), and [NO_3] at this well stayed below the 2 mg N L^{-1} threshold for NO_3-limitation during rain events. Time series of [NO_3] at both bioreactors during high and low flow events suggest that mixing is less uniform at lower flows. If higher flows decrease size of dead zones and short-circuiting in bioreactors it would decrease the probability of NO_3-limiting conditions at any given distance from inlet.

Variable [NO_3] throughout the woodchip matrix can be depicted at a series of probability density functions (PDF) for given distances from the inlet (Figure 5-19). Variable [NO_3] within the bioreactor was seen at both IA and NZ bioreactors and is a result of cumulative removal and

variable conditions (e.g. water chemistry, flow rates). At low flows or when flow is non-uniform (e.g. preferential flow, non-uniform mixing) the range of $[NO_3]$ values at a given distance from the inlet will be greater, with variable local residence times resulting in more variable $[NO_3]$. Relating a wide density function with low flows is based on the premise that mixing is less uniform at low flows. Closer to the bioreactor inlet, NO_3-limiting conditions are less likely to occur if $[NO_3]_{in}$ is sufficiently high . Near the outlet, while mean $[NO_3]$ may be above limiting conditions, there will be a given proportion of locations where NO_3 removal is N-limited. Nitrate removal under such conditions would be transport-limited ($Da_{hz}>1$) and would result in an apparent decrease in bulk R_{NO3}, since portions of the bioreactor are experiencing N-limited denitrification. It is worth repeating that the assumed caustion of lower flows leading to greater preferential flow is based on 1) the limited data collected in this study during high flow events and tracer injections; 2) the assumption that lower hydraulic head at lower flow in field bioreactors would provide insufficient pressure head to overcome clogging of some pores via biofilm (Vandevivere and Baveye, 1992; Suchomel et al., 1998; Rockhold et al., 2002; Seifert and Engesgaard, 2007) or biogas (Beckwith and Baird, 2001; Kellner et al., 2004) accumulation, effectively creating dead zones; and 3) that solute transport via dispersion is greater at higher pore-water velocities (Bear, 1972; Brusseau, 1993)

Wide density curves under non-ideal, low flow conditions would contrast with the narrower density curves under ideal, high flow conditions. When mixing is uniform and preferential flow minimized, the dispersion of $[NO_3]$ around the mean is decreased. Under this scenario, even if mean $[NO_3]$ at a location are constant, the likelihood of NO_3-limitation is reduced. In Figure 5-19, at non-uniform mixing an N-limitation threshold of 3 mg N L^{-1} might be reported since some sites are experiencing N-limited denitrification, whereas no reduction in R_{NO3} might be apparent at the same $[NO_3]_{out}$ under uniform mixing.

The mean of the $[NO_3]$ probability distribution near the outlet would approximate $[NO_3]_{out}$. This is consistent with IA 2017 and NZ 2018 data where $[NO_3]_{out}$ was a product of lower and higher $[NO_3]$ at deep and shallow wells. Outlet $[NO_3]$ is sometimes used in bioreactor studies to determine whether N-limiting conditions were reached (Lepine et al., 2016; Addy et al., 2016; Halaburka et al., 2017), where $[NO_3]_{out}$ is related to bulk R_{NO3} (i.e., differences in inlet and outlet $[NO_3]$). Therefore, there is a possibility of *flow-dependent* values of the N-limitation threshold,

K_N, for denitrification (units of mg NO_3-N L^{-1}), where flow-dependency relates to either flow rate or flow uniformity. Reported values of K_N would be affected by the shape of the [NO_3] probability density function. Higher values of K_N would be reported when preferential flow is high or at low flow rates, and lower values of K_N would be reported when preferential flow is low or at high flow rates. The data collected in this study through [NO_3] tracking in internal pore water only suggests the possibility of flow-dependent K_N. Further research using similar methods in lab experiments where flow rate and $[NO_3]_{in}$ could be held constant over a wide range are needed for supporting evidence.

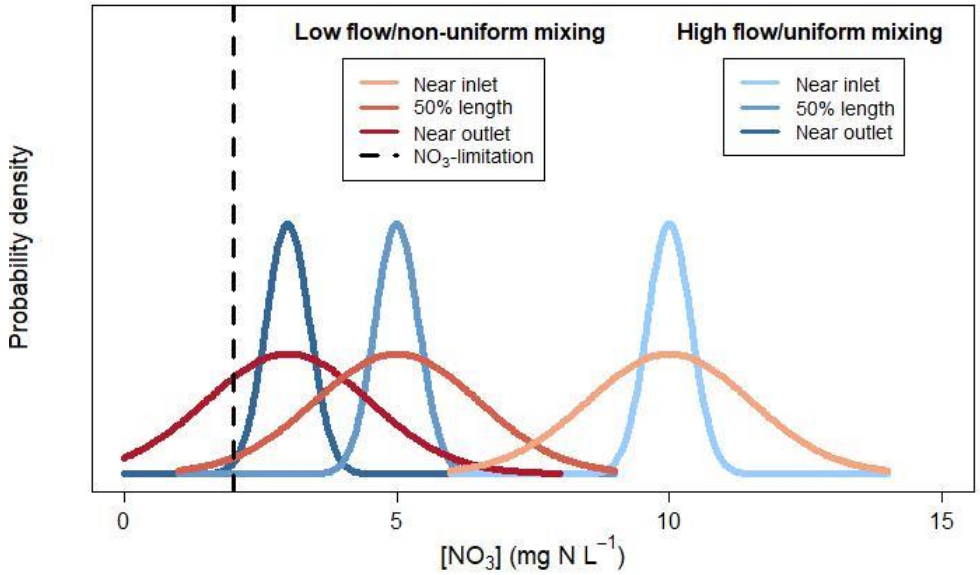

Figure 5-19. Theoretical probability density functions (PDF) of [NO_3] at a given distance from the bioreactor inlet. Non-uniform mixing or high dispersion would result in wide PDF curves, while uniform mixing or low dispersion would result in narrow PDF curves. Wider PDF curves have a higher likelihood of N-limitation even at similar mean [NO_3].

Real [NO_3] within woodchip bioreactors are likely not normally distributed. Figure 5-20 shows PDF of [NO_3] at the IA and NZ bioreactor over a several day period, according to distance from the inlet. The PDF of [NO_3] include measurements at all wells, shallow and deep, at the given distance from inlet, a total of two and four wells at each distance for IA and NZ bioreactors, respectively. In the NZ bioreactor [NO_3] at 0.5 and 3.2 m varied by <2 mg N L^{-1} at each distance, with no observed [NO_3] <2 mg N L^{-1} at well ≤3.2 m. It was unlikely that NO_3-limiting conditions

occurred <3.2 m from the inlet and is supported by higher, linear decreases in [NO_3] across these wells. Mean [NO_3] at 5.9 m was >2 mg N L^{-1} but a broad distribution of [NO_3] had 34% of measurements below the NO_3-limitation threshold. All [NO_3] measurements at 8.5 m were below K_N, consistent with decreases in R_{NO3} over this same distance (Figure 5-12). Although [NO_3] at any well in the IA bioreactor never approached the N-limiting threshold, the [NO_3] PDF was wide due to a bimodal distribution where [NO_3] varied between shallow and deep wells. Changes in NO_3 removal in the IA bioreactor (Figure 5-13), in this case, may not be explained by apparent N-limiting conditions and have to do with differences in water chemistry (e.g. [DO], [DOC]). It is still possible that even when the entire [NO_3] distribution is well above 2 mg N L^{-1} that N-limiting conditions are still occurring within internal woodchip pores, since the MPS only samples mobile flow contained in the drainable porosity.

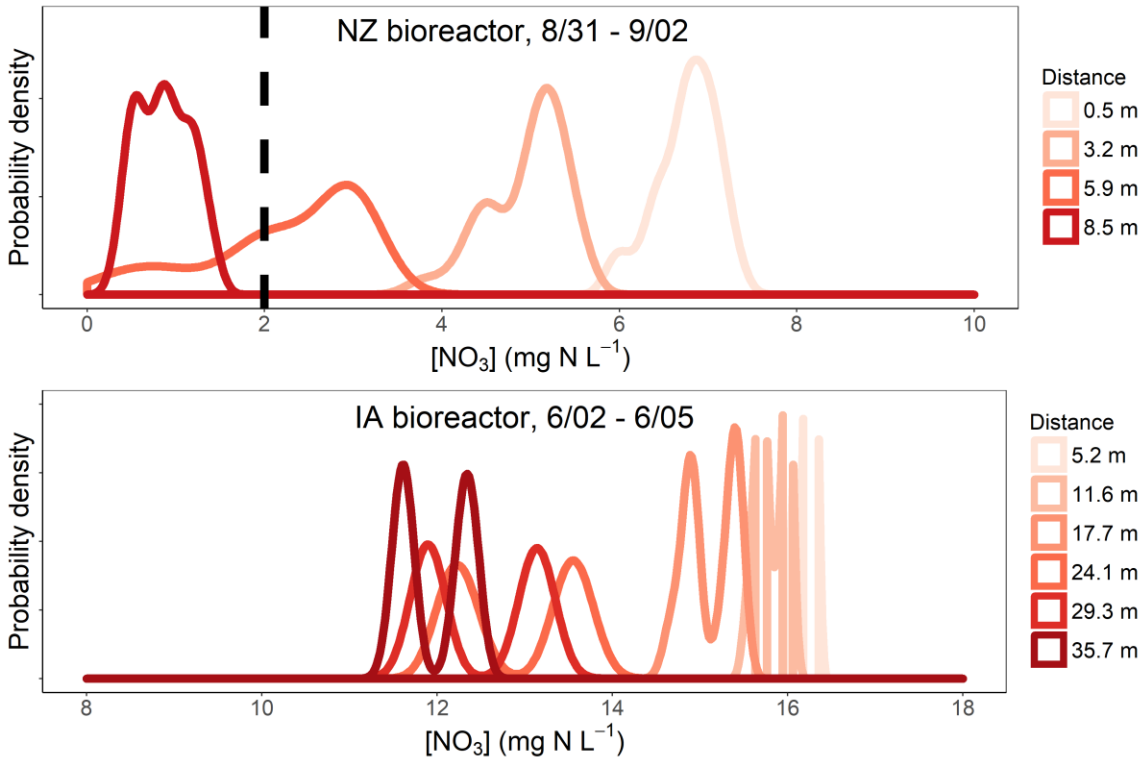

Figure 5-20. Probability density functions (PDF) of measured [NO_3] at all wells according to distance from inlet for select days in the NZ 2018 and IA 2017 data. At the NZ bioreactor [NO_3] below the N-limitation threshold (2 mg N L^{-1}, dashed black line) did not occur in wells ≤3.2 m from inlet. At the IA bioreactor [NO_3] < 2 mg N L^{-1} were not seen at any distance from inlet and PDF had bimodal distributions due to vertical gradients between shallow and deep wells.

5.4.8. Loading versus reaction limited NO_3 removal

At $Da_{hz} < 1$, a chemical reaction is believed to be limited by the rate of reaction, where at $Da_{hz} > 1$ the reaction is believed to be limited by transport rates (Harvey et al., 2013; Oldham et al., 2013). From the IA 2017 and NZ 2018 data it is possible to calculate Da_{hz} over the monitoring period based on calculated cumulative loads in and out of the bioreactor. For IA 2017 and NZ 2018, cumulative loading, as a daily rate, was 7.5 and 0.9 g N m^{-3} d^{-1}, respectively. Cumulative removal rates, CR_{NO3}, were previously calculated as 2.5 and 0.7 g N m^{-3} d^{-1}. This would equate to Da_{hz} of 0.33 and 0.73, respectively, at the IA 2017 and NZ 2018 bioreactors over this monitoring period. The ratio of the Damköhler number also allows for the theoretical calculation of the percentage of a compound converted during a chemical reaction. This calculation is achieved using Equation 5.3 (Fogler, 2006), where *X* is the percent reduction of the substrate concentration (i.e. NO_3), and *n* is the order of the reaction. If we assume the reaction is zero-order (n=0), the calculated values for *X* at the IA 2017 and NZ 2018 bioreactors are 0.33 and 0.73, respectively. These values are almost identical to the mean measured percent reduction (Figure 5-4) during both monitoring periods. This suggests that use of the Damköhler number may be helpful in the design of woodchip bioreactors in the field.

$$\frac{(1-\mathrm{X})^n}{X} = \frac{1}{\mathrm{Da}_{hz}} \qquad \text{Equation 5-3}$$

Although both bioreactors had $Da_{hz} < 1$, suggesting that NO_3 removal was reaction limited, it is important to remember that these ratios were calculated using the observed reaction rates. Calculated CR_{NO3} for the NZ bioreactor were likely low due to N-limiting conditions, with $[NO_3]_{out} < 2$ mg N L^{-1} 56% of the time. In calculating Da_{hz} for this bioreactor, if typical R_{NO3} for field bioreactors is used (2.9 – 7.3 g N m^{-3} d^{-1}; Addy et al., 2016) instead of observed reaction rates, Da_{hz} would be much higher (3.1 – 7.9). It is more likely that the NZ bioreactor was transport limited, considering the high mean HRT and relatively low $[NO_3]_{in}$. Even during high flow events NO_3 removal at the NZ bioreactor was likely transport limited. During the three highest periods of flow loading rate was 1.5 – 1.6 g N m^{-3} d^{-1} with Da_{hz} 1.8 – 4.9, assuming previously observed R_{NO3} in field bioreactors (Addy et al., 2016).

5.5. Conclusion

High-frequency, multi-point sampling provides the means to increase our understanding of bulk and internal processes of field bioreactors. The MPS and spectrophotometer were successfully deployed in three field experiments of 10-30 d. Data from both bioreactors showed that $[NO_3]_{in}$ increased quickly with increasing flow, making it possible to observe NO_3 pulses at internal sampling wells as they made their way through the bioreactor.Times series of $[NO_3]$ at the inlet and outlet showed that using instantaneous values of $[NO_3]$ and flow may give biased estimates of nitrate removal performance. This is especially true when HRT is high (> 1 d), as was the case in the NZ bioreactor. High-frequency sampling made it possible to calculate cumulative N load with reduced uncertainty by decreasing the sampling interval. Calculated removal rate based on cumulative N load was within 1-4% of the mean R_{NO3} values. Subsampling measured R_{NO3} values showed that it is possible to reduce sampling frequency to a daily interval and still get accurate estimates of R_{NO3} when taking the mean of instantaneous rates. While it is tempting to use the large data sets provided by this method to develop relationships between instantaneous R_{NO3} and other variables (e.g. flow, temperature, [DO]), cumulative or mean R_{NO3} values are more robust indicators and require monitoring over longer periods of time and a minimum of daily intervals.

Monitoring of sampling wells helped reveal internal solute transport. At the IA bioreactor, longitudinal [DOC] and [DO] trends were spatially aligned with lower $[NO_3]$ reductions, indicating a zone where peak NO_3 removal occurs where aerobic DOC production is highest and DO is depleted. In the IA bioreactor $[NO_3]$ was lower in deeper wells relative to shallow wells. Although [DO] could have explained these differences, time series of $[NO_3]$ during a high flow event and a tracer injection suggested slower flowpaths around deeper wells. Variable flow rates through the woodchip media explained vertical differences in $[NO_3]$ and [DO], lags in $[NO_3]$ at shallow and deep wells, and indirect evidence of preferential flow from previous studies. Silting and clogging of deeper pores in the 9-year-old bioreactor is a likely cause of decreased hydraulic conductivity. Vertical $[NO_3]$ gradients at the NZ bioreactor are likely to increase over time considering that lower porosity in deeper woodchips is already occurring.

5.5.1. Recommendations for future research

The large data sets provided by the MPS improve the ability to establish relationship between R_{NO3} and flow or temperature compared to previous efforts using infrequent or small data sets (Christianson et al., 2012; David et al., 2016; Hoover et al., 2016; Lepine et al., 2016). Cumulative or mean R_{NO3} are more robust indicators, but would require a monitoring period to be sufficiently long. If flows are variable over the monitoring period, more uncertainty is introduced when selecting an appropriate HRT to attribute to observed R_{NO3}. This uncertainty could be reduced by high-frequency monitoring of a bioreactor where flow rates could be held constant while steady-state conditions are reached (e.g. >10x HRT). This would reduce bias in calculating R_{NO3} and reduce uncertainty in reporting flow since instantaneous flow is approximately mean flow. This would test the previous hypothesis of flow-dependency of the K_N constant. Additional insight would be provided by monitoring internal sampling wells to determine solute dispersion as affected by flow, since N removal efficiency is affected by hydraulic inefficiencies.

Monitoring internal sampling wells provides a better method for determining effect of distributor configuration on overall performance. Cameron and Schipper (2011) found that vertical flow was more uniform than horizontal flow, although the study used based conclusions on inlet/outlet monitoring of a small (2.4 m x 1.2 m) lab bioreactor using fresh maize cobs as the fill media. Inlet and outlet monitoring can show that hydraulic inefficiencies exist, but cannot directly observe how or why they are occurring. Internal sampling wells in this study and Maxwell et al. (2018) were able to show hydraulic dead zones where theoretical flow lines would predict slower flow. Proposed distributor designs should consider practicality of installation in the field. Conclusions on flow uniformity of a distributor design should consider changes in porosity as the bioreactor ages.

Technical issues were experienced from MPS field use. A quartz cuvette insert for the spectrophotometer was used in all three monitoring periods. In all three monitoring periods an acid rinse was not needed since fouling by metals or heavy organics was not an issue. The cuvette did, however, result in lost data when condensation on the cuvette surface occurred. This was especially prevalent at the NZ bioreactor on warm days where humidity was high and

drainage water was cooler than air temperature. Minimal fouling of the cuvette in NZ by organics was resolved by a rinse with tap water at the end of each sampling sequence, where rinsing with chlorinated tap water helped keep optical fouling low. If an acid rinse is not required, use of the quartz cuvette insert is not recommended. This will require additional pumping time when sampling since the dead volume of the manufacturer's cuvette sleeve (~45 mL) is higher than the quartz cuvette (4 mL).

The April 2018 monitoring period showed that the MPS was not able to pump water at temperatures well below freezing. Sampling lines were inserted in black corrugated loom to reduce convective heat loss from wind, and complete freezing of the lines was not observed until temperatures were well below freezing (< -2 °C) for several hours.

Increased spatial and temporal resolution of water chemistry data will be beneficial for improved modeling of woodchip bioreactors. Early modeling used results from infrequent inlet/outlet measurements to build simplified design models (Christianson et al., 2011), while improvements were made when considering woodchip bioreactors as dual-porosity systems (Jaynes et al., 2016). Modeling by Halaburka et al. (2018) concluded that nitrate removal in bioreactors may be simple as zero-order kinetics, but the findings were based on limited observations over a narrow range of conditions in one-dimensional, upflow columns. This research has shown that bioreactors are dynamic systems with a number of factors varying spatially and temporally (e.g. porosity, flow, woodchip age, water chemistry). Well-calibrated models that understand the solute transport dynamics, particularly with regards to solute transport at high and low hydraulic gradients, could help predict the performance of improved bioreactor design and be less costly than constructing and testing prototype designs. Important design parameters include distributor configuration, geometry, and design flow rate.

Additional recommendations include how results are obtained and reported in the existing bioreactor literature. The IA bioreactor was an example of an unlined bioreactor with no impermeable barrier beneath the woodchip to prevent lateral inflows or outflows. Woodchip bioreactor monitoring typically assumes conservation of water mass through the bioreactor. This assumption was unable to be tested since only outflow was measured. Lateral inflows may have been the cause of marginally low apparent R_{NO3} at this site. If bioreactors are unlined and lateral

contributions are likely, it is important to measure inflow, bypass flow, and outflow to calculate the mass balance. Volumetric removal rates, R_{NO3}, are reported in the literature as g N m^{-3} d^{-1}, with volume referring the woodchip-filled bioreactor volume. It is commonly unclear, in the literature, whether the authors use the woodchip-filled volume or the *saturated* woodchip-filled volume when calculating these rates. In the case of the IA bioreactor, only 1/3 of the design volume was saturated. It is important for comparing rates between bioreactors to make this distinction.

5.6. References

Addy, K., Gold, A. J., Christianson, L. E., David, M. B., Schipper, L. A., & Ratigan, N. A. (2016). Denitrifying bioreactors for nitrate removal: A meta-analysis. *Journal of Environmental Quality, 45*(3), 873-881.

Bear, J. (1972). In Dover N. (Ed.), *Dynamics of fluids in porous media* Courier Corporation.

Birgand, F., Aveni-Deforge, K., Smith, B., Maxwell, B., Horstman, M., Gerling, A. B., et al. (2016). First report of a novel multiplexer pumping system coupled to a water quality probe to collect high temporal frequency in situ water chemistry measurements at multiple sites. *Limnology and Oceanography: Methods, 14*(12), 767-783.

Birgand, F., Faucheux, C., Gruau, G., Augeard, B., Moatar, F., & Bordenave, P. (2010). Uncertainties in assessing annual nitrate loads and concentration indicators. part 1: Impact of sampling frequency and load estimation alogorithms. *Transactions of the American Society of Agricultural and Biological Engineers, 53*(2), 437-446.

Bonnett, S., Blackwell, M., Leah, R., Cook, V., O'connor, M., & Maltby, E. (2013). Temperature response of denitrification rate and greenhouse gas production in agricultural river marginal wetland soils. *Geobiology, 11*(3), 252-267.

Brusseau, M. L. (1993). The influence of solute size, pore water velocity, and intraparticle porosity on solute dispersion and transport in soil. *Water Resources Research, 29*(4), 1071-1080.

Cameron, S. G., & Schipper, L. A. (2010). Nitrate removal and hydraulic performance of organic carbon for use in denitrification beds. *Ecological Engineering, 36*(11), 1588-1595.

Cameron, S. G., & Schipper, L. A. (2011). Evaluation of passive solar heating and alternative flow regimes on nitrate removal in denitrification beds. *Ecological Engineering, 37*(8), 1195-1204.

Christianson, L. E., Bhandari, A., Helmers, M. J., Kult, K. J., Sutphin, T., & Wolf, R. (2012). Performance evaluation of four field-scale agricultural drainage denitrification bioreactors in iowa. *Transactions of the ASABE, 55*(6), 2163.

Christianson, L. E., Hanly, J. A., & Hedley, M. J. (2011). Optimized denitrification bioreactor treatment through simulated drainage containment. *Agricultural Water Management, 99*(1), 85-92.

Christianson, L., Helmers, M., Bhandari, A., & Moorman, T. (2013). Internal hydraulics of an agricultural drainage denitrification bioreactor. *Ecological Engineering, 52*, 298-307.

David, M. B., Gentry, L. E., Cooke, R. A., & Herbstritt, S. M. (2016). Temperature and substrate control woodchip bioreactor performance in reducing tile nitrate loads in east-central illinois. *Journal of Environmental Quality, 45*(3), 822-829.

Davidson, E. A., Janssens, I. A., & Luo, Y. (2006). On the variability of respiration in terrestrial ecosystems: Moving beyond Q10. *Global Change Biology, 12*(2), 154-164.

Dupin, H. J., & McCarty, P. L. (2000). Impact of colony morphologies and disinfection on biological clogging in porous media. *Environmental Science & Technology, 34*(8), 1513-1520.

Etheridge, J. R., Birgand, F., Osborne, J. A., Osburn, C. L., Burchell, M. R., & Irving, J. (2014). Using in situ ultraviolet-visual spectroscopy to measure nitrogen, carbon, phosphorus, and suspended solids concentrations at a high frequency in a brackish tidal marsh. *Limnology and Oceanography: Methods, 12*(1), 10-22.

Fenner, N., & Freeman, C. (2011). Drought-induced carbon loss in peatlands. *Nature Geoscience, 4*(12), 895.

Fenner, N., Freeman, C., & Reynolds, B. (2005). Hydrological effects on the diversity of phenolic degrading bacteria in a peatland: Implications for carbon cycling. *Soil Biology and Biochemistry, 37*(7), 1277-1287.

Fogler, S. (2006). Elements of chemical reaction engineering, prentice hall international series in the physical and chemical engineering sciences.

Freeman, C., Evans, C., Monteith, D., Reynolds, B., & Fenner, N. (2001). Export of organic carbon from peat soils. *Nature, 412*(6849), 785.

Freeman, C., Ostle, N., & Kang, H. (2001). An enzymic'latch'on a global carbon store. *Nature, 409*(6817), 149.

Halaburka, B. J., LeFevre, G. H., & Luthy, R. G. (2017). Evaluation of mechanistic models for nitrate removal in woodchip bioreactors. *Environmental Science & Technology, 51*(9), 5156-5164.

Harvey, J. W., Böhlke, J. K., Voytek, M. A., Scott, D., & Tobias, C. R. (2013). Hyporheic zone denitrification: Controls on effective reaction depth and contribution to whole-stream mass balance. *Water Resources Research, 49*(10), 6298-6316.

Healy, M. G., Ibrahim, T. G., Lanigan, G. J., Serrenho, A. J., & Fenton, O. (2012). Nitrate removal rate, efficiency and pollution swapping potential of different organic carbon media in laboratory denitrification bioreactors. *Ecological Engineering, 40*, 198-209.

Herbert Jr, R. B. (2011). Implications of non-equilibrium transport in heterogeneous reactive barrier systems: Evidence from laboratory denitrification experiments. *Journal of Contaminant Hydrology, 123*(1-2), 30-39.

Holmes, R. M., Jones, J. B., Fisher, S. G., & Grimm, N. B. (1996). Denitrification in a nitrogen-limited stream ecosystem. *Biogeochemistry, 33*(2), 125-146.

Holt, D. M., & Jones, E. B. (1983). Bacterial degradation of lignified wood cell walls in anaerobic aquatic habitats. *Applied and Environmental Microbiology, 46*(3), 722-727.

Hoover, N. L., Bhandari, A., Soupir, M. L., & Moorman, T. B. (2016). Woodchip denitrification bioreactors: Impact of temperature and hydraulic retention time on nitrate removal. *Journal of Environmental Quality, 45*(3), 803-812.

Janssens, I. A., & Pilegaard, K. (2003). Large seasonal changes in Q10 of soil respiration in a beech forest. *Global Change Biology, 9*(6), 911-918.

Jaynes, D. B., Moorman, T. B., Parkin, T. B., & Kaspar, T. C. (2016). Simulating woodchip bioreactor performance using a dual-porosity model. *Journal of Environmental Quality, 45*(3), 830-838.

Johnes, P. (2007). Uncertainties in annual riverine phosphorus load estimation: Impact of load estimation methodology, sampling frequency, baseflow index and catchment population density. *Journal of Hydrology, 332*(1), 241-258.

Kim, D., & Fogler, H. S. (2000). Biomass evolution in porous media and its effects on permeability under starvation conditions. *Biotechnology and Bioengineering, 69*(1), 47-56.

Lepine, C., Christianson, L., Sharrer, K., & Summerfelt, S. (2016). Optimizing hydraulic retention times in denitrifying woodchip bioreactors treating recirculating aquaculture system wastewater. *Journal of Environmental Quality, 45*(3), 813-821.

Liu, Y. (2017). The performance of controlled drainage and inline denitrifying woodchip bioreactor for reducing nutrient losses from subsurface drained grassland receiving liquid swine lagoon effluent. (Doctoral Dissertation, NCSU). (http://www.lib.ncsu.edu/resolver/1840.20/34529)

Nordström, A., & Herbert, R. B. (2019). Identification of the temporal control on nitrate removal rate variability in a denitrifying woodchip bioreactor. *Ecological Engineering, 127*, 88-95.

Odier, E., & Monties, B. (1983). Absence of microbial mineralization of lignin in anaerobic enrichment cultures. *Applied and Environmental Microbiology, 46*(3), 661-665.

Oldham, C., Farrow, D., & Peiffer, S. (2013). A generalized damköhler number for classifying material processing in hydrological systems. *Hydrology and Earth System Sciences, 17*(3), 1133-1148.

Parkin, T. B. (1987). Soil microsites as a source of denitrification variability. *Soil Science Society of America Journal, 51*(5), 1194-1199.

Pinay, G., Peiffer, S., De Dreuzy, J., Krause, S., Hannah, D. M., Fleckenstein, J. H., et al. (2015). Upscaling nitrogen removal capacity from local hotspots to low stream orders' drainage basins. *Ecosystems, 18*(6), 1101-1120.

Rieger, L., Langergraber, G., Thomann, M., Fleischmann, N., & Siegrist, H. (2004). Spectral in-situ analysis of NO2, NO3, COD, DOC and TSS in the effluent of a WWTP. *Water Science and Technology : A Journal of the International Association on Water Pollution Research, 50*(11), 143-152.

Robertson, W. (2010). Nitrate removal rates in woodchip media of varying age. *Ecological Engineering, 36*(11), 1581-1587.

Rockhold, M. L., Yarwood, R., Niemet, M., Bottomley, P. J., & Selker, J. S. (2005). Experimental observations and numerical modeling of coupled microbial and transport processes in variably saturated sand. *Vadose Zone Journal, 4*(2), 407-417.

Saraswati, S., Dunn, C., Mitsch, W. J., & Freeman, C. (2016). Is peat accumulation in mangrove swamps influenced by the "enzymic latch" mechanism? *Wetlands Ecology and Management, 24*(6), 641-650.

Schipper, L. A., Barkle, G. F., & Vojvodic-Vukovic, M. (2005). Maximum rates of nitrate removal in a denitrification wall. *Journal of Environmental Quality, 34*(4), 1270-1276.

Schipper, L. A., Robertson, W. D., Gold, A. J., Jaynes, D. B., & Cameron, S. C. (2010). Denitrifying bioreactors—an approach for reducing nitrate loads to receiving waters. *Ecological Engineering, 36*(11), 1532-1543.

Schmidt, C. A., & Clark, M. W. (2013). Deciphering and modeling the physicochemical drivers of denitrification rates in bioreactors. *Ecological Engineering, 60*, 276-288.

Seifert, D., & Engesgaard, P. (2007). Use of tracer tests to investigate changes in flow and transport properties due to bioclogging of porous media. *Journal of Contaminant Hydrology, 93*(1-4), 58-71.

Stewart, T. L., & Fogler, H. S. (2001). Biomass plug development and propagation in porous media. *Biotechnology and Bioengineering, 72*(3), 353-363.

Strohmeier, S., Knorr, K., Reichert, M., Frei, S., Fleckenstein, J., Peiffer, S., et al. (2013). Concentrations and fluxes of dissolved organic carbon in runoff from a forested catchment: Insights from high frequency measurements. *Biogeosciences, 10*(2), 905-916.

Suchomel, B. J., Chen, B. M., & Allen, M. B. (1998). Network model of flow, transport and biofilm effects in porous media. *Transport in Porous Media, 30*(1), 1-23.

Thullner, M. (2010). Comparison of bioclogging effects in saturated porous media within one- and two-dimensional flow systems. *Ecological Engineering, 36*(2), 176-196.

Van Genuchten, M. T., & Wierenga, P. (1977). Mass transfer studies in sorbing porous media: II. experimental evaluation with tritium (3H2O) 1. *Soil Science Society of America Journal, 41*(2), 272-278.

Vandevivere, P., & Baveye, P. (1992). Effect of bacterial extracellular polymers on the saturated hydraulic conductivity of sand columns. *Applied and Environmental Microbiology, 58*(5), 1690-1698.

von Ahnen, M., Pedersen, P. B., Hoffmann, C. C., & Dalsgaard, J. (2016). Optimizing nitrate removal in woodchip beds treating aquaculture effluents. *Aquaculture, 458*, 47-54.

Warneke, S., Schipper, L. A., Bruesewitz, D. A., McDonald, I., & Cameron, S. (2011). Rates, controls and potential adverse effects of nitrate removal in a denitrification bed. *Ecological Engineering, 37*(3), 511-522.

Warneke, S., Schipper, L. A., Matiasek, M. G., Scow, K. M., Cameron, S., Bruesewitz, D. A., et al. (2011). Nitrate removal, communities of denitrifiers and adverse effects in different carbon substrates for use in denitrification beds. *Water Research, 45*(17), 5463-5475.

Williams, M. R., King, K. W., Macrae, M. L., Ford, W., Van Esbroeck, C., Brunke, R. I., et al. (2015). Uncertainty in nutrient loads from tile-drained landscapes: Effect of sampling frequency, calculation algorithm, and compositing strategy. *Journal of Hydrology, 530*, 306-316.

Woli, K. P., David, M. B., Cooke, R. A., McIsaac, G. F., & Mitchell, C. A. (2010). Nitrogen balance in and export from agricultural fields associated with controlled drainage systems and denitrifying bioreactors. *Ecological Engineering, 36*(11), 1558-1566.

Zeikus, J., Wellstein, A., & Kirk, T. (1982). Molecular basis for the biodegradative recalcitrance of lignin in anaerobic environments. *FEMS Microbiology Letters, 15*(3), 193-197.

APPENDICES

Appendix A: Supplementary Material for Chapter 1

Optical methods for estimating NO_3^- concentrations

The s::can spectro::lyser (s::can^{TM}, Vienna, Austria) was used for the optical measurement of NO_3^- concentrations during the source and cross contamination trials (Sec. 2.3.1 and 2.3.2), as well as the woodchip bioreactor and stream mesocosm applications. The probe's estimates for NO_3^- were used to determine source/cross contamination due to the probe's low coefficient of variance for NO_3^- measurements and ability to detect small changes in NO_3^- concentration. Measurement of NO_3^- by the spectrophotometer is made possible by the principle of Behr's law and measuring the absorbance of a water volume over the 200 – 750 nm range. The resulting absorbance fingerprint provides absolute absorbance values at each 2.5 nm interval, with NO_3^- showing an absorbance peak at 200-205 nm. The spectrophotometer was configured for the 4 mm pathlength cuvette by changing the measurement pathlength of the spectrophotometer, and a baseline using deionized water was set using the manufacturer's specifications. While the spectro::lyser provides estimates of NO_3^- concentrations based on the manufacturer's global calibration, a local calibration is often recommended, particularly as the presence of organic matter absorbing at UV wavelengths can interfere with measurement of nitrate. During the cross and source contamination, the global calibration of the probe was used. In the bioreactor and stream applications, a local calibration was performed using PLSR methods detailed further in Etheridge et al. (2014). The R package *pls* was used to construct a model using the 240 raw absorbance values as predictors for the lab samples analyzed for NO_3^- by the NCSU Environmental Analysis Lab.

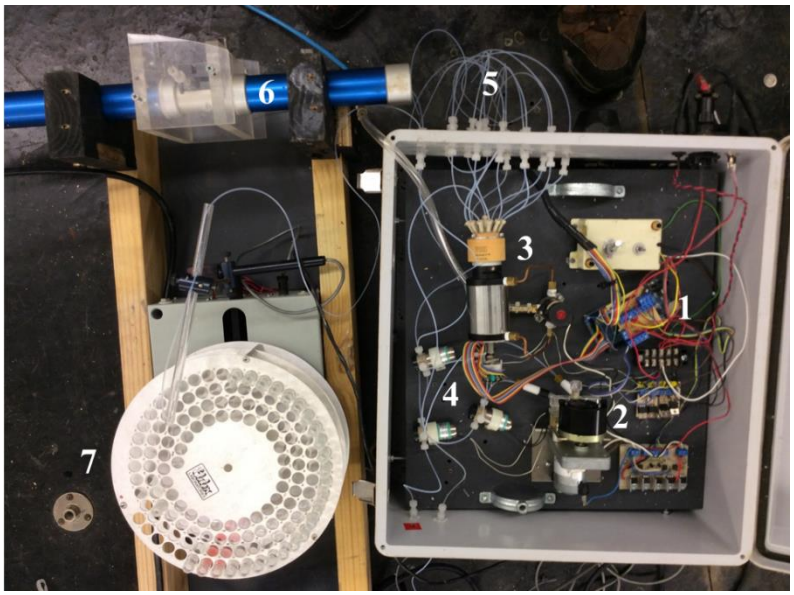

Figure A-1. Photo of the small volume multiplexer with 1) Arduino control board, 2) bidirectional peristaltic pump, 3) 12 port air-actuated valve, 4) 3 way valve manifold, 5) 0.9 mm ID PFTE tubing, 6) s::can spectrophotometer with housing for 1.1 mL, 4 mm path length cuvette, and 7) fractional volume collector (optional).

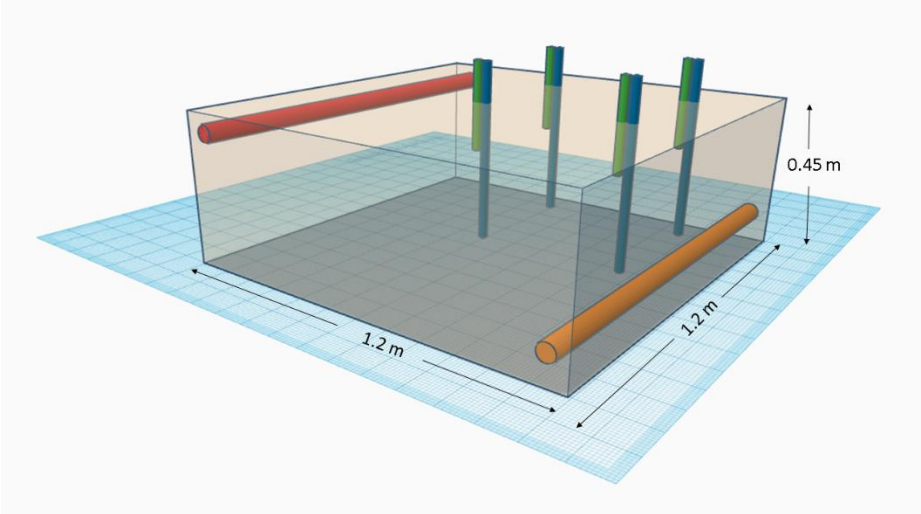

Figure A-2. Diagram of lab bioreactor at NCSU facility. Eight sampling wells were located in four well pairs placed at 20.9 and 41.9 cm depth, at 55.9 and 100.2 cm from the inlet, and in transects along the centerline of flow and 21.6 cm from left sidewall. Shallow and deep wells are shown in green and blue, respectively. Flow was diagonal downflow from the inlet header (red) to the outlet header (orange).

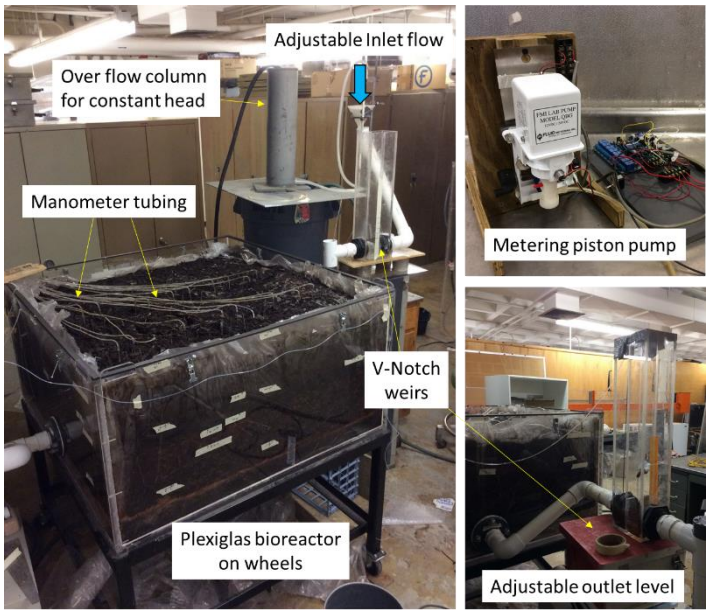

Figure A-3. Photo of the lab bioreactor at the NCSU facility using V-notch weirs to measure flow, overflow constant head column for uniform flow, the metering piston pump for KNO_3 additions, and an adjustable outlet weir to stop flow or drain bioreactor.

Figure A-4. Photo of the small volume MPS being deployed in the Sand section of Goldsboro stream. Four open-bottom Sediment mesocosms were inserted into the stream bottom and a fifth closed-bottom Control mesocosm was used as a baseline for nitrate fluxes occurring in the water column. The small volume MPS sampled each mesocosm every 6 min for a 36 min data interval on each mesocosm.

Figure A-5. Photo of the small volume MPS being deployed in the Muck section of Goldsboro stream. Recirculating pumps were installed on the mesocosm sidewall to mimic advective flow of the stream.

Figure A-6. Photo of the small volume MPS being deployed in the Muck section of Goldsboro stream. Emergent vegetation along the banks during March trials resulted in large variability in nitrate decreases over the 24 h experiment.

Appendix B: Supplementary Material for Chapter 2

Sample ID	Sediment type	% carbon	% nitrogen
S1	Sand	0.21	0.009
S2	Sand	1.34	0.052
S3	Sand	0.41	0.014
M1	Muck	4.43	0.220
M2	Muck	2.84	0.170
M3	Muck	0.31	0.015

Figure B-1. Carbon and nitrogen content analysis of Sand and Muck sediments. Carbon and nitrogen content was significantly higher in Muck sediments, illustrating the more organic nature of this sediment zone.

Appendix C: Supplementary Material for Chapter 3

Table C-1. Analysis of woodchips obtained from field bioreactor. TC and TN were measured following combustion at 1350 °C then measurement by infrared detector for C and thermal conductivity detector for N. pH measured using Standard Methods 4500-H^+ B or EPA Method 150.1. TP measured using K_2SO_4-$CuSO_4$ digestion, ortho phosphate-molybdate-antimony-ascorbic acid colorimetry on Bran & Leubbe Autoanalyzer System (Norderstedt,Germany), Standard Methods 4500-P F.

Sample ID	TP, mg/kg DW	pH	Total C, g/kg DW	Total N, g/kg DW	C/N
Woodchip S1 9/11	204.42	6.56	445.8	9.26	48.1
Woodchip S2 9/11	191.32	6.43	343.1	6.38	53.8
Woodchip S3 9/11	158.90	6.32	386.4	7.20	53.7

Standard Methods. 2017. 4500-H^+ B. Standard methods for examination of water and wastewater.
Standard Methods. 2017. 4500-P F. Standard methods for examination of water and wastewater.

Table C-2. Mean temperatures and hydraulic residence time (HRT) for SAT and DRW groups across all periods. Temperature was measured in the top 3 cm of the column woodchips.

	DRW mean temp. (°C)	SAT mean temp. (°C)	DRW mean HRT (h)	SAT mean HRT (h)
Period 0a	22.06	22.07	9.52	8.86
Period 0b	23.10	23.20	9.69	8.94
Period 0c	22.08	22.13	10.05	11.60
Period 1	23.31	23.38	9.27	9.21
Period 2	24.18	24.19	8.84	9.02
Period 3	24.49	24.55	9.03	9.04
Period 4	23.44	23.50	7.37	7.75
Period 5	22.02	22.03	7.61	8.14
Period 6	21.31	21.32	7.31	7.62
Period 7	21.64	21.65	7.26	7.06
Period 8	24.26	24.39	7.55	7.27
Period 9	21.28	21.77	7.39	6.83
Period 10	20.68	20.80	6.74	7.98
Period 11	23.45	23.15	6.90	7.46
Period 19	20.23	20.23	7.65	7.52
Period 20	19.49	19.49	8.78	8.86
Period 21	19.20	19.20	6.93	6.82
Period 22	19.43	19.40	7.18	6.88
Period 35	22.81	22.82	6.92	7.41
Period 36	21.37	21.38	7.18	8.05
Period 37	21.60	21.59	7.80	8.23
Period 38	23.78	23.92	8.45	8.94
Period 39	22.24	22.63	8.72	8.97

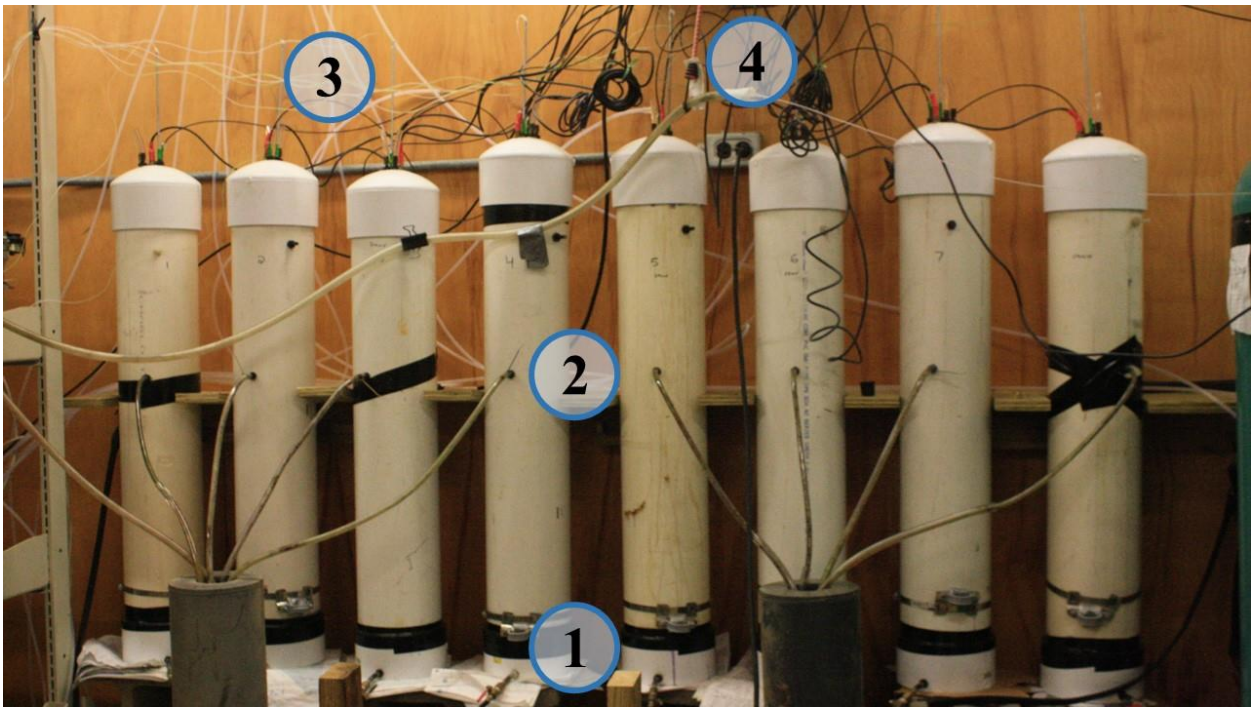

Figure C-1. Photo of eight experimental columns in the lab facility at North Carolina State University. Flow entered columns through the bottom side-wall (1), passing through 6 cm of gravel and 50 cm of woodchips, before exiting through the column sidewall at 56 cm height (2) and discharging to drain. Columns were sampled from the top by the multiplexed pumping system (MPS) using 0.9 mm internal diameter tubing (thin clear tubing seen at 3). Presens® temperature and dissolved oxygen sensors also entered from the column top (black cables seen at 4).

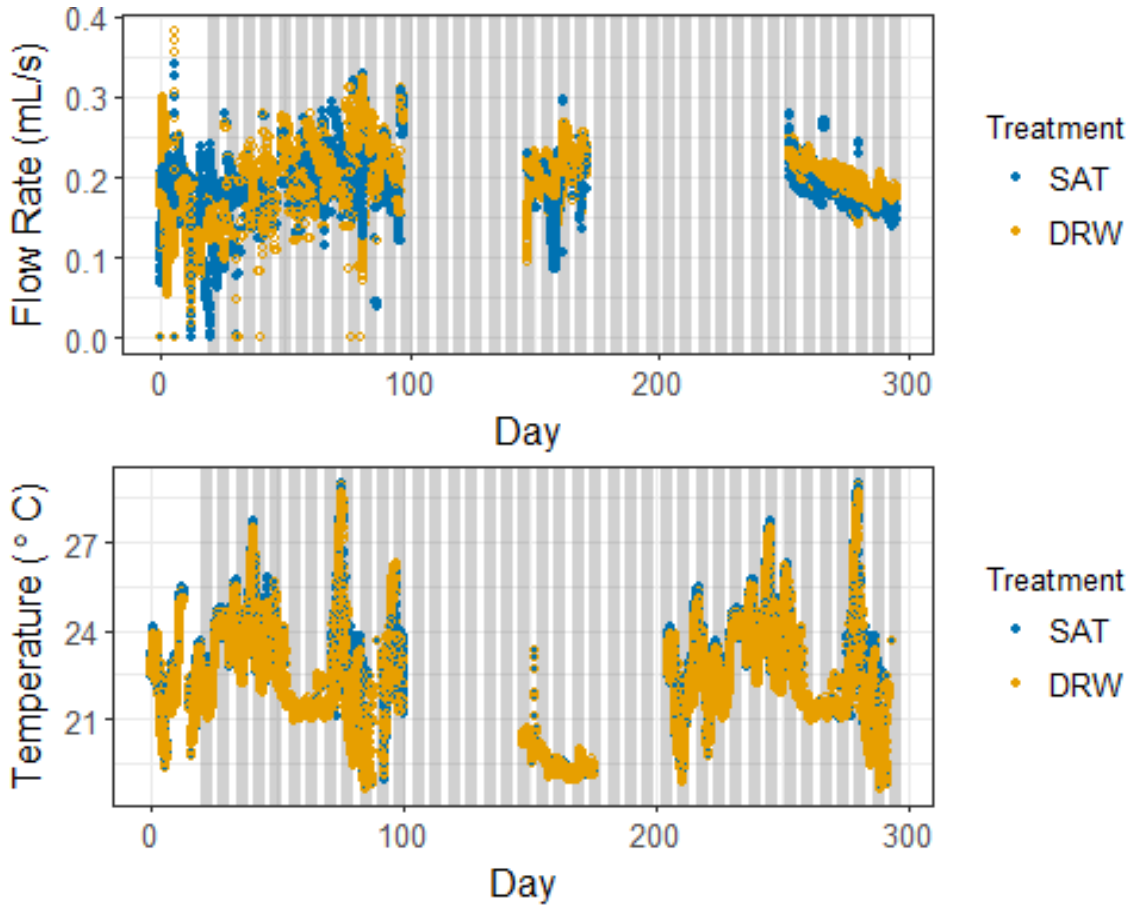

Figure C-2. Flow rates and temperature for SAT and DRW columns over the entire experiment. Flow rates from Day 0-100 were highly variable due to HVAC issues and bioclogging of pump tubing. Temperature and flow stabilized after Day 100 by replacing pump tubing more frequently (once a week) and HVAC replacement. Grey vertical bars denote DRW events.

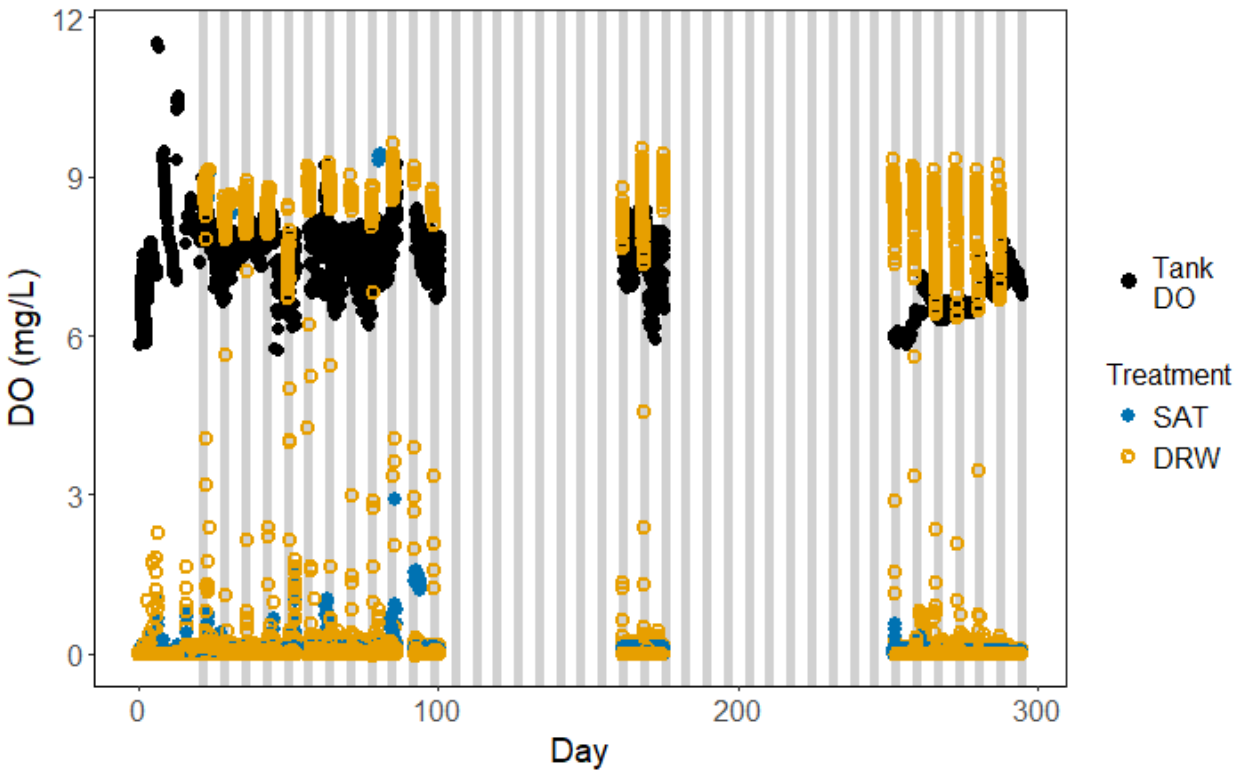

Figure C-3. Dissolved oxygen in the stock tank and column outlet for SAT and DRW columns. Dissolved oxygen in DRW columns increased briefly when woodchips were unsaturated, exposing the DO sensors to unsaturated woodchips. Dissolved oxygen in SAT columns briefly rose on several occasions when tubing was disconnected and water level fell below the DO sensor. Grey vertical bars denote DRW events.

Table C-3. Mean volumetric removal rates for SAT and DRW groups across periods. Removal rates over each week following DRW event are used to calculate difference in means (standard deviation). †In Period 22, data was collected for the first three days following rewetting only, explaining the apparent increased difference in means.

	DRW Volumetric Rate (g N m^{-3} d^{-1})	SAT Volumetric Rate (g N m^{-3} d^{-1})	Difference in Means (s.d.)	Days
Period A	5.62	5.02	0.60 (0.28)	0 - 7
Period B	5.14	5.22	-0.082 (0.17)	7 - 14
Period C	14.50	14.99	-0.49 (0.34)	14 - 21
Period 1	20.54	20.82	-0.28 (0.34)	21 - 28
Period 2	25.38	23.79	1.59 (0.37)	28 - 35
Period 3	24.91	21.49	3.42 (0.25)	35 - 42
Period 4	23.80	18.77	5.03 (0.40)	42 - 49
Period 5	16.96	14.14	2.82 (0.23)	49 - 56
Period 6	15.18	12.94	2.24 (0.19)	56 - 63
Period 7	16.57	13.16	3.41 (0.26)	63 - 70
Period 8	22.02	16.09	5.93 (0.45)	70 - 77
Period 9	17.01	12.60	4.41 (0.37)	77 - 84
Period 10	13.07	9.71	3.36 (0.36)	84 - 91
Period 11	18.13	13.38	4.75 (0.36)	91 - 98
Period 19	11.96	8.35	3.60 (0.11)	147 - 154
Period 20	12.07	8.42	3.64 (0.11)	154 - 161
Period 21	10.92	7.63	3.29 (0.11)	161 - 168
Period 22†	14.22	7.88	6.34 (0.20)	168 - 171
Period 35	11.43	8.05	3.38 (0.13)	252 - 259
Period 36	12.04	8.91	3.13 (0.12)	259 - 266
Period 37	13.24	9.54	3.70 (0.13)	266 - 273
Period 38	12.67	9.30	3.37 (0.12)	273 - 280
Period 39	12.06	8.82	3.24 (0.13)	280 – 287

SAS Code

```
Proc mixed data=a ;
class Period Treatment Column Day;
Model VolumetricRate=Period Treatment Period*Treatment;
random Column*Treatment Column*Treatment*Period;
lsmeans Period*Treatment / slice=Period adjust=tukey;
repeated Day/subject = Column type = ar(1);
Run;
```

Table C-4. SAS output for proc mixed model, testing all column data from Periods 2-39 for significance of fixed effects (Treatment and Period) and their interaction. An AR(1) autocorrelation structure proved to be the best covariance structure in the linear mixed model. AIC was minimized when selecting an AR(1) covariance structure with an estimated value of 0.76 for the AR(1) covariance parameter, indicating evidence of autocorrelation in the repeated measurements of the column experiment.

	Num DF	**F Value**	**Pr < F**
Period	17	111.34	<0.0001
Treatment	1	29.2	0.0017
Period*Treatment	17	1.24	0.2504

Table C-5. SAS output for proc mixed model slice testing, testing the significance of Treatment effect within each period (Periods 2-39). The overall model indicated Treatment effect as significant, and Treatment effect was consistently significant within each period. Analysis excluded Period 22 where data was collected in the first 3 days of rewetting only

Period	**Num DF**	**F Value**	**Pr < F**
2	1	4.3	0.0407
3	1	11.89	8e-04
4	1	17.06	1e-04
5	1	9.11	0.0032
6	1	4.6	0.0344
7	1	13.16	4e-04
8	1	34.5	1e-04
9	1	21.83	1e-04
10	1	14.53	2e-04
11	1	12.79	5e-04
19	1	12.28	7e-04
20	1	8.67	0.004
21	1	8.37	0.0047
35	1	7.29	0.0081
36	1	11.93	8e-04
37	1	16.18	1e-04
38	1	11.5	0.001
39	1	9.24	0.003

Table C-6. SAS output for proc mixed model, testing all column data from Periods 19-39 for significance of fixed effects (Treatment and Period Day) and their interaction.

	Num DF	F Value	Pr < F
Period Day	6	66.52	<0.0001
Treatment	1	921.82	<0.0001
Period Day*Treatment	5	122.29	<0.0001

Figure C-4. Volumetric nitrate removal rates (R_{NO3}) over number of days since rewetting for Periods 2 -11. Flow and temperature were less stable during these periods due to lab facility HVAC issues and bioclogging of pump tubing. In later Periods 19-22 and 35-39 it was more clearly observed that R_{NO3} decreased with number of days since rewetting.

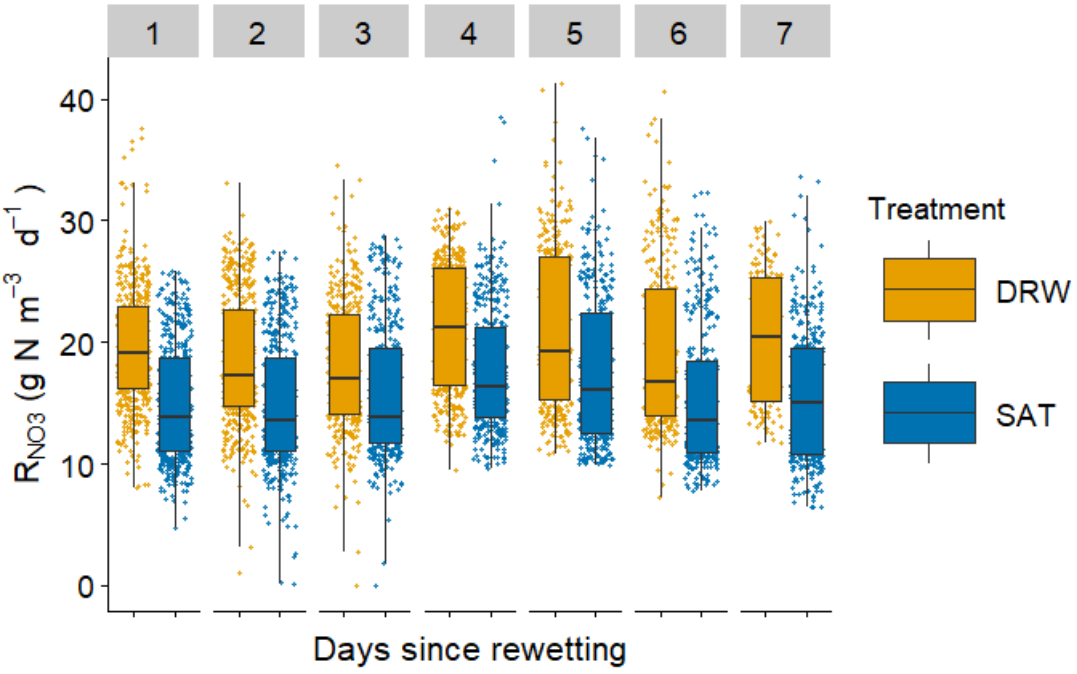

Appendix D: Supplementary Material for Chapter 4

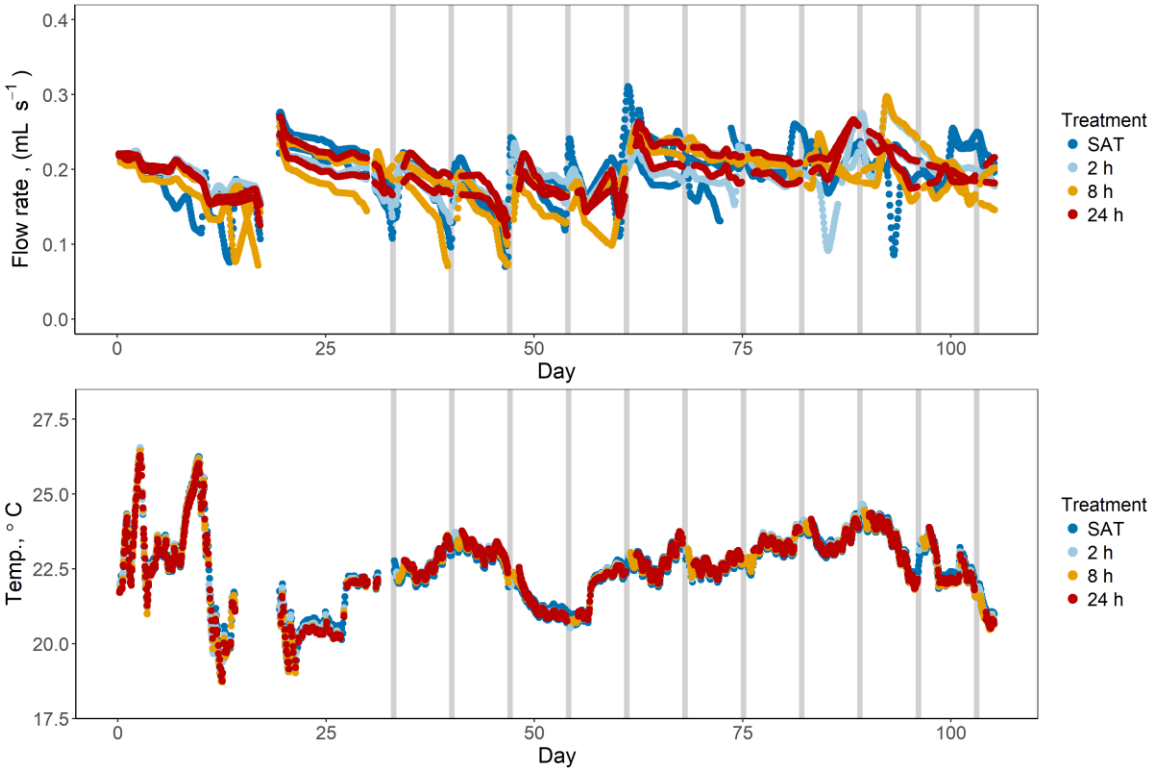

Figure D-1. Flow rates and temperature time series for all eight columns in the DRW 2018 experiment. Flow rates were generally close to the target flow rate was 0.2 mL s^{-1}. Flow rates were similar between groups with no consistent differences. Temperatures differences between columns were <0.5 °C. Grey vertical bars denote DRW events.

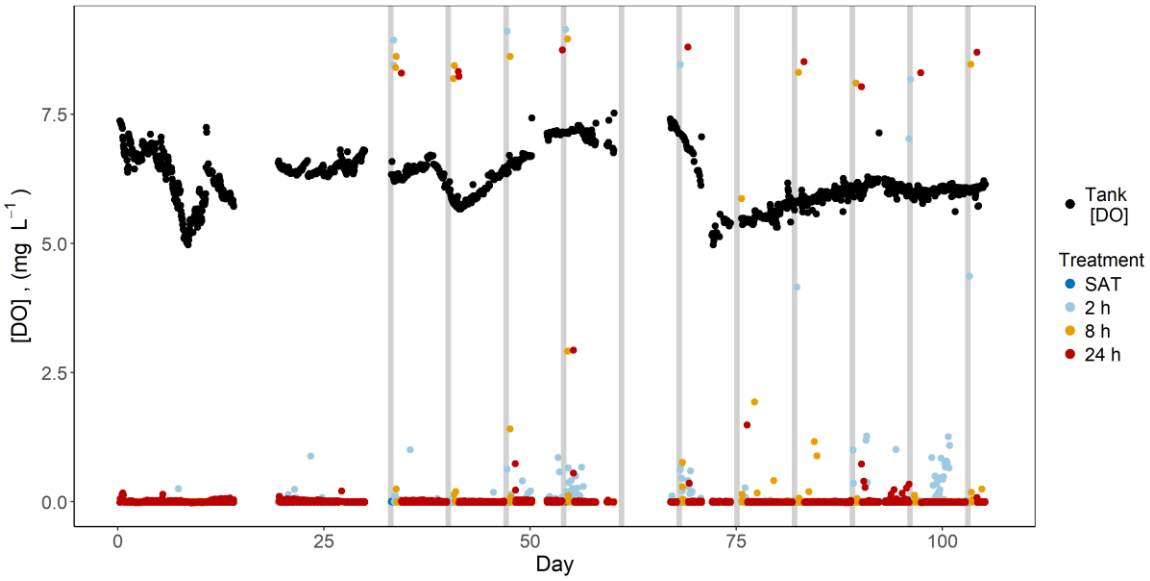

Figure D-2. Dissolved oxygen in the stock tank and column outlet for all columns. Dissolved oxygen in DRW columns increased briefly when woodchips were unsaturated, exposing the DO sensors to unsaturated woodchips. Grey vertical bars denote DRW events.

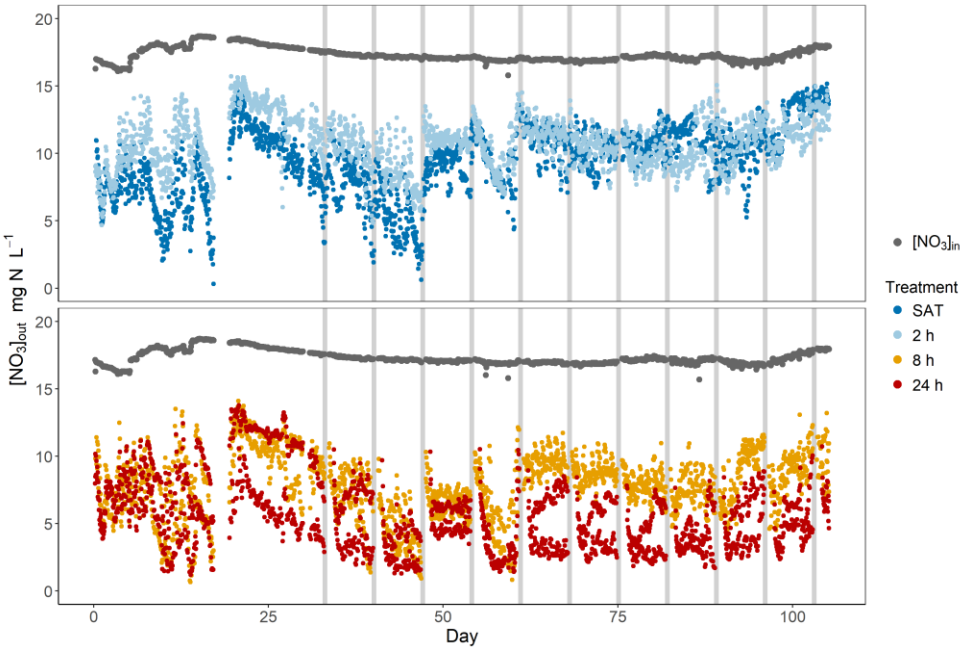

Figure D-3. Nitrate concentrations in the stock tank $[NO_3]_{in}$ and outflow of all columns $[NO_3]_{out}$ over the experiment for SAT, 2 h, 8 h, and 24 h DRW groups. Grey vertical bars denote DRW events. Measurements of $[NO_3]_{out}$ were collected over the entire 105 d experiment.

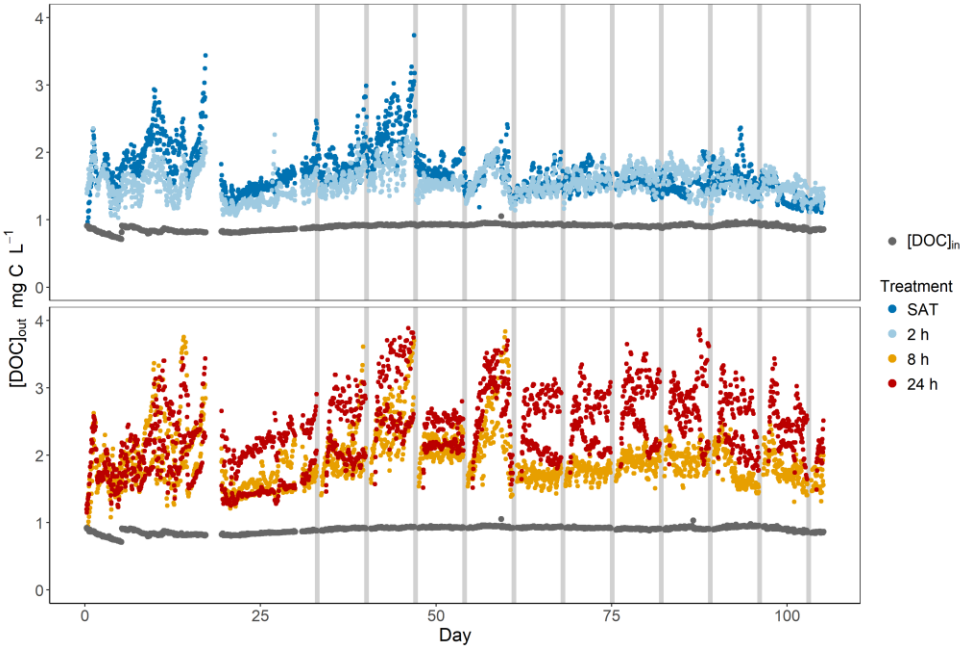

Figure D-4. Dissolved organic carbon (DOC) in the stock tank $[DOC]_{in}$ and outflow of all columns $[DOC]_{out}$ over the experiment for SAT, 2 h, 8 h, and 24 h DRW groups. Grey vertical bars denote DRW events. Measurements of $[DOC]_{out}$ were collected over the entire 105 d.

Table D-1. Mean R_{NO3} for each treatment group over the experiment, with period 0 being the 33 d baseline period where all columns received the SAT treatment.

Volumetric NO_3 removal rates (R_{NO3}), g N m^{-3} d^{-1}					
Period	SAT	2 h DRW	8 h DRW	24 h DRW	Days
0	16.48	12.13	15.83	18.77	0 - 33
1	16.02	12.02	16.31	21.78	33 - 40
2	17.6	13.97	17.68	21.87	40 - 47
3	13.96	11.17	16.24	20.11	47 - 54
4	12.15	11.46	15.35	20.75	54 - 61
5	11.85	11.47	16.92	25.58	61 - 68
6	12.58	12.63	17.07	24.35	68 - 75
7	12.75	13.86	18.36	25.51	75 - 82
8	12.41	12.93	18.45	28.07	82 - 89
9	12.55	12.96	16.96	24.6	89 - 96
10	9.7	11.63	15.37	22.64	96 - 105
11	7.59	9.4	12.91	20.68	103 - 105

Table D-2. Results of ANOVA analysis showing significance of the two-way interaction effects of main effects temperature, HRT, and L_{DOC} on nitrate removal rates and coefficients DRW 2018 and DRW 2017 experiments. All two-way interactions were significant in both experiments. Coefficients for all two-way interactions were negative in both experiments.

DRW 2018 results – model 3					
Effect	**Estimate**	**Std Error**	**DF**	**t Value**	**Pr > |t|**
L_{DOC}	15.11	1.05	3439	14.41	<.0001
HRT	1.10	0.56	3439	1.98	0.0476
Temperature	1.24	0.21	3439	5.92	<.0001
L_{DOC} *Temperature	-0.34	0.04	3439	-8.27	<.0001
HRT*Temperature	-0.05	0.02	3439	-2.19	0.0282
L_{DOC} *HRT	-0.19	0.03	3439	-7.73	<.0001
DRW 2017 results – model 3					
L_{DOC}	13.32	0.38	9528	35.08	<.0001
HRT	1.17	0.13	9528	8.96	<.0001
Temperature	0.82	0.06	9528	14.09	<.0001
L_{DOC} *Temperature	-0.23	0.02	9528	-14.95	<.0001
HRT*Temperature	-0.06	0.01	9528	-9.31	<.0001
L_{DOC} *HRT	-0.26	0.02	9528	-12.61	<.0001

Figure D-5. Leaching rates of DOC (L_{DOC}) in SAT and 8 h DRW columns from the DRW 2017 study, with four replicates in each treatment group. Grey vertical bars denote DRW events.

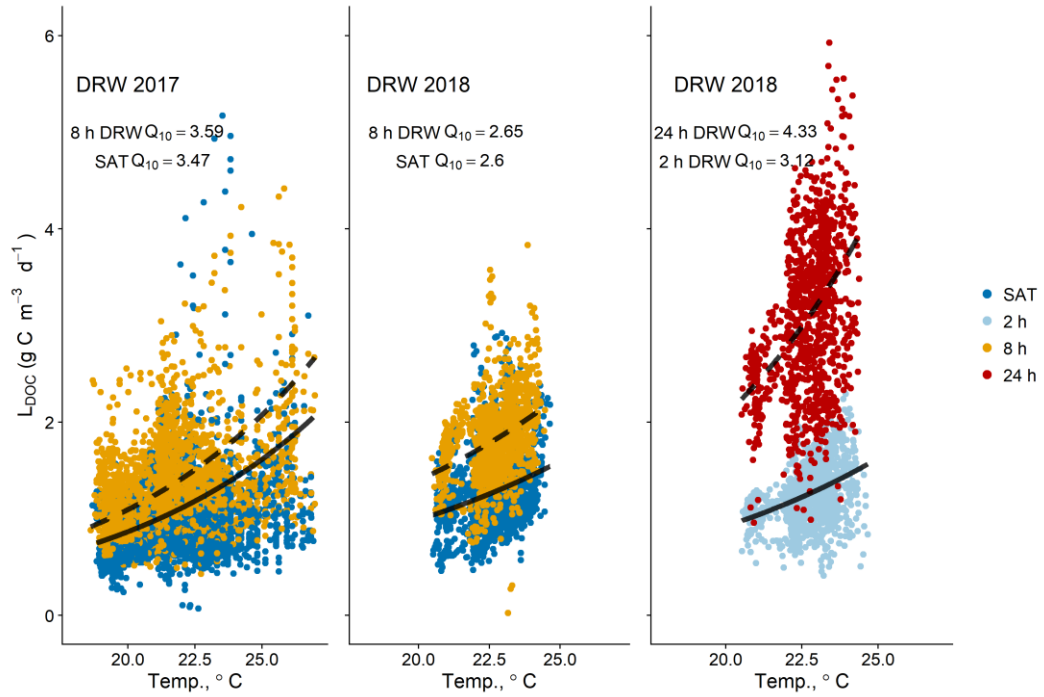

Figure D-6. Leaching rates of DOC plotted against temperature in the DRW 2017 and DRW 2018 experiments. Leaching was positively correlated with temperature in all treatment groups, with Q_{10} of 2.60 – 4.33. Calculated L_{DOC} Q_{10} was highest in the 24 h DRW group.

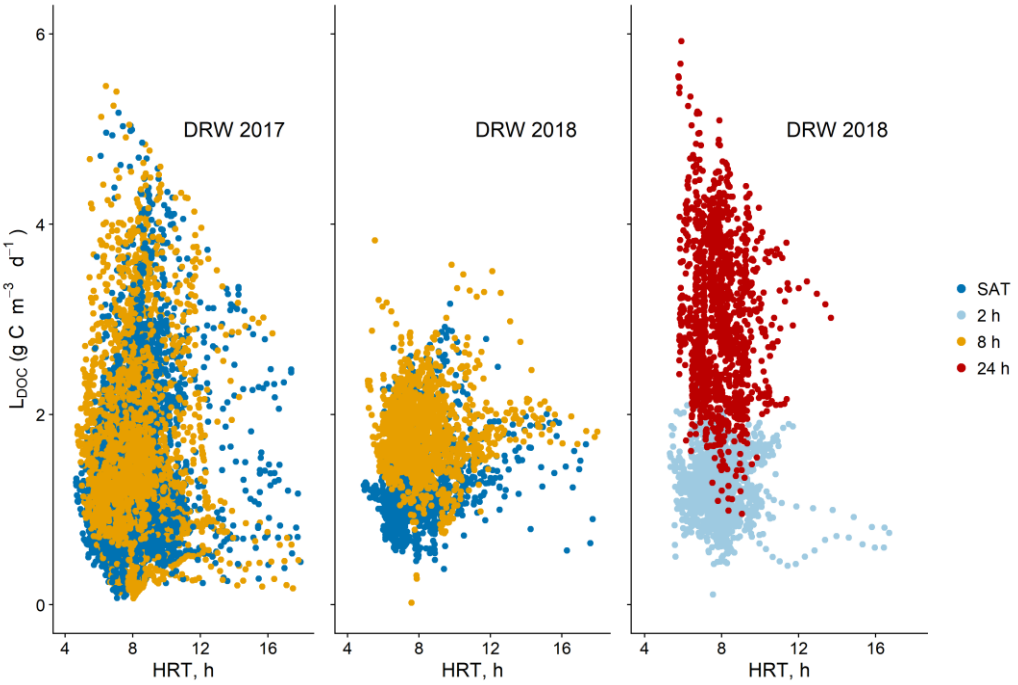

Figure D-7. DOC leaching rates plotted against hydraulic residence time (HRT) in the DRW 2017 and DRW 2018 experiments. In general, L_{DOC} was not strongly correlated with HRT.

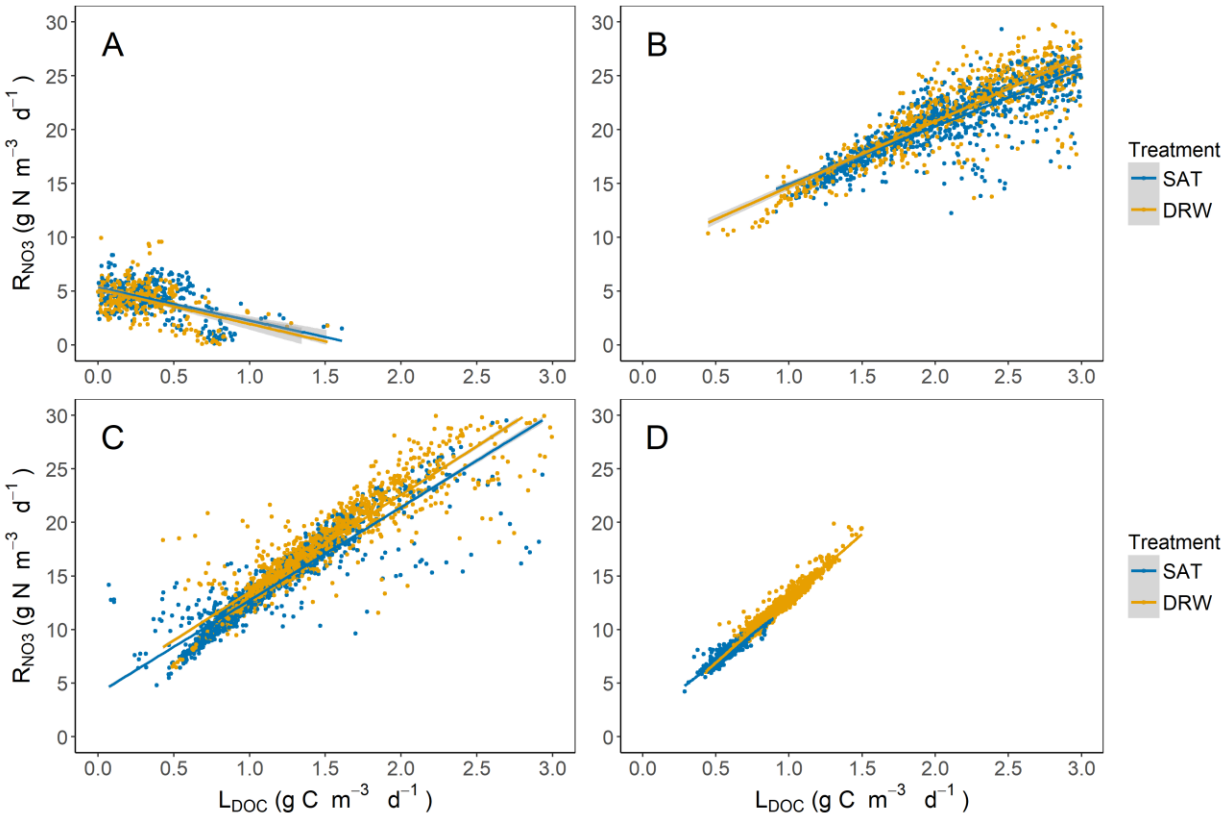

Figure D-8. Nitrate removal rates plotted against DOC leaching rates in the DRW 2017 experiment for Days 2-11 (A), Days 20-50 (B), Days 50-100 (C), and Days 147-172 (D). The slope of the R_{NO3} : L_{DOC} relationship changed slightly over the course of the experiment.

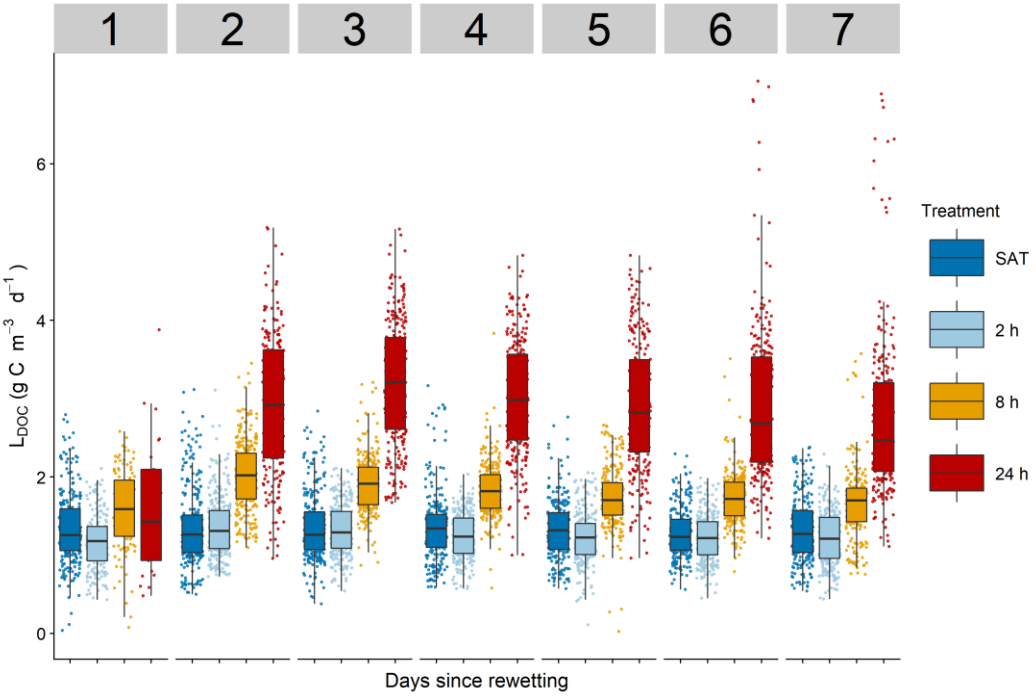

Figure D-9. Box plots of DOC leaching rates for each treatment group according to the number of days since rewetting. Nitrate removal peaked on the second day after rewetting, although subsequent declines in L_{DOC} were not as high as the previous DRW 2017 experiment.

Appendix E: Supplementary Material for Chapter 5

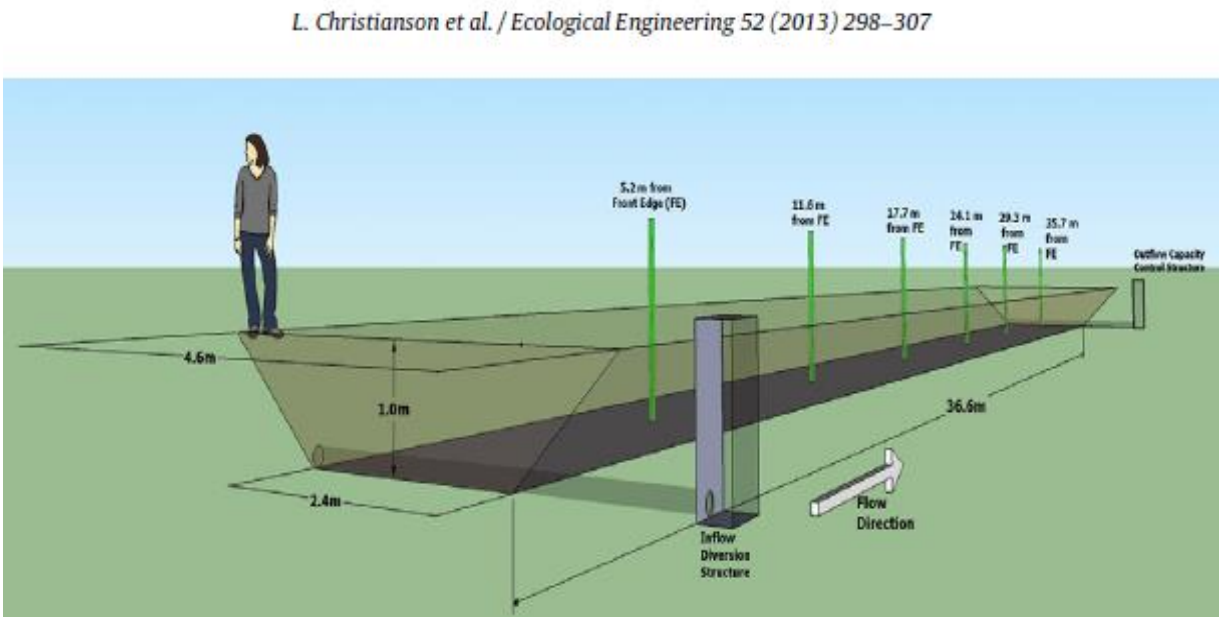

Figure E-1. Diagram of the IA bioreactor (figure produced in Christianson et al., 2013). The bioreactor is an unlined trapezoidal channel with bottom-to-bottom distributor configuration constructed in 2009.

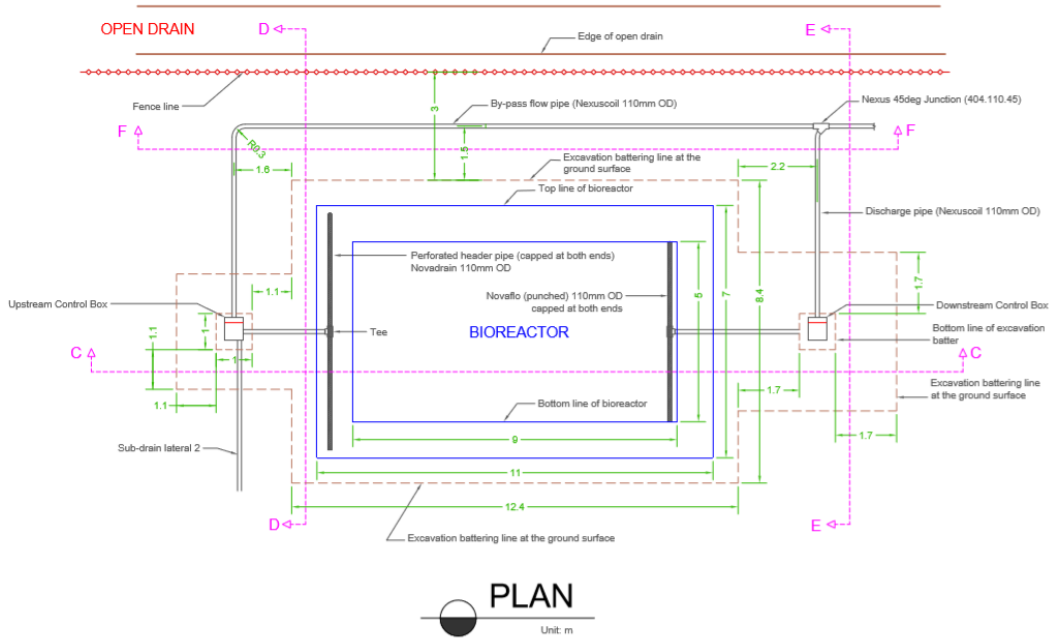

Figure E-2. Plan view of the NZ bioreactor (figure produced by Lincoln Agritech).

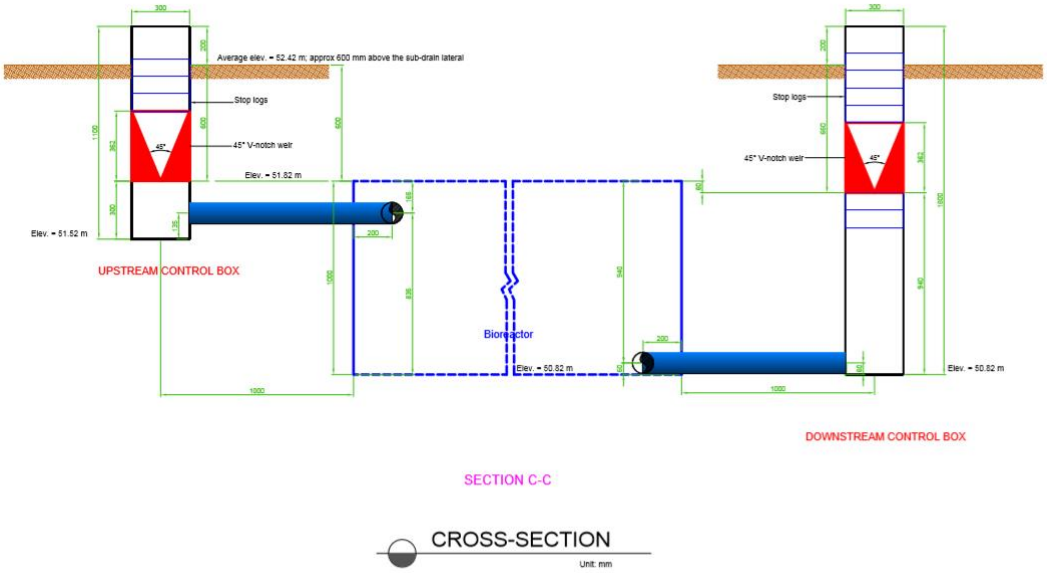

Figure E-3. Side view of NZ bioreactor. The NZ bioreactor is designed from permanent saturation below the annual water table. It is a lined bioreactor with diagonal downflow distributor configuration.

Table E-1. Description of sampling sequences and wells sampled by each MPS for IA and NZ bioreactors. Sample cycle duration refers to the interval of time between measurements at any given location.

Site	Sampler	Wells sampled (listed in order of sampling sequence)	Sample cycle duration
IA bioreactor			
	MPS #1	Inlet, S1, D1, S2, D2, S3, D3	40 min
	MPS #2	S4, D4, S5, D5, S6, D6, Outlet	5 – 40 min
NZ bioreactor			
	MPS #1	Inlet, LS1, LD1, RS1, RD1, LS2, LD2, RS2, RD2, C1, C2	60 min
	MPS #2	LS3, LD3, RS3, RD3, LS4, LD4, RS4, RD4, C3, Outlet	55 min

Table E-2. Number of samples collected, fits of PLSR and linear regression from probe calibrations during each monitoring periods. *indicates the statistical method used for probe calibration. **indicates neither method was suitable and a probe results were not used. NA indicates lab analysis was not available.

Site (Year)	Probe #	Nutrient	# of samples submitted	Conc. range (mg L^{-1})	PLSR r^2, RMSEP (# of components)	Lin. Reg. r^2, RMSEP
IA (2017)						
	Probe #1	NO_3	22	13.8 – 17.7	0.90, 0.27 (4)	0.67, 0.49*
		DOC	30	0.6 – 1.3	0.64, 0.11 (3)*	0.28, 0.16
	Probe #2	NO_3	25	10.8 – 14.4	0.93, 0.25 (5)	0.72, 0.52*
IA (2018)		DOC	21	1.0 – 1.3	0.20, 0.06 (1)*	0.09, 0.06
	Probe #1	NO_3	24	9.7 – 20.9	0.99, 0.18 (4)	0.99, 0.21*
		DOC	22	1.0 – 2.5	0.95, 0.13 (7)**	-0.03, 0.6
	Probe #2	NO_3	24	11.2 – 13.5	0.88, 0.22 (3)	0.60, 0.39*
		DOC	27	1.0 – 2.6	0.49, 0.32 (1)**	0.32, 0.34
NZ (2018)						
	Probe #1	NO_3	10	0.8 – 9.8	0.83, 1.13 (1)	0.87, 0.99*
		DOC	NA	NA		
	Probe #2	NO_3	9	0.3 – 2.2	0.95, 0.13 (1)	0.89, 0.21*
		DOC	NA	NA		

Figure E-4. Nitrate concentrations in shallow and deep wells during the IA 2018 monitoring period, according to distance from bioreactor inlet. Nitrate concentrations were higher in shallow wells relative to deep wells >5.2 m from inlet, similar to trends seen during the IA 2018 monitoring period.

Table E-3. Summary of Q_{10} values reported previously for nitrate removal in woodchip bioreactors. Conditions among lab studies varied significantly and may contribute to the variability in reported Q_{10}.

Study	Q_{10}	Carbon source (age in years)	Temperature °C	HRT hours	$[NO_3]_{in}$ mg L^{-1}
Hoover et al. (2016)	2.2	Hardwood chips (NA)	10 - 15	12.8	20 - 30
	2.9	Hardwood chips (NA)	15 - 20	12.8	20 - 30
Lepine et al. (2016)	1.6	Hardwood chips (NA)	14 - 20	10 - 13	60 - 80
Cameron and Schipper (2010)	2.0	Hardwood chips (<1)	14 -24	30 - 50	140 - 160
	1.3	Maize cobs (<1)	14 -24	30 - 50	140 - 160
	1.4	Hardwood chips (1-2)	14 -24	30 - 50	140 - 160
	0.8	Maize cobs (1-2)	14 -24	30 - 50	140 - 160
Warneke et al. (2011)	1.2	Hardwood, maize (>2)	17 - 27	40 - 50	15 - 20
Schmidt and Clark (2013)	4.7	Sawdust (NA)	8 - 24	24 - 96	6 - 8

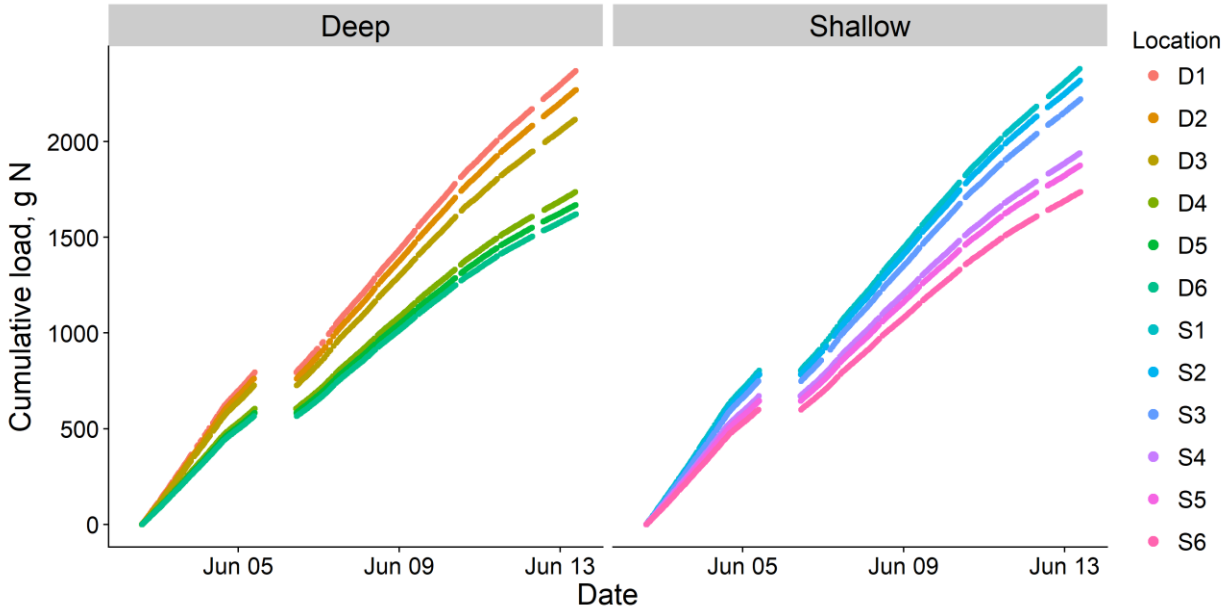

Figure E-5. Cumulative load at shallow and deep wells at the IA bioreactor during 2017.

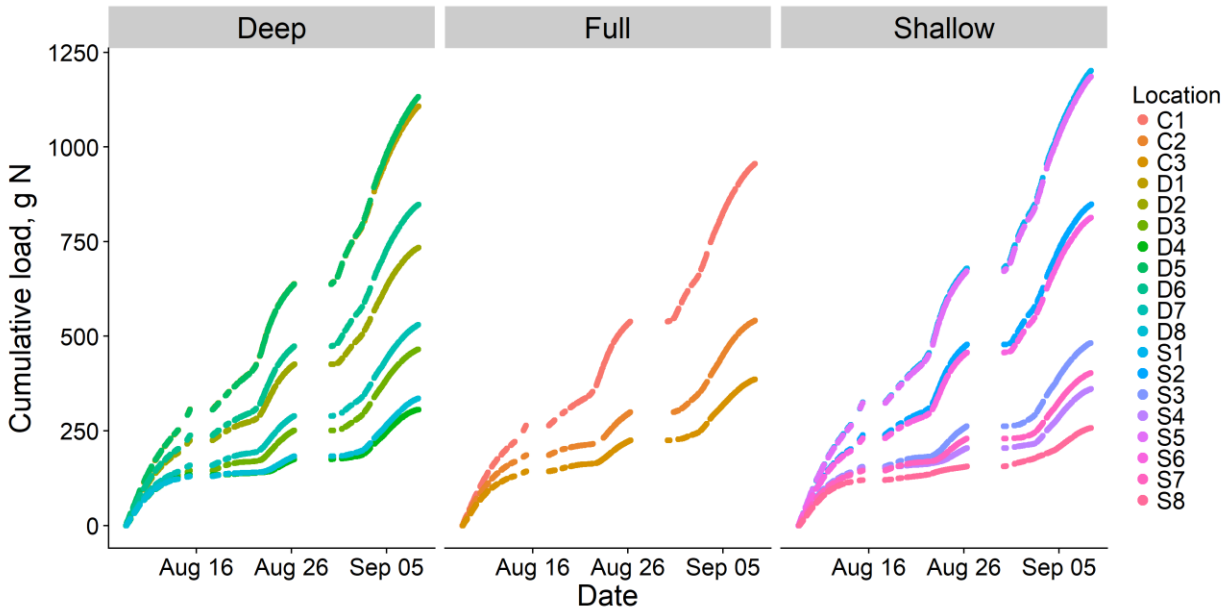

Figure E-6. Cumulative concentration at shallow, deep, and fully screened wells at the NZ bioreactor during 2018. Full refers to fully screened wells along the bioreactor centerline.

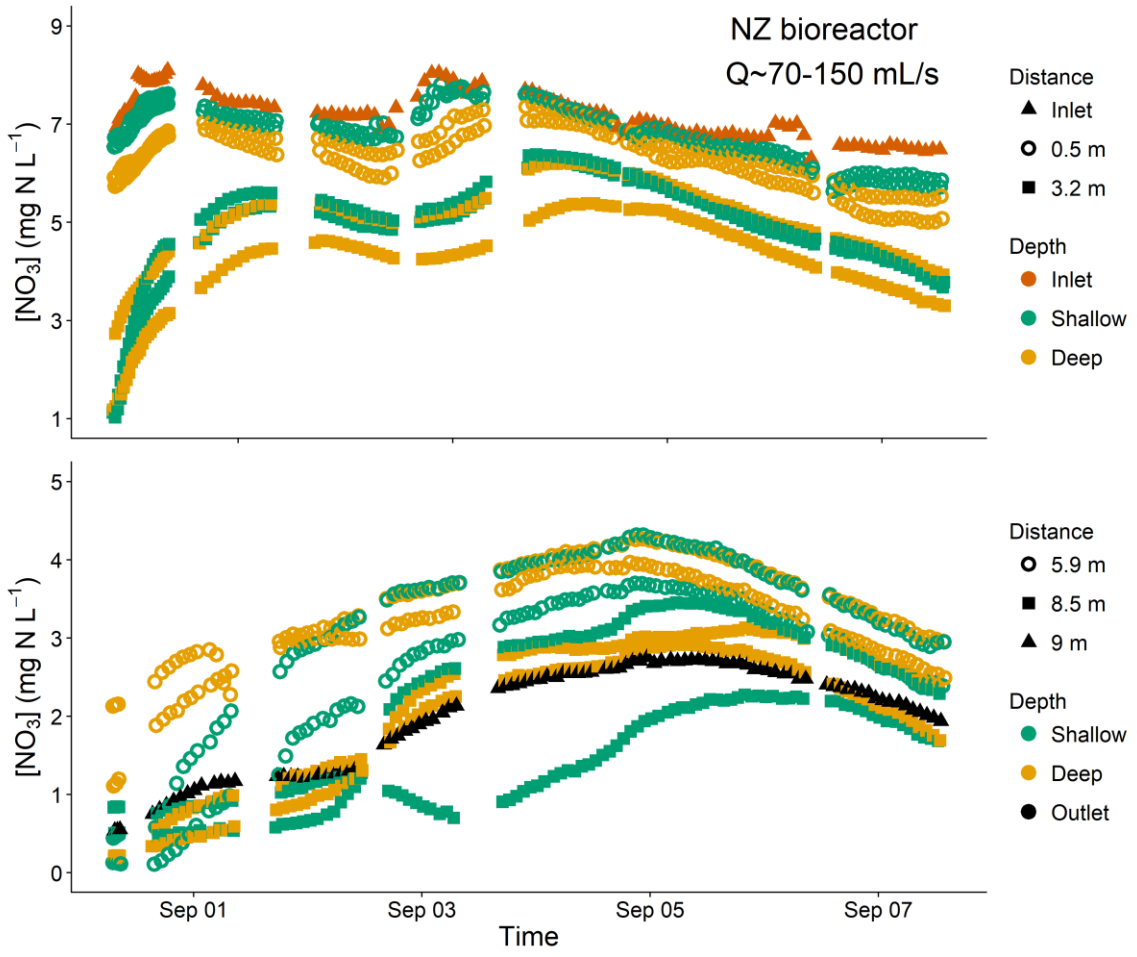

Figure E-7. Time series of [NO_3] in the NZ bioreactor following a rain event. Increased [NO_3] at the inlet was followed by relatively uniform [NO_3] increases throughout the bioreactor. Longitudinal [NO_3] trends at shallow and deep well were similar to the event on August 23 (Figure 5-17). Nitrate was generally higher in shallow ≤3.2 m, although [NO_3] was not consistently higher in deep wells ≥5.9 m. The same shallow well closest to the outlet showed a significant dead zone above the outlet distributor.